

Curso 2009/10  
**CIENCIAS Y TECNOLOGÍAS/21**  
I.S.B.N.: 978-84-7756-964-0

**GABRIEL BIHAIN**

**Objetos subestelares en cúmulos abiertos**

**Director**  
**RAFAEL REBOLO LÓPEZ**



**SOPORTES AUDIOVISUALES E INFORMÁTICOS**  
**Serie Tesis Doctorales**

# Resumen

Los objetos subestelares (masas  $M \lesssim 0.075 M_{\odot}$ ) tienen temperaturas centrales demasiado bajas para producir una fusión estable del hidrógeno. Esto implica que progresivamente se van contrayendo y enfriando. Centenares de enanas marrones ( $M \approx 0.013 - 0.075 M_{\odot}$ ) y otros centenares de objetos de masa planetaria ( $M \lesssim 0.013 M_{\odot}$ ) o candidatos han sido descubiertos en los últimos quince años. Las enanas marrones han sido caracterizadas por tipos espectrales ultra-fríos M, L, y T. Debido al progresivo debilitamiento de su luminosidad – especialmente rápido a edades  $\lesssim 0.1$  Ga, los objetos subestelares se detectan mejor cuando son jóvenes. Los cúmulos abiertos cercanos con edades y metalicidades bien determinadas son regiones idóneas para identificarlos y comprobar las predicciones de los modelos teóricos. En esta tesis doctoral presentamos la búsqueda, identificación y caracterización de nuevos objetos subestelares en los cúmulos abiertos de las Pléyades y  $\sigma$  Orionis, y con masas teóricas de  $\sim 35$ – $25$  y  $\sim 4$  veces la masa de Júpiter ( $M_{\text{Jup}}$ ), respectivamente.

El cúmulo abierto de las Pléyades ha recibido gran atención en la literatura, gracias a su riqueza en objetos, cercanía al Sol ( $\sim 120$  pc), juventud ( $\sim 120$  Ma), notable movimiento propio y baja extinción interestelar. Debido a que su población de enanas marrones más débiles y de tipo espectral L era poco conocida, hemos realizado una búsqueda de estos objetos. Hemos analizado datos fotométricos del óptico e infrarrojo cercano (bandas  $RIJ$ ) en un área de  $1.8 \text{ deg}^2$  y hemos identificado 18 candidatos. Posteriormente hemos realizado un seguimiento de ellos en el infrarrojo cercano (bandas  $HK_s$ ), obteniendo medidas fotométricas y espectroscópicas para comprobar su pertenencia al cúmulo y determinar sus características espectrales. Confirmamos nueve miembros por movimiento propio, que nos permiten mejorar la determinación del espectro de masas subestelares de las Pléyades  $dN/dM$  (número de objetos por unidad de masa). En el rango  $\sim 0.5$ – $0.026 M_{\odot}$ , el espectro de masas puede ser ajustado por una ley de potencias  $M^{-\alpha}$  con un índice  $\alpha = 0.5 \pm 0.2$ . Este índice es similar al de otros cúmulos abiertos mucho más jóvenes, lo que sugiere que la evaporación diferencial de las enanas marrones de baja masa respecto a los objetos más masivos no es significativa. Este resultado apunta a la existencia de objetos subestelares aun menos masivos en las Pléyades. Los espectros obtenidos para seis miembros del cúmulo muestran tipos espectrales desde L temprano a L medio. Al menos dos de ellos tienen rasgos espectrales que pueden ser relacionados con baja gravedad superficial, polvo, y juventud. Las enanas marrones de tipo L de las Pléyades parecen ser intrínsecamente tan débiles como las enanas de tipo L del campo con paralaje trigonométrico conocido, en desacuerdo con las predicciones de luminosidad de los modelos teóricos. Es posible que las enanas marrones de

tipo L de las Pléyades se hayan contraído más rápidamente de lo que indican los modelos.

En el cúmulo abierto  $\sigma$  Orionis, de edad  $\sim 3$  Ma, baja extinción, y relativa cercanía ( $\sim 360$ – $440$  pc), hemos buscado candidatos a masa planetaria y de tipo espectral T, adicionales a los ya conocidos S Ori 69 y S Ori 70. Hemos obtenido y analizado datos fotométricos desde el rojo lejano hasta el infrarrojo medio en un área de  $\sim 840$  arcmin<sup>2</sup>. Hemos descubierto tres nuevos candidatos a masa planetaria que por sus colores tendrían tipos espectrales L, transición L/T, y T medio, respectivamente. El candidato de tipo L está situado cerca de una estrella de tipo solar perteneciente al cúmulo (separación angular de 11.8 arcsec). Las masas teóricas estimadas de estos nuevos candidatos están en el rango 2–7  $M_{\text{Jup}}$ , teniendo en cuenta las incertidumbres en la edad, distancia y fotometría. De confirmarse como miembros del cúmulo serían algunos de los objetos de masa planetaria menos masivos identificados por imagen directa fuera del Sistema Solar. No obstante, es probable que algunos de ellos sean enanas del campo (mucho más viejas y cercanas) o galaxias contaminantes, en cuyo caso el espectro de masas tendría un fuerte cambio en la pendiente, que podría ser evidencia del llamado límite de opacidad para la fragmentación de nubes moleculares.

# Abstract

Substellar objects (mass  $M \lesssim 0.075 M_{\odot}$ ) have core temperatures too low to produce stable hydrogen fusion. Therefore, they progressively contract and cool down. Hundreds of brown dwarfs ( $M \approx 0.013 - 0.075 M_{\odot}$ ) and fewer hundreds of planetary-mass objects ( $M \lesssim 0.013 M_{\odot}$ ) or candidates have been discovered in the last fifteen years. Brown dwarfs have been characterized by ultra-cool spectral types M, L, and T. Due to their progressive dimming – especially rapid at ages  $\lesssim 0.1$  Gyr, substellar objects can be better detected when they are young. Nearby open clusters of well determined age and metallicity are idoneous regions to find such objects and test the predictions of theoretical models. In this PhD thesis we present the search, identification, and characterization of new substellar objects in the Pleiades and  $\sigma$  Orionis open clusters, and with theoretical masses of  $\sim 35-25$  and  $\sim 4$  times the mass of Jupiter ( $M_{\text{Jup}}$ ), respectively.

The Pleiades open cluster has received great attention in the litterature, due to its richness in objects, its proximity to the Sun ( $\sim 120$  pc), youth ( $\sim 120$  Myr), notable proper motion and small interstellar extinction. Because its population of fainter, L-type brown dwarfs was poorly known, we performed a search for these objects. We analyzed optical and near infrared imaging data ( $RIJ$  bands) in an area of  $1.8 \text{ deg}^2$  and we found 18 candidates. Subsequently, we performed a follow-up of these candidates in the near infrared ( $HK_s$  bands), obtaining photometric and spectroscopic measurements to verify membership to the cluster and determine spectral characteristics. We confirm nine cluster members by proper motion, which allow us to improve the determination of the Pleiades substellar mass spectrum  $dN/dM$  (number of objects per unit of mass). In the range  $\sim 0.5-0.026 M_{\odot}$ , the mass spectrum can be fit by a power law  $M^{-\alpha}$  with an index  $\alpha = 0.5 \pm 0.2$ . This index is similar to those of open clusters about thirty times younger, suggesting that the differential evaporation of the low mass brown dwarfs relative to the more massive objects is insignificant. This result points to the existence of substellar objects of even lower mass in the Pleiades. The spectra obtained for six cluster members show early- to mid L spectral types. At least two of them have spectral features which can be related to low surface gravity, dust, and youth. The Pleiades L-type brown dwarfs appear to be intrinsically as faint as field L-type dwarfs of known trigonometric parallax, which disagrees with luminosity predictions of theoretical models. A possible explanation could be that the Pleiades L-type brown dwarfs may have contracted faster than what the models indicate.

In the  $\sim 3$  Myr old, extinction free, and relatively nearby ( $\sim 360-440$  pc)  $\sigma$  Orionis open cluster, we searched for additional T-type planetary-mass candidates to S Ori 69 and



S Ori 70. We collected and analyzed photometric data from the far red to the mid infrared in an area of  $\sim 840$  arcmin<sup>2</sup>. We discovered three new planetary-mass candidates whose spectral types based on their colours would be L, transition L/T, and mid T, respectively. The L-type candidate is located near to a solar-type star belonging to the cluster (angular separation of 11.8 arcsec). The estimated theoretical masses of these candidates are in the range 2–7  $M_{\text{Jup}}$ , accounting for age, distance, and photometric uncertainties. If confirmed as cluster members, they would be some of the least massive planetary-mass objects identified by direct imaging outside the Solar System. Nevertheless, some of them are probably contaminating field dwarfs (that are much older and nearby) or galaxies, in which case the cluster mass spectrum would have a strong change in the slope, which could be evidence of the so-called opacity limit for the fragmentation of molecular clouds.

# Agradecimientos

Primero, agradezco a mi madre y mi padre, mis hermanos, cercanas/cercanos quienes me han motivado directamente o indirectamente en este proyecto (inter)cultural. Segundo agradezco a Rafael Rebolo López, Víctor Sánchez Béjar y María Rosa Zapatero-Osorio por su maestría científica, filosofía resistente y habilidad veloz inspiradoras. Agradezco también a José Antonio Caballero, Jonay Isaí González Hernández y a muchas otras personas relacionadas con el Instituto de Astrofísica de Canarias (IAC) por su ayuda y su compañía. Finalmente, agradezco al IAC por haberme permitido disfrutar de su dinamismo, logística e instrumentación astronómica.

# Index

<b>1</b>	<b>Introduction</b>	<b>1</b>
1.1	Searches for substellar objects . . . . .	1
1.2	Photometric and spectroscopic properties . . . . .	4
1.3	Formation and evolution . . . . .	4
1.4	Young open clusters and substellar evolution . . . . .	14
1.5	The Pleiades open cluster . . . . .	16
1.6	The $\sigma$ Orionis open cluster . . . . .	19
<b>2</b>	<b>Objectives</b>	<b>24</b>
2.1	L-type brown dwarfs in the Pleiades open cluster . . . . .	24
2.1.1	Pleiades low-mass brown dwarfs: the cluster L dwarf sequence . . . . .	25
2.1.2	Near-infrared low-resolution spectroscopy of Pleiades L-type brown dwarfs . . . . .	25
2.2	T-type planetary-mass objects in the $\sigma$ Orionis open cluster . . . . .	25
<b>3</b>	<b>Methodology</b>	<b>26</b>
3.1	Searches in databases . . . . .	26
3.2	Observational method . . . . .	27
3.2.1	Context . . . . .	27
3.2.2	Imaging . . . . .	28
3.2.3	Spectroscopy . . . . .	28
3.3	Data reduction . . . . .	29
3.3.1	Imaging data . . . . .	30
3.3.2	Spectroscopic data . . . . .	31
3.4	Data analysis . . . . .	33
3.4.1	Colour–magnitude- and colour–colour diagrams and broad-band luminosity functions . . . . .	33
3.4.2	Proper motions . . . . .	35
3.4.3	Spectral classification and magnitude- and colour–spectral type diagrams . . . . .	36
3.4.4	Bolometric luminosities, effective temperatures, and masses . . . . .	36

<b>4</b>	<b>Results and discussion</b>	<b>38</b>
4.1	L-type brown dwarfs in the Pleiades open cluster . . . . .	38
4.2	T-type candidates in the $\sigma$ Orionis open cluster . . . . .	41
<b>5</b>	<b>Conclusions</b>	<b>43</b>
5.1	Further studies . . . . .	44

# List of Figures

1.1	Far-red optical spectra of MLT-type field dwarfs . . . . .	5
1.2	Optical- to mid-infrared spectra of MLT-type dwarfs. . . . .	6
1.3	Optical–near-infrared $I - J$ and $I - K$ colours of ML-type field dwarfs . . .	7
1.4	Near-infrared $J - K_s$ , $H - K_s$ and $J - H$ colours of MLT-type field dwarfs	8
1.5	Theoretical evolution of luminosity . . . . .	10
1.6	Theoretical isomasses and isochrones in a radius versus effective temperature diagram . . . . .	11
1.7	Theoretical isomasses and isochrones in a luminosity versus effective temperature diagram (Hertzsprung–Russell diagram) . . . . .	12
1.8	Theoretical evolution of central temperature . . . . .	13
1.9	Lithium abundance versus effective temperature for Pleiades members of a wide mass range (left panel). Theoretical lithium fraction as a function of mass, for different ages (right panel) . . . . .	14
1.10	$4.0 \times 2.6$ deg <sup>2</sup> image of the Pleiades open cluster . . . . .	16
1.11	Colour-magnitude diagram in the $IK$ bands for Pleiades low mass members	17
1.12	Pleiades mass function from $0.030$ to $10 M_{\odot}$ . . . . .	18
1.13	$18 \times 18$ arcmin <sup>2</sup> image of the $\sigma$ Orionis open cluster . . . . .	20
1.14	$I_C$ -band magnitudes of $\sigma$ Orionis KMLT-type low-mass members or candidates	21
1.15	$\sigma$ Orionis mass histogram (top panel) and mass spectrum (bottom panel) from $0.110$ to $0.006 M_{\odot}$ . . . . .	22
3.1	Example of near-infrared imaging data reduction: Pleiades $J$ -band images .	30
3.2	Example of near-infrared spectroscopic data reduction: Pleiades brown dwarf spectrum . . . . .	32
3.3	Pleiades $J$ versus $I - J$ , $J - H$ , and $J - K$ colour–magnitude diagrams . .	33
3.4	$\sigma$ Orionis $I - J$ versus $J - K_s$ colour–colour diagram . . . . .	34
3.5	Near-infrared spectral classification of the Pleiades low-mass member PPl 1	37
4.1	Near-infrared low-resolution spectra of Pleiades late-M- and L-type brown dwarfs . . . . .	40
4.2	Hertzsprung–Russell diagram of Pleiades ML-type members . . . . .	41
4.3	$\sigma$ Orionis mass spectrum from $0.110$ to $0.004 M_{\odot}$ . . . . .	42

# 1

---

## Introduction

Puedes decir que el mundo es porque tú eres con tus sentidos. El mundo no es otra cosa que vista, oído, olfato, gusto, tacto. Pero después de la percepción directa, superpones un concepto a la sensación para calificar el mundo; la percepción cesa entonces porque percepción y concepto no pueden existir simultáneamente. Una vez se detiene la conceptualización, queda la quietud, el silencio, la conciencia, la percepción pura. Todas estas palabras apuntan al Ser.

Jean Klein (La sencillez de ser, 1986)

In 1963, Kumar presents models of very low-mass stellar structure and evolution, showing that young contracting stars less massive than  $0.07\text{--}0.09 M_{\odot}$  (high–low metallicity) “cannot reach the main sequence stage, because the temperature and density at the center are too low for hydrogen-burning to start”. Instead, they cool down, mainly, and become completely degenerate. These objects are called “brown dwarfs” (Tarter 1975) or “substellar objects”, designating thus self-gravitating objects that do not have enough mass to maintain a sufficiently high temperature in their cores for stable hydrogen fusion. A recent theoretical estimate of the stellar–substellar boundary mass at solar metallicity is of  $0.075 M_{\odot}$  (Chabrier & Baraffe 2000). Substellar objects with masses below the theoretical minimum for deuterium burning ( $\sim 0.013 M_{\odot}$ , Saumon et al. 1996) are usually called “planetary-mass objects”, or planets if they orbit around stars.

### 1.1 Searches for substellar objects

After about three decades of observational efforts, two brown dwarfs are found: Teide 1, member of the  $\sim 120$  Myr Pleiades open cluster (Rebolo et al. 1995) and Gl 229B, companion to the nearby M2-type star Gl 229 (Nakajima et al. 1995). The same year, the giant planet 51 Pegasi b is found in a 4.2 days-period orbit around the G5V-type star 51 Pegasi (Mayor & Queloz 1995). This discovery follows that of three low-mass planets around the pulsar PSR 1257+12 (Wolszczan & Frail 1992) and the confirmed early identifications of giant planets orbiting in periods of years the K0–2 III–V-type stars  $\gamma$  Cep,  $\epsilon$  Eri, and  $\beta$  Gem (Campbell et al. 1988; Hatzes & Cochran 1993; Hatzes et al. 2003; Benedict et al. 2006; Hatzes et al. 2006; Walker 2008). As of June 2010, numbers of discovered brown-dwarfs

and planets reach both several hundreds<sup>1</sup>. We note that the substellar nature of several candidates remains unconfirmed, such as the companion of the F9V-type star HD 114762 (Latham et al. 1989; Mazeh et al. 1996).

Most of the brown dwarf candidates are discovered by wide-field imaging in star-forming regions and young stellar clusters (molecular clouds, associations, and open clusters) and the field (e.g. Kelu-1, by Ruiz et al. 1997 using the DENIS survey; see Table 1.1). Some brown dwarf candidates are discovered as companions to stars, by wide- or narrow-field imaging (e.g. G196-3B, by Rebolo et al. 1998; see also White et al. 1999; Burgasser et al. 2000; Close et al. 2002, 2003; Gizis et al. 2003; Bouy et al. 2003; Chauvin et al. 2005c; ?). In smaller numbers they are discovered indirectly, as by monitoring of stellar radial velocities or proper motions (e.g. HD 29587B y HD 127506B, Halbwachs et al. 2000; Frankowski et al. 2007). In particular, a “hot brown dwarf” companion (CoRoT-3B) in a 4.26 days orbit has even been discovered by photometric and radial-velocity monitoring of a F3V-type star (i.e. by the transit- and radial velocity methods; Deleuil et al. 2008). Stellar clusters are advantageous relative to field single or multiple systems, because their age can be determined more precisely, for instance by the methods of upper-main-sequence turn-off or lithium-depletion boundary (Stauffer et al. 1998). But the first are located at distances greater than a few tens of parsecs to the Sun (cf. the nearby AB Doradus- and Ursa Major associations and the Hyades open cluster). The general field, on the other hand, provides very nearby, large proper-motion, isolated-or-bound, faint, and mostly evolved substellar candidates. The nearest known brown dwarf is a T-type<sup>2</sup> binary, in a wide orbit (physical separation of 1500 AU) around the star Epsilon Indi, at 3.6 pc (Scholz et al. 2003; McCaughrean et al. 2004; King et al. 2009).

Most of the exoplanet candidates are discovered around “solar type” stars (FGK V-type stars) by the radial velocity method (e.g. with the CORALIE, ELODIE, and HARPS searches of the Geneva group, see Mayor et al. 2004, and the HIRES, HAMILTON, and AAT searches of the California group, Marcy et al. 2005). In smaller numbers, they are discovered around giant stars (Hatzes et al. 2005; Sato et al. 2007; Lovis & Mayor 2007; Han et al. 2010) or low-mass stars via radial velocity (Marcy et al. 1998; Bonfils et al. 2005; Charbonneau et al. 2009), around pulsars via timing (Wolszczan & Frail 1992; Rasio 1994), low-mass stars via gravitational lensing (Bond et al. 2004; Udalski et al. 2005; Gould et al. 2006; Beaulieu et al. 2006), and solar type stars via transiting (Charbonneau et al. 2000; Alonso et al. 2004; Dvorak et al. 2009; Shporer et al. 2009; Anderson et al. 2010) or direct imaging (Neuhäuser et al. 2005; Chauvin et al. 2005b; Kalas et al. 2008; Lafrenière et al. 2008; Marois et al. 2008). A planetary-mass object has even been found as a companion to a brown dwarf (2M1207) by direct imaging and proper motion (Chauvin et al. 2004, 2005a). We note that the acquisition of images resolving planetary-mass objects at very small angular separations of stars or brown dwarfs remains still a technical challenge, due to the large flux contrast of the objects. Finally, free-floating planetary-mass candidates are discovered among brown dwarfs and stars in star-forming regions, such as  $\sigma$  Orionis (Zapatero Osorio et al. 2000; Caballero 2006), Trapezium (Lucas & Roche 2000; Lucas et al. 2005), IC 348 (Najita et al. 2000), Chamaeleon I (Luhman et al. 2005b,a), and Taurus (Luhman et al. 2009; Barrado

<sup>1</sup>See e.g. the Dwarf Archives at <http://www.dwarfarchives.org> and J. Schneider’s Extrasolar Planets Encyclopaedia at <http://exoplanet.eu/>, and the references in Table 1.1.

<sup>2</sup>In Sect. 1.2, we describe the spectral types later than O, B, A, F, G, K, and M.



Table 1.1: Examples of brown dwarf wide imaging searches.

Type of region	Examples
Molecular cloud	Chamaeleon (Neuhäuser & Comerón 1999), IC 348 (Luhman 1999), $\rho$ Ophiuchus (Williams et al. 1995; Wilking et al. 1999), Taurus (Briceño et al. 1998), Trapezium (Hillenbrand 1997)
Association	TW Hydrae (Gizis 2002), Upper Scorpius (Lodieu et al. 2007),
Open cluster	$\sigma$ Orionis (Béjar 2000; Zapatero Osorio et al. 1999a, 2000), $\alpha$ Persei (Barrado y Navascués et al. 2002) Pleiades (Zapatero Osorio et al. 1997a,b; Bouvier et al. 1998), Praesepe (Magazzu et al. 1998; Chappelle et al. 2005) Hyades (Bouvier et al. 2008; Hogan et al. 2008)
Field	DENIS project (Delfosse et al. 1997; Phan-Bao et al. 2003), 2MASS project (Kirkpatrick et al. 1999a; Burgasser et al. 1999; Kirkpatrick et al. 2000; Cruz et al. 2003; Burgasser et al. 2003a), SDSS project (Strauss et al. 1999; Hawley et al. 2002; Schneider et al. 2002), UKIDSS project (Lawrence et al. 2007; Kendall et al. 2007), CFBDS project (Delorme et al. 2008)

et al. 2009). One of the least massive free-floating candidates is S Ori 70 in the  $\sigma$  Orionis open cluster (Zapatero Osorio et al. 2002a, 2008; Martín & Zapatero Osorio 2003). It has an estimated theoretical mass of 2–7  $M_{Jup}$  ( $1M_{Jup} \approx 0.00095M_{\odot}$ ,  $1M_{\odot} \approx 1047M_{Jup}$ ) and a spectral type T6. S Ori 70 is the precursor of other T-type planetary-mass candidates recently discovered in stellar clusters (Bihain et al. 2009; Burgess et al. 2009; Marsh et al. 2010).

While the precision of radial velocity measurements increases and the detection of objects with the mass of Neptune (McArthur et al. 2004) down to a few Earths (Rivera et al. 2005; Mayor et al. 2009) is reached, there appears a clear paucity of brown dwarfs orbiting at less than 4–5 AU of solar type stars (Marcy & Butler 2000; Jorissen et al. 2001; Marcy et al. 2005). Also, there appears a paucity at distances larger than 50 UA, by direct imaging searches (Oppenheimer et al. 2001; McCarthy & Zuckerman 2004). These paucities are called “short and wide deserts of brown dwarfs”, respectively. However, brown dwarfs appear more frequently in tight orbits around low-mass stars and brown dwarfs, at separation of semi-major axis of  $\sim 4$  UA (Bouy et al. 2003; Gizis et al. 2003). They appear thus more as binaries (high mass ratio  $q = m_2/m_1 \sim 1$ , where  $m_1$  and  $m_2$  are the masses of the primary and secondary, respectively) than as substellar companions to stars (low mass ratio  $q$ ). Finally, the binary fraction is found to decrease continuously from 50% for the G-type dwarfs (Duquennoy & Mayor 1991) to  $\sim 10\%$  for the T-type dwarfs (Burgasser et al. 2003b). This points to the possibility that the separation of semi-major axis and the fraction of binaries would decrease with the mass of the primary, from the stellar- to the

substellar domain (Siegler et al. 2005).

## 1.2 Photometric and spectroscopic properties

The observation of low-mass stars and substellar objects has allowed to extend the classification of spectral types (O, B, A, F, G, K, M) with L and T, corresponding to effective temperatures  $T_{\text{eff}} \sim 2300\text{--}1400$  K y  $\sim 1400\text{--}700$  K, respectively (Martín et al. 1997, 1999; Kirkpatrick et al. 1999b; Burgasser et al. 2002; Geballe et al. 2002; Dahn et al. 2002). In comparison with the M-type dwarfs (Fig. 1.1), the L-type dwarfs are characterized in the optical by the weakening of the metal-oxide TiO y VO bands due to the condensation of the metals Ti and V in dust grains (that can affect significantly the atmospheric structure and the emerging spectrum; cf. DUSTY models of Chabrier et al. 2000). The metal-hydrides CrH, FeH, and CaH bands begin to be more intense, as well as the neutral alkali metal Na, K, Rb, and Cs lines (Chabrier & Baraffe 2000; Basri 2000). In the near-infrared (Fig. 1.2), the water bands at 1.3–1.51, 1.75–2.05, and 2.3–3.2  $\mu\text{m}$  intensify, and also the FeH bands at  $\sim 1.0$ , 1.2, and 1.6  $\mu\text{m}$ . Finally, the appearance of CH<sub>4</sub> bands at 1.1–1.24, 1.6–1.8, and 2.15–2.5  $\mu\text{m}$  characterizes the T-type dwarf sequence. From M- to early L-type, the Na I resonance doublet at  $\sim 1.14$   $\mu\text{m}$  and the K I resonance doublets at 1.17 and 1.25  $\mu\text{m}$  intensify, and then from early L- to T-type they weaken. CO bands at 2.294, 2.323, and 2.352  $\mu\text{m}$  are present at spectral types M to mid-L, and progressively disappear at later types.

These ultra-cool atmospheres are thus characterized by strong molecular line-blanketing (or “greenhouse” effect) and condensation of species with decreasing effective temperature, which change the chemical equilibrium composition. The formation and evolution of dust cloud patterns could be related with the observed temporal variability in L- and early-T-type dwarfs (Bailer-Jones & Mundt 2001; Koen 2003; Littlefair et al. 2008).

As shown in Fig. 1.3 and in Fig. 1.4, the colours of late M-type dwarfs are bluer than  $I - J \sim 3.3$ ,  $I - K \sim 4.7$ ,  $J - K_s \sim 1.4$ , and  $J - H \sim 0.8$  mag. L-type dwarfs have redder colours, which increase from early to late spectral subclasses and are related to the formation of dust in the atmospheres (Chabrier et al. 2000). The colours  $J - K_s$  and  $J - H$  appear to saturate at  $\sim 2.0$  and  $\sim 1.3$  mag, respectively, for spectral types L4–L8. For T-type dwarfs, these two colours become bluer, reaching even negative values. This effect is attributed to the gravitational settling of some dust grains below the photosphere (Chabrier et al. 2000). From L6 to T8, the  $I - J$  colour increases from  $\sim 4.0$  to  $\sim 5.6$  mag (see also Table 1.2), whereas the  $I - K$  colour increases up to  $\sim 6.0$  mag for L6–T2 and then decreases to  $\sim 5.0\text{--}5.5$  mag for  $\sim$ T8 (Caballero et al. 2008).

## 1.3 Formation and evolution

From stars to free-floating brown dwarfs and planetary-mass objects, observations indicate accretion discs (Barrado y Navascués et al. 2003; Mohanty et al. 2005; Luhman et al. 2005c,a) and, at least in the  $\sigma$  Orionis open cluster and the Chamaeleon I cloud, a continuity of the mass function<sup>3</sup> (Béjar et al. 2001; Caballero et al. 2007; Luhman 2007). In the NGC

<sup>3</sup>See definition in Sect. 1.5.

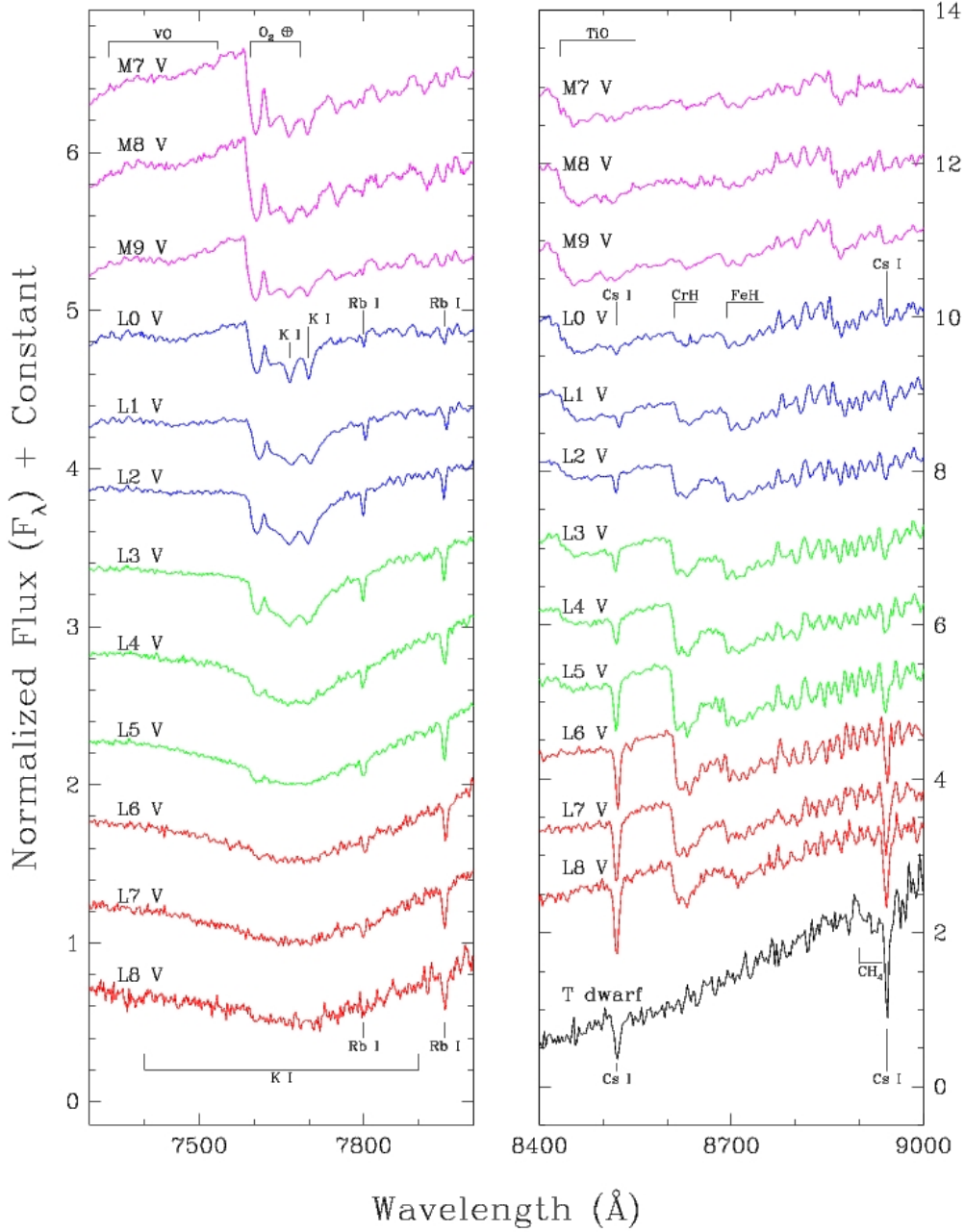


Figure 1.1: Comparison of line and band strength changes as a function of spectral type (or temperature) for two feature-rich portions of the far-red optical spectrum. From Kirkpatrick et al. (1998).

1333 cloud, an apparent mass function cutoff at  $\sim 0.015 M_\odot$  has been found (Scholz et al. 2009) - previously suggested by (Greissl et al. 2007), which could be interpreted as due to an opacity mass limit<sup>4</sup> for gravitational fragmentation of collapsing molecular clouds (Hoyle

<sup>4</sup>This study is relatively recent. It was accepted for publication about two weeks before that of Bihain et al. (2009) on the same topic, in the  $\sigma$  Orionis cluster.

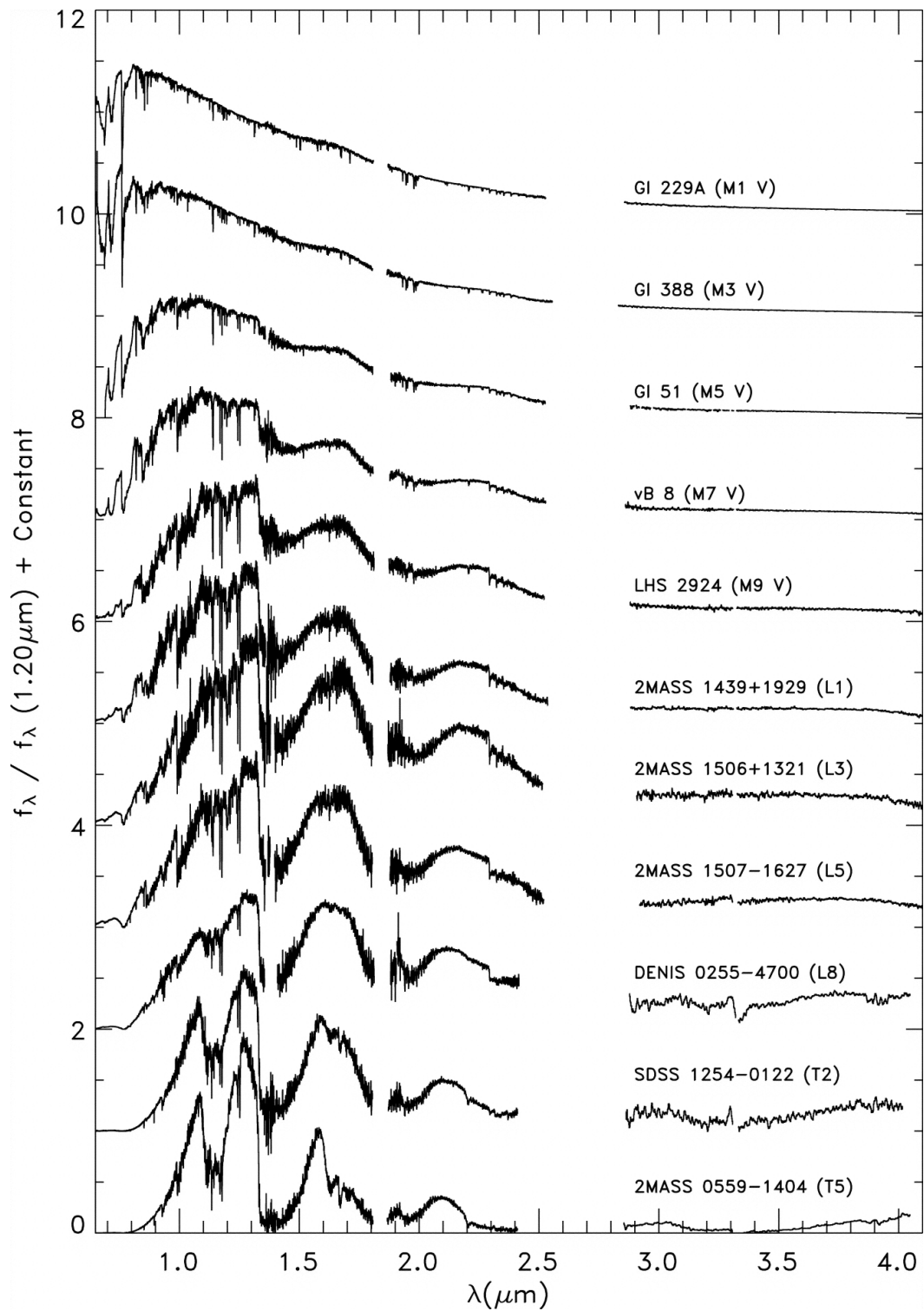


Figure 1.2: 0.6–4.1  $\mu\text{m}$  sequence of M-, L-, and T-type dwarfs. From Cushing et al. (2005).

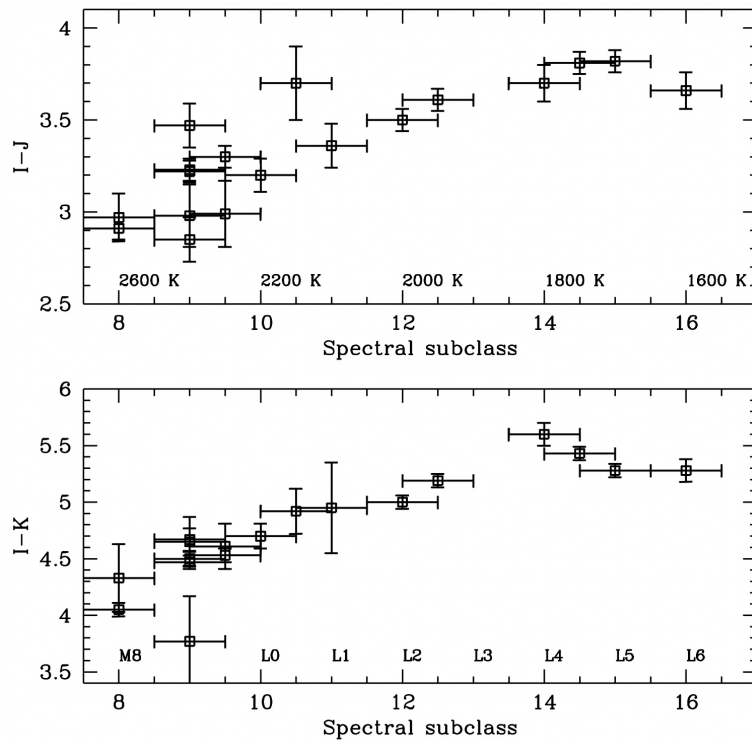


Figure 1.3: Optical–near-infrared  $I - J$  and  $I - K$  colours of ML-type field dwarfs. The numbers in the x-axis correspond to the spectral subclasses (M8=8, L0=10). From Martín et al. (1999).

1953; Larson 1973; Low & Lynden-Bell 1976; Rees 1976; Silk 1977). Besides, observations indicate a higher disc frequency for brown dwarfs than for stars (Caballero et al. 2007; Zapatero Osorio et al. 2007; Luhman et al. 2008). All these observations suggest that free-floating substellar objects could form as stars (fragmentation of collapsing molecular clouds) or stellar embryos that are fragmented, photo-eroded or ejected before they can accrete sufficient mass to become stars (Reipurth & Clarke 2001; Whitworth & Zinnecker 2004; Bate & Bonnell 2005; Whitworth & Goodwin 2005). The short desert of brown dwarfs in Sun-like stars (Grether & Lineweaver 2006), as opposed to the higher proportion of brown dwarfs around low-mass stars and brown dwarfs, may indicate that they would form less similarly as planetary companions than as stellar binaries.

Planets are usually considered as secondary by-products of star formation, resulting from accretion of planetesimals and then of gas in the disc surrounding the proto-star (Hayashi et al. 1985; Lissauer 1993; Marcy & Butler 1998; Ikoma et al. 2000; Wuchterl et al. 2000; Hubickyj et al. 2005) or directly from gravitational instability in the gas disc (Boss 1997; Mayer et al. 2002; Whitworth & Stamatellos 2006). Due to dynamical interaction, some may eventually be ejected into interstellar space (Veras et al. 2009; Stamatellos & Whitworth 2009). The planetary formation may also produce some of the observed gaps and asymmetries in accretion discs of very young stars (Mouillet et al. 1997; Heap et al. 2000; Wyatt 2003; Quillen et al. 2004; Grady et al. 2005; Telesco et al. 2005). Half of the planets detected by the radial velocity method at less than 5 AU of solar type stars

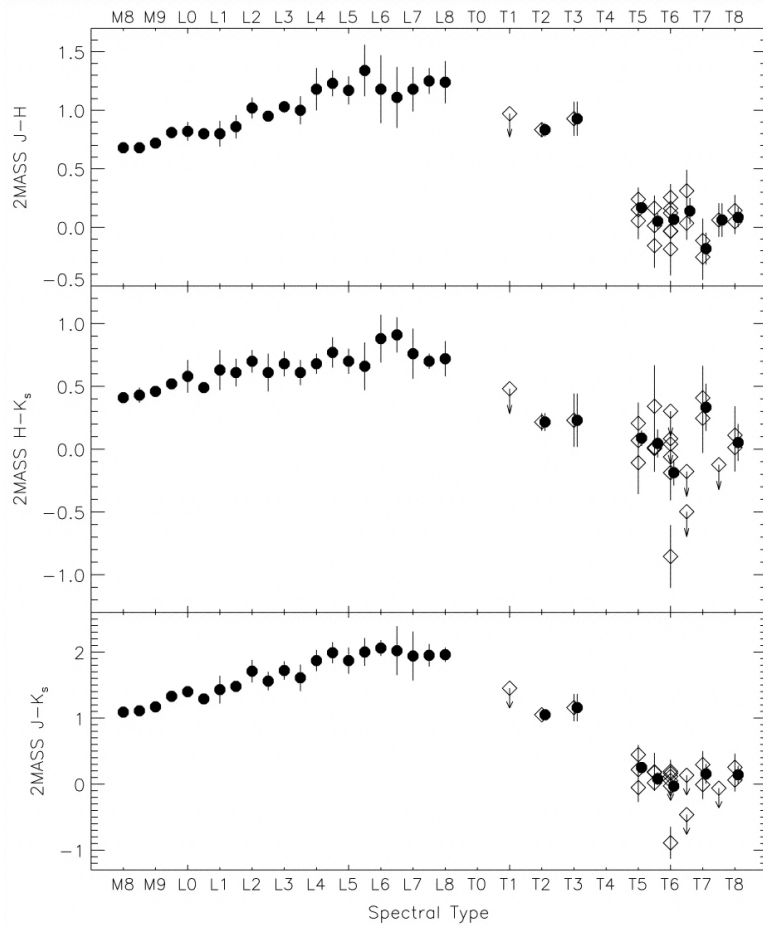


Figure 1.4: Near-infrared  $J - K_s$ ,  $H - K_s$  and  $J - H$  colours of MLT-type field dwarfs. Individual T-type dwarf colours with errors are indicated by open symbols, with upper-limit detections indicated by downward arrows. Weighted averages at each half-subtype are indicated by slightly offset filled circles. L-type dwarf mean colours (with  $1 \sigma$  scatter) are taken from Kirkpatrick et al. (2000). From Burgasser et al. (2002).

have minimum masses ( $M \sin(i)$ , where  $i$  is the inclination of the stellar system relative to the sky plane) smaller than  $1.5 M_{\text{Jup}}$ . In the other half, the planets distribute until a dozen  $M_{\text{Jup}}$  with a frequency inversely proportional to their mass (Marcy et al. 2005). The frequency of radial velocity planets with masses  $\sim 5\text{--}14 M_{\text{Jup}}$  at less than 5 AU of field solar type stars is  $\sim 1.5 \%$ , whereas the frequency of free-floating objects in the same mass range in comparison to solar type stars in the sigma Orionis cluster is  $\sim 50 \%$  (Caballero 2006). These statistics may suggest that giant planets are much less frequent around stars than their mass counterparts in interstellar space, and thus, that planets would form (*i*) mostly at small masses by core accretion (Solar system paradigm) or (*ii*) also at larger masses (e.g., by gravitational instability in the gas disc) and be ejected into the free-floating population (Stamatellos & Whitworth 2009). The low giant-planet statistics are supported by the null results of several high-resolution deep imaging surveys of stars probing greater separations 20–100 AU, providing a probability of less than 20 % for planets more massive than  $4 M_{\text{Jup}}$

Table 1.2: Numerical volume densities, absolute  $J$ -band magnitudes, and  $I - J$  colours of MLT-type field dwarfs (Caballero 2006).

SpT	$\rho$ ( $10^3 pc^{-3}$ )	$M_J$ (mag)	$I - J$ (mag)	$J$ (@360 pc)
M3V	19.6	7.11	1.3	14.9
M4V	16.3	8.60	1.5	16.4
M5V	9.81	8.81	1.8	16.6
M6V	4.90	10.23	2.2	18.0
M7V	1.907	10.63	2.8	18.4
M8V	1.285	11.15	3.1	18.9
M9V	0.768	11.64	3.4	19.4
L0V	0.435	11.62	3.4	19.4
L1V	0.456	12.00	3.5	19.8
L2V	0.477	12.38	3.6	20.2
L3V	0.394	12.76	3.7	20.5
L4V	0.332	13.14	3.8	20.9
L5V	0.373	13.52	3.9	21.3
L6V	0.312	13.90	4.0	21.7
L7V	0.250	14.28	4.1	22.1
L8V	0.229	14.66	4.2	22.4
T0V	0.379	14.79	4.4	22.6
T1V	0.443	14.60	4.5	22.4
T2V	0.368	14.33	4.7	22.1
T3V	0.181	14.26	4.9	22.0
T4V	0.587	14.36	5.0	22.1
T5V	0.439	14.64	5.1	22.4
T6V	2.33	15.11	5.3	22.9
T7V	0.345	15.75	5.5	23.5

(Nielsen et al. 2008). But the range 5–20 AU where the radial velocity and imaging technics have low sensitivity remains to be further probed. There are also claims that (young) giant planets may be much fainter than predicted, and therefore much more difficult to detect by imaging (Fortney et al. 2008). In fact, the few theoretical studies predicting the planet fluxes by coupling the atmosphere models to the thermal evolution models (Burrows et al. 1997; Chabrier et al. 2000; Baraffe et al. 2003) assume arbitrary initial conditions, i.e. without coupling to the formation models.

Due to the lack of sufficient thermonuclear energy, substellar objects are expected to contract and cool down. The evolution of a brown dwarf can be described schematically in three phases (Stevenson 1978):

- the collapse phase, during which a homogeneous low-density gas sphere (essentially of hydrogen and helium) contracts adiabatically along the vertical Hayashi track in the Hertzsprung-Russell diagram. This phase is difficult to modelize as for the pre-main sequence T Tauri stars (asymmetry, turbulence, accretion, magnetic fields, opacity,



and external triggering);

- the deuterium burning<sup>5</sup> which occurs during the degenerate cooling. It is also referred as the deuterium 'main sequence', where the luminosity decreases less rapidly;
- the degenerate cooling<sup>6</sup>, during which the luminosity decreases with the rhythm of release of the internal and gravitational potential energies. Lower mass objects are less luminous as illustrated in Fig. 1.5.

Evolution of luminosity with time for different masses

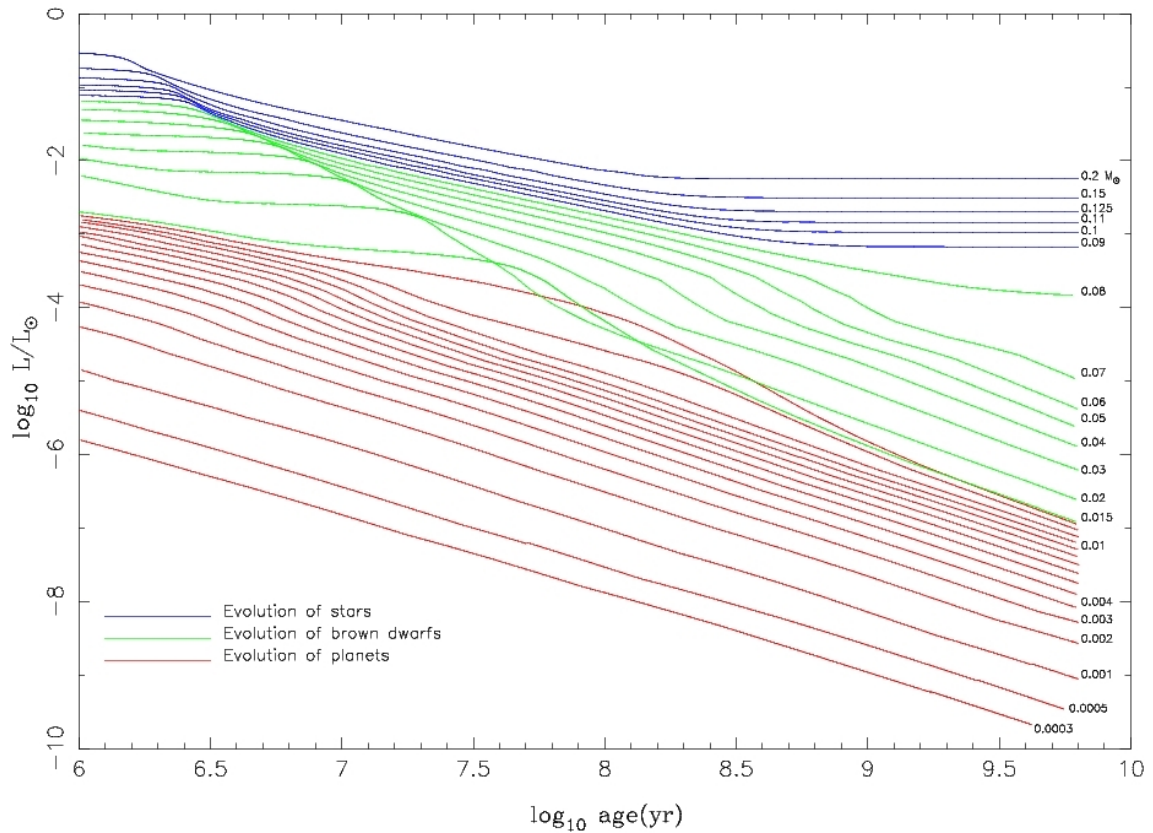


Figure 1.5: Evolution of the luminosity (in  $L_{\odot}$ ) of solar-metallicity M-type dwarfs and substellar objects versus time (in yr) after formation. The isomasses of stars, brown dwarfs, and planetary-mass objects are represented by blue, green, and red curves, respectively. The masses (in  $M_{\odot}$ ) label most of the curves, with the lowest three corresponding to the mass of Saturn, half the mass of Jupiter, and the mass of Jupiter. From Burrows et al. (1997).

From Figs. 1.6 and 1.7, high-mass brown dwarfs are expected to evolve slowly from late M-type in the initial phase to L-type at an intermediate age (several hundreds of Myr), and

<sup>5</sup>The thermonuclear reaction is  ${}^2\text{D}(p,\gamma){}^3\text{He}$  ( $T_D \sim 4 \times 10^5 \text{K}$ ). D and He are fully ionized and treated as classical gases, whereas the electrons are treated as a mostly quantum-degenerate gas.

<sup>6</sup>The degeneracy of the electrons gas implies that the gas can hardly get denser and the cooling implies that the degeneracy increases. Therefore the density is mostly constant, and so the radius of the brown dwarf ( $\sim 1 R_{Jup}$ ).

at ages large enough (a few Gyr), to T-type, and then beyond. Low-mass brown dwarfs and massive planetary-mass objects of late M-type are expected to reach faster the L- and later types.

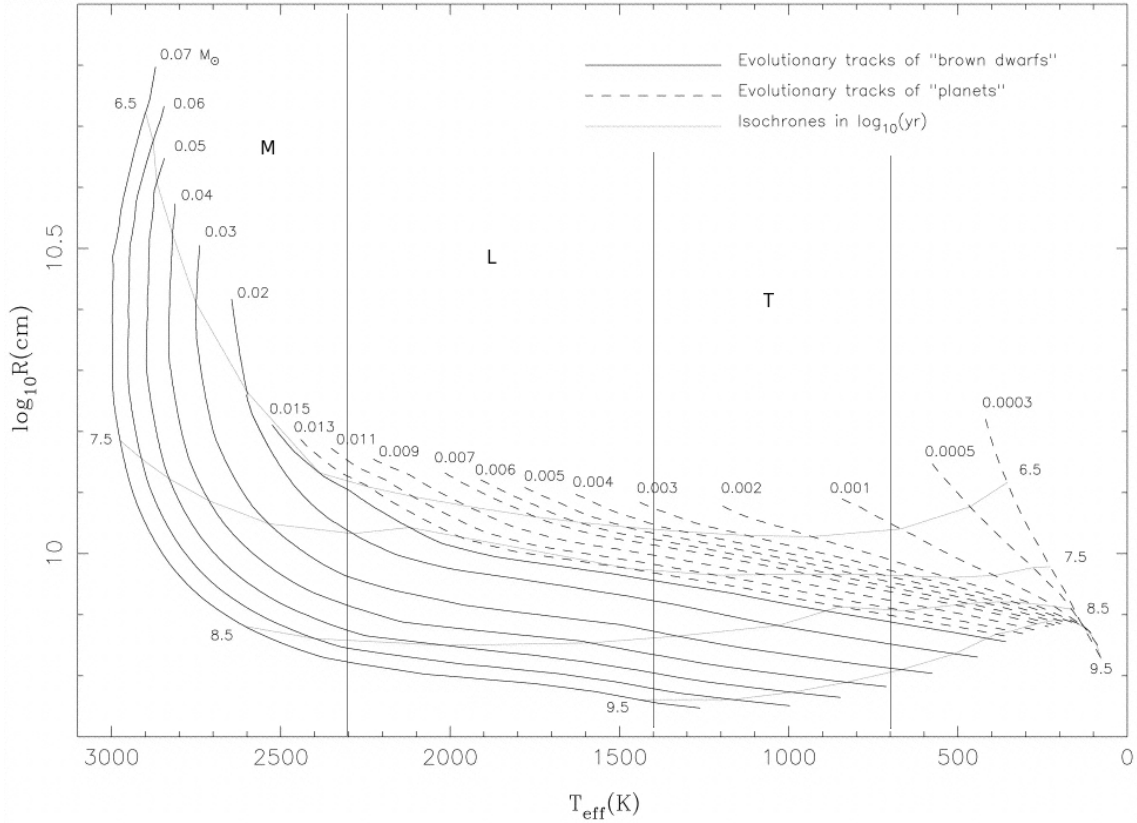


Figure 1.6: Evolutionary tracks in a  $\log_{10}$  radius versus effective temperature diagram. Isochrones for the ages of  $\approx 3.2$ , 32, 320 Myr, and 3.2 Gyr are shown from top to bottom. The  $T_{\text{eff}}$  ranges of MLT spectral types are indicated. This plot has the advantage over an Hertzsprung–Russell diagram in that considerably more detail can be shown over the range of conditions considered. In all cases, radius decreases with time. For the more massive brown dwarfs the effective temperature initially increases before decreasing. Adapted from Burrows et al. (1997).

Figures 1.5 and 1.7 show that young brown dwarfs could have the same luminosity as older low-mass stars<sup>7</sup>. Because the theoretical models are relatively untested at various ages, metallicities, and low-mass stellar- and substellar masses, this further complicates the search for substellar objects among field dwarfs of spectral types later than mid-M.

Therefore, a direct measurement of the mass is the most suitable. Binary systems, preferentially of short periods, permit the estimation of the dynamical mass (see e.g., Zapatero Osorio et al. 2004; Dupuy et al. 2009a,b; ?, 2010). However numerous objects are observed free-floating or in some cases in rather long period systems.

One way to distinguish low-mass stars from brown dwarfs is the lithium test (Rebolo

<sup>7</sup>Although Fig. 1.7 indicates that low-mass substellar objects of spectral types late M and early L would always be brighter than higher mass objects of same effective temperature.

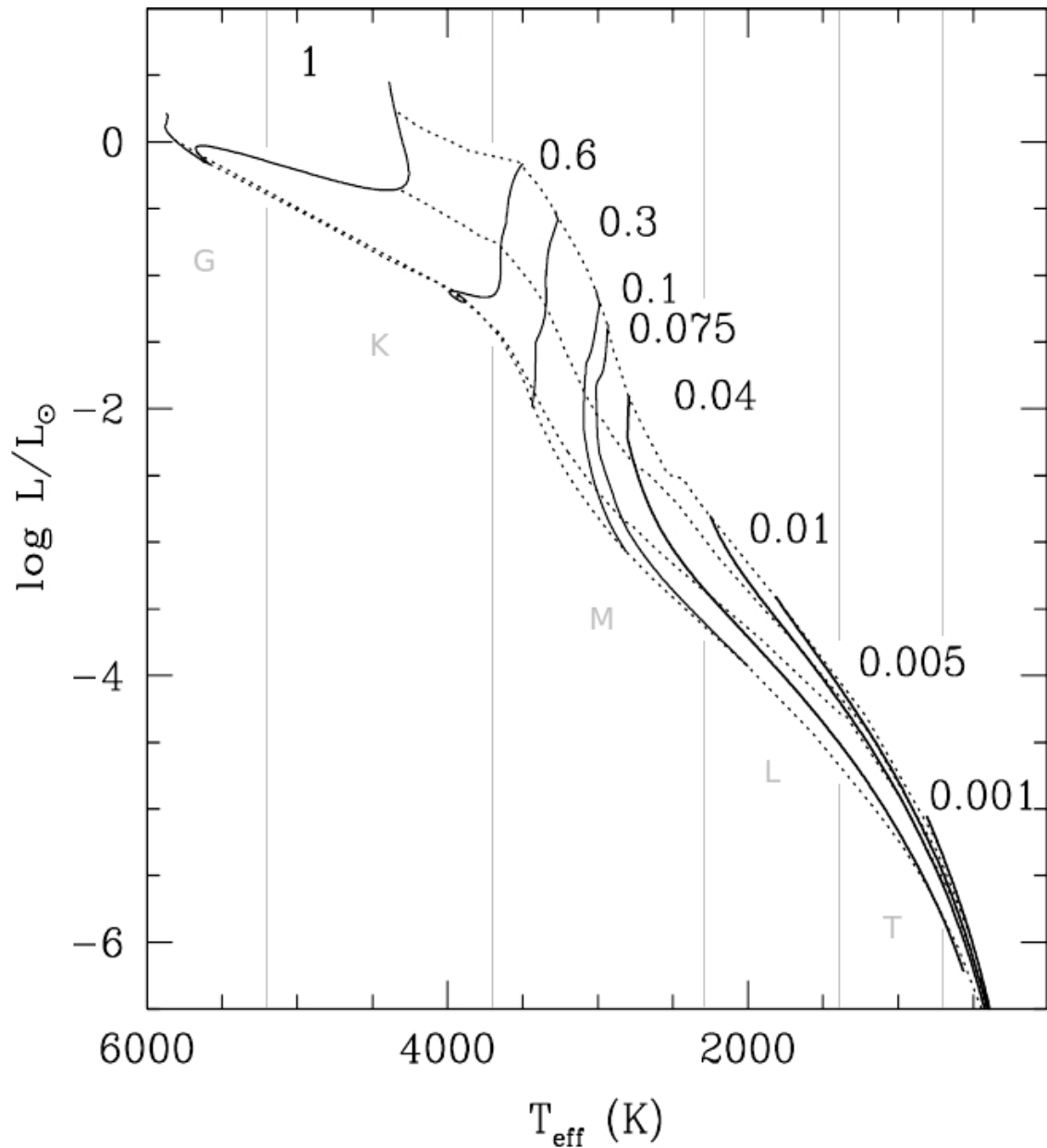


Figure 1.7: Theoretical Hertzsprung–Russell diagram for various masses (labeled in  $M_{\odot}$ ). The weak dependence of radius on mass for substellar objects yields the merging of the tracks for the lowest-mass objects. Dotted lines represent 1, 10, 100 Myr, and 5 Gyr isochrones from right to left. Adapted from Chabrier & Baraffe (2000).

et al. 1992; Magazzu et al. 1993; Pavlenko et al. 1995).  ${}^7\text{Li}$  nuclei are burned via proton collisions [ ${}^7\text{Li}(p,\alpha){}^4\text{He}$ ] in interiors at relatively low temperatures of  $\sim 2 \times 10^6$  K (near the H burning temperature; Fig. 1.8). The strong convection of very low-mass stars ( $M < 0.3 M_{\odot}$ ) brings the lithium into the deeper and hotter layers where it is burned and causes an atmospheric lithium depletion. But for substellar objects with masses below  $0.06 M_{\odot}$ ,

this temperature is not reached, and they thus preserve largely their initial lithium content. The atmospheric lithium abundance can be measured spectroscopically using the resonance doublet at 6708 Å, which is detectable for effective temperatures down to  $\sim 1500\text{--}1000$  K. At  $T_{\text{eff}} < 1500$  K, the doublet becomes less intense because of the increase of lithium in molecular forms like LiCl and LiOH (Lodders 1999). Nevertheless, the overall  $T_{\text{eff}}$  range covers largely the range relevant for brown dwarfs, at ages young enough ( $\lesssim 0.5$  Gyr).

The left panel in Fig. 1.9 illustrates the lithium depletion or preservation for members of the Pleiades open cluster. The cool objects Teide 1 (Rebolo et al. 1995) and Calar 3 (Rebolo et al. 1996) have preserved their initial lithium content and are substellar. The same is expected for Pleiades dwarfs fainter than Teide 1 (see Sect. 1.5), which can thus be used to interpret the lithium amounts of field dwarfs of same spectral type. The right panel in Fig. 1.9 shows how the theoretical lithium fraction (the ratio of the number of Li atoms at a given time over the initial number of Li atoms) depends on mass and age. Brown dwarfs with masses smaller than  $0.055 M_{\odot}$  preserve during at least 10 Gyr half of their initial lithium content, whereas those with masses greater than  $0.06 M_{\odot}$  deplete in less than 0.5 Gyr all their lithium. The figure suggests that the lithium test differentiates neatly a brown dwarf from a low-mass star of same age when the mass of complete lithium depletion is below the hydrogen burning mass limit, i.e. when the age is  $>0.1$  Gyr.

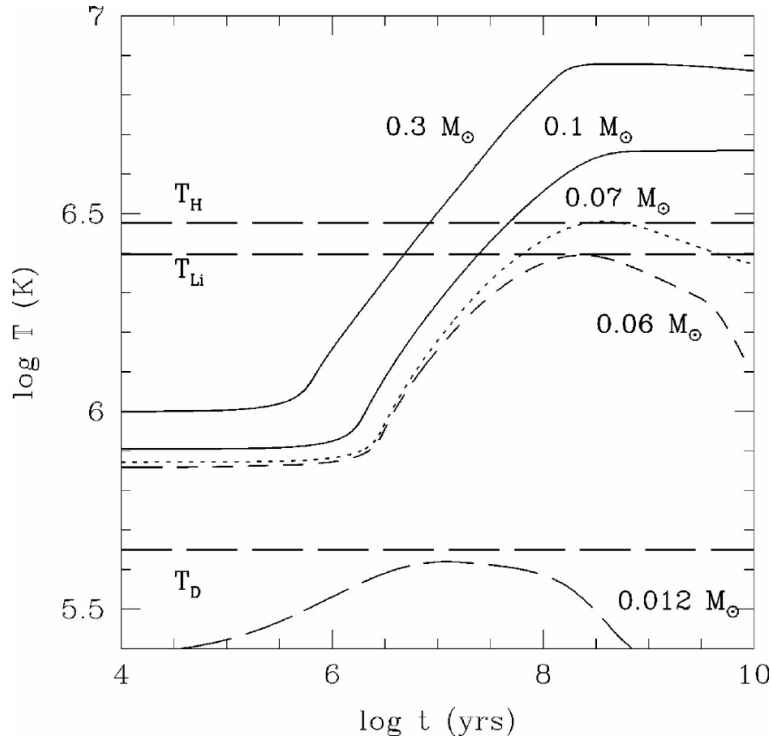


Figure 1.8: Central temperature as a function of age for different masses.  $T_{\text{H}}$ ,  $T_{\text{Li}}$  and  $T_{\text{D}}$  indicate the hydrogen, lithium, and deuterium burning temperatures, respectively. From Chabrier & Baraffe (2000).

However, the substellarity of an ultra-cool object with lithium can be further constrained by evolutionary models. Indeed, the highest-mass brown dwarf sets the maximum substellar luminosity and effective temperature at which lithium begins to be fully depleted

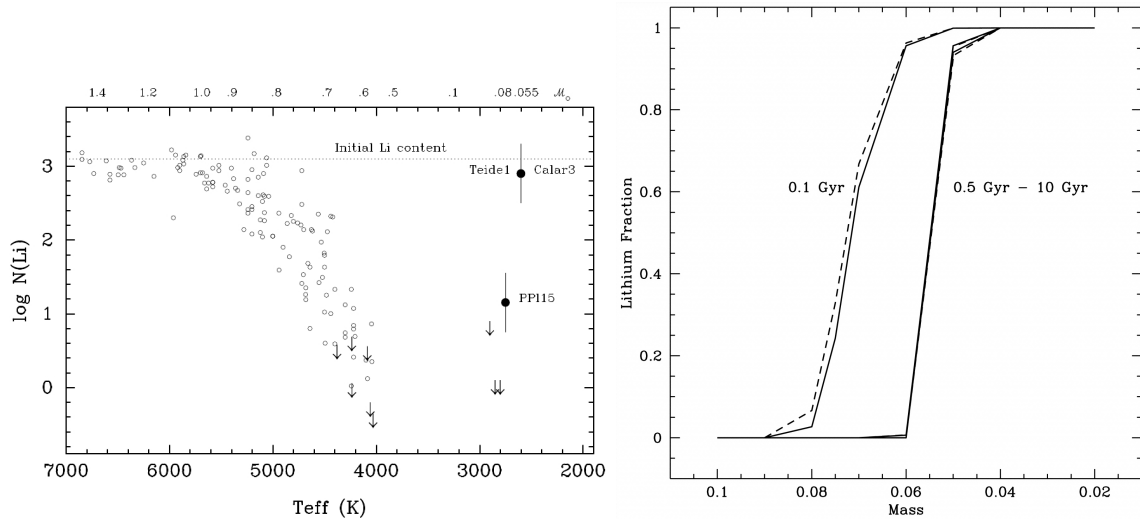


Figure 1.9: Left: lithium abundance versus effective temperature for Pleiades members of a wide mass range. Abundances are given in the usual scale  $N(H) = 12$ . Open circles and arrows (which indicate upper limits) are taken from the literature. From Rebolo et al. (1996). Right: theoretical lithium fraction as a function of mass, for different ages. The solid and dashed lines represent the NextGen and Dusty models, respectively (Baraffe et al. 1998; Chabrier et al. 2000); the lines for ages 0.5–10 Gyr overlap. From Martín et al. (1999).

( $\log(L/L_{\odot}) = -3.05$  dex and  $T_{\text{eff}} = 2670$  K, respectively), so that a fainter and cooler dwarf with lithium will be a brown dwarf (Basri 1998). The maximum effective temperature corresponds to an optical spectral type M8V (Kirkpatrick et al. 2008).

Besides, low-mass stars are predicted not to reach effective temperatures cooler than those of early L-type dwarfs (about 2000 K, as estimated using the 10 Gyr Dusty model from Chabrier et al. 2000, and corresponding to an optical spectral type  $\sim$ L3). Therefore, a spectral type T would certainly be conclusive for substellarity.

In the case of substellar candidates of spectral types mid M and L, spectral shapes and features indicative of low surface gravity and youth, such as weak Na I, K I, Rb I, and Cs I absorption lines and strong VO bands (McGovern et al. 2004), can be compared to emergent spectra of model atmospheres and allow to estimate the effective temperature and surface gravity (Béjar 2000; Basri et al. 2000; Mohanty et al. 2004a; Kirkpatrick et al. 2006). From a measured distance and the difference between predicted and observed magnitudes, it is possible to estimate the radius, which together with the estimates of the effective temperature and surface gravity allows to derive the luminosity and mass, respectively (Mohanty et al. 2004b).

#### 1.4 Young open clusters and substellar evolution

To test the contraction- and cooling rates of substellar objects predicted by theoretical models, age- and mass benchmark objects are required (see e.g., Chabrier & Baraffe 2000). Once the models are calibrated, they can be used to determine and understand the Galactic substellar population (Kroupa & Bouvier 2003; Burgasser 2004; Allen et al. 2005; Pinfield

et al. 2006), as well as the substellar populations outside our Galaxy.

For ultracool field dwarfs, it is in general difficult to obtain precisely the age, due to the large uncertainties in their effective temperature, luminosity, and metallicity (obtained from spectroscopy, photometry, and astrometry) as compared to the closeness of the theoretical isochrones of low-mass stellar and substellar evolutionary models in the Hertzsprung–Russell diagram, as well as due to the uncertainties in the theoretical isochrones themselves. In the case of large samples of members of open- and globular clusters, the age can be estimated more reliably, using for example model isochrones in colour–magnitude diagrams (or the Hertzsprung–Russell diagram) and the upper–main–sequence turn-off method, although there remain uncertainties even for the stellar evolutionary models (Soderblom 2010). In open- and globular clusters, binaries can be more easily identified, by their overluminosity with respect to the lower cluster sequence of singles in the colour–magnitude diagrams, sequence whose faint and cool tail is defined by the less massive (substellar) objects. Thus, a stellar cluster allows to obtain a photometric and spectroscopic snapshot for a whole mass sequence of stars and substellar objects at a specific age, and finally, to derive statistically significant properties as a function of mass and age.

From Fig. 1.5, we see that younger substellar objects are brighter, even brighter than older low-mass stars. They are thus easier to detect in nearby young open clusters, allowing us furthermore to reach lower mass domains. Also from Figs. 1.6 and 1.5, we see that the radius and luminosity decrease more rapidly at  $\lesssim 0.1$  Gyr than at older ages, implying that using open clusters that young we could test more easily whether the theoretical models describe well the evolution of substellar objects and can be used for later ages.

Table 1.3: Theoretical fundamental parameters of a  $0.030 M_{\odot}$  brown dwarf at the ages of 3, 120 Myr, and 1 Gyr (Baraffe et al. 1998; Chabrier et al. 2000). The absolute magnitude difference  $\Delta M$  is relative to 3 Myr. Spectral type based on  $T_{\text{eff}}$  is also given (Kirkpatrick et al. 2008; Testi 2009).

Age (Myr)	$T_{\text{eff}}$ (K)	$\log L/L_{\odot}$ (dex)	$\Delta M$ (mag)	$\log g$ (dex)	SpT
3	2613	-2.24	0.	3.77	$\approx$ M8.5
120	1782	-3.86	4.05	4.73	$\approx$ L4.5
1000	958	-5.11	7.18	4.90	early T

As an example, in Table<sup>8</sup> 1.3 we show the predicted luminosity of a  $0.030 M_{\odot}$  brown dwarf at the ages of 3, 120 Myr, and 1 Gyr (Baraffe et al. 1998; Chabrier et al. 2000). The former two ages are those estimated for the  $\sigma$  Orionis and Pleiades open clusters, respectively, which we have chosen to explore in this PhD Thesis. Both young clusters are very suitable observationally, because they are populous, nearby, compact in the sky, and relatively free of interstellar extinction.

<sup>8</sup>In this Table, we derive also the absolute magnitude, which is the magnitude of the object as it would appear at a distance of 10 pc from the observer:  $M = -2.5 \log(L/(4\pi r^2)) + C$  with  $r = 10$  pc and  $C$  a constant depending of the photometric system. The absolute magnitude can be expressed relative to the Sun,  $M - M_{\odot} = -2.5 \log(L/L_{\odot})$ , where  $M_{\odot} = 4.74$  mag and  $L_{\odot} = 3.856 \times 10^{33}$  erg.s<sup>-1</sup> (Bessell et al. 1998). In continuation, we will refer to it as the absolute *bolometric* magnitude ( $M_{\text{bol}}$ ), i.e. including the emission of light at all wavelengths, to differentiate it from absolute magnitudes limited to small wavelength ranges (as for example  $M_J$  in Table 1.2). To convert the last to the bolometric magnitude, bolometric corrections are required and they depend of the spectral type of the object.

### 1.5 The Pleiades open cluster

The Pleiades open cluster (M45) is one of the nearest open clusters of intermediate young age, with a distance of  $\sim 120$  pc (revised Hipparcos distance, van Leeuwen 2009) and an approximately solar metallicity (Funayama et al. 2009; Soderblom et al. 2009). It has equatorial coordinates (RA =  $3^h 47.0^m$ , DEC =  $+24^\circ 07'$ ) and galactic coordinates ( $l=166.57^\circ$ ,  $b=-23.52^\circ$ ). Because of its relatively high galactic latitude, searches of brown dwarfs have small visual contamination by red giants from the Galactic disc. The Pleiades cluster contains more than 1200 stars (for a total cluster mass of  $\sim 800\text{--}900 M_\odot$ , Adams et al. 2001; Converse & Stahler 2008), distributed spherically in its central part and slightly elliptically ( $e=0.17$ ) in its external part (Raboud & Mermilliod 1998).

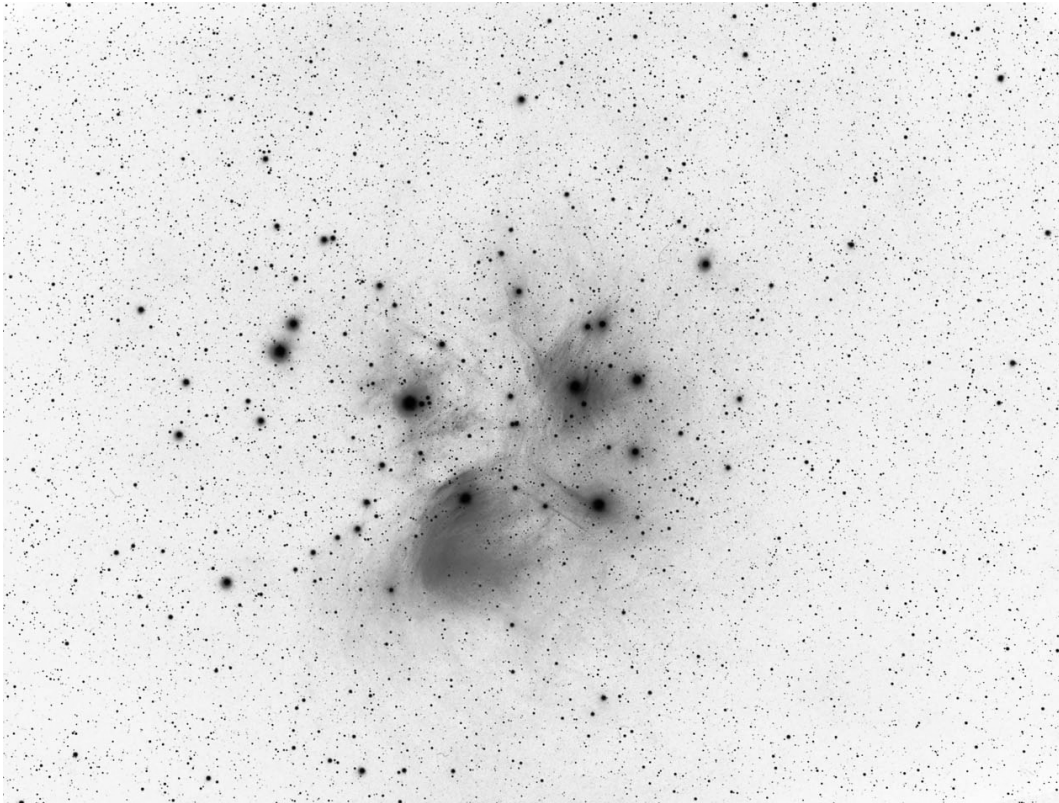


Figure 1.10:  $4.0 \times 2.6$  deg<sup>2</sup> image of the Pleiades open cluster in the visible. From George Greaney (<http://www.astroimages.com/index.html>).

Figure 1.10 shows a  $4.0 \times 2.6$  deg<sup>2</sup> image of the cluster in the visible. The expected tidal radius of the cluster, where the gravitational potential of the Galaxy equals the cluster potential, is of about 6 deg (13.1 pc, Pinfield et al. 1998). Several B-type massive stars populate the central region, among which the seven brightest Alcyone, Atlas, Electra, Maia, Merope, Taygeta and Pleione, with visual magnitudes  $V=2.86\text{--}5.09$  mag. The extinction in the Pleiades is relatively small, possibly in the range  $E(R-I)=0.02\text{--}0.14$  mag (Taylor 2008), except near the star Merope, where a star-like concentration of nebulous matter lays (IC 349). The overall blue nebulous matter observed among several of the massive stars is



reflective and is not a remainder of the proto-cluster nebula, because its radial velocities differ to that of the cluster. It corresponds in fact to illuminated parts of passing-by dust clouds (see e.g. White 2003).

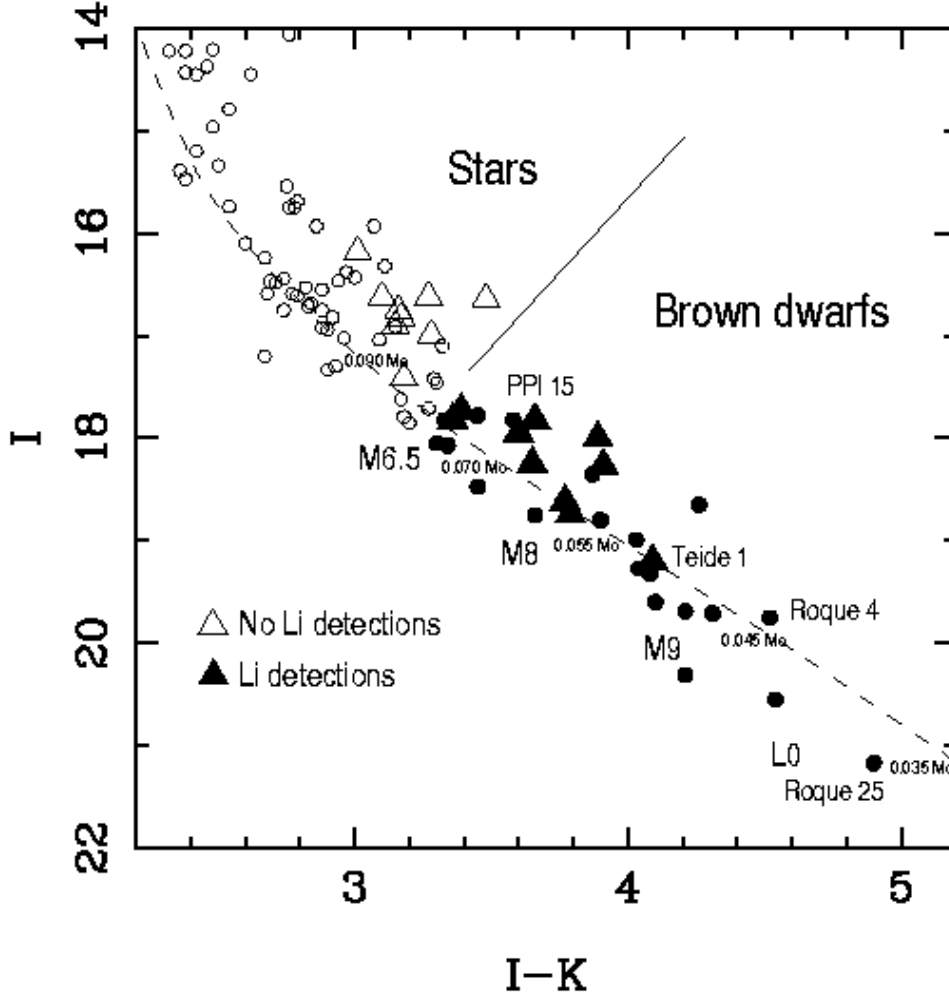


Figure 1.11: Colour-magnitude diagram in the  $IK$  bands for Pleiades low mass stars (open symbols) and brown dwarfs (filled symbols). The substellar limit ( $0.075 M_{\odot}$ ) at the age of the cluster is given by the reappearance of the lithium feature in the spectra of Pleiades objects (denoted with triangle-shaped symbols in this diagram). Spectral types are provided on the left side of the cluster sequence. Overplotted to the data is the theoretical dust-free, NextGen 120 Myr-isochrone (dashed line) from Baraffe et al. (1998) shifted to the distance and reddening of the Pleiades. Masses in solar units are indicated. From Rebolo & Zapatero Osorio (2000).

The Pleiades average proper motion  $(\mu_{\alpha}\cos\delta, \mu_{\delta}) = (19.15 \pm 0.23, -45.72 \pm 0.18)$  mas/yr (Robichon et al. 1999) is large, so that membership can be easily confirmed by proper motion measurements. The comparison of the  $I$ -band magnitude corresponding to complete

lithium depletion with that predicted by theoretical models provides a Pleiades cluster age of  $\sim 120$  Myr (Martín et al. 1998a; Stauffer et al. 1998). Because at this age the mass corresponding to the complete lithium depletion is very near to the hydrogen burning mass limit (see Sect. 1.3), the lithium test is particularly useful to confirm brown dwarfs in the Pleiades.

The Pleiades open cluster served for decades as a reference stellar laboratory where models were put in contrast with observations (stellar rotation, binary statistics, chromospheric activity, stellar distribution and luminosity function, etc.). Since the discovery of the Pleiades brown dwarfs Teide 1 and PPL 1, subsequent studies have provided numerous fainter substellar candidates (Zapatero Osorio et al. 1997a,b; Festin 1998; Bouvier et al. 1998; Zapatero Osorio et al. 1999b; Pinfield et al. 2000), from which a fraction has been confirmed by lithium detection (Rebolo et al. 1996; Martín et al. 1998a; Stauffer et al. 1998; Martín et al. 2000) or by proper motion (Moraux et al. 2001). In Fig. 1.11 a colour-magnitude diagram in the  $IK$ -bands summarizes some of the results obtained for low mass stars and brown dwarfs in the cluster. The coolest object for which a spectral type is obtained is the (L0-type) brown dwarf Roque 25 (Martín et al. 1998b), with an estimated mass of  $\sim 0.035 M_{\odot}$ . Deep photometric searches have unveiled a dozen other faint sources in the Pleiades, of which some were confirmed by proper motion (Moraux et al. 2003; Bouy et al. 2006). Proper motion measurements of such objects have not been published explicitly prior to our study (Bihain et al. 2006).

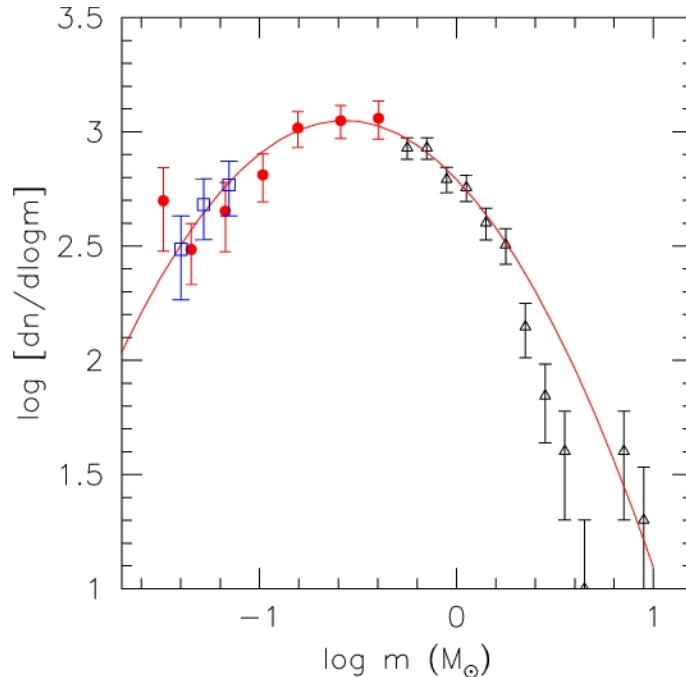


Figure 1.12: Pleiades mass function from  $0.030$  to  $10 M_{\odot}$ . The log-normal fit of Moraux et al. (2003) is shown as a solid line. From Moraux et al. (2004).

On the other hand, very large area proper motion surveys (Hambly et al. 1999; Pinfield et al. 2000; Deacon & Hambly 2004) have provided significant coverage of the stellar-

substellar boundary population of the cluster. Regarding radial distribution, Moraux et al. (2003) find that it is more dispersed for substellar objects than for stars, indicating that mass segregation has taken place in the past (Moraux et al. 2004). In Fig. 1.12, we present the Pleiades mass function from Moraux et al. (2004) for the mass range  $10\text{--}0.03 M_{\odot}$ . The mass function is defined as the number of objects  $dN$  per logarithmic mass unit  $d\log M$ ,

$$\xi(\log M) = \frac{dN}{d\log M} \quad (1.1)$$

or equivalently, as the number of objects  $dN$  per mass unit  $dM$  and multiplied by the mass  $M$  and  $\ln 10$  ( $dN/dM \times M \times \ln 10$ ). Here it is fitted by a log normal function

$$\xi(\log M) \propto \exp \left[ \frac{-(\log M - \log \langle M \rangle)^2}{2\sigma_{\log M}^2} \right], \quad (1.2)$$

where  $\langle M \rangle \simeq 0.25$  is the peak mass value and  $\sigma_{\log M} \simeq 0.52$  is the dispersion (Moraux et al. 2003). Sometimes, an alternative representation is used, which is that of the mass spectrum  $dN/dM$  (see for example Deacon & Hambly 2004). In small mass ranges, the mass spectrum can be approximated by a power law  $dN/dM \propto M^{-\alpha}$  and the spectral index  $\alpha$  can be compared to that obtained by other studies. Dobbie et al. (2002) and Moraux et al. (2003) find that in the mass range  $0.6\text{--}0.03 M_{\odot}$  the spectral index  $\alpha$  is  $\sim 0.6\text{--}0.8$ . It is similar to that found in much younger clusters, as  $\sigma$  Orionis where  $\alpha = 0.8 \pm 0.4$  for  $0.2 < M(M_{\odot}) < 0.013$  (Béjar et al. 2001). This similitude implies that differential evaporation<sup>9</sup> of low-mass members relative to more massive ones has not been very significant (Moraux et al. 2003, 2004; Moraux & Clarke 2005).

## 1.6 The $\sigma$ Orionis open cluster

The  $\sigma$  Orionis open cluster is one of the youngest ( $3 \pm 2$  Myr; Zapatero Osorio et al. 2002c) and relatively nearby ( $360_{-60}^{+70}$  pc, Brown et al. 1994;  $444 \pm 20$  pc, Sherry et al. 2008) open clusters without significant extinction ( $A_V < 1$  mag; Sherry et al. 2008). Also, it has a solar metallicity (González Hernández et al. 2008). Its name comes from its central star  $\sigma$ , which is located in the Orion constellation, or more precisely, in the Ori OB 1b association (see e.g., Brown et al. 1994). The massive star is about half a degree West and slightly to the North of the Horsehead Nebula, where there is a very high extinction at optical and near-infrared wavelengths. The  $\sigma$  Orionis open cluster has equatorial coordinates  $(\alpha, \delta) = (5^h 38.7^m, -2^{\circ} 36')$  and galactic coordinates  $(l, b) = (206.8, -17.3)^{\circ}$ , implying a sufficiently high galactic latitude so that searches of brown dwarfs have small visual contamination by red giants from the Galactic disc. The cluster contains about 340 stars and brown dwarfs in the mass range  $\sim 18\text{--}0.03 M_{\odot}$  (Caballero 2008b); its total mass is of  $2 \times 10^2 M_{\odot}$  (Sherry et al. 2004). The distribution of the cluster members is approximately radial and of two components: a dense core extending to  $\sim 20$  arcmin and a rarefied halo at larger separations (Caballero 2008a). Figure. 1.13 shows a  $18 \times 18$  arcmin<sup>2</sup> image of the cluster in combined

<sup>9</sup>Due to the release of energy in weak encounters of cluster members, members of lower masses are dispersed with larger velocities, reaching larger distances to the cluster centre (mass segregation) and eventually escaping into the field population (see also Converse & Stahler 2010).

optical and infrared light. The star  $\sigma$  Orionis, with visual magnitude  $V \approx 2.8$  mag, is quintuple at least, with stellar components A, B, C, D, and E of spectral type O9.5V, B0.5V, A0V, B2V, and B2Vp, respectively.

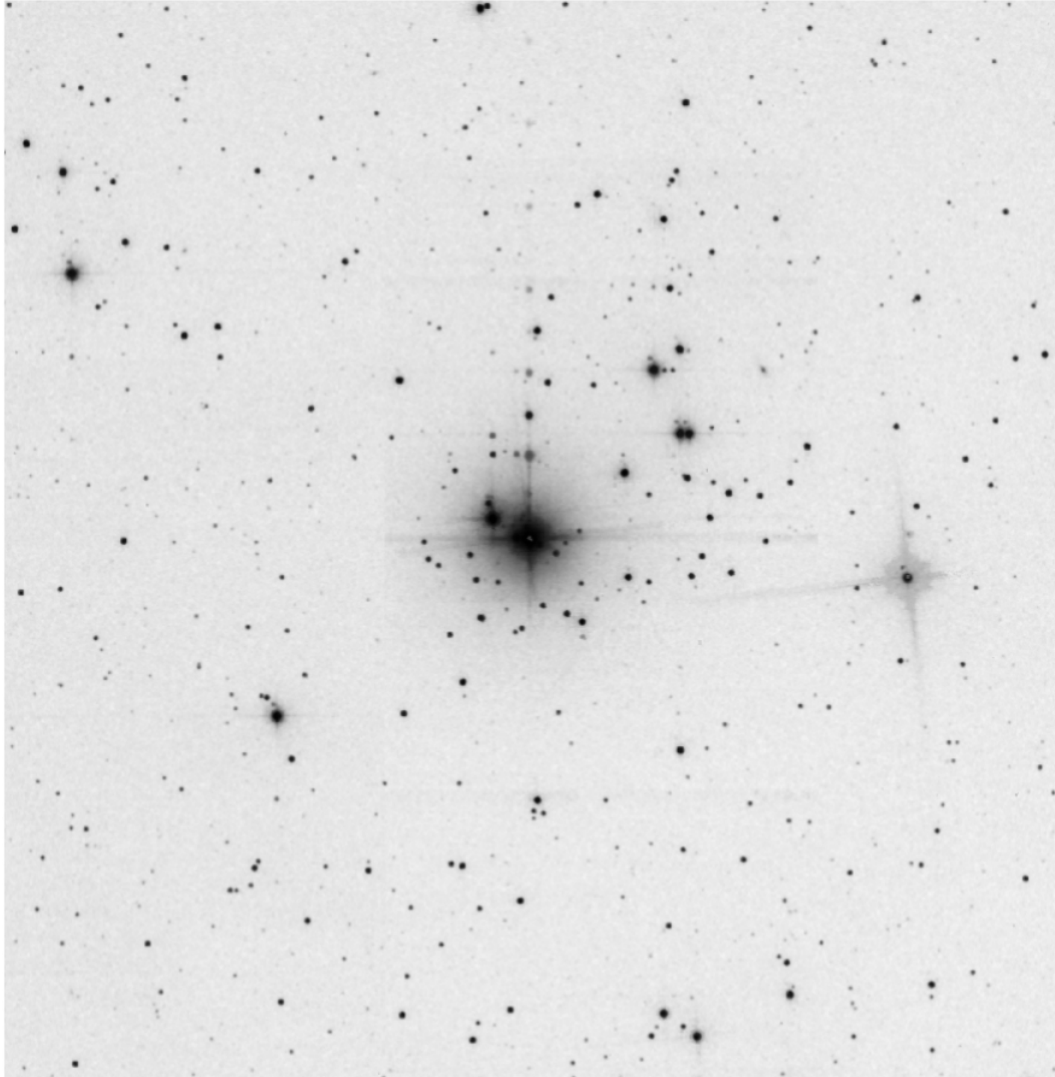


Figure 1.13:  $18 \times 18$  arcmin<sup>2</sup> image of the  $\sigma$  Orionis open cluster in combined optical and infrared light. North is up and East is left. From J. A. Caballero (<http://www.ucm.es/info/Astrof/users/cab/sigmaOrionis.jpg>).

The proper motion of cluster members is very small – for  $\sigma$  Orionis AB,  $(\mu_{\alpha} \cos \delta, \mu_{\delta}) = (4.61 \pm 0.88, -0.40 \pm 0.53)$  mas/yr (Perryman et al. 1997), requiring thus a large time baseline to be measured accurately, in contrast to other objects in the line of sight that might move relatively faster. However, the radial velocity of cluster members is of about  $\sim 30$  km s<sup>-1</sup> and can be used more easily to confirm the membership of photometric candidates, together with spectroscopic criteria of youth such as lithium preservation, intense H $_{\alpha}$  emission and weak Na I absorption (see e.g., Zapatero Osorio et al. 2002c; Kenyon et al. 2005). Finally, some of the photometric candidates present infrared excesses (as revealed

by unusually red colours) probably related to discs, supporting their cluster membership (Oliveira et al. 2006; Hernández et al. 2007).

The substellar content of the  $\sigma$  Orionis cluster has been studied for about a decade, since the discovery of brown-dwarf- and planetary-mass members (Béjar et al. 1999; Zapatero Osorio et al. 1999a, 2000). Deeper photometric and spectroscopic studies have provided additional cluster members and candidates down to planetary-masses (Béjar et al. 2001; Zapatero Osorio et al. 2000), further confirmed by spectroscopy (Martín et al. 2001; Barrado y Navascués et al. 2001, 2002; Zapatero Osorio et al. 2002c,b). A deep survey has even allowed to find a mid-T-type object with a mass of  $\sim 2\text{--}7 M_{\text{Jup}}$  (S Ori 70, Zapatero Osorio et al. 2002a) and an L0-type low-mass brown dwarf of extreme  $H_{\alpha}$  emission (S Ori 71, Barrado y Navascués et al. 2002). Other, mainly photometric surveys (Barrado y Navascués et al. 2003; Béjar et al. 2004b,a; Caballero 2006; González-García et al. 2006; Caballero et al. 2007) have allowed to increase the census of substellar members and candidates in the cluster.

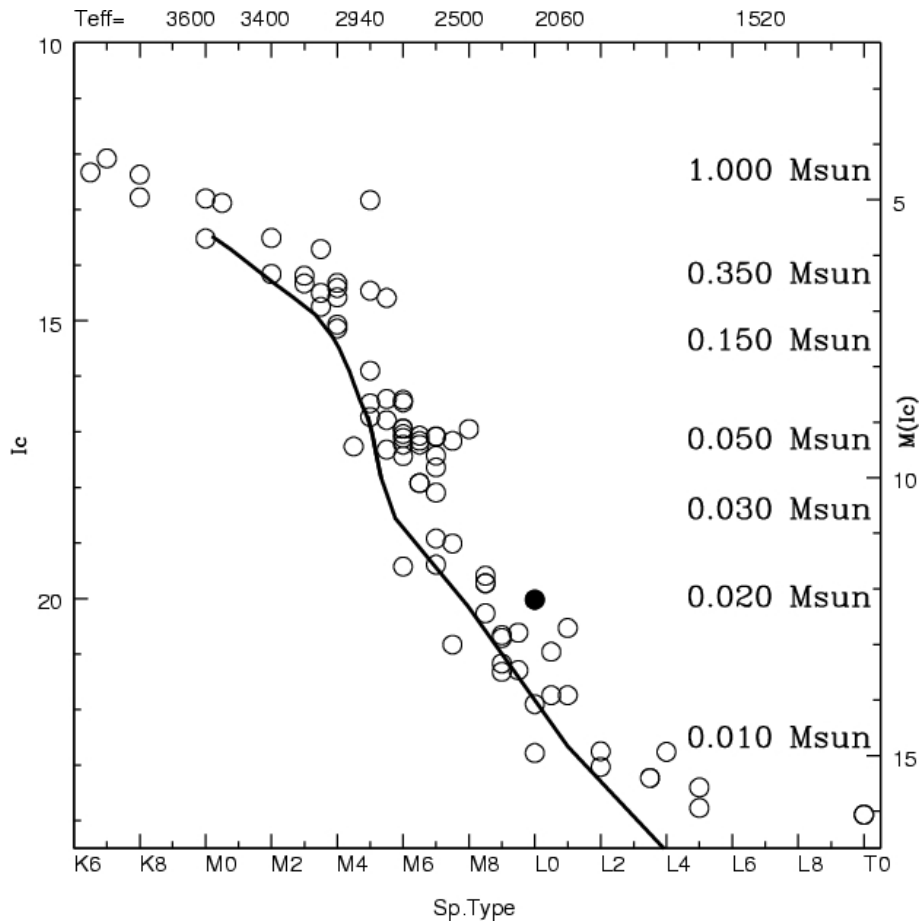


Figure 1.14:  $I_C$ -band magnitude versus spectral type for low-mass members or candidates of the  $\sigma$  Orionis cluster. The solid line represents a 3 Myr-isochrone from Baraffe et al. (1998). Absolute magnitudes and masses are indicated to the right of the diagram, and effective temperatures (in K) are indicated at the top. The filled circle is S Ori 71. Adapted from Barrado y Navascués et al. (2002).

Figure 1.14 shows a spectral type –  $I_C$ -band magnitude diagram, including most of the reported late-type cluster members and candidates observed by spectroscopy. The coolest object with measured spectral type, later than the T0-type S Ori 69 candidate (right-most in the figure), remains the candidate  $2\text{--}7 M_{\text{Jup}}$  S Ori 70 (Zapatero Osorio et al. 2008; Scholz & Jayawardhana 2008; Luhman et al. 2008).

Studies of infrared excesses find a disc frequency  $\geq 45\%$  for cluster substellar members and candidates, larger than that for low- and intermediate-mass stars (Caballero et al. 2007; Zapatero Osorio et al. 2007; Luhman et al. 2008). Similar results of an increase of the disc frequency with decreasing mass are found in other star forming regions and may suggest longer lifetimes of the circumsubstellar accretion discs.

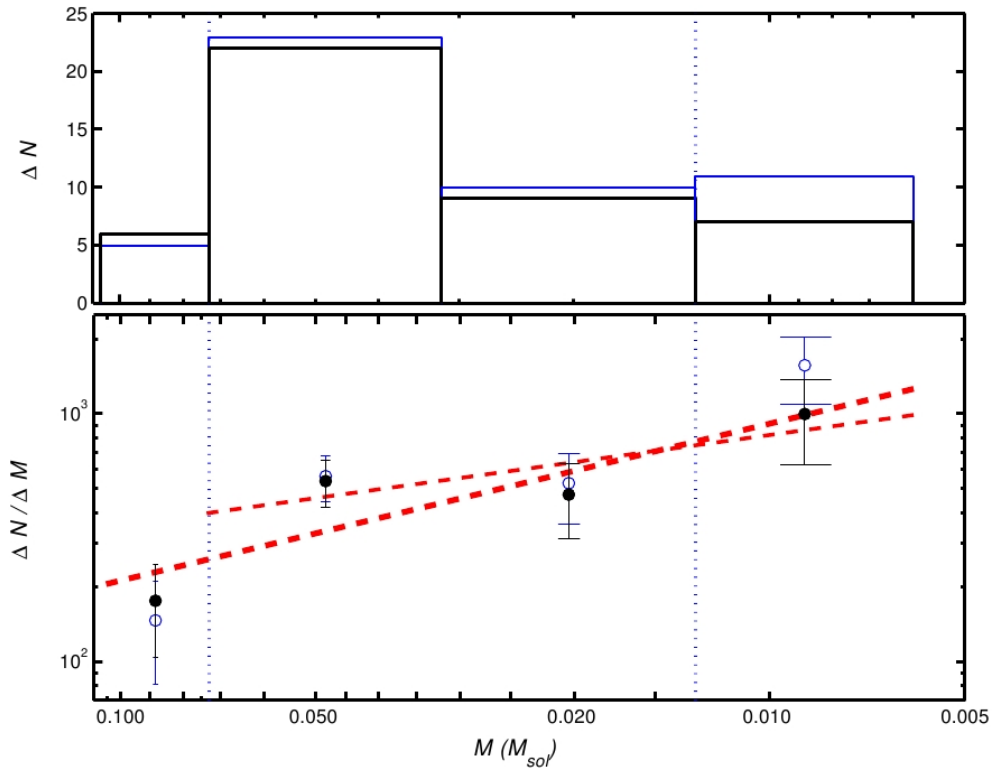


Figure 1.15: Number of objects within each mass interval (top panel) and mass spectrum (bottom panel) from  $0.110$  to  $0.006 M_{\odot}$ . Dotted vertical lines denote the hydrogen (left) and deuterium (right) burning mass limits. The values not corrected for contamination are shown with thin lines (top panel) and open circles (bottom panel), while the values corrected for contamination are shown with thick lines (top panel) and filled circles (bottom panel). The fits of the mass spectrum in the three substellar bins (thin dashed line) and the four bins (thick dashed line) are also shown. From Caballero et al. (2007).

Several of the census studies of brown dwarfs and planetary-mass objects in the young  $\sigma$  Orionis cluster have derived the mass spectrum in an attempt to elucidate the formation mechanisms of these substellar objects (e.g., Béjar et al. 2001). A mass cutoff in the spectrum, for example, would favour an opacity mass limit (Hoyle 1953; Larson 1973; Low & Lynden-Bell 1976; Rees 1976; Silk 1977) for gravitational fragmentation of collapsing molecular clouds (Bate & Bonnell 2005; Bate 2005, 2009), whereas an approximately log-

---

normal, shallower drop would favour a turbulent fragmentation of the clouds (Padoan & Nordlund 2002, 2004; Padoan et al. 2007). The most complete mass spectrum in the mass range  $0.110\text{--}0.006 M_{\odot}$  is that of Caballero et al. (2007), shown in Fig. 1.15. Its shape can be approximated by a power law  $dN/dM \propto M^{-\alpha}$  with a spectral index  $\alpha = 0.6 \pm 0.2$ . In the substellar domain, the index is found to be slightly smaller, of  $0.4 \pm 0.2$ . Clearly, the mass spectrum of Caballero et al. (2007) indicates no cutoff, but a more or less smooth increase towards planetary masses.



# 2

---

## Objectives

We might try our lives by a thousand simple tests; as, for instance, that the same sun which ripens my beans illumines at once a system of earths like ours. If I had remembered this it would have prevented some mistakes. This was not the light in which I hoed them. The stars are the apexes of what wonderful triangles! What distant and different beings in the various mansions of the universe are contemplating the same one at the same moment! Nature and human life are as various as our several constitutions. Who shall say what prospect life offers to another? Could a greater miracle take place than for us to look through each other's eyes for an instant? We should live in all the ages of the world in an hour; ay, in all the worlds of the ages.

Henry David Thoreau (Walden, 1854)

In this PhD Thesis, we would like to search, identify, and characterize new substellar objects in the Pleiades and  $\sigma$  Orionis open clusters, and with spectral types L and T, respectively. We would like to study specifically the Pleiades L-type brown dwarfs to constrain: (i) the substellar evolution (in particular, that of luminosity and effective temperature) at an age of  $\sim 120$  Myr and spectral type L, and (ii) the Pleiades substellar mass spectrum for  $M \lesssim 0.040 M_{\odot}$ , because it will give us clues on the differential evaporation at these masses in the  $\sim 120$  Myr open cluster and the existence of a population of free-floating planetary-mass members. Also, we would like to study T-type planetary-mass objects in the very young ( $\sim 3$  Myr)  $\sigma$  Orionis open cluster, because their very low masses ( $\lesssim 6 M_{\text{Jup}}$ ) and their number density may help us to determine the lowest mass by which they can form as stars by gravitational fragmentation of collapsing molecular clouds.

### 2.1 L-type brown dwarfs in the Pleiades open cluster

The research objectives for the Pleiades are further detailed in the publications "Pleiades low-mass brown dwarfs: the cluster L dwarf sequence" (Bihain et al. 2006) and "Near-infrared low-resolution spectroscopy of Pleiades L-type brown dwarfs" (Bihain et al. 2010) and briefly outlined below:

### 2.1.1 Pleiades low-mass brown dwarfs: the cluster L dwarf sequence

- **Search for the Pleiades lower-mass brown dwarfs ( $M < 0.035 M_{\odot}$ ) corresponding to the L-type dwarf sequence.** We search for red and faint objects using near-IR and optical images. Our candidates will then be followed-up for complementary photometry and proper motion measurements, which will allow us to confirm their membership to the Pleiades open cluster.
- **Compare our photometric results to model predictions and field dwarfs translated to the cluster distance.** Because the open cluster has a well known age and metallicity, the photometric properties of the Pleiades L-type brown dwarfs will provide useful constraints to models predicting the evolution of substellar objects.
- **Obtain the Pleiades mass spectrum.** We will complement our results with the most constrained results based on proper motion and lithium confirmations. This will provide us a good estimation of the mass spectrum, to be compared with that of other clusters, and thus allowing us to determine whether the differential evaporation of the lower-mass brown dwarfs relative to the more massive cluster members is significant or not and whether free-floating planetary-mass objects are likely to be found in the open cluster.

### 2.1.2 Near-infrared low-resolution spectroscopy of Pleiades L-type brown dwarfs

- **Characterize spectroscopically the candidate L-type Pleiades members by proper motion.** We obtain follow-up near-infrared low resolution spectroscopy for these Pleiades members, that will allow us to confirm their spectral type L and discuss possible spectroscopic features of youth.
- **Compare the spectrophotometric properties to those of models and field dwarfs translated to the cluster distance.** Because the open cluster has a well known age and metallicity, the spectrophotometric properties of Pleiades L-type brown dwarfs will provide useful constraints to models predicting the evolution of luminosity and effective temperature for substellar objects.

## 2.2 T-type planetary-mass objects in the $\sigma$ Orionis open cluster

The research objectives for  $\sigma$  Orionis are detailed further in the publication "Candidate free-floating super-Jupiters in the young  $\sigma$  Orionis open cluster" (Bihain et al. 2009) and briefly outlined below:

- **Search for new  $\sigma$  Orionis T-type few-Jupiter mass candidates.** We search for red and faint objects using a dataset of optical and infrared images.
- **Obtain the  $\sigma$  Orionis mass spectrum.** We complement our results with constrained results at greater masses. This will provide us a hint of the trend of the mass spectrum towards lower planetary masses and will allow us to consider possible formation mechanisms.

# 3

---

## Methodology

Men frequently say to me, “I should think you would feel lonesome down there, and want to be nearer to folks, rainy and snowy days and nights especially.” I am tempted to reply to such, – This whole earth which we inhabit is but a point in space. How far apart, think you, dwell the two most distant inhabitants of yonder star, the breadth of whose disk cannot be appreciated by our instruments? Why should I feel lonely? is not our planet in the Milky Way? This which you put seems to me not to be the most important question. What sort of space is that which separates a man from his fellows and makes him solitary? I have found that no exertion of the legs can bring two minds much nearer to one another. What do we want most to dwell near to?

Henry David Thoreau (Walden, 1854)

To search and characterize fainter substellar objects in the Pleiades and  $\sigma$  Orionis open clusters, we used collaboration- and new optical-to-near-infrared data from instruments at various telescopes of class 2–8 m. According to the expected spectral energy distributions for the type of objects we were interested to discover (L- and T type objects), we designed observations in various bands, mainly in the range 1.0–2.4  $\mu\text{m}$ . In addition, we made use of digital databases to complement our data. Photometry and astrometry were used to search for these objects and spectroscopy was used to characterize them further. Comparison with available theoretical models and with nearby reference objects of L and T-type were carried out to determine the existence of peculiar features associated with age. Luminosities, effective temperatures, and masses were estimated. Mass functions constructed and discussed in the light of current formation theories for low-mass substellar objects.

### 3.1 Searches in databases

To obtain information on celestial objects, prepare astronomical observations, and select photometric and astrometric calibrators, I used World Wide Web interfaces (i) of the NASA (Astrophysics Data System –ADS– Bibliographic Services, Infrared Processing and Analysis Center –IPAC– archives), (ii) of the Centre de Données Astronomiques de Strasbourg in France (SIMBAD Astronomical Database, VizieR Service, Aladin Sky Atlas, and Catalogues) and (iii) more specific ones (e.g., Wide Field Camera –WFCAM– Science Archive of the United Kingdom Infra-Red Telescope –UKIRT). I also used the SAOImage DS9 display programme (Joye & Mandel 2003), which can retrieve images and information from

Web databases. Examples of source catalogues or image archives accessed are those of the United States Naval Observatory (USNO, A2.0 and B1.0 catalogues, Monet & et al. 1998; Monet et al. 2003), Sloan Digital Sky Survey (SDSS, Abazajian et al. 2009), Two Micron All Sky Survey (2MASS, Skrutskie et al. 2006), UKIRT Infrared Deep Sky Survey (UKIDSS, Lawrence et al. 2007), and the *Spitzer Space Telescope*.

## 3.2 Observational method

### 3.2.1 Context

Because the Pleiades L-type brown dwarfs and  $\sigma$  Orionis T-type planetary-mass objects would be very faint, with far-red optical magnitudes  $I \gtrsim 21.0$  and  $24.0$  mag (see the cluster spectroscopic sequences in Figs. 1.10 and 1.13), due to their lower masses and the distances of the open clusters to the Sun, we chose broad-band near-infrared imaging as the primary observational technique. Also, we studied regions at intermediate angular separations to the centre of each cluster: not too small (loss of flux contrast because of the bright central stars) and not too large (rarefied halo). We ensured that the Pleiades and  $\sigma$  Orionis surveys were wide enough ( $1.8$  and  $0.8$  deg<sup>2</sup>, respectively) to find several candidates, as estimated from numerical surface densities. These later were obtained by extrapolating linearly published mass spectra. For example, for our  $\sigma$  Orionis survey area, a linear extrapolation of the mass spectrum  $dN/dM \propto M^{-0.4 \pm 0.2}$  of Caballero et al. (2007) imply 3–7 objects in the mass range  $\sim 0.006$ – $0.004 M_{\odot}$ .

Practically, in the Pleiades study we performed an *HK*-band imaging follow-up of *IJ*-band L-type brown dwarf candidates (see Sect. 3.4.1), allowing us to confirm some by proper motion. Then, for a fraction of the later, we performed near-infrared spectroscopy. We used the following instruments and telescopes for the imaging follow-up: the Cámara Infrarroja (CAIN-II) mounted on the 1.55 m Telescopio Carlos Sánchez (TCS; Observatorio del Teide –OT–, Tenerife, Spain), the Long-Slit Intermediate Resolution Infrared Spectrograph (LIRIS) on the 4.2 m William Herschel Telescope (WHT; Observatorio del Roque de Los Muchachos –ORM–, La Palma, Spain), and Omega2000 on the 3.5 m Telescope (Centro Astronómico Hispano-Alemán de Calar Alto –CAHA–, Spain). For the spectroscopic follow-up, we used the Near Infrared Camera Spectrometer (NICS) and its Amici prism mounted on the 3.6 m Telescopio Nazionale Galileo (TNG; ORM) and WHT/LIRIS.

In the  $\sigma$  Orionis study, we performed mainly an extension by *ZJHK*-band imaging of a multi-band search for T-type planetary-mass candidates initiated by the research team in the early 2000’s. We used the Wide Field Camera (WFC) mounted on the 2.5 m Isaac Newton Telescope (INT, ORM), CAHA 3.5 m/Omega2000, the Son of Isaac (SofI) on the 3.6 m New Technology Telescope (NTT; La Silla Observatory, Chile), and WHT/LIRIS.

More details on the instruments and specific observations can be found in the appended papers. The observations that I performed or was helped to perform are indicated in Table 3.1. In these and most of the other observations, I contributed to the choice, priority and observational requirements of the targets.

Table 3.1: Observations that I performed or was helped to perform.

Paper	Observations
Pleiades phot.	WHT/LIRIS 2005 Jan. 23–24 and Mar. 25; all TCS/CAIN-II nights
Pleiades spec.	TNG/NICS 2005 Sep 18 and Nov 20
$\sigma$ Orionis phot.	NTT/Soff 2006 Dec. 24–27

### 3.2.2 Imaging

The near-infrared broad-band imaging of target fields consisted typically of short-time exposures (of a few seconds), repeated several times over each of several dither positions 15–20 arcsec apart (20 times a seeing of 0.75–1.0) or along a scan pattern (to obtain a mosaic). The exposures are (i) short enough to avoid that the level of counts of the sky atmospheric background enters the non-linear regime of the detector and (ii) long enough to ensure that the noise is background limited (in this case, the signal-to-noise ratio is proportional to the square root of the exposure time, permitting to anticipate the total exposure time needed to reach a specific image depth). The dithering displaces point-like sources over the detector sufficiently so that blank sky can be mapped everywhere; the higher counts of the sources can then be easily rejected during the ulterior computation of the median sky background (see Sect. 3.3.1). Due to the dithering, however, the area of 100% overlap of the images – i.e. the deepest area – is always smaller than the total area covered, and this more significantly for detectors of smaller fields of view.

Typical calibration images were flats and darks. The flats are obtained from images taken at different illumination levels of a spatially uniform source of light such as the sky or doom lamps, to allow to correct for the varying efficiency of the individual pixels, which are exposed to the important near-infrared heat radiation of the instrumental installation (telescope, optic, cryostat and surrounding dome). There are thus different types: sky-, doom-, and super-flats. The later ones are obtained from the science target images themselves. The darks are images taken with the same short exposure times and detector operating temperature as for the target images, but with the light entrance blocked. These images are integrations of the noise due in part to thermally excited current carriers in the detector (“dark current”). Darks are required when the detector temperature is not low enough<sup>1</sup>.

In the case of far red images (*IZ*-band), exposure times were typically larger (a few- to several minutes) due to the lower sky atmospheric emission. No dithering was performed, unless for correction of fringing. Flats and biases were also obtained. Biases are essentially darks of zero exposure time (therefore they are also called “zero” frames) and allow to correct for pixel-to-pixel variations.

### 3.2.3 Spectroscopy

The collection of dispersed near-infrared light of the faint Pleiades targets consisted of longer exposures (a fraction to a few minutes), dithered over two or three positions (separated

<sup>1</sup>The photodetectors of the near-infrared instruments CAIN-II, LIRIS, Omega2000, NICS, and Soff are all mercury cadmium telluride (HgCdTe or MCT) detectors, which operate best at cryogenic temperatures (as for example the liquid nitrogen temperature, 77 K); the first one is a NICMOS3 256x256 array and the latter ones are Hawaii 1024x1024 arrays, from the constructor Rockwell.

by about 20 times the seeing) along the spectrometer slit. A brighter source of known separation and polar angle to each science target was used as reference in the slit during the exposures.

Early A-type stars were used usually as telluric standard stars, for two reasons (Vacca et al. 2003): (i) their spectra contain relatively few metal lines, with strengths that are generally only a few percent of the continuum and (ii) the near-infrared continua can be reasonably well approximated by a blackbody with a temperature of  $\sim 10,000$  K. The standard stars were observed in general close in celestial coordinates and time to the targets (to minimize differences in airmass, and atmospheric- and instrumental conditions), to correct for the telluric absorption and instrumental response. Spectroscopic flats were obtained using tungsten- or halogen lamps within the vacuum optics or weak dome lamps. Wavelength calibration spectra were obtained from argon or xenon arc lamps within the vacuum optics.

In the case of optical spectra, exposure time are relatively larger (a good fraction of an hour), because of the lower atmospheric sky emission. Flats and biases are also obtained.

### 3.3 Data reduction

The reduction of the data was performed mostly within the Image Reduction and Analysis Facility<sup>2</sup> (IRAF) environment. Details on specific software packages used are provided in the appended papers. Also, I elaborated several IRAF data reduction scripts, based on the shared knowledge of the research team, IAC colleagues, and guidelines and publications for the specific instruments and observational modes. These scripts allow semi-automatic data reduction and were frequently updated to optimize the depth and resolution of the images. The data reduction that I performed or was helped to perform are indicated in Table 3.1.

Table 3.2: Data that I reduced.

Paper	Data reduction
Pleiades phot.	<i>J</i> -band survey and <i>HK<sub>s</sub></i> -band follow-up
Pleiades spec.	All data, except that of 2005 Sep 18 (collaboration)
$\sigma$ Orionis phot.	new <i>JHK<sub>s</sub></i> -band data, published VLT <i>J</i> -band survey, and published 3.5-m Calar/Omega2000 data of Zapatero Osorio et al. (2008); photometry and astrometry for all the optical and near-infrared data

After the Pleiades photometric paper, I reduced TNG/NICS and WHT/LIRIS *HK<sub>s</sub>*-band imaging data of the Pleiades L-type candidates BRB 25 and BRB 32 (Bihain et al. 2006), obtained on the observing nights of 2005 September 18 and 2006 December 28, respectively. These data and their results were not published. The NICS data was reduced using the Speedy Near-IR data Automatic reduction Pipeline (SNAP; Filippo Mannucci), whereas the WHT/LIRIS data was reduced as in Bihain et al. (2006). Also, I reduced spectroscopic data corresponding to the Pleiades brown dwarfs BRB 27 and 28 (Bihain et al. 2006), obtained on the observing nights of 2005 October 27–28 with the Near-IR Spectrograph (NIRSPEC) mounted on the 10 m Keck II telescope (Mauna Kea Observatory).

<sup>2</sup>IRAF is distributed by the National Optical Astronomy Observatories, which are operated by the Association of Universities for Research in Astronomy, Inc., under cooperative agreement with the National Science Foundation.

The spectra are consistent with L-type, but their too low  $S/N$  and small wavelength coverage (1.15–1.37  $\mu\text{m}$ ) impede their spectral classification at the sub-type level as intended in Bihain et al. (2010).

### 3.3.1 Imaging data

Near-infrared raw images were pre-processed depending of the instrument (e.g., pixel-mapping- and row-cross-talk corrections, dark subtraction), then flat divided, sky subtracted, their elements flagged for bad pixel, aligned using several reference stars, distortion corrected (depending also of the instrument), and combined (see Fig. 3.1 for an example).

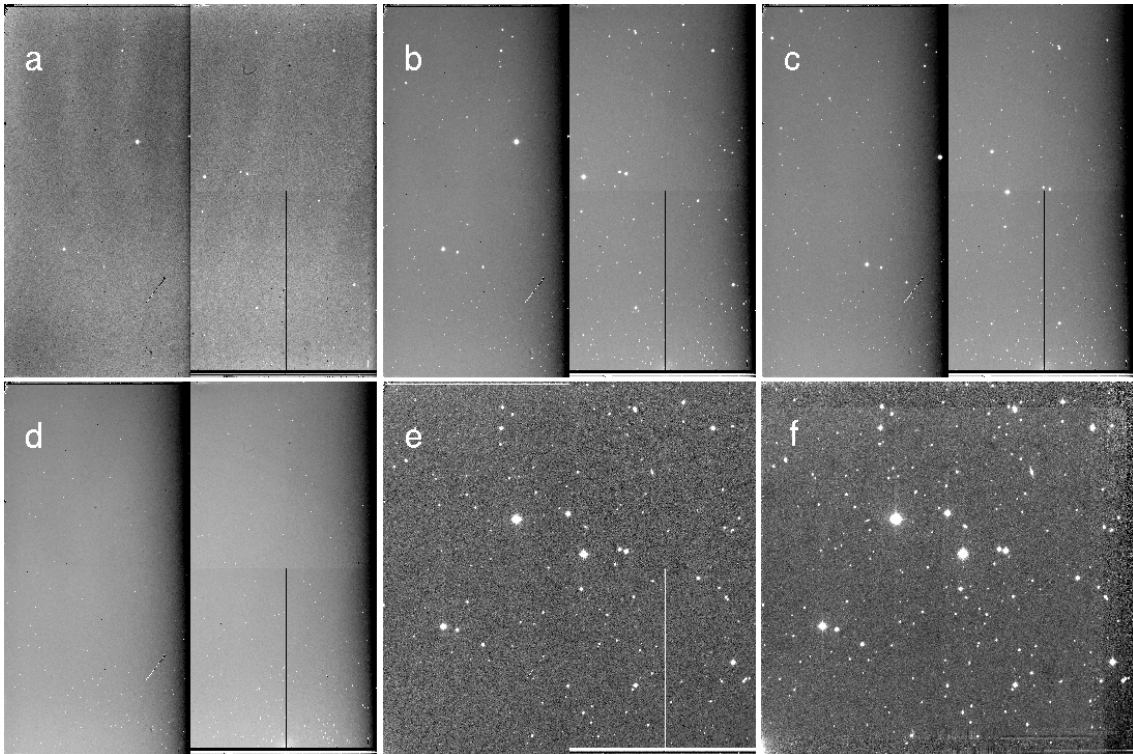


Figure 3.1: Example of near-infrared imaging data reduction: 3.5 m Telescope (CAHA)/Omega-Prime (1024×1024 pixels, 0.40 arcsec/pixel, 6.8×6.8 arcmin<sup>2</sup>)  $J$ -band survey images of the Pleiades (as reduced on April 2010): (a) raw image, (b) the same image but flat divided, (c) another flat-divided image but with a pointing offset, (d) median sky obtained from several of such flatfielded images, (e) sky subtraction, (f) combination of all the flat-divided-, sky-subtracted- and aligned images.

In the optical, the raw CCD images were overscan subtracted, trimmed, bias subtracted, flat or superflat divided (superflats obtained from dithered images allow to correct the fringing), aligned using several reference stars, and combined. The overscan corresponds to the dark current determined in the “overscan” region, not exposed to observation photons and situated along one of the borders. This and other border regions are cut after use (image trimming).

### Photometry

The images were analyzed for aperture- and point-spread-function (PSF) photometry using routines within the DAOPHOT package, which is specifically designed for stellar photometry of crowded fields (such as those of stellar clusters).

The following steps were performed using scripts I wrote in IDL. Sources with counts in the linear regime were correlated with 2MASS or UKIDSS point sources of magnitude errors smaller than 0.1 mag. An average difference between the instrumental and reference magnitudes was then computed (rejecting iteratively deviant sources) and used to calibrate the PSF photometry. The completeness (limiting) magnitude of an image was estimated at the maximum (fainter half maximum) of the histogram of object counts per magnitude bin. However, in the particular case where the source detection – using the routines FINDSTAR (Almoznino) or DAOFIND – was pushed to very low signal-to-noise ratios ( $S/N \sim 3$ ) and the number of sources at faint magnitudes increased substantially, the completeness and limiting magnitudes were estimated from the vector of average instrumental magnitude error per magnitude bin: the faintest magnitude bins where the average errors are  $\leq 0.10$  and 0.20 mag, respectively (corresponding to  $S/N = 10$  and 5, respectively, see e.g., Newberry 1991).

### Astrometry

For the astrometry, I used published point-source catalogues (e.g., USNO-B1, 2MASS, UKIDSS) as references and an IRAF script that I adapted from the `myasrtrom.cl` script of E. Puddu. It correlates catalogue sources with those in the image, starting from an assumed orientation and pixel scale (A). Then it computes the plate solution (B) and uses it for an improved source correlation (A'), which in turn allows to compute a new plate solution (B'). One or two more iterations (A''B'', A'''B''') permit to optimize further the correlation and the plate solution. The last plate solution is then used to transform ( $x,y$ ) pixel coordinates into (*right ascension, declination*) coordinates.

### Multi-band source catalogues

In the case of the Pleiades photometric study, I obtained  $IJ$ -band source catalogues for each of the 120  $J$ -band images overlapping with the  $I$ -band images, from a correlation of the pixel coordinates of the  $I$ - and  $J$ -band sources (using the FORTRAN program CORREL, kindly provided by M. R. Zapatero Osorio).

In the  $\sigma$  Orionis study, where several survey images of different bandpasses overlapped ( $IZJHK$ ), I used a less time-consuming method, thanks to a more systematic and precise astrometric calibration of the images. First I joined together the source catalogues of different images but same bandpass, then I correlated the (*right ascension, declination*) coordinates of the sources of different bandpasses (using an IDL script). I obtained mainly  $IJHK$ -band source catalogues.

#### 3.3.2 Spectroscopic data

Near-infrared raw spectroscopic images were pre-processed depending of the instrument (e.g., pixel mapping and row cross-talk corrections), then the spectra were sky-subtracted,



flat-fielded, aligned, combined, optimally extracted (i.e. traced and validated in the images), and wavelength calibrated. The LIRIS spectra were wavelength calibrated before they were shifted and combined. The instrumental response and telluric bands were removed dividing by the telluric standard spectra and multiplying by black-body spectra with the same effective temperature (see Fig. 3.2). Resolved intrinsic lines in telluric standard spectra (LIRIS spectra) were removed before dividing the target spectra. Spectra of different wavelength ranges (LIRIS  $zJ$  and  $HK$  spectra) were flux calibrated using published broad-band photometry of the corresponding objects and the appropriate filter bandpasses.

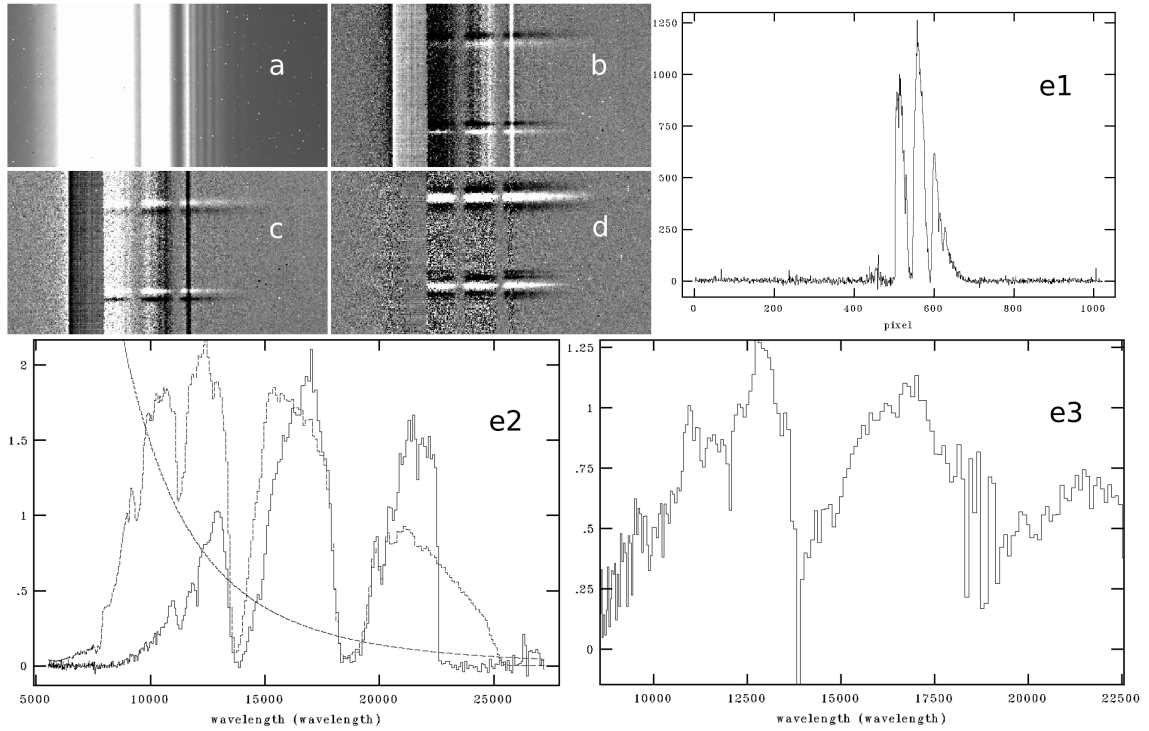


Figure 3.2: Example of near-infrared spectroscopic data reduction: TNG/NICS-Amici data of the Pleiades brown dwarf BRB 23. The block of four expanded images shows: (a) a raw spectral image, (b) and (c) two consecutive offsetted spectral images that are subtracted by each other to remove the contribution of the sky, and (d) the combination of 10 sky-subtracted and aligned spectral images. Panel (e1) shows the extracted spectrum of BRB 23, corresponding to the lower trace in the spectral images. Panel (e2) shows three normalized spectra: the wavelength calibrated spectra of BRB 23 (solid line) and its telluric standard (dashed line; it is the A0-type hot star SAO 56596, with  $T_{\text{eff}} \sim 10000$  K) and the blackbody spectra with the same  $T_{\text{eff}}$  than the telluric standard (concave dashed line). Finally, panel (e3) shows the spectrum of BRB 23 divided by the telluric standard spectra and multiplied by the black-body spectra – i.e. corrected in principle for the instrumental response and the telluric bands.

### 3.4 Data analysis

#### 3.4.1 Colour–magnitude- and colour–colour diagrams and broad-band luminosity functions

Sources of multi-band source catalogues were represented in different diagrams to identify new candidate members of the young open clusters.

In the colour–magnitude diagrams, we used in general as ordinate magnitude the band-pass of the images allowing the best detection of the candidates (usually in the near-infrared), although it is not a strict rule. “Normal” candidates were expected to appear along the sequence of known or probable low-mass stellar- and substellar members. Lower mass candidates were expected to follow the extrapolation of the sequence at fainter magnitudes (lower luminosities) and more evolved colours (cooler effective temperatures), in general anticipated using the field dwarf sequence shifted to the distance of the open cluster. Predicted magnitudes and colours of evolutionary models could also be used as a guide, although these remain less reliable, because of incomplete knowledge of opacities and dust properties in substellar photospheres (Helling et al. 2008).

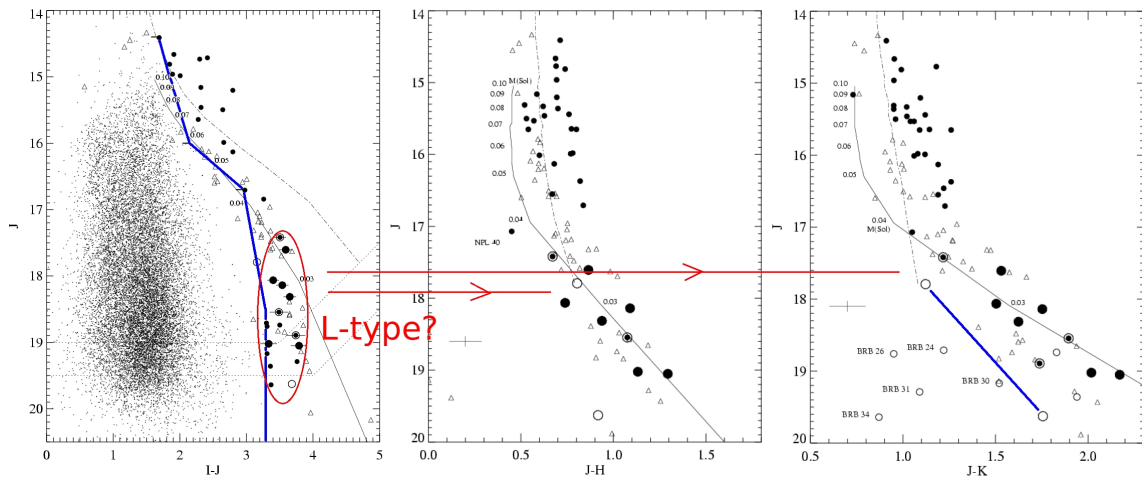


Figure 3.3: Pleiades  $J$  versus  $I - J$ ,  $J - H$ , and  $J - K$  colour–magnitude diagrams (*Left, middle, and right panel, respectively*). In the  $J$  versus  $I - J$  diagram, the circular symbols are the candidate- or confirmed cluster members, with redder  $I - J$  colours than the “bluer” envelope (blue line). At  $J > 17.4$  mag, some of the L-type candidates are Pleiades members (large filled circles), possible members (circled filled circles) and non-members (large empty circles) by proper motion (see Sect. 3.4.2). The upper and lower dotted lines at the bottom indicate the completeness and limiting magnitudes of the survey, respectively. In all three diagrams, the solid line and the dash-dotted line represent the  $\sim 120$  Myr DUSTY isochrone (Chabrier et al. 2000) and the  $\sim 125$  Myr NextGen isochrone (Baraffe et al. 1998), respectively, shifted to the distance of the cluster. The small triangles correspond to field dwarfs shifted to the distance of the cluster. In the  $J$  versus  $J - H$  and  $J - K$  diagrams, additional reported Pleiades very low-mass stars and brown dwarfs with lithium or proper motion consistent with cluster membership are shown (additional small filled circles at  $J < 17.2$  mag). In these diagrams, the typical photometric error for the candidate L-type probable and possible cluster members by proper motion is represented by a cross, on the left. In the  $J$  versus  $J - K$  diagram, the small empty circles at  $J > 18.5$  mag represent the IJ candidates without proper motion measurements: five of them have  $J - K$  colours less red than the segment connecting the two non-members by proper motion (blue line) and are thus probable photometric contaminants. Adapted from Bihain et al. (2006).

In the Pleiades study, for example, we built  $I$  versus  $I - J$  colour–magnitude diagrams for each of our 120 catalogues of pixel cross-matched sources, detected both in the  $I$ - and  $J$  band (for the search of the Pleiades L-type dwarfs, these optical and near-infrared images had similar depth). Then we considered a lower envelope defined by the bluest known cluster members and extended it at fainter magnitudes to a slightly redder colour, for the search of L-type dwarfs. We selected as cluster member candidates all the point-like sources redder than this boundary. In a further step, we made an  $HK_s$ -band follow-up of the candidates to verify if they had red  $J - H$  and  $J - K_s$  colours as expected for L-type dwarfs. To assess their cluster membership, we built  $J$  versus  $J - H$  and  $J - K_s$  diagrams, where each candidate could be located. We flagged as most probable cluster member candidates those with the reddest colours and prioritized them for proper motion follow-up. This allowed us to consolidate the Pleiades L-type sequence using the colour-magnitude diagrams. Figure 3.3 summarizes this procedure.

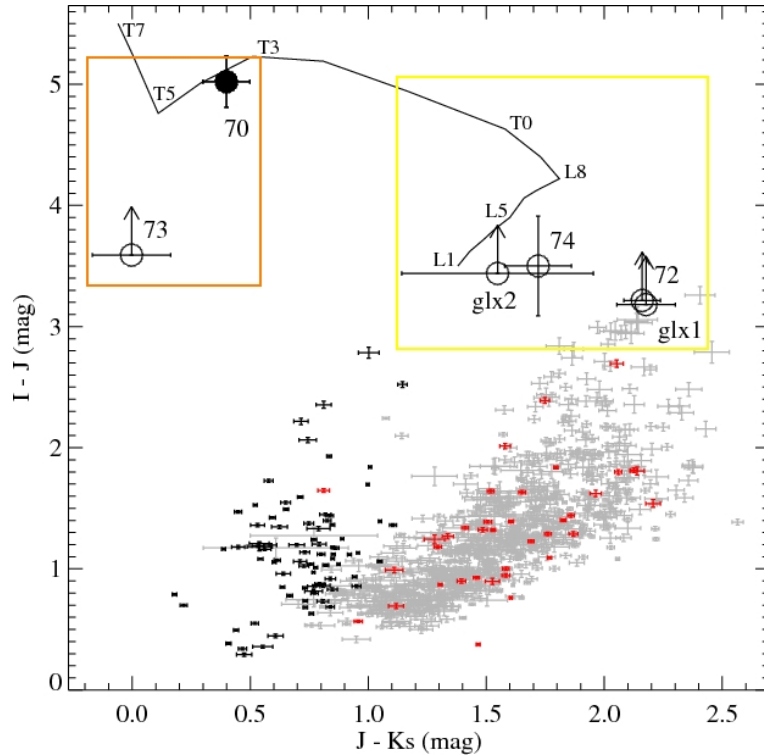


Figure 3.4:  $I - J$  versus  $J - K_s$  colour-colour diagram of stars (black crosses), active galactic nuclei (red crosses), and galaxies (grey crosses) from the GOODS-MUSIC catalogue (Grazian et al. 2006), in the magnitude range  $19.5 < J < 21.5$  mag. The solid line represents the field L1–T7-type dwarf sequence, the filled circle represents S Ori 70, and the open circles represent new member candidates of the  $\sigma$  Orionis open cluster. The new candidate in the orange rectangle is probably a mid T-type object. The candidates in the yellow rectangle could either be L- or T-type objects or galaxies or active galactic nuclei (considering that if the GOODS-MUSIC area would be scaled up to  $\sigma$  Orionis search area, then the colour distributions of galaxies and active galactic nuclei would probably be slightly broader and overlap more with the locations of the candidates in the yellow rectangle). Adapted from Bihain et al. (2009).

Colour–colour diagrams were also used in our studies to determine photometrically the

spectral type, nature, or properties of candidates, comparing them with field LT-type dwarfs and galaxies (see Fig. 3.4).

Finally, (single broad-band filter) luminosity functions, i.e. histograms of the number of cluster members and member candidates per magnitude bin, were obtained. Like the colour–magnitude- and colour–colour diagrams, they provide observational fingerprints of open-cluster populations<sup>3</sup>.

### 3.4.2 Proper motions

The proper motion measurements were obtained as follows. First I selected non-saturated and well defined ( $S/N > 10$ ) single objects among all those that appeared within  $\sim 3'$  of a substellar candidate. I measured their centres in the first- and the second-epoch images with the IRAF task `CENTER` (`DIGIPHOT`.`DAOPHOT` package).

Then I computed the transformation from second-epoch image to first-epoch image with `GEOMAP` – if the first-epoch image had a more accurate equatorial astrometry (because of wider field of view, smaller pixel scale, point sources with smaller full-width-half-maximum –FWHM– or larger  $S/N$ ); else I computed the transformation from first-epoch image to second-epoch image. With `GEOMAP` I selected the objects whose positions minimized the transformation error and could thus be considered as reference objects. A Legendre function of order 3 was used when more than 12 objects were available, and of order 2 for fewer objects.

With `GEOXYTRAN` I used the transformation to predict the positions  $(x_{1p}, y_{1p})$  of the reference objects and the candidate in the first-epoch (or destination) image, and compared them with the measured ones,  $(x_1, y_1)$ , obtaining the pixel shifts  $(\Delta_{x_1}, \Delta_{y_1}) = (x_{1p} - x_1, y_{1p} - y_1)$ . This already allowed us to determine whether the candidate had a pixel shift larger than the dispersion of the pixel shifts of the reference objects, centred on zero.

Using the plate solution of the first-epoch image and `WCSCTAN`, I converted, for the candidate, the predicted and measured pixel positions in equatorial coordinates,  $(RA_{1p}, Dec_{1p})$  and  $(RA_1, Dec_1)$ , respectively, and obtained the corresponding equatorial shift  $(\Delta_{RA_1}, \Delta_{Dec_1}) = (RA_{1p} - RA_1, Dec_{1p} - Dec_1)$ . I then obtained the proper motion:

$$(\mu_\alpha \cos \delta, \mu_\delta) = \left( \frac{\Delta_{RA_1}}{\Delta t}, \frac{\Delta_{Dec_1}}{\Delta t} \right), \quad (3.1)$$

where  $\Delta t$  is the time in Julian years between the two epochs of observation. The proper motion units are arcseconds per year. Therefore,  $\Delta_{RA_1}$  should be multiplied by 15 if it was measured initially in seconds.

In general, the precision of the equatorial astrometry was relatively high ( $\sigma \sim 0.1''$ ), so that its error contribution to the proper motion was negligible. I computed the proper motion error using a linear approximation of the plate solution at the position of the candidate. This linear approximation can be expressed as follows, assuming RA and Dec along x and y, respectively:

---

<sup>3</sup>Nevertheless, they depend of the selection criteria used for cluster membership, which rely on *a priori* and sometimes implicit assumptions based on previous observations and predictions of evolutionary- and atmospheric models.

$$(\sigma_{\mu_\alpha \cos \delta}, \sigma_{\mu_\delta}) = \left( \frac{|\mu_\alpha \cos \delta|}{|\Delta_{x_1}|} \sqrt{\sigma_{x_1}^2 + \sigma_{x_2}^2 + \sigma_{tx}^2}, \frac{|\mu_\delta|}{|\Delta_{y_1}|} \sqrt{\sigma_{y_1}^2 + \sigma_{y_2}^2 + \sigma_{ty}^2} \right), \quad (3.2)$$

where  $\sigma_{x_1, y_1, x_2, y_2}$  are the errors of the  $(x, y)$  pixel positions in the first- (1) and second-epoch (2) images and  $\sigma_{tx, ty}$  the error of the transformation between these images.

The proper motions of the substellar candidates were then compared to those expected for members of the young open cluster in consideration, for example in a proper motion diagram.

### 3.4.3 Spectral classification and magnitude- and colour–spectral type diagrams

Spectra of cluster members were classified by comparing them visually and automatically with published dwarf spectra of similar bandpass coverage and resolution. All the spectra were normalized before in the same wavelength range. For the visual comparison, I made an IDL script that overplots the spectrum of interest on dwarf spectra sorted by increasing spectral type (e.g., L0 to L8). This allowed me to determine the best spectral match and approximate match range (see Fig. 3.5), accounting for the progressive change of spectral features with spectral type (e.g., 0.85–1.3  $\mu\text{m}$  continuum shape and depth of water bands between the *J*, *H*, and *K* bands). For the automatic comparison, I used the FORTRAN program SINTET kindly provided by M. R. Zapatero Osorio. This program converted all the spectra to the same resolution and determined the best match to the spectrum of interest by chi-squared minimization. I then verified the proposed spectral match visually.

In some cases, the spectra had peculiar features (of youth or low surface gravity), which I could identify by eye comparing with young field objects.

Magnitude- and colour–spectral type diagrams were obtained to further study cluster members.

### 3.4.4 Bolometric luminosities, effective temperatures, and masses

We obtained bolometric luminosities using bolometric corrections – e.g.,  $BC_J$  for the *J* band – established for field dwarfs (Cushing et al. 2006), assuming thus that these bolometric corrections are also valid for our young substellar candidates. Theoretical masses were obtained interpolating linearly between model points of evolutionary models using our estimated luminosities. Finally, average effective temperatures were adopted from field dwarfs of same spectral type than our substellar candidates. The luminosities and effective temperatures were used to compare with theoretical isochrones in the Hertzsprung-Russell diagram, whereas masses were used to build substellar mass spectra and discuss them considering formation mechanisms.

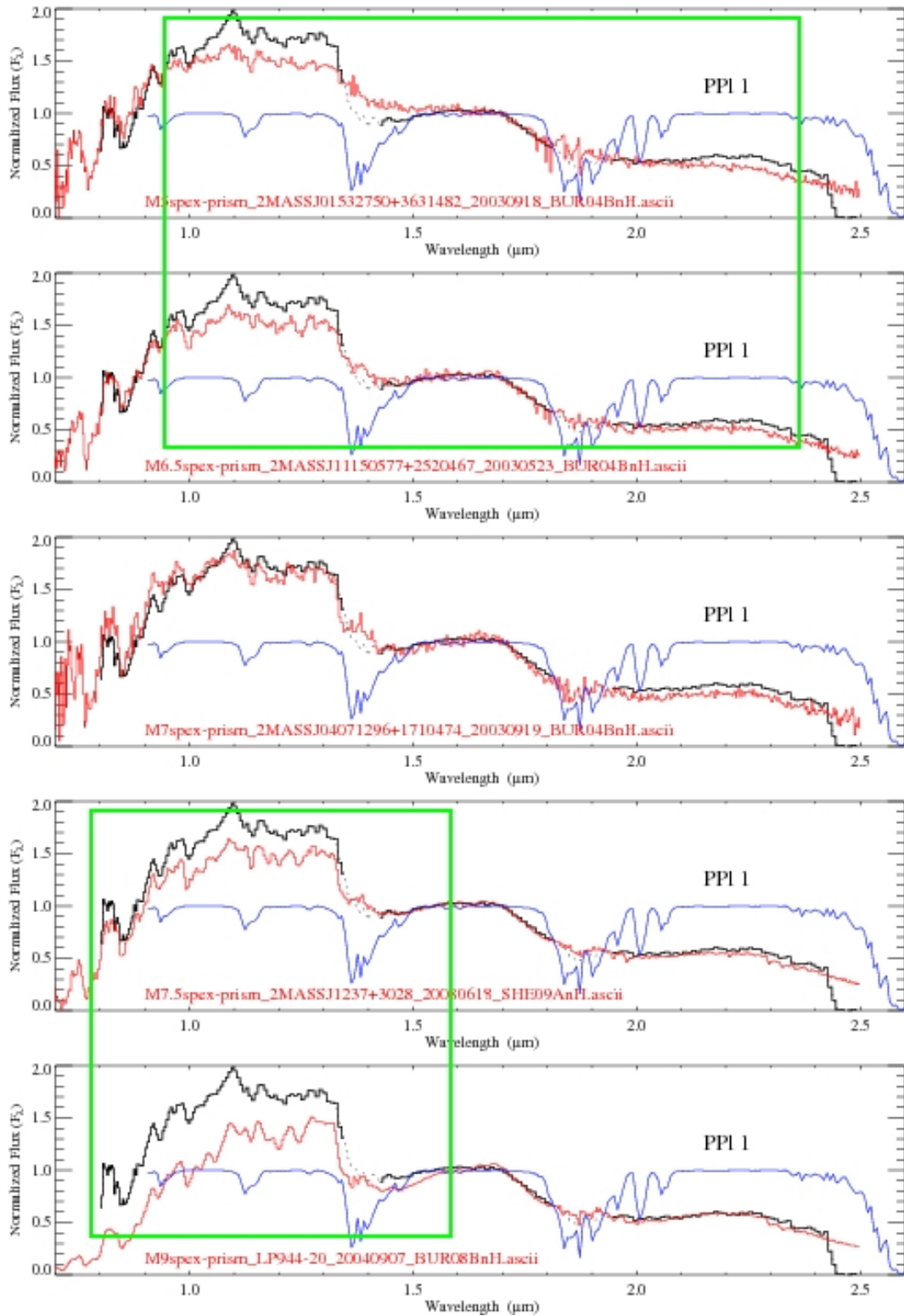


Figure 3.5: Schematic summary of the near-infrared spectral classification of the Pleiades low-mass member PPI 1. Its TNG/NICS-Amici low-resolution spectrum (black line) is compared to spectra of M-type field dwarfs (red lines). A model atmospheric transmission of Hammersley (1998) is also shown (blue line). The best spectral match is at spectral type M7. At spectral types  $\leq M6.5$ , the 1.0–2.4  $\mu\text{m}$  region becomes straighter, with weaker water bands at  $\sim 1.4$  and  $\sim 1.85$   $\mu\text{m}$ . At spectral types  $\geq M7.5$ , the 0.8–1.3  $\mu\text{m}$  flux decreases relative to that at  $H$  band and the  $\sim 1.4$   $\mu\text{m}$  water band becomes deeper. The references of the comparison M-type spectra are: 2MASS J01532750+3631482, 2MASS J11150577+2520467, 2MASS J04071296+1710474 (Burgasser et al. 2004), 2MASS J12373441+3028596 (Sheppard & Cushing 2009), LP944-20 (Burgasser et al. 2008). Practically, PPI 1 was classified spectroscopically comparing to 88 M-type dwarfs.

# 4

---

## Results and discussion

The very globe continually transcends and translates itself, and becomes winged in its orbit.

Henry David Thoreau (Walden, 1854)

### 4.1 L-type brown dwarfs in the Pleiades open cluster

In our 1.8 deg<sup>2</sup> *RIJ*-band search in the Pleiades open cluster,

- 1) We find 18 L-type candidates, with  $I \gtrsim 21$  mag (and  $R - I \gtrsim 2.0$  mag when measurable),  $17.4 < J < 19.7$  mag, and  $I - J > 3.3$  mag.
- 2) Our  $HK_s$ -bands follow-up confirms that (Teide 1, Roque 25, and) 9 out of the 11 candidates with proper motion measurements are Pleiades members, considering a larger intrinsic velocity dispersion of the cluster low mass members than for the more massive members. Five of the seven other photometric candidates are probable contaminants, considering their less red near-infrared colours<sup>1</sup>.
- 3) The intrinsic velocity dispersion of the candidate L-type Pleiades members is estimated to be of  $>4$  mas yr<sup>-1</sup>, at least four times that of Pleiades stars with masses  $\gtrsim 1 M_\odot$  (Jones 1970; Pinfield et al. 1998) and appears consistent with the linear relationship of equipartition of energy, between the velocity dispersion and the inverse square root of the mass for cluster members, as expected in an nearly relaxed cluster (Pinfield et al. 1998 and Fig. 4 therein).
- 4) The Pleiades sequence in the  $J$  versus  $I - J$  colour-magnitude diagram at  $J > 18$  mag is bluer than that predicted by the Dusty atmospheres model (Chabrier et al. 2000), whereas it agrees with those predicted in the  $J$  versus  $J - H$  and  $J - K$  diagrams, suggesting that the far red flux ( $I$  band) might be underestimated relative to the near-infrared flux ( $JHK$  bands).

---

<sup>1</sup>Our unpublished, additional  $HK_s$ -band imaging of the two remaining and redder candidates BRB 25 and BRB 32 (see, in the  $J$  versus  $J - K$  diagram of Fig. 3.3, the two small empty circles at  $J > 18.5$  mag and with redder  $J - K$  colours than the blue-colour segment) imply proper motions inconsistent with cluster membership.

- 5) Also, the Pleiades L-type sequence overlaps in the three colour–magnitude diagrams with that of field L-type dwarfs with known trigonometric parallax, contrary to what happens at M-type, suggesting that the Pleiades and field L-type dwarfs may have comparable spectral energy distributions and luminosities (L). If the effective temperatures ( $T_{\text{eff}}$ ) estimated from the spectral energy distribution do not depend much on the surface gravity, then, the Pleiades and field L-type dwarfs may have also similar effective temperatures and therefore radii (from the black body relation  $L = 4\pi R^2 \sigma T_{\text{eff}}^4$ , where  $\sigma$  is the Stefan–Boltzmann constant).
- 6) Correcting for contaminants and including the proper motion objects from Deacon & Hambly (2004) in our survey fields, we obtain a substellar mass spectrum. For a power law  $dN/dM \propto M^{-\alpha}$  fit in the mass range 0.5–0.026  $M_{\odot}$ , we find a spectral index  $\alpha$  of  $0.5 \pm 0.2$ . It agrees with that of Moraux et al. (2003),  $\alpha = 0.60 \pm 0.11$  (0.48–0.03  $M_{\odot}$ ), based mainly in the 0.04–0.03  $M_{\odot}$  mass range on photometric candidates. Again, this slope is similar to that of open clusters a few Myr old, such as  $\sigma$  Orionis (Béjar et al. 2001) and  $\lambda$  Orionis (Barrado y Navascués et al. 2004), implying that differential evaporation of low-mass members relative to more massive ones has not been very significant and that Pleiades members of even lower masses are probably to be found in our survey area. Indeed, from log-normal and power law extrapolations of the mass spectrum, we predict 3–5 brown dwarfs of 0.026–0.013  $M_{\odot}$  and 1–4 planetary-mass objects of 0.013–0.005  $M_{\odot}$  in our survey area.
- 7) The near-infrared spectra obtained for six of our L-type candidates confirmed by proper motion imply spectral types early- to mid L, whereas those obtained for the well known Pleiades late M-type PPL 1, Calar 3, and Teide 1 confirm their optical spectral types (see Fig. 4.1 for the Amici spectra).
- 8) The spectra of the earliest L-type Pleiades brown dwarfs PLIZ 28 and BRB 17 (the latter is not shown in Fig. 4.1) present a triangular shape in the  $H$ -band spectral region, a noticeable VO band at 1.06  $\mu\text{m}$ , and an entire apparently peculiar continuum shape (relative to typical L0-type field dwarfs), probably associated to low-surface gravity, dust and youth. These spectra indicate that the triangular  $H$ -band continuum shape, a peculiar spectral feature that has been previously reported for substellar members of stellar associations of a few Myr to a few tens of Myr only (the oldest object with such feature is the early-L-type AB Pic B in the  $\sim 30$  Myr old Tucana-Horologium association, Chauvin et al. 2005b; Bonnefoy et al. 2010), persists until at least the age of the Pleiades.
- 9) We build a Pleiades spectrophotometric sample of 45 low-mass stars and brown dwarfs, adding to our nine spectroscopic targets 36 reported M5–L0-type members of the open cluster. In  $M_J$ ,  $M_H$ , and  $M_K$  absolute-magnitude– and  $I - J$ ,  $Z - J$ ,  $Y - J$ ,  $J - H$ ,  $H - K$ , and  $J - K$  colour–spectral type diagrams, we confirm that there are no significant differences in absolute magnitudes (obtained using trigonometric parallax distances) and colours between the Pleiades and field dwarf sequences at spectral type L, supporting thus the interpretation of similar spectral energy distributions and luminosities. Nevertheless, adopting a larger cluster distance (such as obtained by main-sequence fitting using field stars), the luminosities of the Pleiades L-type brown dwarfs would be brighter and less similar to those of the field L-type dwarfs.



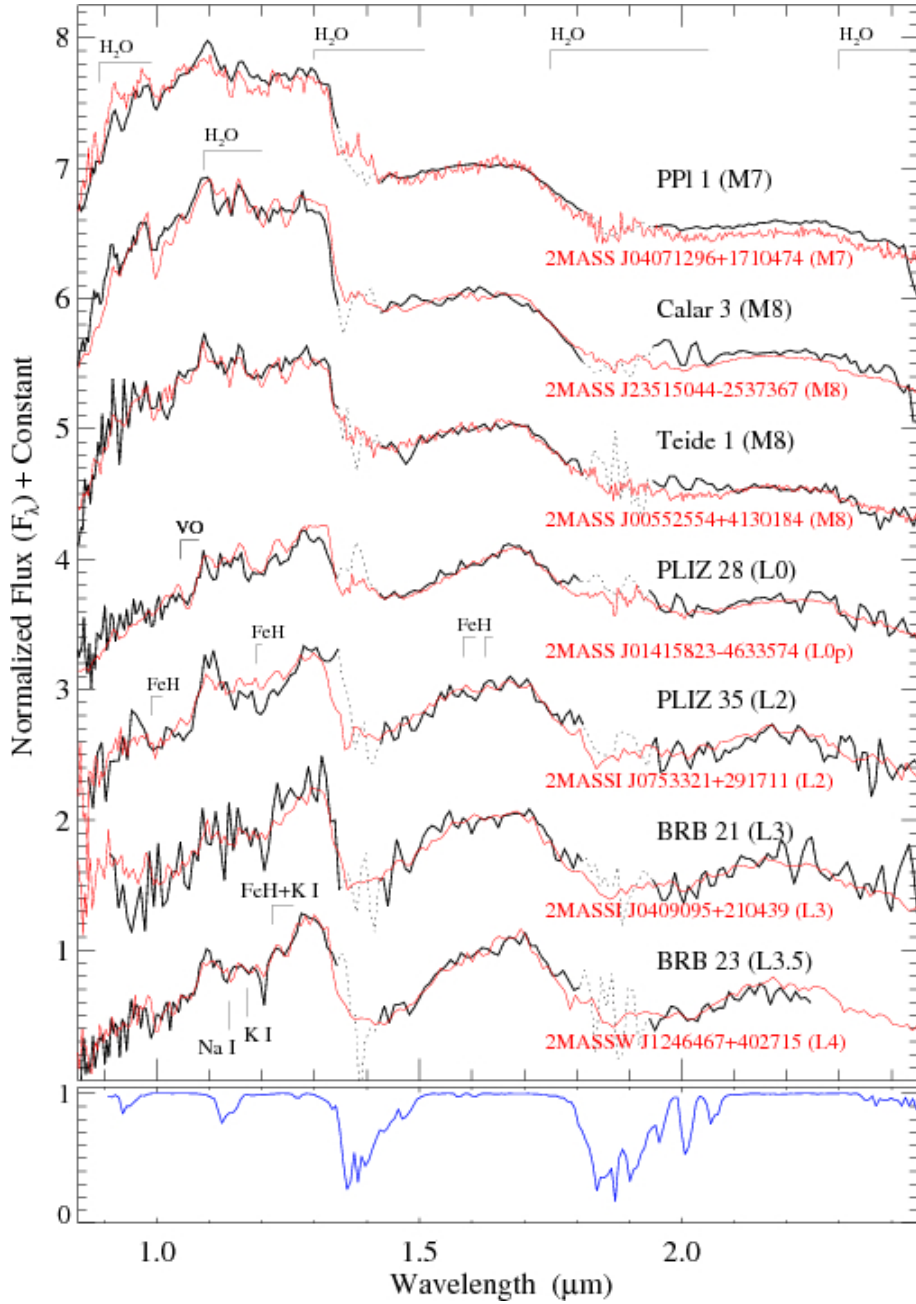


Figure 4.1: NICS/Amici low-resolution 0.85–2.40  $\mu\text{m}$  spectra of Pleiades low-mass members, in air wavelengths. The spectra are normalized to the average flux between 1.56 and 1.74  $\mu\text{m}$  and offset by constants. The main regions affected by tellurics are represented by dotted lines. Field dwarf spectra are overplotted in red. For PLIZ 28, the comparison field dwarf spectra is that of the low-surface gravity 2MASS J00552554+4130184 (Kirkpatrick et al. 2006). A model atmospheric transmission rebinned to a dispersion of 7 nm  $\text{pix}^{-1}$  is represented in blue in the lower panel. From Bihain et al. (2010).

- 10) Besides, from this comparison we find that the Pleiades mid-M to mid-L-type dwarfs have a  $J - K$  colour marginally redder by  $0.1 \pm 0.2$  mag than their field counterparts,

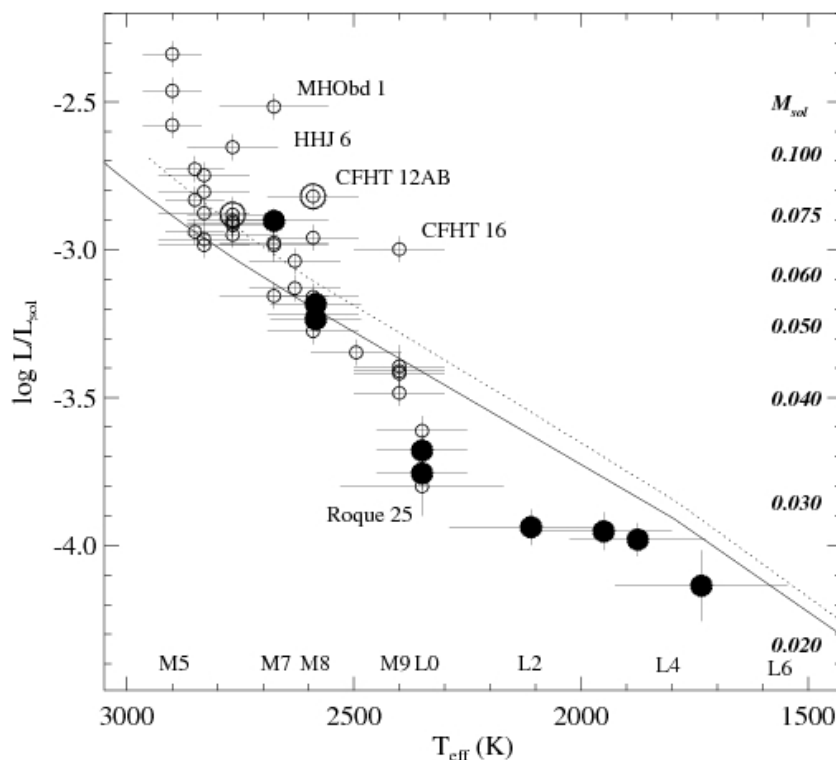


Figure 4.2: Hertzsprung–Russell diagram of Pleiades low-mass stars and brown dwarfs, shown as black filled circles (our new data) and black small open circles (previous data). Theoretical 120 Myr isochrones of Chabrier et al. (2000, DUSTY) and Burrows et al. (1997) are represented by dotted and solid lines, respectively. Spectral types and DUSTY theoretical masses are indicated. From Bihain et al. (2010).

possibly related to both reddening and youth.

- 11) In the Hertzsprung–Russell diagram (see Fig. 4.2), the Pleiades sequence at spectral types later than M ( $T_{\text{eff}} \lesssim 2400$  K) drops below the  $\sim 120$  Myr theoretical isochrones, suggesting that the Pleiades early- to mid- L-type brown dwarfs may have contracted faster than predicted for their age. The theoretical masses for their luminosities are estimated to be in the range  $0.035\text{--}0.025 M_{\odot}$ .

## 4.2 T-type candidates in the $\sigma$ Orionis open cluster

In our  $\sim 840$  arcmin<sup>2</sup>  $IJ$ -band search ( $J = 19.5 - 21.5$  mag) in the  $\sim 3$  Myr old  $\sigma$  Orionis open cluster, complemented with  $ZHK[3.6][4.5][5.8][8.0]$ -band data,

1. We recover S Ori 70 and two other known cluster member candidates.
2. We find three new candidates S Ori 72–74 and two probable galaxies with  $J \sim 21$  mag. S Ori 73 is a T-type candidate, S Ori 72 an L/T-type transition candidate, and S Ori 74 an L-type candidate and at 11.8 arcsec ( $\sim 4250$  AU) from the K7.5-type cluster member Mayrit 260182, itself possibly forming a triple system with two cluster lower-mass members.

3. If S Ori 72–74 indeed belong to the  $\sigma$  Orionis open cluster, then they would have masses of  $4_{-2}^{+3} M_{\text{Jup}}$  and be some of the least massive free-floating objects detected by direct imaging outside the Solar System.
4. These new cluster member candidates and S Ori 70 are located within 12 arcmin of the cluster centre, whereas most of the previously reported more massive planetary-mass candidates are further away. If the cluster membership census and the masses are confirmed, this configuration could be explained by several mechanisms, including e.g. a possible photo-erosion by the central OB stars in the deep gravity well.

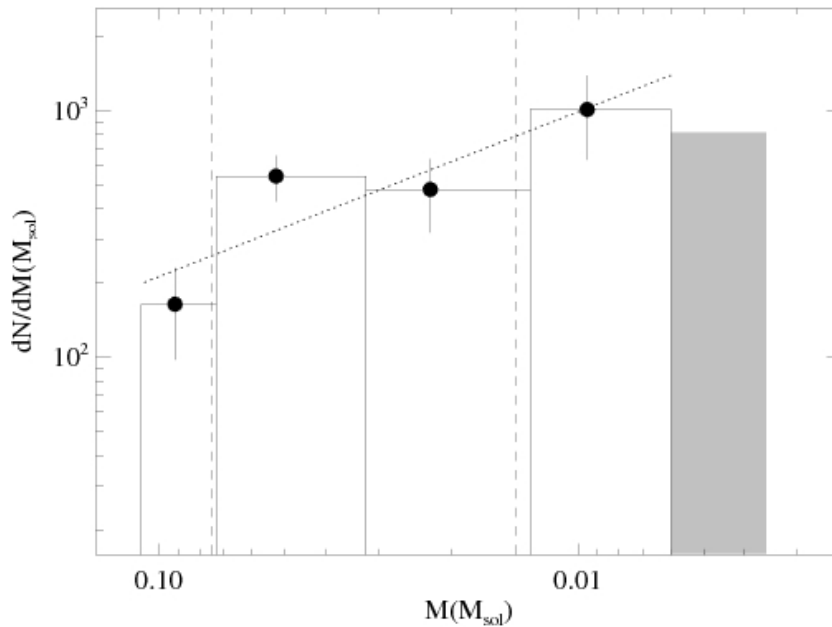


Figure 4.3: Mass spectrum with contamination-corrected data. The dotted segment represents the linear fit to the data points from Caballero et al. (2007) in the mass range  $0.110\text{--}0.006 M_{\odot}$ , which are previously scaled to the total area. The shaded region is our estimate of 0–2 cluster members in the mass range  $0.006\text{--}0.004 M_{\odot}$ . From left to right, the vertical dashed lines represent the hydrogen and deuterium burning mass limits, respectively. From Bihain et al. (2009).

5. Accounting for field contaminants in the effective search area of  $\sim 790 \text{ arcmin}^2$  complete to  $J = 21.1$  mag, there would remain nevertheless between zero and two cluster members in the mass interval  $6\text{--}4 M_{\text{Jup}}$ . This together with previous results at higher masses may hint at a possible turnover or even a sharp drop in the substellar mass spectrum (see Fig. 4.3) of this  $\sim 3$  Myr old cluster. If confirmed, it would suggest in the latter case that we may have reached the opacity limit for fragmentation of molecular clouds.

# 5

---

## Conclusions

Any argument or point of view that makes solipsism look no less likely may be discounted.

Iain M. Banks (Transition, 2009)

The fundamental results of our studies presented in this Thesis are the following:

- We confirm nine Pleiades L-type brown dwarf candidates to be cluster members based on photometric, proper motion and spectroscopic measurements. These young open cluster members have theoretical masses estimated to be in the range  $0.035\text{--}0.025 M_{\odot}$  and permit us to determine:
  - (i) an intrinsic velocity dispersion of  $>4 \text{ mas yr}^{-1}$  for these objects, consistent with a nearly dynamically relaxed cluster,
  - (ii) a mass spectrum  $dN/dM \propto M^{-\alpha}$  with a spectral index  $\alpha$  of  $0.5 \pm 0.2$  in the mass range  $0.5\text{--}0.026 M_{\odot}$ , similar to that of open clusters about thirty times younger, implying by extrapolation the existence of Pleiades free-floating planetary-mass objects of spectral type T,
  - (iii) the Pleiades early- to mid L-type spectrophotometric sequence that (a) besides some small differences associable to youth, appears to overlap with the sequence of field L-type dwarfs, implying that the Pleiades and field L-type dwarfs may have comparable spectral energy distributions and luminosities, and thus possibly similar radii, and (b) appears to be fainter or warmer than predicted by theoretical models of substellar evolution, suggesting that the cluster L-type brown dwarfs may have contracted faster than predicted.
- We find three new free-floating planetary-mass candidates in the  $\sigma$  Orionis open cluster, based on photometric measurements. One of them, S Ori 73, is probably a T-type object, as the already known S Ori 70. If cluster members, the three new objects would have estimated theoretical masses of  $4_{-2}^{+3} M_{\text{Jup}}$ , implying that they would be some of the least massive free-floating or companion objects detected by direct imaging outside the Solar System. However, contamination by field dwarfs and galaxies is very probable. This implies a possible turnover or even a sharp drop in

the substellar mass spectrum, suggesting in the latter case that the opacity limit for fragmentation of molecular clouds may have been reached.

### 5.1 Further studies

Pleiades free-floating planetary-mass objects will probably have spectral types late-L and T, and thus magnitudes  $J \sim 20$  mag or fainter (translating the field dwarf magnitudes to the cluster distance). These magnitudes are well within the completeness range of modern survey instrumentation (e.g., the 4-m class Visible and Infrared Survey Telescope for Astronomy – VISTA –). In fact, Casewell et al. (2007) already found in the meantime promising candidate Pleiades T-type sources with  $J = 20.0 - 20.3$  mag, using published  $IZ$ -band data and new near-infrared imaging data of moderate depth. We are presently reducing  $J$ - and  $H$ -band data obtained in 1998 and 2007 with the 3.5 m Telescope CAHA/Omega-Prime and Omega-2000, respectively, with limiting magnitudes of 21.5 mag in both bands and covering an area of 1 deg<sup>2</sup>. These data will allow us to identify additional planetary-mass T-type candidates in the Pleiades by photometry and proper motion. Further characterization of the atmospheres of the Pleiades L- and T-type members, by optical to mid-infrared photometry and spectroscopy, will allow us to improve their comparison to field dwarfs, young objects of other stellar clusters, and the predictions of substellar evolution models.

In the case of the mass spectrum of  $\sigma$  Orionis, a survey of one square degree (about the area of the cluster) and complete to  $I = 27$  mag and  $J = 23$  mag (using 10 and 4-m class telescopes, respectively) could permit us to detect other T-type candidates and confirm the possible turnover or sharp drop at low planetary masses, with probable implications on how we understand their formation.

# Bibliography

- Abazajian, K. N., et al. 2009, *ApJS*, 182, 543
- Adams, J. D., Stauffer, J. R., Monet, D. G., Skrutskie, M. F., & Beichman, C. A. 2001, *AJ*, 121, 2053
- Allen, P. R., Koerner, D. W., Reid, I. N., & Trilling, D. E. 2005, *ApJ*, 625, 385
- Alonso, R., et al. 2004, *ApJ*, 613, L153
- Anderson, D. R., et al. 2010, *ApJ*, 709, 159
- Bailer-Jones, C. A. L., & Mundt, R. 2001, *A&A*, 367, 218
- Baraffe, I., Chabrier, G., Allard, F., & Hauschildt, P. H. 1998, *A&A*, 337, 403
- Baraffe, I., Chabrier, G., Barman, T. S., Allard, F., & Hauschildt, P. H. 2003, *A&A*, 402, 701
- Barrado, D., et al. 2009, *A&A*, 508, 859
- Barrado y Navascués, D., Béjar, V. J. S., Mundt, R., Martín, E. L., Rebolo, R., Zapatero Osorio, M. R., & Bailer-Jones, C. A. L. 2003, *A&A*, 404, 171
- Barrado y Navascués, D., Bouvier, J., Stauffer, J. R., Lodieu, N., & McCaughrean, M. J. 2002, *A&A*, 395, 813
- Barrado y Navascués, D., Stauffer, J. R., Bouvier, J., Jayawardhana, R., & Cuillandre, J.-C. 2004, *ApJ*, 610, 1064
- Barrado y Navascués, D., Zapatero Osorio, M. R., Béjar, V. J. S., Rebolo, R., Martín, E. L., Mundt, R., & Bailer-Jones, C. A. L. 2001, *A&A*, 377, L9
- Barrado y Navascués, D., Zapatero Osorio, M. R., Martín, E. L., Béjar, V. J. S., Rebolo, R., & Mundt, R. 2002, *A&A*, 393, L85
- Basri, G. 1998, in *Astronomical Society of the Pacific Conference Series*, Vol. 134, *Brown Dwarfs and Extrasolar Planets*, ed. R. Rebolo, E. L. Martin, & M. R. Zapatero Osorio, 394

- Basri, G. 2000, *ARA&A*, 38, 485
- Basri, G., Mohanty, S., Allard, F., Hauschildt, P. H., Delfosse, X., Martín, E. L., Forveille, T., & Goldman, B. 2000, *ApJ*, 538, 363
- Bate, M. R. 2005, *MNRAS*, 363, 363
- . 2009, *MNRAS*, 392, 590
- Bate, M. R., & Bonnell, I. A. 2005, *MNRAS*, 356, 1201
- Beaulieu, J.-P., et al. 2006, *Nature*, 439, 437
- Béjar, V. J. S. 2000, PhD thesis, Universidad de La Laguna
- Béjar, V. J. S., Caballero, J. A., Rebolo, R., Zapatero Osorio, M. R., & Y Navascués, D. B. 2004a, *Ap&SS*, 292, 339
- Béjar, V. J. S., Zapatero Osorio, M. R., & Rebolo, R. 1999, *ApJ*, 521, 671
- . 2004b, *Astronomische Nachrichten*, 325, 705
- Béjar, V. J. S., et al. 2001, *ApJ*, 556, 830
- Benedict, G. F., et al. 2006, *AJ*, 132, 2206
- Bessell, M. S., Castelli, F., & Plez, B. 1998, *A&A*, 333, 231
- Bihain, G., Rebolo, R., Béjar, V. J. S., Caballero, J. A., Bailer-Jones, C. A. L., Mundt, R., Acosta-Pulido, J. A., & Manchado Torres, A. 2006, *A&A*, 458, 805
- Bihain, G., Rebolo, R., Zapatero Osorio, M. R., Béjar, V. J. S., & Caballero, J. A. 2010, *A&A*, in press (eprint ArXiv:1005.3249),
- Bihain, G., et al. 2009, *A&A*, 506, 1169
- Bond, I. A., et al. 2004, *ApJ*, 606, L155
- Bonfils, X., et al. 2005, *A&A*, 443, L15
- Bonnefoy, M., Chauvin, G., Rojo, P., Allard, F., Lagrange, A., Homeier, D., Dumas, C., & Beuzit, J. 2010, *A&A*, 512, A52
- Boss, A. P. 1997, *Science*, 276, 1836
- Bouvier, J., Stauffer, J. R., Martín, E. L., Barrado y Navascues, D., Wallace, B., & Bejar, V. J. S. 1998, *A&A*, 336, 490
- Bouvier, J., et al. 2008, *A&A*, 481, 661
- Bouy, H., Brandner, W., Martín, E. L., Delfosse, X., Allard, F., & Basri, G. 2003, *AJ*, 126, 1526

- Bouy, H., Moraux, E., Bouvier, J., Brandner, W., Martín, E. L., Allard, F., Baraffe, I., & Fernández, M. 2006, *ApJ*, 637, 1056
- Briceño, C., Hartmann, L., Stauffer, J., & Martín, E. 1998, *AJ*, 115, 2074
- Brown, A. G. A., de Geus, E. J., & de Zeeuw, P. T. 1994, *A&A*, 289, 101
- Burgasser, A. J. 2004, *ApJS*, 155, 191
- Burgasser, A. J., Kirkpatrick, J. D., McElwain, M. W., Cutri, R. M., Burgasser, A. J., & Skrutskie, M. F. 2003a, *AJ*, 125, 850
- Burgasser, A. J., Kirkpatrick, J. D., Reid, I. N., Brown, M. E., Miskey, C. L., & Gizis, J. E. 2003b, *ApJ*, 586, 512
- Burgasser, A. J., Liu, M. C., Ireland, M. J., Cruz, K. L., & Dupuy, T. J. 2008, *ApJ*, 681, 579
- Burgasser, A. J., McElwain, M. W., Kirkpatrick, J. D., Cruz, K. L., Tinney, C. G., & Reid, I. N. 2004, *AJ*, 127, 2856
- Burgasser, A. J., et al. 1999, *ApJ*, 522, L65
- . 2000, *ApJ*, 531, L57
- . 2002, *ApJ*, 564, 421
- Burgess, A. S. M., Moraux, E., Bouvier, J., Marmo, C., Albert, L., & Bouy, H. 2009, *A&A*, 508, 823
- Burrows, A., et al. 1997, *ApJ*, 491, 856
- Caballero, J. A. 2006, PhD thesis, Universidad de La Laguna, Spain
- . 2008a, *MNRAS*, 383, 375
- . 2008b, *VizieR On-line Data Catalog*, J/A+A/478/667
- Caballero, J. A., Burgasser, A. J., & Klement, R. 2008, *A&A*, 488, 181
- Caballero, J. A., et al. 2007, *A&A*, 470, 903
- Campbell, B., Walker, G. A. H., & Yang, S. 1988, *ApJ*, 331, 902
- Casewell, S. L., Dobbie, P. D., Hodgkin, S. T., Moraux, E., Jameson, R. F., Hambly, N. C., Irwin, J., & Lodieu, N. 2007, *MNRAS*, 378, 1131
- Chabrier, G., & Baraffe, I. 2000, *ARA&A*, 38, 337
- Chabrier, G., Baraffe, I., Allard, F., & Hauschildt, P. 2000, *ApJ*, 542, 464
- Chappelle, R. J., Pinfield, D. J., Steele, I. A., Dobbie, P. D., & Magazzù, A. 2005, *MNRAS*, 361, 1323



- Charbonneau, D., Brown, T. M., Latham, D. W., & Mayor, M. 2000, *ApJ*, 529, L45
- Charbonneau, D., et al. 2009, *Nature*, 462, 891
- Chauvin, G., Lagrange, A.-M., Dumas, C., Zuckerman, B., Mouillet, D., Song, I., Beuzit, J.-L., & Lowrance, P. 2004, *A&A*, 425, L29
- . 2005a, *A&A*, 438, L25
- Chauvin, G., et al. 2005b, *A&A*, 438, L29
- . 2005c, *A&A*, 430, 1027
- Close, L. M., Potter, D., Brandner, W., Lloyd-Hart, M., Liebert, J., Burrows, A., & Siegler, N. 2002, *ApJ*, 566, 1095
- Close, L. M., Siegler, N., Freed, M., & Biller, B. 2003, *ApJ*, 587, 407
- Converse, J. M., & Stahler, S. W. 2008, *ApJ*, 678, 431
- . 2010, *MNRAS*, in press (eprint ArXiv:1002.2229)
- Cruz, K. L., Reid, I. N., Liebert, J., Kirkpatrick, J. D., & Lowrance, P. J. 2003, *AJ*, 126, 2421
- Cushing, M. C., Rayner, J. T., & Vacca, W. D. 2005, *ApJ*, 623, 1115
- Cushing, M. C., et al. 2006, *ApJ*, 648, 614
- Dahn, C. C., et al. 2002, *AJ*, 124, 1170
- Deacon, N. R., & Hambly, N. C. 2004, *A&A*, 416, 125
- Deleuil, M., et al. 2008, *A&A*, 491, 889
- Delfosse, X., et al. 1997, *A&A*, 327, L25
- Delorme, P., et al. 2008, *A&A*, 484, 469
- Dobbie, P. D., Kenyon, F., Jameson, R. F., Hodgkin, S. T., Pinfield, D. J., & Osborne, S. L. 2002, *MNRAS*, 335, 687
- Dupuy, T., Liu, M., Bowler, B., Cushing, M., Helling, C., Witte, S., & Hauschildt, P. 2010, *ApJ*, in press (eprint ArXiv:1007.4197)
- Dupuy, T. J., Liu, M. C., & Ireland, M. J. 2009a, *ApJ*, 692, 729
- . 2009b, *ApJ*, 699, 168
- Duquennoy, A., & Mayor, M. 1991, *A&A*, 248, 485

- Dvorak, R., Schneider, J., Lammer, H., Barge, P., Wuchterl, G., & the CoRoT team. 2009, Proceeding of the BDEP Meeting "New Technologies for Probing the Diversity of Brown Dwarfs and Exoplanets" (Shanghai, China, 2009 July 19–24), EPJ Web of Conferences, in press (eprint ArXiv: 0912.4655)
- Festin, L. 1998, *A&A*, 333, 497
- Fortney, J. J., Marley, M. S., Saumon, D., & Lodders, K. 2008, *ApJ*, 683, 1104
- Frankowski, A., Jancart, S., & Jorissen, A. 2007, *A&A*, 464, 377
- Funayama, H., Itoh, Y., Oasa, Y., Toyota, E., Hashimoto, O., & Mukai, T. 2009, *PASJ*, 61, 930
- Geballe, T. R., et al. 2002, *ApJ*, 564, 466
- Gizis, J. E. 2002, *ApJ*, 575, 484
- Gizis, J. E., Reid, I. N., Knapp, G. R., Liebert, J., Kirkpatrick, J. D., Koerner, D. W., & Burgasser, A. J. 2003, *AJ*, 125, 3302
- González-García, B. M., Zapatero Osorio, M. R., Béjar, V. J. S., Bihain, G., Barrado Y Navascués, D., Caballero, J. A., & Morales-Calderón, M. 2006, *A&A*, 460, 799
- González Hernández, J. I., Caballero, J. A., Rebolo, R., Béjar, V. J. S., Barrado y Navascués, D., Martín, E. L., & Zapatero Osorio, M. R. 2008, *A&A*, 490, 1135
- Gould, A., et al. 2006, *ApJ*, 644, L37
- Grady, C. A., Woodgate, B., Heap, S. R., Bowers, C., Nuth, III, J. A., Herczeg, G. J., & Hill, H. G. M. 2005, *ApJ*, 620, 470
- Grazian, A., et al. 2006, *A&A*, 449, 951
- Greissl, J., Meyer, M. R., Wilking, B. A., Fanetti, T., Schneider, G., Greene, T. P., & Young, E. 2007, *AJ*, 133, 1321
- Grether, D., & Lineweaver, C. H. 2006, *ApJ*, 640, 1051
- Halbwachs, J. L., Arenou, F., Mayor, M., Udry, S., & Queloz, D. 2000, *A&A*, 355, 581
- Hambly, N. C., Hodgkin, S. T., Cossburn, M. R., & Jameson, R. F. 1999, *MNRAS*, 303, 835
- Hammersley, P. L. 1998, *New Astronomy Review*, 42, 533
- Han, I., Lee, B. C., Kim, K. M., Mkrtichian, D. E., Hatzes, A. P., & Valyavin, G. 2010, *A&A*, 509, A24+
- Hatzes, A. P., & Cochran, W. D. 1993, *ApJ*, 413, 339

- Hatzes, A. P., Cochran, W. D., Endl, M., McArthur, B., Paulson, D. B., Walker, G. A. H., Campbell, B., & Yang, S. 2003, *ApJ*, 599, 1383
- Hatzes, A. P., Guenther, E. W., Endl, M., Cochran, W. D., Döllinger, M. P., & Bedalov, A. 2005, *A&A*, 437, 743
- Hatzes, A. P., et al. 2006, *A&A*, 457, 335
- Hawley, S. L., et al. 2002, *AJ*, 123, 3409
- Hayashi, C., Nakazawa, K., & Nakagawa, Y. 1985, in *Protostars and Planets II*, ed. D. C. Black & M. S. Matthews, 1100–1153
- Heap, S. R., Lindler, D. J., Lanz, T. M., Cornett, R. H., Hubeny, I., Maran, S. P., & Woodgate, B. 2000, *ApJ*, 539, 435
- Helling, C., et al. 2008, *MNRAS*, 391, 1854
- Hernández, J., et al. 2007, *ApJ*, 662, 1067
- Hillenbrand, L. A. 1997, *AJ*, 113, 1733
- Hogan, E., Jameson, R. F., Casewell, S. L., Osbourne, S. L., & Hambly, N. C. 2008, *MNRAS*, 388, 495
- Hoyle, F. 1953, *ApJ*, 118, 513
- Hubickyj, O., Bodenheimer, P., & Lissauer, J. J. 2005, *Icarus*, 179, 415
- Ikoma, M., Nakazawa, K., & Emori, H. 2000, *ApJ*, 537, 1013
- Jones, B. F. 1970, *AJ*, 75, 563
- Jorissen, A., Mayor, M., & Udry, S. 2001, *A&A*, 379, 992
- Joye, W. A., & Mandel, E. 2003, in *PASPC*, Vol. 295, *Astronomical Data Analysis Software and Systems XII*, ed. H. E. Payne, R. I. Jedrzejewski, & R. N. Hook, 489
- Kalas, P., et al. 2008, *Science*, 322, 1345
- Kendall, T. R., et al. 2007, *A&A*, 466, 1059
- Kenyon, M. J., Jeffries, R. D., Naylor, T., Oliveira, J. M., & Maxted, P. F. L. 2005, *MNRAS*, 356, 89
- King, R. R., McCaughrean, M. J., Homeier, D., Allard, F., Scholz, R., & Lodieu, N. 2009, *ArXiv e-prints*
- Kirkpatrick, J. D., Allard, F., Bida, T., Zuckerman, B., Becklin, E. E., Chabrier, G., & Baraffe, I. 1999a, *ApJ*, 519, 834
- Kirkpatrick, J. D., Barman, T. S., Burgasser, A. J., McGovern, M. R., McLean, I. S., Tinney, C. G., & Lowrance, P. J. 2006, *ApJ*, 639, 1120

- Kirkpatrick, J. D., et al. 1998, *Bulletin of the American Astronomical Society*, 30, 899
- . 1999b, *ApJ*, 519, 802
- . 2000, *AJ*, 120, 447
- . 2008, *ApJ*, 689, 1295
- Koen, C. 2003, *MNRAS*, 346, 473
- Kroupa, P., & Bouvier, J. 2003, *MNRAS*, 346, 369
- Kumar, S. S. 1963, *ApJ*, 137, 1121
- Lafrenière, D., Jayawardhana, R., & van Kerkwijk, M. H. 2008, *ApJ*, 689, L153
- Larson, R. B. 1973, *MNRAS*, 161, 133
- Latham, D. W., Stefanik, R. P., Mazeh, T., Mayor, M., & Burki, G. 1989, *Nature*, 339, 38
- Lawrence, A., et al. 2007, *MNRAS*, 379, 1599
- Lissauer, J. J. 1993, *ARA&A*, 31, 129
- Littlefair, S. P., Dhillon, V. S., Marsh, T. R., Shahbaz, T., Martín, E. L., & Copperwheat, C. 2008, *MNRAS*, 391, L88
- Lodders, K. 1999, *ApJ*, 519, 793
- Lodieu, N., Hambly, N. C., Jameson, R. F., Hodgkin, S. T., Carraro, G., & Kendall, T. R. 2007, *MNRAS*, 374, 372
- Lovis, C., & Mayor, M. 2007, *A&A*, 472, 657
- Low, C., & Lynden-Bell, D. 1976, *MNRAS*, 176, 367
- Lucas, P. W., & Roche, P. F. 2000, *MNRAS*, 314, 858
- Lucas, P. W., Roche, P. F., & Tamura, M. 2005, *MNRAS*, 361, 211
- Luhman, K. L. 1999, *ApJ*, 525, 466
- . 2007, *ApJS*, 173, 104
- Luhman, K. L., Adame, L., D'Alessio, P., Calvet, N., Hartmann, L., Megeath, S. T., & Fazio, G. G. 2005a, *ApJ*, 635, L93
- Luhman, K. L., D'Alessio, P., Calvet, N., Allen, L. E., Hartmann, L., Megeath, S. T., Myers, P. C., & Fazio, G. G. 2005b, *ApJ*, 620, L51
- Luhman, K. L., Hernández, J., Downes, J. J., Hartmann, L., & Briceño, C. 2008, *ApJ*, 688, 362

- Luhman, K. L., Mamajek, E. E., Allen, P. R., & Cruz, K. L. 2009, *ApJ*, 703, 399
- Luhman, K. L., et al. 2005c, *ApJ*, 631, L69
- Magazzu, A., Martin, E. L., & Rebolo, R. 1993, *ApJ*, 404, L17
- Magazzu, A., Rebolo, R., Zapatero Osorio, M. R., Martin, E. L., & Hodgkin, S. T. 1998, *ApJ*, 497, L47
- Marcy, G., Butler, R. P., Fischer, D., Vogt, S., Wright, J. T., Tinney, C. G., & Jones, H. R. A. 2005, *Progress of Theoretical Physics Supplement*, 158, 24
- Marcy, G. W., & Butler, R. P. 1998, *ARA&A*, 36, 57
- . 2000, *PASP*, 112, 137
- Marcy, G. W., Butler, R. P., Vogt, S. S., Fischer, D., & Lissauer, J. J. 1998, *ApJ*, 505, L147
- Marois, C., Macintosh, B., Barman, T., Zuckerman, B., Song, I., Patience, J., Lafrenière, D., & Doyon, R. 2008, *Science*, 322, 1348
- Marsh, K. A., Kirkpatrick, J. D., & Plavchan, P. 2010, *ApJ*, 709, L158
- Martín, E. L., Basri, G., Delfosse, X., & Forveille, T. 1997, *A&A*, 327, L29
- Martín, E. L., Basri, G., Gallegos, J. E., Rebolo, R., Zapatero Osorio, M. R., & Bejar, V. J. S. 1998a, *ApJ*, 499, L61
- Martín, E. L., Basri, G., Zapatero Osorio, M. R., Rebolo, R., & López, R. J. G. 1998b, *ApJ*, 507, L41
- Martín, E. L., Brandner, W., Bouvier, J., Luhman, K. L., Stauffer, J., Basri, G., Zapatero Osorio, M. R., & Barrado y Navascués, D. 2000, *ApJ*, 543, 299
- Martín, E. L., Delfosse, X., Basri, G., Goldman, B., Forveille, T., & Zapatero Osorio, M. R. 1999, *AJ*, 118, 2466
- Martín, E. L., & Zapatero Osorio, M. R. 2003, *ApJ*, 593, L113
- Martín, E. L., Zapatero Osorio, M. R., Barrado y Navascués, D., Béjar, V. J. S., & Rebolo, R. 2001, *ApJ*, 558, L117
- Mayer, L., Quinn, T., Wadsley, J., & Stadel, J. 2002, *Science*, 298, 1756
- Mayor, M., & Queloz, D. 1995, *Nature*, 378, 355
- Mayor, M., Udry, S., Naef, D., Pepe, F., Queloz, D., Santos, N. C., & Burnet, M. 2004, *A&A*, 415, 391
- Mayor, M., et al. 2009, *A&A*, 507, 487

- Mazeh, T., Latham, D. W., & Stefanik, R. P. 1996, *ApJ*, 466, 415
- McArthur, B. E., et al. 2004, *ApJ*, 614, L81
- McCarthy, C., & Zuckerman, B. 2004, *AJ*, 127, 2871
- McCaughrean, M. J., Close, L. M., Scholz, R.-D., Lenzen, R., Biller, B., Brandner, W., Hartung, M., & Lodieu, N. 2004, *A&A*, 413, 1029
- McGovern, M. R., Kirkpatrick, J. D., McLean, I. S., Burgasser, A. J., Prato, L., & Lowrance, P. J. 2004, *ApJ*, 600, 1020
- Mohanty, S., Basri, G., Jayawardhana, R., Allard, F., Hauschildt, P., & Ardila, D. 2004a, *ApJ*, 609, 854
- Mohanty, S., Jayawardhana, R., & Basri, G. 2004b, *ApJ*, 609, 885
- . 2005, *ApJ*, 626, 498
- Monet, D., & et al. 1998, *VizieR Online Data Catalog*, 1252, 0
- Monet, D. G., et al. 2003, *AJ*, 125, 984
- Morau, E., Bouvier, J., & Stauffer, J. R. 2001, *A&A*, 367, 211
- Morau, E., Bouvier, J., Stauffer, J. R., & Cuillandre, J.-C. 2003, *A&A*, 400, 891
- Morau, E., & Clarke, C. 2005, *A&A*, 429, 895
- Morau, E., Kroupa, P., & Bouvier, J. 2004, *A&A*, 426, 75
- Mouillet, D., Larwood, J. D., Papaloizou, J. C. B., & Lagrange, A. M. 1997, *MNRAS*, 292, 896
- Najita, J. R., Tiede, G. P., & Carr, J. S. 2000, *ApJ*, 541, 977
- Nakajima, T., Oppenheimer, B. R., Kulkarni, S. R., Golimowski, D. A., Matthews, K., & Durrance, S. T. 1995, *Nature*, 378, 463
- Neuhäuser, R., & Comerón, F. 1999, *A&A*, 350, 612
- Neuhäuser, R., Guenther, E. W., Wuchterl, G., Mugrauer, M., Bedalov, A., & Hauschildt, P. H. 2005, *A&A*, 435, L13
- Newberry, M. V. 1991, *PASP*, 103, 122
- Nielsen, E. L., Close, L. M., Biller, B. A., Masciadri, E., & Lenzen, R. 2008, *ApJ*, 674, 466
- Oliveira, J. M., Jeffries, R. D., van Loon, J. T., & Rushton, M. T. 2006, *MNRAS*, 369, 272
- Oppenheimer, B. R., Golimowski, D. A., Kulkarni, S. R., Matthews, K., Nakajima, T., Creech-Eakman, M., & Durrance, S. T. 2001, *AJ*, 121, 2189

- Padoan, P., & Nordlund, Å. 2002, *ApJ*, 576, 870
- . 2004, *ApJ*, 617, 559
- Padoan, P., Nordlund, Å., Kritsuk, A. G., Norman, M. L., & Li, P. S. 2007, *ApJ*, 661, 972
- Pavlenko, Y. V., Rebolo, R., Martin, E. L., & Garcia Lopez, R. J. 1995, *A&A*, 303, 807
- Perryman, M. A. C., et al. 1997, *A&A*, 323, L49
- Phan-Bao, N., et al. 2003, *A&A*, 401, 959
- Pinfield, D. J., Hodgkin, S. T., Jameson, R. F., Cossburn, M. R., Hambly, N. C., & Devereux, N. 2000, *MNRAS*, 313, 347
- Pinfield, D. J., Jameson, R. F., & Hodgkin, S. T. 1998, *MNRAS*, 299, 955
- Pinfield, D. J., Jones, H. R. A., Lucas, P. W., Kendall, T. R., Folkes, S. L., Day-Jones, A. C., Chappelle, R. J., & Steele, I. A. 2006, *MNRAS*, 368, 1281
- Quillen, A. C., Blackman, E. G., Frank, A., & Varnière, P. 2004, *ApJ*, 612, L137
- Raboud, D., & Mermilliod, J.-C. 1998, *A&A*, 333, 897
- Rasio, F. A. 1994, *ApJ*, 427, L107
- Rebolo, R., Martín, E. L., Basri, G., Marcy, G. W., & Zapatero Osorio, M. R. 1996, *ApJ*, 469, L53
- Rebolo, R., Martín, E. L., & Magazzù, A. 1992, *ApJ*, 389, L83
- Rebolo, R., & Zapatero Osorio, M. R., eds. 2000, *Very Low-mass Stars and Brown Dwarfs*
- Rebolo, R., Zapatero Osorio, M. R., Madrugá, S., Bejar, V. J. S., Arribas, S., & Licandro, J. 1998, *Science*, 282, 1309
- Rebolo, R., Zapatero Osorio, M. R., & Martín, E. L. 1995, *Nature*, 377, 129
- Rees, M. J. 1976, *MNRAS*, 176, 483
- Reipurth, B., & Clarke, C. 2001, *AJ*, 122, 432
- Rivera, E. J., et al. 2005, *ApJ*, 634, 625
- Robichon, N., Arenou, F., Mermilliod, J.-C., & Turon, C. 1999, *A&A*, 345, 471
- Ruiz, M. T., Leggett, S. K., & Allard, F. 1997, *ApJ*, 491, L107
- Sato, B., et al. 2007, *ApJ*, 661, 527
- Saumon, D., Hubbard, W. B., Burrows, A., Guillot, T., Lunine, J. I., & Chabrier, G. 1996, *ApJ*, 460, 993

- Schneider, D. P., et al. 2002, *AJ*, 123, 458
- Scholz, A., Geers, V., Jayawardhana, R., Fissel, L., Lee, E., Lafreniere, D., & Tamura, M. 2009, *ApJ*, 702, 805
- Scholz, A., & Jayawardhana, R. 2008, *ApJ*, 672, L49
- Scholz, R.-D., McCaughrean, M. J., Lodieu, N., & Kuhlbrodt, B. 2003, *A&A*, 398, L29
- Sheppard, S. S., & Cushing, M. C. 2009, *AJ*, 137, 304
- Sherry, W. H., Walter, F. M., & Wolk, S. J. 2004, *AJ*, 128, 2316
- Sherry, W. H., Walter, F. M., Wolk, S. J., & Adams, N. R. 2008, *AJ*, 135, 1616
- Shporer, A., et al. 2009, *ApJ*, 690, 1393
- Siegler, N., Close, L. M., Cruz, K. L., Martín, E. L., & Reid, I. N. 2005, *ApJ*, 621, 1023
- Silk, J. 1977, *ApJ*, 214, 152
- Skrutskie, M. F., et al. 2006, *AJ*, 131, 1163
- Soderblom, D. R. 2010, in press (eprint ArXiv: 1003.6074)
- Soderblom, D. R., Laskar, T., Valenti, J. A., Stauffer, J. R., & Rebull, L. M. 2009, *AJ*, 138, 1292
- Stamatellos, D., & Whitworth, A. P. 2009, *MNRAS*, 392, 413
- Stauffer, J. R., Schultz, G., & Kirkpatrick, J. D. 1998, *ApJ*, 499, L199
- Stevenson, D. J. 1978, *Proceedings of the Astronomical Society of Australia*, 3, 227
- Strauss, M. A., et al. 1999, *ApJ*, 522, L61
- Tarter, J. C. 1975, Ph.D. Thesis
- Taylor, B. J. 2008, *AJ*, 136, 1388
- Telesco, C. M., et al. 2005, *Nature*, 433, 133
- Testi, L. 2009, *A&A*, 503, 639
- Udalski, A., et al. 2005, *ApJ*, 628, L109
- Vacca, W. D., Cushing, M. C., & Rayner, J. T. 2003, *PASP*, 115, 389
- van Leeuwen, F. 2009, *A&A*, 497, 209
- Veras, D., Crepp, J. R., & Ford, E. B. 2009, *ApJ*, 696, 1600
- Walker, G. A. H. 2008, ArXiv e-prints



- White, R. E. 2003, *ApJS*, 148, 487
- White, R. J., Ghez, A. M., Reid, I. N., & Schultz, G. 1999, *ApJ*, 520, 811
- Whitworth, A. P., & Goodwin, S. P. 2005, *Astron. Nachr.*, 326, 899
- Whitworth, A. P., & Stamatellos, D. 2006, *A&A*, 458, 817
- Whitworth, A. P., & Zinnecker, H. 2004, *A&A*, 427, 299
- Willing, B. A., Greene, T. P., & Meyer, M. R. 1999, *AJ*, 117, 469
- Williams, D. M., Comeron, F., Rieke, G. H., & Rieke, M. J. 1995, *ApJ*, 454, 144
- Wolszczan, A., & Frail, D. A. 1992, *Nature*, 355, 145
- Wuchterl, G., Guillot, T., & Lissauer, J. J. 2000, *Protostars and Planets IV*, 1081
- Wyatt, M. C. 2003, *ApJ*, 598, 1321
- Zapatero Osorio, M. R., Béjar, V. J. S., Martín, E. L., Rebolo, R., Barrado y Navascués, D., Bailer-Jones, C. A. L., & Mundt, R. 2000, *Science*, 290, 103
- Zapatero Osorio, M. R., Béjar, V. J. S., Martín, E. L., Rebolo, R., Barrado y Navascués, D., Mundt, R., Eisloffel, J., & Caballero, J. A. 2002a, *ApJ*, 578, 536
- Zapatero Osorio, M. R., Béjar, V. J. S., Rebolo, R., Martín, E. L., & Basri, G. 1999a, *ApJ*, 524, L115
- Zapatero Osorio, M. R., Béjar, V. J. S., Martín, E. L., Barrado y Navascués, D., & Rebolo, R. 2002b, *ApJ*, 569, L99
- Zapatero Osorio, M. R., Béjar, V. J. S., Pavlenko, Y., Rebolo, R., Allende Prieto, C., Martín, E. L., & García López, R. J. 2002c, *A&A*, 384, 937
- Zapatero Osorio, M. R., Lane, B. F., Pavlenko, Y., Martín, E. L., Britton, M., & Kulkarni, S. R. 2004, *ApJ*, 615, 958
- Zapatero Osorio, M. R., Rebolo, R., & Martín, E. L. 1997a, *A&A*, 317, 164
- Zapatero Osorio, M. R., Rebolo, R., Martín, E. L., Basri, G., Magazzu, A., Hodgkin, S. T., Jameson, R. F., & Cossburn, M. R. 1997b, *ApJ*, 491, L81
- Zapatero Osorio, M. R., Rebolo, R., Martín, E. L., Hodgkin, S. T., Cossburn, M. R., Magazzù, A., Steele, I. A., & Jameson, R. F. 1999b, *A&AS*, 134, 537
- Zapatero Osorio, M. R., et al. 2007, *A&A*, 472, L9
- . 2008, *A&A*, 477, 895

# Pleiades low-mass brown dwarfs: the cluster L dwarf sequence

G. Bihain<sup>1,2</sup>, R. Rebolo<sup>1,2</sup>, V. J. S. Béjar<sup>1,3</sup>, J. A. Caballero<sup>1</sup>, C. A. L. Bailer-Jones<sup>4</sup>,  
R. Mundt<sup>4</sup>, J. A. Acosta-Pulido<sup>1</sup>, and A. Manchado Torres<sup>1,2</sup>

<sup>1</sup> Instituto de Astrofísica de Canarias, c/ Vía Láctea, s/n, 38205 La Laguna, Tenerife, Spain  
e-mail: [gbihain;rrl;zvezda;jap;amt]@ll.iac.es;victor.bejar@gtc.iac.es

<sup>2</sup> Consejo Superior de Investigaciones Científicas, Spain

<sup>3</sup> GTC Project, Instituto de Astrofísica de Canarias

<sup>4</sup> Max-Planck-Institut für Astronomie, Königstuhl 17, 69117 Heidelberg, Germany  
e-mail: [calj;mundt]@mpia-hd.mpg.de

Received 1 March 2006 / Accepted 3 August 2006

## ABSTRACT

**Aims.** We present a search for low-mass brown dwarfs in the Pleiades open cluster. The identification of Pleiades members fainter and cooler than those currently known allows us to constrain evolutionary models for L dwarfs and to extend the study of the cluster mass function to lower masses.

**Methods.** We conducted a 1.8 deg<sup>2</sup> near-infrared *J*-band survey at the 3.5 m Calar Alto Telescope, with completeness  $J_{\text{cpl}} \sim 19.0$ . The detected sources were correlated with those of previously available optical *I*-band images ( $I_{\text{cpl}} \sim 22$ ). Using a *J* versus *I* – *J* colour–magnitude diagram, we identified 18 faint red L-type candidates, with magnitudes  $17.4 < J < 19.7$  and colours  $I - J > 3.2$ . If Pleiades members, their masses would span  $\sim 0.040$ – $0.020 M_{\odot}$ . We performed follow-up *HK<sub>s</sub>*-band imaging to further confirm their cluster membership by photometry and proper motion.

**Results.** Out of 11 *IJ* candidates with proper motion measurements, we find six cluster members, two non-members and three whose membership is uncertain and depends on the intrinsic velocity dispersion of Pleiades brown dwarfs. This dispersion ( $>4 \text{ mas yr}^{-1}$ ) is at least four times that of cluster stars with masses  $\geq 1 M_{\odot}$ . Five of the seven other *IJ* candidates are discarded because their *J* – *K<sub>s</sub>* colours are bluer than those of confirmed members. Our least massive proper motion members are BRB 28 and 29 ( $\sim 25 M_{\text{Jup}}$ ). The *J* versus *I* – *J* sequence of the L-type candidates at  $J > 18$  is not as red as theoretical models predict; it rather follows the field L-dwarf sequence translated to the cluster distance. This sequence overlapping, also observed in the *J* versus *J* – *H* and *J* – *K* diagrams, suggests that Pleiades and field L dwarfs may have similar spectral energy distributions and luminosities, and thus possibly similar radii. Also, we find  $\alpha = 0.5 \pm 0.2$  for a power-law approximation  $dN/dM \propto M^{-\alpha}$  of the survey mass spectrum in the mass range  $0.5$ – $0.026 M_{\odot}$ . This value is similar to that of much younger clusters, indicating no significant differential evaporation of low-mass Pleiades members relative to more massive ones.

**Key words.** open clusters and associations: individual: Pleiades – stars: low-mass, brown dwarfs – stars: luminosity function, mass function

## 1. Introduction

As a result of progressive cooling, brown dwarfs are expected to evolve from late M spectral type at very early stages (age  $\lesssim 10$  Myr) to L-type ( $T_{\text{eff}}$  in the range  $\sim 2400$  to  $\sim 1400$  K; Dahn et al. 2002), and at sufficiently old ages (a few Gyr), to T-type and beyond ( $T_{\text{eff}} \lesssim 1400$  K). The mass-spectral type and mass-luminosity relationships at different ages remain to be derived from observations of cool dwarfs, which also permit the calibration of the theory of substellar evolution (e.g. Chabrier & Baraffe 2000). In comparison to the spectra of M dwarfs, L dwarfs are characterized in the optical by the weakening of the metal-oxide TiO and VO bands due to the condensation of the metals Ti and V in dust grains that may significantly affect the atmospheric structure and the emergent spectrum (e.g. the DUSTY models from Chabrier et al. 2000). Bands of metal-hydrides CrH, FeH and CaH and bands of water become more intense especially in the near-infrared (IR), whereas the neutral alkali metals Na, K, Rb, Cs and Li become stronger in the optical (Chabrier & Baraffe 2000; Basri 2000). The emergence in the near-IR of CH<sub>4</sub> bands characterizes the beginning of the T dwarf sequence. Field L dwarfs have *I* – *J* and *J* – *K<sub>s</sub>* colours redder

than  $\sim 3.3$  and  $\sim 1.3$  mag, respectively, increasing from early to later spectral subclasses (Martín et al. 1999). For the L4–L8 spectral subclasses the near-IR *J* – *H* and *J* – *K<sub>s</sub>* colours appear to saturate at  $\sim 1.2$  and  $\sim 2.0$  mag (Kirkpatrick et al. 2000; Burgasser et al. 2002), respectively, whereas for T dwarfs these colours become bluer, with values decreasing to below zero (Knapp et al. 2004). From L0 to T8 spectral types the *I* – *J* colour is increasing to  $\sim 5.8$  mag (Dahn et al. 2002). Associated with the other colours it can give a rough indication of the spectral type.

The Pleiades open cluster ( $\sim 120$  Myr,  $\sim 130$  pc) served for decades as a reference stellar laboratory where models were contrasted with observations. Since the discovery of Pleiades brown dwarfs (Rebolo et al. 1995, 1996), subsequent studies have provided numerous fainter substellar candidates with spectral types down to late M (Zapatero Osorio et al. 1997a,b; Bouvier et al. 1998, hereafter B98; Festin 1998a; Zapatero Osorio et al. 1999), from which a fraction is confirmed by lithium detection (Stauffer et al. 1998b; Martín et al. 2000) or by proper motion (Morau et al. 2001, hereafter M01). Very large area proper motion surveys (Hambly et al. 1999; Deacon & Hambly 2004) have obtained on the other hand a significant

census of the stellar-substellar boundary population of the cluster. The coolest object for which a spectral type has been obtained is the L0 brown dwarf candidate Roque 25 (Martín et al. 1998b), with an estimated theoretical mass of  $\sim 0.035 M_{\odot}$ . A dozen fainter objects than Roque 25 have been identified in deep surveys (Festin 1998a; Béjar 2000; Dobbie et al. 2002; Nagashima et al. 2003; Moraux et al. 2003, hereafter M03; Schwartz & Becklin 2005), and some were confirmed by proper motion (Bouy et al. 2006).

The mass spectrum  $dN/dM = f(M)$  of the Pleiades cluster, where  $dN$  stands for the number of objects in the mass range  $dM$ , is best fitted by a lognormal function (M03; Deacon & Hambly 2004), and its approximation by a power law  $M^{-\alpha}$  in the low mass range  $0.6\text{--}0.03 M_{\odot}$  provides a spectral index  $\alpha \sim 0.6\text{--}0.8$  (Dobbie et al. 2002; M03). Similar values are found in other much younger open clusters, as for example  $\sigma$  Orionis ( $\sim 2\text{--}4$  Myr), where  $\alpha = 0.8 \pm 0.4$  for  $0.2 < M(M_{\odot}) < 0.013$  (Béjar et al. 2001), and IC 348 ( $\sim 3$  Myr), where  $\alpha = 0.7 \pm 0.2$  for  $0.5 < M(M_{\odot}) < 0.035$  (Tej et al. 2002). It is important to determine the behaviour of the  $\alpha$  index in the lower mass domain because it can help to discriminate among brown dwarf formation mechanisms. For instance, for the formation of gravitationally unstable cores by turbulent fragmentation (Padoan & Nordlund 2004), the mass spectrum is predicted to be log-normal, with a peak that appears at smaller masses when the sonic Mach number and the mean density of the cores are greater.

In this paper we present a  $1.8 \text{ deg}^2$  deep  $J$ -band survey of the Pleiades open cluster aimed to find lower-mass brown dwarfs ( $< 0.035 M_{\odot}$ ), by comparison with a new analysis of  $I$ -band data obtained by B98. Our goal is to identify L dwarf cluster candidates and study the location of the L dwarf sequence in the colour–magnitude diagram. Preliminary results have been reported in Bihain et al. (2005). Because the cluster has a well known age, the properties of Pleiades L-type brown dwarfs could provide useful constraints to models predicting the evolution of substellar objects. Additionally, we can estimate the cluster mass spectrum of the surveyed area at lower masses.

## 2. Observations and data reduction

### 2.1. $J$ -band survey

We obtained  $J$ -band images on 1998 October 27–28 with the Omega-Prime ( $\Omega'$ ) instrument at the 3.5 m Telescope of the Centro Astronómico Hispano Alemán (CAHA; Calar Alto, Spain). The fields were specifically chosen to cover the optical  $RI$ -band survey from B98 obtained with the 3.6 m Canada-France-Hawaii Telescope (CFHT)/UH8K survey. We observed the fields CFHT 2, 5 (north half), 6, 7, 8, 10, 11 and 13 (see their spatial distribution in Fig. 1). They correspond to an area of the cluster of  $\sim 1.8$  square degrees. The  $\Omega'$  camera has a  $1024 \times 1024$  HgCdTe Hawaii detector with a pixel scale of  $0.40'' \text{ pixel}^{-1}$  and a field of view of  $6.8' \times 6.8'$ . To cover each of the  $29' \times 29'$  UH8K fields (hereafter CFHT fields, as designed in B98) a connecting observation macro was used. The exposure times and repetitions in each pointing were  $16 \text{ s} \times 2$ , except for CFHT7 and CFHT8 ( $16 \text{ s} \times 3$ ), and CFHT6 ( $18 \text{ s} \times 2$ ). Because the offset between successive macro pointings corresponded to one third of an  $\Omega'$  field of view, each area was repeated in total 6–9 times (96–144 s), depending of the CFHT field. The individual images were sky-subtracted, flat-fielded using dome flats, combined and aligned in horizontal strips of  $\sim 30' \times 6.8'$ , using standard scripts and

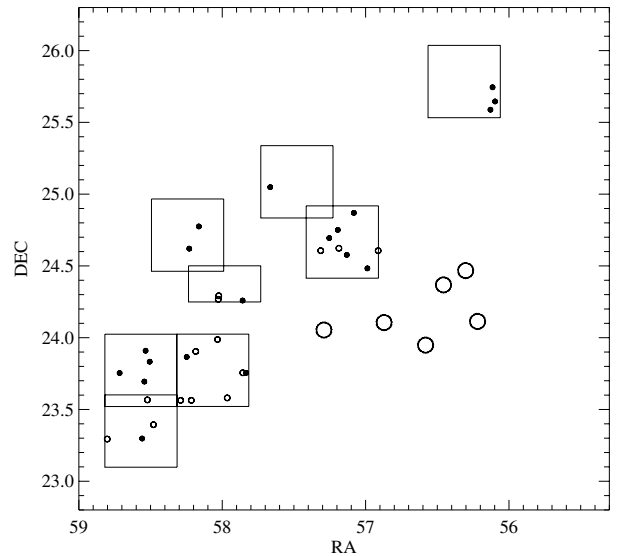


**Fig. 1.** Location of the surveyed Pleiades fields (squares) relative to the brightest Pleiades members with visual magnitude  $V < 5$  (large open circles). The *small open circles* represent the brown dwarf candidates from B98 with lithium or proper motion consistent with cluster membership, and the *filled circles* represent all the other candidates identified in this study.

routines within the IRAF<sup>1</sup> environment. These were later analyzed for aperture and PSF photometry using DAOPHOT. The PSF photometry was calibrated with measurements from the Two Micron All Sky Survey (2MASS) Point Source Catalog (Cutri et al. 2003) and which had errors of less than 0.1 mag. On average, about five 2MASS calibrators were used per horizontal strip. The  $J$ -band completeness (limiting) magnitude was estimated at the maximum (fainter half maximum) of the histogram of object counts per magnitude. We found values of  $\sim 19.0$  and  $\sim 19.5$  mag, respectively.

The optical survey in the  $RI$  bands from B98 was obtained with the UH8K instrument at the CFHT (Mauna Kea, Hawai'i) on 1996 December 9–13. The UH8K camera comprises eight Loral  $2048 \times 4096$  CCD detectors with a pixel scale of  $0.21'' \text{ pixel}^{-1}$ . These data were used initially for a study of brown dwarfs and low-mass stars by B98. In the present paper we use an independent data analysis by Béjar (2000). The photometric calibration of the CFHT fields was performed by comparing our photometry to the Cousins photometry of their candidates and applying an average offset; for the fields CFHT6 and CFHT8 however, different offsets were applied because they were observed through thin cirrus. The completeness and limiting magnitudes were  $\sim 23.5$  and  $\sim 25.0$  mag in the  $R$  band, and  $\sim 22.5$  and  $\sim 23.5$  mag in the  $I$  band, respectively.

To identify fainter and redder objects than those found by B98 and Béjar (2000), we used as reference the detected  $J$ -band sources and searched for their optical counterparts in the  $I$ -band images using a FORTRAN correlation program, CORREL, kindly provided by M. R. Zapatero Osorio. The correlated objects were plotted in a  $J$  versus  $I - J$  diagram (see Fig. 2) and contrasted with the 120 Myr DUSTY isochrone from Chabrier et al. (2000), shifted to the cluster distance of  $133.8 \pm 3.0$  pc

<sup>1</sup> IRAF is distributed by the National Optical Astronomy Observatories, which are operated by the Association of Universities for Research in Astronomy, Inc., under cooperative agreement with the National Science Foundation.

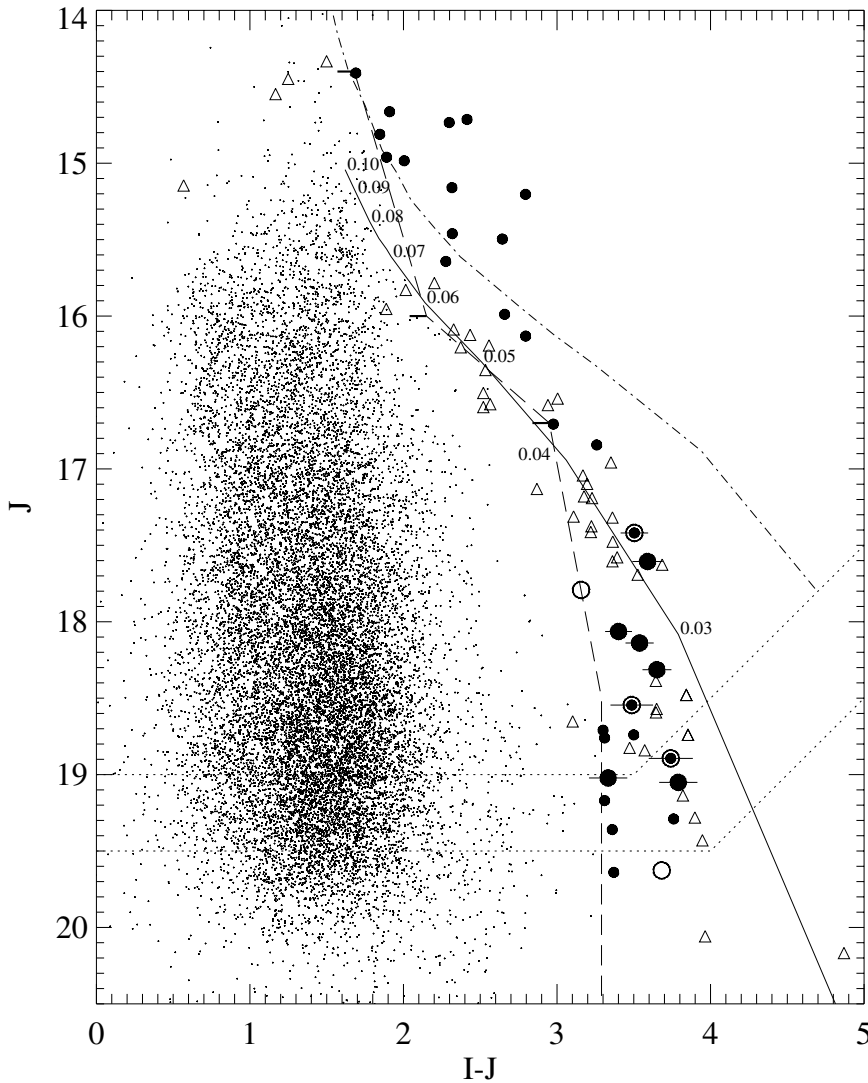


**Fig. 2.**  $J$  versus  $I - J$  colour-magnitude diagram for the correlated survey objects. The circular symbols correspond to  $IJ$  candidate or confirmed cluster members (Table 1), with redder  $I - J$  colours than the dashed line boundary (see text for details). At  $J > 17.4$  we plot: proper motion members (large filled circles), possible proper motion members (circled filled circles) and non-proper motion members (large empty circles). The solid line and the dash-dotted line represent the  $\sim 120$  Myr DUSTY isochrone (Chabrier et al. 2000) and the  $\sim 125$  Myr NextGen isochrone (Baraffe et al. 1998), respectively, shifted to the distance of the cluster. Masses in solar units are indicated for the DUSTY isochrone. The triangles correspond to field dwarfs shifted to the distance of the cluster. Finally, the upper and lower dotted lines at the bottom of the diagram indicate the completeness and limiting magnitudes of the survey, respectively.

(Percival et al. 2005). As most of our faint objects were bluer than the theoretical isochrone in the  $J$  versus  $I - J$  diagram, we decided to establish our selection of candidates based on an empirical criterion. We considered a bluer envelope to cluster candidates (dashed line in Fig. 2), defined by the bluest lithium or proper motion Pleiades objects reported (Martín et al. 2000; M01): CFHT-PI-1, Calar 1 and CFHT-PI-25 (horizontal thick marks in Fig. 2). The envelope was extended to faint magnitudes  $J > 18.5$  at a fixed colour of  $I - J = 3.3$ , to avoid most of the M8–9 dwarf contaminants which have bluer colours. As potential cluster members we have selected 34 objects (named “BRB”) with  $J > 14.4$  and colours  $1.7 < I - J < 3.8$  (Table 1). We checked that these objects had colours  $R - I \geq 1.8$ . Some fainter candidates had unreliable or too faint  $R$ -band magnitudes and no value is given in Table 1. We discarded as contaminants the previously identified non-proper motion candidates CFHT-PI-8 (M01) and CFHT-PLIZ-25 (M03).

Of the 34 BRB candidates, 22 were identified already by previous surveys (e.g. Béjar 2000, B98; see footnote of Table 1 for all the references). In the magnitude range of the brightest objects we identify an additional candidate, BRB 4, which is also in the 2MASS catalog. This object is not mentioned by B98 and is not in the list of proper motion and  $RI$ -band photometric

candidates from Deacon & Hambly (2004). The latter survey overlaps the CFHT survey and its  $R$ -band limiting magnitude is greater than the magnitude of BRB 4,  $R = 19.4$ . Therefore this object should have been detected. Possibly it was blended or it is not a proper motion cluster member.

The magnitude errors of the BRB candidates are 0.06 mag for  $J \sim 14.5$ – $17.0$  and 0.08 mag for  $J \sim 17.0$ – $20.0$ . Comparing our  $J$ -band magnitudes with those available in the literature (Martín et al. 2000; Pinfield et al. 2003), i.e. those in the range  $J \sim 14.5$ – $17.0$ , we find:

1.  $\langle J_{\text{BRB}} - J_{\text{Martin}} \rangle = -0.04 \pm 0.09$ , for the objects in common CFHT-PI-2, 3, 4, 5, 6, 7, 9, 11, 12, 15, 21 and 25. CFHT-PI-6 and CFHT-PI-7 present the greatest differences,  $-0.18$  and  $-0.26$  mag, respectively. Both objects lack of  $H\alpha$  emission (Martín et al. 2000), but CFHT-PI-7 has a proper motion consistent with that of the cluster. In one of our individual  $J$ -band images, the radial profile of CFHT-PI-7 peaks at relatively higher counts and is not well centred, probably due to a cosmic ray; this might explain the greater brightness (it is also supported by the difference with 2MASS,  $J_{\text{BRB}} - J_{\text{2MASS}} = -0.14$ ). For CFHT-PI-6, as discussed by M01, if this is an equal mass binary as suggested by its position well above the cluster sequence in the

**Table 1.** *R**I**J* photometry and coordinates for the low-mass stars and brown dwarf candidates.

Name	Names reported <sup>b</sup>	$R - I \pm \sigma_{R-I}$	$I \pm \sigma_I$	$J \pm \sigma_J$	$I - J$	RA (J2000) (h m s)	Dec (J2000) <sup>c</sup> (° ′ ″)
BRB 1	CFHT-PI-1, BPL 242, MBSC 91, (*)	1.76 ± 0.13	16.10 ± 0.07	14.41 ± 0.03 <sup>d</sup>	1.69	03 51 51.6 +23 34 50.2	
BRB 2	CFHT-PI-2, BPL 267, DH 765, (*)	2.00 ± 0.10	16.57 ± 0.07	14.66 ± 0.06	1.91	03 52 44.3 +23 54 15.2	
BRB 3	CFHT-PI-6, (*)	2.38 ± 0.10	17.13 ± 0.07	14.71 ± 0.05	2.41	03 52 07.9 +23 59 14.6	
BRB 4	(*)	2.38 ± 0.10	17.03 ± 0.07	14.73 ± 0.04	2.30	03 44 23.2 +25 38 44.7	
BRB 5	CFHT-PI-3, HHJ 22, BPL 272, MBSC 99, (*)	1.94 ± 0.10	16.66 ± 0.07	14.81 ± 0.06	1.85	03 52 51.8 +23 33 48.9	
BRB 6	CFHT-PI-4, BPL 280, MBSC 101, (*)	1.92 ± 0.10	16.85 ± 0.07	14.96 ± 0.06	1.89	03 53 09.6 +23 33 48.3	
BRB 7	CFHT-PI-5, DH 590, (*)	2.11 ± 0.10	16.99 ± 0.07	14.98 ± 0.06	2.01	03 48 44.7 +24 37 22.7	
BRB 8	CFHT-PI-7, BPL 253, MBSC 108, (*)	1.84 ± 0.13	17.48 ± 0.07	15.16 ± 0.07	2.32	03 52 05.8 +24 17 31.7	
BRB 9	CFHT-PI-12, BPL 294, CFHT-PLIZ-6, (*)	2.55 ± 0.10	18.00 ± 0.07	15.20 ± 0.03	2.80	03 53 55.1 +23 23 37.4	
BRB 10	CFHT-PI-9, BPL 202, MHOBD 6, (*)	2.17 ± 0.10	17.78 ± 0.07	15.46 ± 0.07	2.32	03 49 15.1 +24 36 22.4	
BRB 11	CFHT-PI-13, Teide 2, BPL 254, CFHT-PLIZ-3, (*)	2.11 ± 0.13	18.14 ± 0.07	15.50 ± 0.07	2.64	03 52 06.7 +24 16 01.4	
BRB 12	CFHT-PI-11, Roque 16, BPL 152, (*)	2.25 ± 0.10	17.92 ± 0.07	15.64 ± 0.07	2.28	03 47 39.0 +24 36 22.1	
BRB 13	CFHT-PI-15, (*)	2.44 ± 0.10	18.65 ± 0.07	15.99 ± 0.07	2.66	03 55 12.5 +23 17 38.0	
BRB 14	CFHT-PI-21, Calar 3, BPL 235, CFHT-PLIZ-12, (*)	2.49 ± 0.11	18.93 ± 0.07	16.13 ± 0.05	2.80	03 51 25.6 +23 45 20.6	
BRB 15	CFHT-PI-25, BPL 303, CFHT-PLIZ-20, (*)	2.70 ± 0.13	19.68 ± 0.07	16.71 ± 0.04	2.98	03 54 05.3 +23 34 00.2	
BRB 16	PIZ 1	–	20.10 ± 0.12 <sup>e</sup>	16.84 ± 0.07	3.26	03 48 31.4 +24 34 37.7	
BRB 17 <sup>a</sup>	(**)	–	20.92 ± 0.07	17.42 ± 0.06	3.50	03 54 08.31 +23 54 33.4	
BRB 18 <sup>a</sup>	CFHT-PLIZ-28, (**)	2.37 ± 0.17	21.20 ± 0.07	17.61 ± 0.07	3.59	03 54 14.08 +23 17 52.2	
BRB 19 <sup>a</sup>	–	2.25 ± 0.14	20.95 ± 0.09	17.79 ± 0.05	3.16	03 54 51.49 +23 45 12.2	
BRB 20 <sup>a</sup>	CFHT-PLIZ-35, (*), (**)	2.55 ± 0.23	21.47 ± 0.06	18.06 ± 0.07	3.40	03 52 39.16 +24 46 29.7	
BRB 21 <sup>a</sup>	(**)	2.34 ± 0.21	21.68 ± 0.08	18.14 ± 0.05	3.54	03 54 10.27 +23 41 40.3	
BRB 22 <sup>a</sup>	CFHT-PLIZ 2141	2.14 ± 0.20	21.97 ± 0.08	18.31 ± 0.05	3.65	03 44 31.27 +25 35 15.1	
BRB 23 <sup>a</sup>	(**)	2.13 ± 0.27	22.03 ± 0.10	18.55 ± 0.10	3.49	03 50 39.53 +25 02 54.5	
BRB 24	(*)	2.95 ± 0.51	22.01 ± 0.09	18.71 ± 0.08	3.30	03 48 19.65 +24 52 09.5	
BRB 25	–	–	22.24 ± 0.09	18.74 ± 0.07	3.50	03 52 59.73 +23 51 56.0	
BRB 26	–	1.93 ± 0.30	22.07 ± 0.08	18.76 ± 0.10	3.31	03 48 56.17 +25 09 43.1	
BRB 27 <sup>a</sup>	CFHT-PLIZ 1262, (**)	2.30 ± 0.32	22.64 ± 0.11	18.89 ± 0.09	3.74	03 44 27.24 +25 44 41.9	
BRB 28 <sup>a</sup>	(*), (**)	2.64 ± 0.45	22.36 ± 0.08	19.02 ± 0.10	3.33	03 52 54.92 +24 37 18.6	
BRB 29 <sup>a</sup>	–	–	22.84 ± 0.10	19.05 ± 0.07	3.79	03 54 01.43 +23 49 58.1	
BRB 30	–	1.98 ± 0.23	22.48 ± 0.10	19.17 ± 0.07	3.31	03 47 56.96 +24 28 58.4	
BRB 31	–	2.50 ± 0.25	23.05 ± 0.10	19.29 ± 0.10	3.76	03 51 25.93 +24 15 32.2	
BRB 32	–	–	22.72 ± 0.12	19.36 ± 0.09	3.36	03 49 00.86 +24 41 38.5	
BRB 33 <sup>a</sup>	–	–	23.31 ± 0.20	19.63 ± 0.09	3.68	03 51 20.15 +23 45 18.4	
BRB 34	–	–	23.01 ± 0.16	19.64 ± 0.09	3.37	03 48 46.55 +24 45 03.2	

<sup>a</sup> With follow-up observation for proper motion measurement (see Table 2).

<sup>b</sup> (\*) (Béjar 2000), CFHT-PI (B98), BPL (Pinfield et al. 2000), MBSC and CFHT-PLIZ (M03), (\*\*) (Bihain et al. 2005), DH (Deacon & Hambly 2004), CFHT-PLIZ (Bouy et al. 2006), HHJ 22 (Hambly et al. 1993), MHOBD 6 (Stauffer et al. 1998a), Teide 2 (Martín et al. 1998a), Roque 16 (Zapatero Osorio et al. 1997b), Calar 3 (Martín et al. 1996), PIZ 1 (Cossburn et al. 1997). In Fig. 1 we overplotted the 14 CFHT-PI objects (open circles) and the 20 other objects (filled circles).

<sup>c</sup> Coordinates of CFHT-PI, CFHT-PLIZ, PIZ 1 and the other objects are from B98, M03, Cossburn et al. (1997) and the present study, respectively.

<sup>d</sup> *J*-band estimate from Martín et al. (2000) because our estimate is bad pixel-contaminated.

<sup>e</sup> *I*-band estimate corrected for a ~0.25 mag reddening due to a close star and ray light traces; the offset was obtained by comparing to objects of similar counts in clean sky areas of the image. Converting the Kitt Peak filter measurement  $I_{KP} = 19.64$  from Cossburn et al. (1997) to Cousins with the transform equation given by Jameson et al. (2002), we find  $I = 19.9$ .

colour–magnitude diagram (B98; see also Fig. 2), the binarity might affect the determination of its short term proper motion and therefore explain its deviance from the cluster peculiar motion. The binarity could also explain some of the magnitude difference observed.

2.  $\langle J_{BRB} - J_{Pinfield} \rangle = 0.04 \pm 0.09$ , for CFHT-PI-2, 3, 4, 7, 9, 11, 12, 13, 21 and 25. CFHT-PI-4 and CFHT-PI-11 present the greatest differences, 0.19 mag and 0.15 mag, respectively. These are also found for 2MASS:  $J_{BRB} - J_{2MASS} = 0.11$  and 0.19, respectively. But CFHT-PI-4 and CFHT-PI-11 have no deviant proper motions or anomalous positions in the colour–magnitude diagram.

Our *I*-band magnitudes rely on an approximate offset to the magnitudes from B98 and have an error of ~0.1 mag. The *I*-band magnitude from B98 is obtained after transformation onto the standard Cousins system, with observation of red Landolt standards. Due to the lack of very red standard stars,

the transformation is linearly extrapolated for the red and faint objects and could produce systematic errors. Comparing our magnitudes to those in the Cousins system from M03, for the candidates in common and 1–2 mag fainter than CFHT-PI-25 (one of the faintest objects from B98), we observe a difference  $I_{BRB} - I_{Moraux} \sim 0.1$ , which is quite small in comparison with the  $I - J > 3.3$  threshold that we applied to select the faint candidates.

Finally, from the 34 BRB Pleiades candidates, the 18 faintest have  $J \gtrsim 17$  and  $I - J \gtrsim 3.3$ , the magnitudes and colours expected for L-type dwarfs.

## 2.2. Follow-up observations

### 2.2.1. *K*<sub>s</sub>-band imaging

Follow-up *K*<sub>s</sub>-band imaging with CAIN-II at the 1.55 m Telescopio Carlos Sánchez (TCS; Teide Observatory, Tenerife)

**Table 2.**  $HK_s$ -band follow-up observations.

Telescope/instrument	Filter(s)	Date	Object(s)	$\langle c \rangle, \langle l \rangle^a$
TCS/CAIN – II	$K_s$	2004 Dec. 7	BRB 17, 18, 21, 23, 26	$\sim 17.6, \sim 18.2$
TCS/CAIN – II	$K_s$	2004 Dec. 8	BRB 20, 28	$\sim 18.1, \sim 18.6$
WHT/LIRIS	$H$	2005 Jan. 23	BRB 17, 23	$\sim 19.5, \sim 20.0$
WHT/LIRIS	$H$	2005 Jan. 24	BRB 20, 28	$\sim 19.0, \sim 19.5$
3.5 m Calar/ $\Omega 2000$	$H$	2005 Feb. 1	BRB 17, 18, 21, Teide 1	$\sim 18.5, \sim 19.3$
TCS/CAIN – II	$K_s$	2005 Mar. 6	BRB 25	$\sim 16.5, \sim 17.0$
WHT/LIRIS	$K_s$	2005 Mar. 25	BRB 27, Teide 1	$\sim 18.8, \sim 19.3$
TCS/CAIN – II	$K_s$	2005 Oct. 17	BRB 19	$\sim 17.5, \sim 18.5$
TCS/CAIN – II	$K_s$	2005 Oct. 18	BRB 22	$\sim 18.0, \sim 19.0$
3.5 m Calar/ $\Omega 2000$	$H$	2005 Oct. 21	BRB 19	$\sim 19.0, \sim 19.5$
TCS/CAIN – II	$K_s$	2005 Oct. 21	BRB 24, 34	$\sim 17.8, \sim 18.8$
3.5 m Calar/ $\Omega 2000$	$H, K_s$	2005 Oct. 22	BRB 22	$\sim 19.0, \sim 19.5$
TCS/CAIN – II	$K_s$	2005 Oct. 22	BRB 29	$\sim 18.0, \sim 19.0$
3.5 m Calar/ $\Omega 2000$	$H$	2005 Oct. 23	BRB 29	$\sim 18.5, \sim 19.0$
TCS/CAIN – II	$K_s$	2005 Oct. 23	BRB 31, 33	$\sim 18.8, \sim 19.5$
3.5 m Calar/ $\Omega 2000$	$K_s$	2005 Oct. 24	BRB 33	$\sim 19.0, \sim 19.5$
3.5 m Calar/ $\Omega 2000$	$H$	2005 Oct. 25	BRB 33	$\sim 19.0, \sim 19.5$
TCS/CAIN – II	$K_s$	2005 Oct. 28	BRB 30, 32	$\sim 18.0, \sim 19.0$

<sup>a</sup> Average completeness and limiting magnitudes.

was performed for all 18  $IJ$ -band photometric substellar candidates (see the observation log in Table 2). The CAIN-II camera has a  $256 \times 256$  HgCdTe Nicmos3 detector with a pixel scale of  $1.00'' \text{ pixel}^{-1}$  in wide field configuration, providing a  $4.2' \times 4.2'$  field of view. The observation macro consisted in 6 s exposures  $\times$  10 repetitions  $\times$  10 dither positions. Total exposure times spanned a range of 10–90 min, depending on the expected brightness of the candidates and the seeing. Data were sky-subtracted, flat-fielded (using sky flats instead of dome flats), aligned and combined in a similar way as for the  $J$ -band data (Sect. 2.1). We also performed the photometry and estimated the completeness and limiting magnitudes as described for the  $J$ -band. On average, about six 2MASS calibrators were used per field. Average completeness and limiting magnitudes during the different nights are indicated in Table 2.

### 2.2.2. $HK_s$ -band imaging for astrometry

For the proper motion determination of the candidates, we obtained subarcsecond  $H$ - and  $K_s$ -band images with the Long-slit Intermediate Resolution Infrared Spectrograph (LIRIS) at the 4.2 m William Herschel Telescope (WHT; Roque de los Muchachos Observatory, La Palma) and  $H$ -band images with  $\Omega 2000$  at the 3.5 m Telescope of CAHA (see Table 2).

We decided also to observe the Pleiades brown dwarf Teide 1 (Rebolo et al. 1995) with both LIRIS and  $\Omega 2000$  to improve its proper motion measurement and to check if there are any systematic errors in the proper motion measurements using different instruments. Our first epoch image was a  $12' \times 12'$  reduced image, obtained with the TEK3 CCD detector ( $0.7'' \text{ pixel}^{-1}$ ) at the prime focus of the 2.5 m Isaac Newton Telescope (INT; Roque de los Muchachos Observatory, La Palma) on 1995 December 19 (Zapatero Osorio 2005, private communication).

The LIRIS camera has a  $1024 \times 1024$  HgCdTe Hawaii detector with a pixel scale of  $0.25'' \text{ pixel}^{-1}$  and a  $4.2' \times 4.2'$  field of view, whereas the  $\Omega 2000$  camera has a  $2048 \times 2048$  HgCdTe Hawaii2 detector with a pixel scale of  $0.45'' \text{ pixel}^{-1}$  and a field of view of  $15.4' \times 15.4'$ . The observation macros consisted of: 5 s exposures  $\times$  18 repetitions  $\times$  5 dithers (LIRIS night

2005 January 23), 5 s exposures  $\times$  12 repetitions  $\times$  5 dithers (LIRIS; January 24), 3 s  $\times$  20 coadds  $\times$  7 dithers ( $\Omega 2000$ ; February 1), 20 s  $\times$  6 repetitions  $\times$  5 dithers (LIRIS; March 25), 2 s  $\times$  20 coadds  $\times$  15 dithers ( $\Omega 2000$ ; October 21, 22 and 23), 2 s  $\times$  15 coadds  $\times$  20 dithers ( $\Omega 2000$ ; October 24) and 3 s  $\times$  15 coadds  $\times$  20 dithers ( $\Omega 2000$ ; October 25). The total exposure times were chosen to achieve enough S/N ( $\geq 20$  in the peak) for precise measurement of the position of the candidates. They ranged between 5 and 40 min, depending on the expected brightness of the candidates and the seeing.

The raw images were first bad-pixel corrected using a bad-pixel mask and the IRAF routine `PROTO.FIXPIX`. The mask was obtained from the flat (sky-flat for LIRIS and dome-flat for  $\Omega 2000$ ) using `NOAO.IMRED.CCDRED.CCDMASK`. The images were then sky-subtracted – sky images were obtained by combining 5–20 consecutive images of similar sky counts – and divided by the flat.

The resulting images were distortion corrected, aligned using 10–20 reference stars and combined. For LIRIS these last three steps were performed with the `LDEDITHER` task within the package `IRAF.LIRIS.LIMAGE` developed by J. A. Acosta-Pulido. For  $\Omega 2000$ , the images were distortion corrected by projecting them on the celestial coordinate grid with `MSCIMAGE`. The grid was obtained by astrometry with the `USNO-A2` catalog and the script `myastrom.cl` from E. Puddu. This script invokes `CCFIND`, that correlates the catalog sources with those in the image, and `CCMAP`, which computes the plate solution. Usually, 50–100 stars were accepted by a Legendre order-4 transformation fit and a rejection threshold of 1.5 sigma, providing a projection transformation with standard deviation  $\sim 0.12''$  in both right ascension and declination. The distortion corrected images of  $\Omega 2000$  were then aligned and combined using the `INTALIGN` task within the LIRIS package.

The  $HK_s$ -band photometry was obtained similarly as for the  $J$ -band data. On average, six and eleven 2MASS calibrators were used per LIRIS and  $\Omega 2000$  field, respectively. The average completeness and limiting magnitudes during the different nights are indicated in Table 2.

**Table 3.** Follow-up  $HK_s$  photometry of the low-mass brown dwarf candidates.

Name	$J$	$I - J \pm \sigma_{I-J}$	$H \pm \sigma_H$	$J - H \pm \sigma_{J-H}$	$K_s \pm \sigma_{K_s}$	$J - K_s \pm \sigma_{J-K_s}$
BRB 17 <sup>a</sup>	17.42	3.50 ± 0.09	16.75 ± 0.02	0.67 ± 0.06	16.20 ± 0.06	1.22 ± 0.08
BRB 18 <sup>a</sup>	17.61	3.59 ± 0.10	16.74 ± 0.06	0.87 ± 0.09	16.08 ± 0.07	1.53 ± 0.09
BRB 19 <sup>a</sup>	17.79	3.16 ± 0.10	16.99 ± 0.05	0.80 ± 0.07	16.67 ± 0.05	1.12 ± 0.07
BRB 20 <sup>a</sup>	18.06	3.40 ± 0.09	17.33 ± 0.05	0.73 ± 0.08	16.56 ± 0.07	1.50 ± 0.10
BRB 21 <sup>a</sup>	18.14	3.54 ± 0.09	17.05 ± 0.07	1.09 ± 0.09	16.39 ± 0.07	1.75 ± 0.09
BRB 22 <sup>a</sup>	18.31	3.65 ± 0.09	17.38 ± 0.04	0.94 ± 0.06	16.69 ± 0.04	1.62 ± 0.06
BRB 23 <sup>a</sup>	18.55	3.49 ± 0.14	17.47 ± 0.06	1.08 ± 0.11	16.65 ± 0.06	1.90 ± 0.11
BRB 24	18.71	3.30 ± 0.12	–	–	17.49 ± 0.07	1.22 ± 0.11
BRB 25	18.74	3.50 ± 0.12	–	–	16.91 ± 0.24	1.83 ± 0.25
BRB 26	18.76	3.31 ± 0.13	–	–	17.81 ± 0.10	0.95 ± 0.14
BRB 27 <sup>a</sup>	18.89	3.74 ± 0.14	–	–	17.16 ± 0.09	1.74 ± 0.12
BRB 28 <sup>a</sup>	19.02	3.33 ± 0.12	17.89 ± 0.05	1.13 ± 0.11	17.00 ± 0.08	2.02 ± 0.13
BRB 29 <sup>a</sup>	19.05	3.79 ± 0.12	17.76 ± 0.05	1.29 ± 0.09	16.88 ± 0.08	2.17 ± 0.11
BRB 30	19.17	3.31 ± 0.12	–	–	17.65 ± 0.09	1.52 ± 0.11
BRB 31	19.29	3.76 ± 0.14	–	–	18.20 ± 0.15	1.09 ± 0.18
BRB 32	19.36	3.36 ± 0.15	–	–	17.42 ± 0.20	1.94 ± 0.22
BRB 33 <sup>a</sup>	19.63	3.68 ± 0.22	18.71 ± 0.07	0.92 ± 0.11	17.87 ± 0.06	1.76 ± 0.11
BRB 34	19.64	3.37 ± 0.18	–	–	18.8 ± 0.5	0.9 ± 0.5

<sup>a</sup> With proper motion measurement.

### 2.3. Proper motion analysis

The proper motion measurements were obtained as follows. First we selected non-saturated and well defined ( $S/N > 10$ ) single objects among all those that appeared within  $\sim 3'$  of a brown dwarf candidate. We measured their centres in the first- and the second-epoch images with the IRAF task CENTER (DIGIPHOT.DAOPHOT package), with a precision of 0.01–0.1 pixels in both image dimensions. For BRB 22 and 33 we used the  $H$ -band  $\Omega 2000$  images as second-epoch images, because they provided greater  $S/N$  for the candidates than the  $\Omega 2000 K_s$ -band images. Then we computed the transformation from second-epoch image to first-epoch image with GEOMAP. For the  $\Omega 2000$  image of Teide 1, we performed a transformation from first- to second-epoch (i.e. from TEK3 to  $\Omega 2000$ ), because the destination image had a wider field and a smaller pixel scale and therefore provided more accurate equatorial astrometry with the USNO-A2 catalog. With GEOMAP we selected the objects whose positions minimized the transformation error and could thus be considered as reference objects. A Legendre function of order 3 was used when more than 12 objects were available, and of order 2 for fewer objects. The error, related to the scatter of these objects, ranged over 0.03–0.15 pixels. For the candidate BRB 23 the error in the  $y$  dimension was as high as 0.6 pixels, because of vertical smearing affecting the object positions in the  $I$ -band image (field CFHT 6). With GEOXYTRAN we used the transformation to predict the candidate position  $(x_{1p}, y_{1p})$  in a first-epoch image, and compared it with the measured one,  $(x_1, y_1)$ , obtaining the pixel shifts  $(\Delta x_1, \Delta y_1) = (x_{1p} - x_1, y_{1p} - y_1)$ . The plate solution of a first-epoch (or destination) image was obtained with the USNO-A2 catalog and the *myasrtrom.cl* script, in a similar way as explained above. Then using WCSSTRAN we converted the shifts in pixels to shifts in equatorial coordinates. Due to the precision of the equatorial astrometry ( $\sigma \sim 0.12''$ ), its error contribution to the proper motion was negligible. But for the LIRIS proper motion measurement of Teide 1, the best first epoch TEK3 fit had a relatively high standard deviation ( $\sigma_{\text{RA}} = 0.6'', \sigma_{\text{DEC}} = 0.7''$ ) and the corresponding proper motion value differed by almost  $\sim 1 \text{ mas yr}^{-1}$  with those derived from less precise fits; thus we added  $\sim 1 \text{ mas yr}^{-1}$  to the proper

motion error in this case. In general, we assumed that the proper motion error was:

$$(\sigma_{\mu_\alpha \cos \delta}, \sigma_{\mu_\delta}) = \left( \frac{f_{\mu_\alpha \cos \delta} (\sigma_{x1}^2 + \sigma_{x2}^2 + \sigma_{tx}^2)}{\Delta t}, \frac{f_{\mu_\delta} (\sigma_{y1}^2 + \sigma_{y2}^2 + \sigma_{ty}^2)}{\Delta t} \right), \quad (1)$$

where  $\sigma_{x1}, y1, x2, y2$  are the errors of the  $(x, y)$  pixel positions in the first- (1) and second-epoch (2) images,  $\sigma_{tx, ty}$  the error of the transformation between these images,  $f_{\mu_\alpha \cos \delta, \mu_\delta}$  the transformation from  $(x, y)$  to (RA, DEC) coordinates, and  $\Delta t$  the time in Julian years between the two epochs of observation.

## 3. Proper motion Pleiades low-mass brown dwarfs

### 3.1. Photometry and proper motion results

The  $HK_s$  magnitudes for the red and faint brown dwarf candidates that we have followed-up are given in Table 3. The  $H$ -band magnitude of BRB 17 is the error-weighted average from the values obtained with  $\Omega 2000$  and LIRIS, and the  $K_s$ -band magnitudes of BRB 22 and 33 are the error-weighted averages from the values obtained with  $\Omega 2000$  and TCS. Our 18 follow-up objects have magnitudes  $20.9 < I < 23.3$ ,  $17.4 < J < 19.6$ , and colours  $3.2 < I - J < 3.8$ ,  $0.7 < J - H < 1.3$  and  $0.9 < J - K_s < 2.2$ . Most of them remain good L dwarf candidates, what supports our  $I - J$  selection criterion. But BRB 24, 26, 30, 31 and 34 present much bluer  $J - K_s$  colours than cluster proper motion members with similar  $J$ -band magnitude (see Fig. 5). Moreover, if they were late L or T dwarfs, they would certainly present much redder  $I - J$  colours ( $> 4 - 5 \text{ mag}$ ). We will assume that these are non-cluster members. Finally BRB 32, with its red  $J - K_s$  and relatively blue  $I - J$  colours, remains a possible cluster member.

The proper motion results obtained for 11 of the brown dwarf candidates and two lithium brown dwarfs (Teide 1 and Calar 3) are listed in Table 4 and are represented by small circles in the vector point diagram of Fig. 3. Because Calar 3 (Martin et al. 1996; Rebolo et al. 1996) is at a few arcminutes from BRB 33, we could also measure its proper motion and found a very good agreement with the measurement of M01. We note that the

**Table 4.** Proper motions of the low-mass brown dwarf candidates and the lithium brown dwarfs Teide 1 and Calar 3.

Name	Instrument	$\mu_\alpha \cos \delta \pm \sigma_{\mu_\alpha \cos \delta}$ (mas yr <sup>-1</sup> )	$\mu_\delta \pm \sigma_{\mu_\delta}$ (mas yr <sup>-1</sup> )
Teide 1	LIRIS	22.5 ± 3.6	-40.5 ± 4.0
Teide 1	Ω2000	19.2 ± 2.5	-45.5 ± 3.4
Calar 3	Ω2000	24.5 ± 2.2	-32.6 ± 2.2
BRB 17	LIRIS	20.9 ± 1.5	-22.8 ± 2.4
BRB 17	Ω2000	17.7 ± 2.9	-20.7 ± 3.1
BRB 18	Ω2000	28.4 ± 2.7	-37.4 ± 2.7
BRB 19	Ω2000	75.7 ± 1.0	-143.9 ± 7.7
BRB 20	LIRIS	21.8 ± 3.0	-48.1 ± 2.0
BRB 21	Ω2000	18.1 ± 3.4	-49.1 ± 4.1
BRB 22	Ω2000	18.8 ± 3.5	-51.9 ± 2.9
BRB 23	LIRIS	29.2 ± 3.0	-25.6 ± 14.7
BRB 27	LIRIS	35.3 ± 3.7	-48.8 ± 2.0
BRB 28	LIRIS	15.1 ± 3.1	-37.4 ± 2.1
BRB 29	Ω2000	26.4 ± 3.3	-48.8 ± 2.9
BRB 33	Ω2000	-4.1 ± 3.0	-5.2 ± 3.7

double-check measurements of Teide 1 and BRB 17 are fully consistent within the statistic errors. In Fig. 3 are represented also: (i) the reference objects used to estimate the proper motions (asterisks), (ii) the circle of radius three times the greatest component of the average proper motion error derived from Table 4 ( $(\langle \sigma_{\mu_\alpha \cos \delta} \rangle, \langle \sigma_{\mu_\delta} \rangle) = (3.0, 4.3)$  mas yr<sup>-1</sup>). This circle is centred on the cluster average proper motion,  $(\mu_\alpha \cos \delta, \mu_\delta) = (19.15 \pm 0.23, -45.72 \pm 0.18)$  mas yr<sup>-1</sup> (Robichon et al. 1999), and we will assume that the objects within are cluster members.

The L dwarf candidates BRB 17, 23 and 27 lie outside the circle in Fig. 3 and their membership is considered uncertain. The proper motion dispersion of the seven objects within this circle is (5.2, 5.9) mas yr<sup>-1</sup>. Subtracted quadratically by the average proper motion error, it yields (4.3, 4.1) mas yr<sup>-1</sup>, as an estimate<sup>2</sup> of the intrinsic velocity dispersion of Pleiades brown dwarfs. This velocity dispersion is at least four times that of Pleiades stars with masses  $\geq 1 M_\odot$  (Jones 1970; Pinfield et al. 1998) and appears consistent with the linear relationship of equipartition of energy, between the velocity dispersion and the inverse square root of the mass for cluster members, as expected in a nearly relaxed cluster (Pinfield et al. 1998 and Fig. 4 therein).

We cannot rule out that some of the *IJ* candidates located close to the region surrounding the circle in Fig. 3 are in fact cluster members (although field contaminants are neither excluded, see Sect. 4.1 and Table 5). This is actually the case of the Pleiades lithium brown dwarf Calar 3, suggesting that the intrinsic velocity dispersion of brown dwarfs could be even greater than our previous estimate. We need further data (for instance from lithium observations) to study the membership of the peculiar *IJ* candidates. Note also the case of CFHT-PI-15 (B98), which has a proper motion of  $(66.5 \pm 8.1, -54.1 \pm 8.1)$  mas yr<sup>-1</sup> (M01), thus located far from the cluster point in the proper motion diagram, although it presents a radial velocity consistent with that of the cluster, Li absorption, H $\alpha$  emission and a red *I - K<sub>s</sub>* colour (Stauffer et al. 1998b; Martín et al. 2000).

However, BRB 19 and BRB 33 appear clearly to be non-proper motion members; BRB 19 has an especially high proper motion. Finally, our error-weighted average estimate for Teide 1 is  $(20.3 \pm 2.1, -43.4 \pm 2.6)$  mas yr<sup>-1</sup>, very close to the cluster proper motion. It also agrees with the measurement obtained

<sup>2</sup> At the cluster distance, it corresponds to a tangential velocity of  $\sim 2.5$  km s<sup>-1</sup>.

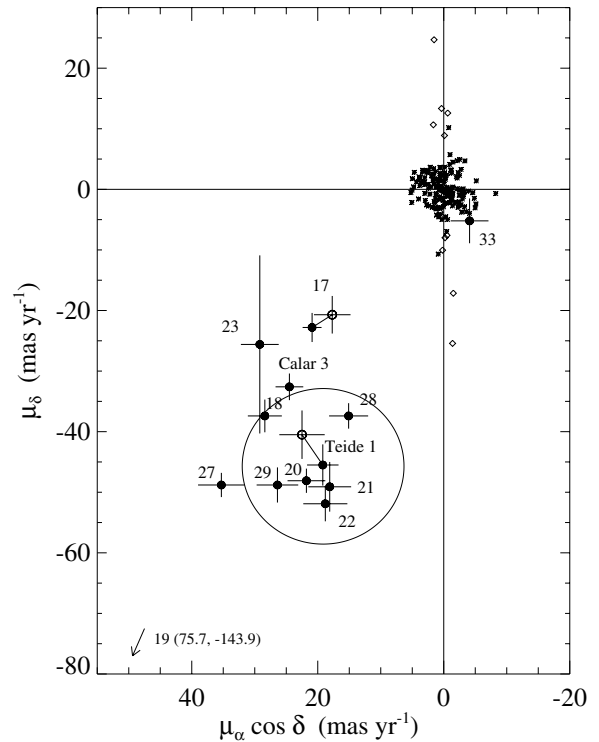


**Fig. 3.** Vector point diagram of proper motion for the candidates (small circles with BRB number indicated) and the reference objects (asterisks). The results for the Pleiades lithium brown dwarfs Teide 1 and Calar 3 are also shown. Double-check objects are linked by a solid line. The plotted large circle is centred on the Pleiades average proper motion (see text for details). The reference objects of BRB 23 (small squares) present a large dispersion in declination which causes the large error bar of this candidate. The arrow plotted for BRB 19 indicates a location outside the diagram.

by Rebolo et al. (1995), the only previous estimate  $(16 \pm 9, -35 \pm 16)$  mas yr<sup>-1</sup>, but with large conservative errors. These measurements, together with the clear lithium detection (Rebolo et al. 1996), thus fully confirm Teide 1 as a Pleiades brown dwarf. Also, the photometry obtained with Ω2000 and LIRIS,  $H = 15.54 \pm 0.06$  and  $K_s = 15.07 \pm 0.09$ , respectively, agrees with that of Jameson et al. (2002),  $H = 15.65 \pm 0.09$  and  $K = 15.08 \pm 0.05$ .

### 3.2. Pleiades L dwarf sequence

In the *J* versus *I - J* colour–magnitude diagram (Fig. 2), the six cluster proper motion members (large filled circles) define the Pleiades L dwarf sequence. Note that the three possible members with relatively high proper motion (circled filled circles) share the same sequence (as well as in the near-IR colour–magnitude diagrams, Figs. 4 and 5).

In Fig. 2 we also present theoretical predictions for the *I* and *J* bandpasses. The solid line corresponds to the DUSTY isochrone and the dash-dotted line corresponds to the NextGen isochrone from Baraffe et al. (1998) for an age 125 Myr. Masses in solar units are shown for the first isochrone. The NextGen model provides a good fit for  $J < 16.0$ – $16.5$  and the DUSTY model provides a good fit for  $J \lesssim 18$ . Both models fail to reproduce the photometric sequence at fainter magnitudes; the former does not account for the onset of dust formation in cooler atmospheres, whereas the latter overestimates the *I - J* colour.



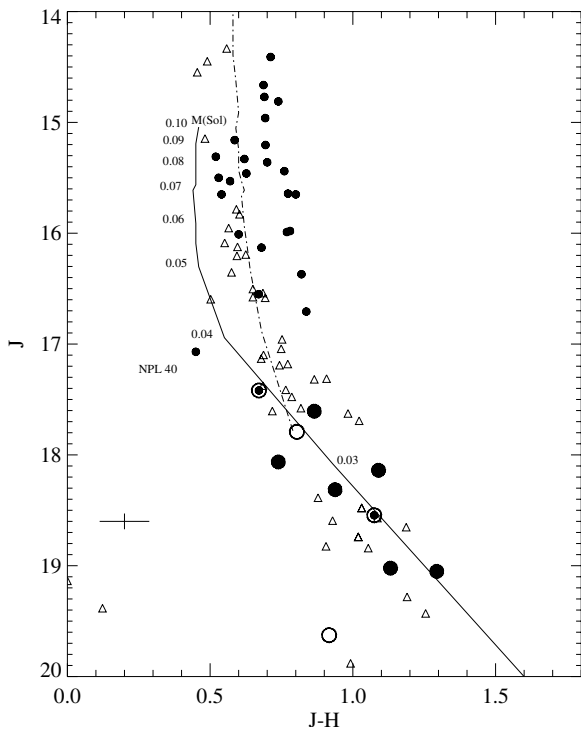


**Fig. 4.**  $J$  versus  $J - H$  colour-magnitude diagram for all the Pleiades very low-mass star and brown dwarf candidates with lithium or proper motion consistent with membership (filled circles). Their photometry was compiled from the present study, Martín et al. (2000), the 2MASS catalog, Zapatero Osorio et al. (1997b), Béjar (2000) and Jameson et al. (2002). The circular symbols ( $J > 17.4$ ), lines and triangles are defined as in Fig. 2. The typical error bars for the probable and possible cluster members by proper motion are represented on the left.

Also in Fig. 2 we show the sequence of field dwarfs (triangles) with parallactic distances, translated to the distance of the Pleiades cluster. These nearby cool dwarfs are compiled from the literature by Caballero (2006). Their  $I$ - and  $JHK_s$ -band photometry are from Dahn et al. (2000, 2002) and the 2MASS Point Source Catalog, respectively. For the M dwarfs, the parallaxes are from Dahn et al. (2000, 2002) and the spectral types are from Golimowski et al. (2004), Leggett et al. (2000, 2002) and Dahn et al. (2002). For the L and T dwarfs, the parallaxes are from Perryman et al. (1997), Dahn et al. (2002) and Vrba et al. (2004), and the spectral types are mostly from Vrba et al. (2004), else from Leggett et al. (2002) and Geballe et al. (2001). In Fig. 2 the spectral types range over  $\sim M3$ – $T2$  from top to bottom. At magnitudes  $J < 17$  the field dwarfs are bluer than the cluster brown dwarfs, but at  $J > 17$  the field sequence begins to intercept that of the cluster and to follow it slightly towards redder colours.

In the  $J$  versus  $J - H$  and  $J - K$  diagrams (Figs. 4 and 5), we show the Pleiades very low-mass stars and brown dwarf candidates having lithium in their atmospheres or proper motions consistent with membership in the cluster (filled circles). The circular symbols ( $J > 17.4$ ), lines and triangles are defined as in Fig. 2. The DUSTY and NextGen isochrones provide relatively good colour predictions for  $J > 17$  and  $J < 17$ , respectively, in both diagrams. The fact that the DUSTY model agrees with the observations in the  $J$  versus  $J - H$  and  $J - K$  diagrams but not in the  $J$  versus  $I - J$  diagram supports the possible underestimation of the far red flux ( $I$  band) relative to the near-IR flux ( $J$ -,  $H$ - and  $K$  bands). In Fig. 4, the M9 Pleiades brown dwarf

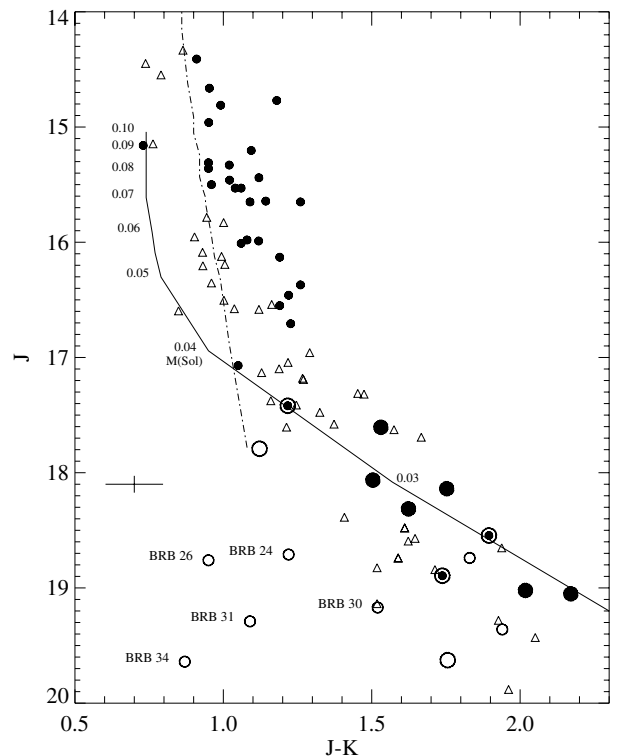


**Fig. 5.**  $J$  versus  $J - K$  colour-magnitude diagram, with the same definition of symbols and error bars as in Fig. 4. The small empty circles represent the  $IJ$  candidates without proper motion measurements.

NPL 40 (Festin 1998a,b) has a very blue  $J - H$  colour, as noted by Pinfield et al. (2003). In Fig. 5, the brown dwarf CFHT-PI-7, with its magnitude  $J = 15.16$  probably enhanced by a cosmic ray, is positioned at the left of the upper sequence, and the five very blue candidates at  $J > 18.5$  (empty circles) are probable contaminants.

In these near-IR colour-magnitude diagrams, where field dwarfs are also represented ( $\sim M3$ – $L6$ ), similar sequence overlaps appear at  $J > 17$  as in the  $J$  versus  $I - J$  diagram. Thus the sequence of the L brown dwarf candidates of the Pleiades is nearly indistinguishable from that of the field dwarfs shifted to the cluster distance. Note that the average errors in the distances of the sample field dwarfs are  $\langle \sigma_d \rangle = 0.4$  pc ( $M5$ – $M9$ ) and 1.0 pc ( $L0$ – $L7$ ), and the average errors in their translated  $J$ -band magnitudes, including the photometric errors and the distance error of 3 pc for the Pleiades cluster, is of only 0.08 and 0.12 mag, respectively. The average error in their  $I - J$  colours is 0.03 mag ( $M5$ – $M9$ ) and 0.06 mag ( $L0$ – $L7$ ). These magnitude and colour errors are small in comparison to the (field and cluster) trends observed.

From the  $J$  versus  $I - J$ ,  $J - H$  and  $J - K$  diagrams it appears that, opposite to the Pleiades late M dwarfs, many of the Pleiades L dwarf candidates have the same colours and absolute magnitudes as their field counterparts. This suggests that they may have the same spectral energy distributions and luminosities. If the effective temperatures estimated from the spectral energy distribution do not depend much on the gravity (as indicated by spectral synthesis), then, they may have also the same effective temperatures. These objects would therefore have the same radii. From Allen et al. (2005), the mean age of field L dwarfs is in the range 3–4 Gyr and the mean mass is in the range  $0.06$ – $0.07 M_\odot$ , which according to the DUSTY models imply radii of  $\sim 0.09 R_\odot$ .

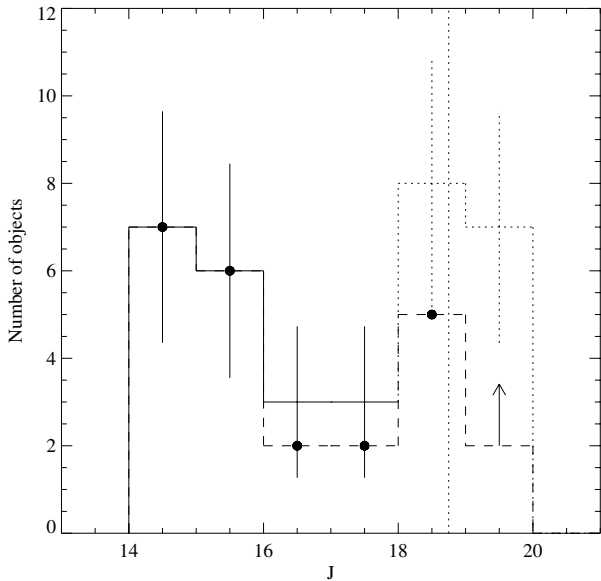


**Fig. 6.** Luminosity function for all the survey candidates (solid and dotted lines) and after contaminant correction (dashed line). The vertical dotted line represents the completeness limit of the survey.

These objects have almost reached the end of the contraction. We note however, that according to the same models (and using the luminosity estimates from Sect. 5), the radii of the Pleiades L brown dwarf candidates are of  $\sim 0.125 R_{\odot}$ , a value inconsistent with the previous one. Either the predicted evolution of radii with time may have to be revisited by the models, so the Pleiades L dwarfs reach radii of  $0.09 R_{\odot}$  in about 120 Myr or, the estimated masses and ages of the field L dwarfs may require a revision toward higher masses or smaller ages. A determination of the radii from the luminosities and the effective temperatures require precise spectroscopic observations which are beyond the scope of the present study.

#### 4. Substellar luminosity function

The  $J$ -band luminosity function, the number of objects versus bin of  $J$ -band magnitude, is represented in Fig. 6 for BRB 1–34, our Pleiades very low-mass star and brown dwarf  $IJ$ -band candidates ( $J < 18$ : solid line,  $J > 18$ : dotted line). The error bars are Poissonian errors, i.e. the square root of the number of candidates per bin. The vertical dotted line delimits the completeness of the survey, at  $J \sim 18.75$ . For this and fainter magnitudes, the present luminosity function is incomplete (dotted line).

##### 4.1. Contaminants

The number of field M and L dwarfs that may contaminate our sample is obtained as follows. First we subdivide the region in the  $J$  versus  $I - J$  diagram occupied by the 34 objects of Table 1 in small rectangular sections. These sections have heights of half  $J$ -band magnitude and widths delimited by the bluer envelope (dashed line in Fig. 2) and the reddest object.

Then, we consider the typical  $I - J$  colours of M- and L-type dwarfs as a function of the spectral type, based on the same sample of nearby cool dwarfs as mentioned in Sect. 3.2. Contaminants in our survey are essentially M5–L4 dwarfs. Using the relation from Dahn et al. (2002) between the spectral type of M7–L8 dwarfs and the maximum distance at which they

can be observed for a given  $J$ -band magnitude (a relation that we assume also valid for M5 and M6 dwarfs), we compute for any spectral type contaminating a given rectangular section the pair of distances associated to the  $J$ -band magnitude boundaries of the section. Each pair of distances defines a volume towards the Pleiades, e.g. a truncated right pyramid with a square base, with top and base surfaces subtended by the survey angular area,  $1.8 \text{ deg}^2$ . This volume is located at the average of the pair of distances ( $\langle d \rangle$ ).

We use the densities of dwarfs in the solar neighbourhood provided by Kirkpatrick et al. (1994) for M5 and M6 spectral types, and by Cruz et al. (2003) for M7–L4 at  $d < 20 \text{ pc}$ . We take into account the completeness and sky coverage of these surveys. Chen et al. (2001) studied the star counts of the Sloan Digital Sky Survey for several hundred thousands stars at high latitudes north and south of the Galactic plane. They obtain an exponential scale height of the old thin disk of  $330 \pm 3 \text{ pc}$  (late-type stars) and a Sun’s distance from the plane of  $27 \pm 4 \text{ pc}$ . We assume that this scale height applies also for early L dwarfs. To compute the numerical density of a given spectral type dwarf at an average distance  $\langle d \rangle$  from the Sun, we multiply the solar neighbourhood density by an exponential  $\exp(-(|\langle d \rangle \sin(b_{\text{Pl}}) - z_{\odot}|/z_{\text{h}}))$ , where  $z_{\text{h}}$  is the scale height,  $z_{\odot}$  the Sun’s distance to the Galactic plane,  $b_{\text{Pl}} = -23.52^{\circ}$  the Pleiades cluster’s galactic latitude.

Finally we multiply the volumes by the corresponding densities and obtain the statistical numbers of contaminants. Each section in the  $J$  versus  $I - J$  diagram is thus contaminated by field dwarfs of different spectral types at different distances and with different densities. In Table 5, we summarize our estimate of contaminants. In the first column we indicate the  $J$ -mag range, in Col. “ $N_{\text{can}}$ ”, the number of  $IJ$  candidates (including CFHT-PLIZ-25 and CFHT-PLIZ-25) and in Col. “Confirmed”, the BRB numbers of the proper motion and lithium Pleiades members. In the next three columns, we give the estimated numbers of contaminants for the spectral type ranges M5–M7, M8–M9 and L0–L4. In Col. “total”, the total number of contaminants is provided for the entire spectral type range M5–L4. Nine contaminants are already found (Col. “Contaminants found”): (i) CFHT-Pl-8 (M01), CFHT-PLIZ-25 (M03), BRB 19 and BRB 33; (ii) BRB 24, 26, 30 31 and 34. The first set of objects is found by proper motion measurements and the second set by  $J - K_{\text{s}}$  photometry (Col. “Measurement”). The numbers of contaminants found in each spectral type range are indicated in parenthesis. Subtracting these from the total number of contaminants, we obtain the number of remaining contaminants that we may find among our survey candidates (Col. “ $N_{\text{r.c.}}$ ”).

After correcting the number of  $IJ$  candidates for contaminants in each  $J$ -mag range, we find an agreement with the number of confirmed Pleiades members, except for 15.0–16.0 and 19.0–20.0 mag. In these ranges one more contaminant than observed is predicted. For the latter range, this can be explained by its incompleteness. In both cases, we assume the observed number of confirmed members as the effective value when deriving the effective luminosity and mass functions, thus decreasing by one the value of  $N_{\text{r.c.}}$ . In Fig. 6, the effective luminosity function is represented by the dashed histogram.

#### 5. Substellar mass function

Finally, we present the implications of our results in the substellar mass function of the cluster surveyed area. The bolometric luminosity and effective temperature predictions of the DUSTY and NextGen models are mostly independent of the atmospheric properties (Chabrier et al. 2000), in contrast to the predicted

**Table 5.** Contaminants among our low-mass star and substellar candidates.

$J$ range	$N_{\text{can}}^a$	Confirmed <sup>b</sup> (Li or pm)	Estimated numbers of contaminants				Contaminants found	Measurement	$N_{\text{r.c.}}^c$
			M5–M7	M8–M9	L0–L4	total			
14.5–15.0	7 <sup>d</sup>	1, 2, 3, 5, 6, 7	0.3	–	–	0.3	–	–	0
15.0–16.0	7	8, 9, 10, 11, 12, 13	1.6(1)	–	–	1.7	CFHT-PI-18	prop. mot.	1
16.0–17.0	3	14, 15	0.8	0.3	0.1	1.2	–	–	1
17.0–18.0	4	17, 18	–	1.3(2)	0.3	1.6	CFHT-PLIZ-25, BRB 19	prop. mot.	0
18.0–19.0	8	20, 21, 22, 23, 27	–	1.7(2)	1.3	3.0	BRB 24, 26	$J - K_s$	1
(19.0–20.0)	7	28, 29	–	2.0(2)	3.8(2)	5.9	BRB 30, 31, 33, 34	$J - K_s$ , prop. mot.	2

<sup>a</sup> Including CFHT-PI-18 and CFHT-PLIZ-25.

<sup>b</sup> BRB number.

<sup>c</sup> We assume only 0 and 1 contaminants that remain to be found in the  $J$  ranges 15.0–16.0 and 19.0–20.0, respectively, when deriving the effective luminosity and mass functions (see text, Sect. 4.1).

<sup>d</sup> Including BRB 1 which has  $J = 14.41$ .

**Table 6.** Mass bins for our mass function.

$\Delta J$	$\Delta M$ ( $M_{\odot}$ )	$N_{\text{BRB}}$	$N_{\text{cont}}$	$N_{\text{eff}}$
14.41–14.97	0.147–0.104	6	0	6
14.97–15.57	0.104–0.075	5	0	5
15.57–17.51	0.075–0.039	6	1	5
17.51–18.75	0.039–0.026	8	3	5
(18.75–19.65)	0.026–0.018	9	6	3

magnitudes (e.g. for the M–L transition), which are not. We decided to infer a bolometric luminosity using a  $J$ -band bolometric correction and then to compare it with the model prediction for the distance and age of the Pleiades to obtain the mass.

Adopting the Pleiades cluster distance from Percival et al. (2005), we convert the  $J$ -band magnitudes to absolute magnitudes  $M_J$ , and add a bolometric correction  $BC_J$  depending on  $I - J$ . This bolometric correction is obtained by Caballero (2006) from a fit to  $(M_{\text{bol}} - M_J, I - J)$  of the nearby cool dwarfs mentioned in Sect. 3.2. Binaries, peculiar dwarfs and dwarfs with line emission are not taken into account in the fit. For the nearby M dwarfs, the bolometric magnitudes are from Golimowski et al. (2004), Leggett et al. (2000, 2002) and Dahn et al. (2002). For the nearby L and T dwarfs, these are mostly from Vrba et al. (2004), else from Leggett et al. (2002) and Geballe et al. (2001). The bolometric magnitudes  $M_{\text{bol}} = M_J + BC_J$  that we obtained are then normalized to the solar value  $M_{\text{bol},\odot} = 4.74$  (Livingston 2002) and converted to luminosities. Using these luminosities, we interpolate linearly the theoretical data points (DUSTY model for BRB 8–34 and NextGen model for BRB 1–7) and obtain the masses. These are grouped into five bins: two low-mass stellar and three substellar bins (see Table 6). The lowest mass bin is incomplete ( $J \gtrsim 18.75$ ). The differences between the masses derived from the bolometric luminosities of the NextGen- and DUSTY models for the fainter objects BRB 8–22, which extend into the lower luminosity range of the NextGen model, are smaller than  $0.002 M_{\odot}$  and do not affect the distribution of objects in these bins. Each bin contains numbers of BRB candidates ( $N_{\text{BRB}}$ ) and contaminants ( $N_{\text{cont}}$ ), identifiable from Tables 1 and 5. The width of the mass bins within the completeness of the survey is such that each bin contains approximately the same effective number of objects,  $N_{\text{eff}} = N_{\text{BRB}} - N_{\text{cont}}$ .

In Fig. 7, we show our results in the mass spectrum representation,  $\log dN/dM$ ,  $\log M$ . Error bars refer to the Poissonian error. We show also the bins for the  $\sim 50$  massive proper motion Pleiades objects from Deacon & Hambly (2004) which

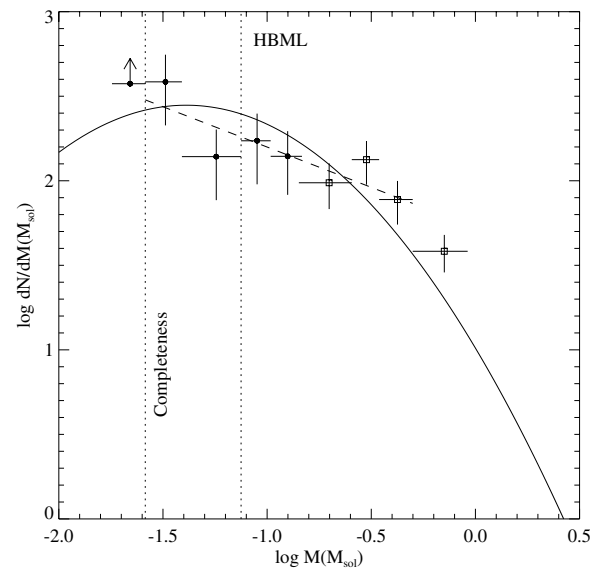


**Fig. 7.** The derived mass function for the Pleiades survey area. The filled circles are for the BRB objects, whereas the squares are for the objects from Deacon & Hambly (2004). The right dotted line indicates the hydrogen-burning mass limit. The lower limit arrow for the lowest mass bin indicates that this bin is incomplete. The curve represents the log normal function obtained by Deacon & Hambly (2004) scaled down to the total number of objects in the survey area and between  $0.5 M_{\odot}$  and the completeness mass limit  $0.026 M_{\odot}$  (56). The dashed line represents the power law fit to the data points between  $0.5$  and  $0.026 M_{\odot}$ , with  $\alpha = 0.5 \pm 0.2$ .

are present in our fields<sup>3</sup>. For the  $\sim 35$  fainter objects, corresponding essentially to M dwarfs ( $T_{\text{eff}} \lesssim 3600$  K), we obtain the masses with the method explained above, but using  $I$ - and  $J$ -band magnitudes from Deacon & Hambly (2004) and 2MASS, respectively, because these objects are saturated in our images. For the brighter ones we proceed similarly but, this time, using a synthetic  $K$ -band bolometric correction, function of the  $(J - K)_{\text{CIT}}$  colour and determined by Houdashelt et al. (2000) for FGK stars with  $4000 \text{ K} \leq T_{\text{eff}} \leq 6500 \text{ K}$ . We assume solar metallicity and  $\log g = 4$ . The CIT colour is transformed into the 2MASS equivalent (see the Explanatory Supplement to

<sup>3</sup> The objects in common with our sample, DH 765 and DH 590, are taken into account only once and in our mass spectrum bins.

the 2MASS All Sky Data Release<sup>4</sup>, Cutri et al. 2006) and the bolometric correction is applied on 2MASS  $JK_s$ -band photometry. For the objects in the  $K-M$  transition, the masses obtained by any of these two methods are within the highest mass bin ( $M > 0.5 M_\odot$ ), thus fixing the number of objects in this bin. A linear fit to all the data points between 0.5 and  $0.026 M_\odot$  provides an  $\alpha = 0.5 \pm 0.2$  for the power law  $dN/dM \propto M^{-\alpha}$ . It is compatible with the mass bin beyond the completeness limit of the survey (lower limit arrow at the left of the vertical dotted line, Fig. 7), defined by the three lowest mass possible or probable cluster members by proper motion, BRB 27, 28 and 29. Our estimate of  $\alpha$  is in agreement with that from M03,  $0.60 \pm 0.11$ , and signifies that the number of objects per unit mass still increases at these low masses. In Fig. 7 the lognormal function obtained by Deacon & Hambly (2004) is also represented, scaled down so that its integral over the mass range  $0.5-0.026 M_\odot$  is equal to the number of objects in the survey area and in this mass range (56).

Our estimate of  $\alpha$  is similar to those for younger clusters as  $\alpha$  Per ( $\sim 80$  Myr), IC 4665 (30–100 Myr) and  $\lambda$  Orionis ( $\sim 5$  Myr). Their values are:  $0.56$  ( $0.2 > M(M_\odot) > 0.06$ ; Barrado y Navascués et al. 2002),  $0.6$  ( $1 > M(M_\odot) > 0.04$ ; de Wit et al. 2006) and  $0.60 \pm 0.06$  ( $0.86 > M(M_\odot) > 0.024$ ; Barrado y Navascués et al. 2004), respectively. The presence of low-mass brown dwarfs after more than 100 Myr in the Pleiades open cluster, in numbers relative to stars which are similar to those found in other younger clusters, implies that differential evaporation of low-mass members relative to more massive ones has not been very significant – in contrast to what may occur in the  $\sim 600$  Myr old Praesepe open cluster (Chappelle et al. 2005). Comparison of observations to evolutionary models of the Pleiades cluster suggests indeed that only marginal differential evaporation of the massive brown dwarfs has occurred (Moraux et al. 2004; Moraux & Clarke 2005). Therefore searches for the lowest mass brown dwarfs and even planetary-mass objects should be conducted. A Pleiades giant planetary-mass object at the deuterium-burning mass limit has a predicted effective temperature of  $\sim 1300$  K (DUSTY and COND models). This effective temperature corresponds to late L and early T field dwarfs (Golimowski et al. 2004) and magnitudes  $J > 20$  (Knapp et al. 2004) when scaled to the distance of the cluster. Such a free-floating object in the Pleiades open cluster may be detected in a photometric search with mid-size telescopes ( $\sim 4$  m) but spectroscopic classification will require a very large telescope of 8–10 m class. The discovery of such low-mass Pleiades objects will permit to compare with free-floating low-gravity candidates in the solar neighbourhood, as for example the T6 brown dwarf SDSS J111010.01+011613.1 (Knapp et al. 2004). Extrapolating the mass spectrum slope to lower masses, we find that our survey area may contain five brown dwarfs with masses  $0.026-0.013 M_\odot$  and four planetary-mass objects with masses  $0.013-0.05 M_\odot$  (or two per square degree). In the case where the mass spectrum is log normal down to planetary masses, these values drop to three and one, respectively (or one planetary-mass object per square degree).

## 6. Conclusions

As a result of an  $IJ$ -band survey in the Pleiades, we have found 18 brown dwarf candidates, most likely of L-type. They have  $17.4 < J < 19.7$ ,  $I - J > 3.2$  and theoretical masses  $\sim 0.040-0.020 M_\odot$ . The near-IR follow-up for proper motion

of 11 candidates permits us to confirm six as cluster members. Another three remain as possible members. Two are clear non-members. The near-IR photometric follow-up of the seven other candidates indicates that at least five are probable contaminants, because their  $J - K_s$  colours are bluer than those of the cluster proper motion members. These latter determine the L brown dwarf photometric sequence of the Pleiades. The sequence in the  $J$  versus  $I - J$  colour-magnitude diagram at  $J > 18$  is bluer than that predicted by the DUSTY atmospheres model, whereas it agrees with the predictions in the  $J$  versus  $J - H$  and  $J - K$  diagrams. Moreover the sequence overlaps that of the field L dwarfs shifted to the cluster distance in the three colour-magnitude diagrams, suggesting that the Pleiades and field L dwarfs may have comparable spectral energy distributions and luminosities, and thus possibly similar radii.

We find evidence for an intrinsic velocity dispersion of Pleiades brown dwarfs at least four times that of Pleiades stars more massive than the Sun. The estimated value  $> 4$  mas yr<sup>-1</sup> appears consistent with the kinematical expectations for brown dwarfs in a nearly relaxed cluster.

Correcting for contaminants and comparing with the proper motion objects from Deacon & Hambly (2004) in the same fields, we obtain a substellar mass spectrum for the surveyed area of the cluster. For a power law  $dN/dM \propto M^{-\alpha}$  fit in the mass range  $0.5-0.026 M_\odot$ , we find a spectral index  $\alpha = 0.5 \pm 0.2$  and in agreement with previous results. The slope is similar to that of much younger open clusters, suggesting the absence of significant differential evaporation of the low-mass brown dwarfs in the Pleiades. This supports deeper searches to detect lower mass free-floating objects in the cluster.

*Acknowledgements.* The 3.5 m Telescope is operated jointly by the Max-Planck Institut für Astronomie and the Instituto de Astrofísica de Andalucía (CSIC) at the Centro Astronómico Hispano Alemán (CAHA) at Calar Alto. The Canada-France-Hawaii Telescope (CFHT) is operated by the National Research Council of Canada, the Institut National des Sciences de l'Univers of the Centre National de la Recherche Scientifique of France, and the University of Hawaii. The William Herschel Telescope (WHT) is operated on the island of La Palma by the Isaac Newton Group in the Spanish Observatorio del Roque de los Muchachos of the Instituto de Astrofísica de Canarias. The Carlos Sánchez Telescope (TCS) is operated by the Instituto de Astrofísica de Canarias at the Teide Observatory, Tenerife. This publication makes use of data products from the Two Micron All Sky Survey, which is a joint project of the University of Massachusetts and the Infrared Processing and Analysis Center/California Institute of Technology, funded by the National Aeronautics and Space Administration and the National Science Foundation. We would like to thank J. Bouvier for allowing us to use the  $RI$ -band data and for refereeing this paper. We thank Terry Mahonay for the English corrections. The LIRIS observations were obtained with the assistance and help of the LIRIS commissioning team. We thank J. I. González Hernández and I. Villo for obtaining near-IR data for us, during LIRIS night 2005 January 24 and  $\Omega 2000$  night 2005 February 1, respectively. We thank also N. Deacon, H. Bouy, E. Martín, M. R. Zapatero Osorio and E. Delgado-Donate for valuable discussions. J.A.P. & A.M. acknowledge the Plan Nacional de Astronomía y Astrofísica (AYA2004-03136), which supported part of this work.

## References

- Allen, P. R., Koerner, D. W., Reid, I. N., & Trilling, D. E. 2005, *ApJ*, 625, 385
- Baraffe, I., Chabrier, G., Allard, F., & Hauschildt, P. H. 1998, *A&A*, 337, 403
- Barrado y Navascués, D., Bouvier, J., Stauffer, J. R., Lodieu, N., & McCaughrean, M. J. 2002, *A&A*, 395, 813
- Barrado y Navascués, D., Stauffer, J. R., Bouvier, J., Jayawardhana, R., & Cuillandre, J.-C. 2004, *ApJ*, 610, 1064
- Basri, G. 2000, *ARA&A*, 38, 485
- Béjar, V. J. S. 2000, Ph.D. Thesis, Universidad de La Laguna
- Béjar, V. J. S., Martín, E. L., Zapatero Osorio, M. R., et al. 2001, *ApJ*, 556, 830
- Bihain, G., Rebolo, R., Béjar, V. J. S., et al. 2005, *Astron. Nachr.*, 326, 1057
- Bouvier, J., Stauffer, J. R., Martín, E. L., et al. 1998, *A&A*, 336, 490
- Bouy, H., Moraux, E., Bouvier, J., et al. 2006, *ApJ*, 637, 1056
- Burgasser, A. J., Kirkpatrick, J. D., Brown, M. E., et al. 2002, *ApJ*, 564, 421
- Caballero, J. A. 2006, Ph.D. Thesis, Universidad de La Laguna

<sup>4</sup> <http://www.ipac.caltech.edu/2mass/releases/allsky/doc/explsup.html>

- Chabrier, G., & Baraffe, I. 2000, *ARA&A*, 38, 337
- Chabrier, G., Baraffe, I., Allard, F., & Hauschildt, P. 2000, *ApJ*, 542, 464
- Chappelle, R. J., Pinfield, D. J., Steele, I. A., Dobbie, P. D., & Magazzù, A. 2005, *MNRAS*, 361, 1323
- Chen, B., Stoughton, C., Smith, J. A., et al. 2001, *ApJ*, 553, 184
- Cosburn, M. R., Hodgkin, S. T., Jameson, R. F., & Pinfield, D. J. 1997, *MNRAS*, 288, L23
- Cruz, K. L., Reid, I. N., Liebert, J., Kirkpatrick, J. D., & Lowrance, P. J. 2003, *AJ*, 126, 2421
- Cutri, R. M., Skrutskie, M. F., van Dyk, S., et al. 2003, *VizieR Online Data Catalog*, 2246, 0
- Dahn, C. C., Guetter, H. H., Harris, H. C., et al. 2000, in *ASP Conf. Ser.*, 212, *From Giant Planets to Cool Stars*, 74
- Dahn, C. C., Harris, H. C., Vrba, F. J., et al. 2002, *AJ*, 124, 1170
- de Wit, W. J., Bouvier, J., Palla, F., et al. 2006, *A&A*, 448, 189
- Deacon, N. R., & Hambly, N. C. 2004, *A&A*, 416, 125
- Dobbie, P. D., Kenyon, F., Jameson, R. F., et al. 2002, *MNRAS*, 335, 687
- Festin, L. 1998a, *A&A*, 333, 497
- Festin, L. 1998b, *MNRAS*, 298, L34
- Geballe, T. R., Saumon, D., Leggett, S. K., et al. 2001, *ApJ*, 556, 373
- Golimowski, D. A., Leggett, S. K., Marley, M. S., et al. 2004, *AJ*, 127, 3516
- Hambly, N. C., Hawkins, M. R. S., & Jameson, R. F. 1993, *A&AS*, 100, 607
- Hambly, N. C., Hodgkin, S. T., Cosburn, M. R., & Jameson, R. F. 1999, *MNRAS*, 303, 835
- Houdashelt, M. L., Bell, R. A., & Sweigart, A. V. 2000, *AJ*, 119, 1448
- Jameson, R. F., Dobbie, P. D., Hodgkin, S. T., & Pinfield, D. J. 2002, *MNRAS*, 335, 853
- Jones, B. F. 1970, *AJ*, 75, 563
- Kirkpatrick, J. D., McGraw, J. T., Hess, T. R., Liebert, J., & McCarthy, D. W. 1994, *ApJS*, 94, 749
- Kirkpatrick, J. D., Reid, I. N., Liebert, J., et al. 2000, *AJ*, 120, 447
- Knapp, G. R., Leggett, S. K., Fan, X., et al. 2004, *AJ*, 127, 3553
- Leggett, S. K., Allard, F., Dahn, C., et al. 2000, *ApJ*, 535, 965
- Leggett, S. K., Golimowski, D. A., Fan, X., et al. 2002, *ApJ*, 564, 452
- Livingston, W. C. 2002, in *Allen's Astrophysical Quantities*, ed. A. N. Cox (4th ed.; New York: Springer), 151
- Martin, E. L., Rebolo, R., & Zapatero-Osorio, M. R. 1996, *ApJ*, 469, 706
- Martín, E. L., Basri, G., Gallegos, J. E., et al. 1998a, *ApJ*, 499, L61
- Martín, E. L., Basri, G., Zapatero Osorio, M. R., Rebolo, R., & López, R. J. G. 1998b, *ApJ*, 507, L41
- Martín, E. L., Delfosse, X., Basri, G., et al. 1999, *AJ*, 118, 2466
- Martín, E. L., Brandner, W., Bouvier, J., et al. 2000, *ApJ*, 543, 299
- Moraux, E., & Clarke, C. 2005, *A&A*, 429, 895
- Moraux, E., Bouvier, J., & Stauffer, J. R. 2001, *A&A*, 367, 211
- Moraux, E., Bouvier, J., Stauffer, J. R., & Cuillandre, J.-C. 2003, *A&A*, 400, 891
- Moraux, E., Kroupa, P., & Bouvier, J. 2004, *A&A*, 426, 75
- Nagashima, C., Dobbie, P. D., Nagayama, T., et al. 2003, *MNRAS*, 343, 1263
- Padoan, P., & Nordlund, Å. 2004, *ApJ*, 617, 559
- Percival, S. M., Salaris, M., & Groenewegen, M. A. T. 2005, *A&A*, 429, 887
- Perryman, M. A. C., Lindgren, L., Kovalevsky, J., et al. 1997, *A&A*, 323, L49
- Pinfield, D. J., Jameson, R. F., & Hodgkin, S. T. 1998, *MNRAS*, 299, 955
- Pinfield, D. J., Hodgkin, S. T., Jameson, R. F., et al. 2000, *MNRAS*, 313, 347
- Pinfield, D. J., Dobbie, P. D., Jameson, R. F., et al. 2003, *MNRAS*, 342, 1241
- Rebolo, R., Zapatero Osorio, M. R., & Martín, E. L. 1995, *Nature*, 377, 129
- Rebolo, R., Martín, E. L., Basri, G., Marcy, G. W., & Zapatero Osorio, M. R. 1996, *ApJ*, 469, L53
- Robichon, N., Arenou, F., Mermilliod, J.-C., & Turon, C. 1999, *A&A*, 345, 471
- Schwartz, M. J., & Becklin, E. E. 2005, *AJ*, 130, 2352
- Stauffer, J. R., Schild, R., Barrado y Navascues, D., et al. 1998a, *ApJ*, 504, 805
- Stauffer, J. R., Schultz, G., & Kirkpatrick, J. D. 1998b, *ApJ*, 499, L199
- Tej, A., Sahu, K. C., Chandrasekhar, T., & Ashok, N. M. 2002, *ApJ*, 578, 523
- Vrba, F. J., Henden, A. A., Luginbuhl, C. B., et al. 2004, *AJ*, 127, 2948
- Zapatero Osorio, M. R., Rebolo, R., & Martín, E. L. 1997a, *A&A*, 317, 164
- Zapatero Osorio, M. R., Rebolo, R., Martín, E. L., et al. 1997b, *ApJ*, 491, L81
- Zapatero Osorio, M. R., Rebolo, R., Martín, E. L., et al. 1999, *A&AS*, 134, 537

## Candidate free-floating super-Jupiters in the young $\sigma$ Orionis open cluster

G. Bihain<sup>1,2</sup>, R. Rebolo<sup>1,2</sup>, M. R. Zapatero Osorio<sup>1</sup>, V. J. S. Béjar<sup>1</sup>, I. Villó-Pérez<sup>3</sup>, A. Díaz-Sánchez<sup>3</sup>, A. Pérez-Garrido<sup>3</sup>, J. A. Caballero<sup>4</sup>, C. A. L. Bailer-Jones<sup>5</sup>, D. Barrado y Navascués<sup>6,7</sup>, J. Eislöffel<sup>8</sup>, T. Forveille<sup>9</sup>, B. Goldman<sup>5</sup>, T. Henning<sup>5</sup>, E. L. Martín<sup>1,10</sup>, and R. Mundt<sup>5</sup>

<sup>1</sup> Instituto de Astrofísica de Canarias, c/ vía Láctea, s/n, 38205 La Laguna, Tenerife, Islas Canarias, Spain  
e-mail: gbihain@ll.iac.es

<sup>2</sup> Consejo Superior de Investigaciones Científicas, Spain

<sup>3</sup> Universidad Politécnica de Cartagena, Campus Muralla del Mar, 30202 Cartagena, Murcia, Spain

<sup>4</sup> Dpto. de Astrofísica y Ciencias de la Atmósfera, Facultad de Física, Universidad Complutense de Madrid, 28040 Madrid, Spain

<sup>5</sup> Max-Planck-Institut für Astronomie, Königstuhl 17, 69117 Heidelberg, Germany

<sup>6</sup> Laboratorio de Astrofísica Espacial y Exoplanetas, Centro de Astrobiología (LAEFF-CAB, INTA-CSIC), European Space Astronomy centre (ESAC), PO Box 78, 28691 Villanueva de la Cañada, Madrid, Spain

<sup>7</sup> Spanish Virtual Observatory thematic network, Spain

<sup>8</sup> Thüringer Landessternwarte Tautenburg, Sternwarte 5, 07778 Tautenburg, Germany

<sup>9</sup> Laboratoire d'Astrophysique de Grenoble, Observatoire de Grenoble, Université Joseph Fourier, CNRS, UMR 571, Grenoble, France

<sup>10</sup> University of Central Florida, Department of Physics, PO Box 162385, Orlando, FL 32816-2385, USA

Received 26 March 2009 / Accepted 31 July 2009

### ABSTRACT

**Context.** Free-floating substellar candidates with estimated theoretical masses of as low as  $\sim 5$  Jupiter masses have been found in the  $\sim 3$  Myr old  $\sigma$  Orionis open cluster. As the overlap with the planetary mass domain increases, the question of how these objects form becomes important. The determination of their number density and whether a mass cut-off limit exists is crucial to understanding their formation.

**Aims.** We propose to search for objects of yet lower masses in the cluster and determine the shape of the mass function at low mass.

**Methods.** Using new- and (re-analysed) published *IZJHK*<sub>s</sub>[3.6]–[8.0]-band data of an area of 840 arcmin<sup>2</sup>, we performed a search for LT-type cluster member candidates in the magnitude range  $J = 19.5$ – $21.5$  mag, based on their expected magnitudes and colours.

**Results.** Besides recovering the T type object S Ori 70 and two other known objects, we find three new cluster member candidates, S Ori 72–74, with  $J \approx 21$  mag and within 12 arcmin of the cluster centre. They have theoretical masses of  $4_{-2}^{+3} M_{\text{Jup}}$  and are among the least massive free-floating objects detected by direct imaging outside the Solar System. The photometry in archival *Spitzer* [3.6]–[5.8]-band images infers that S Ori 72 is an L/T transition candidate and S Ori 73 a T-type candidate, following the expected cluster sequence in the mid-infrared. Finally, the L-type candidate S Ori 74 with lower quality photometry is located at 11.8 arcsec ( $\sim 4250$  AU) of a stellar member of  $\sigma$  Orionis and could be a companion. After contaminant correction in the area complete to  $J = 21.1$  mag, we estimate that there remain between zero and two cluster members in the mass interval  $6$ – $4 M_{\text{Jup}}$ .

**Conclusions.** We present S Ori 73, a new candidate T type and candidate  $\sigma$  Orionis member of a few Jupiter masses. Our result suggests a possible turnover in the substellar mass spectrum below  $\sim 6$  Jupiter masses, which could be investigated further by wider and deeper photometric surveys.

**Key words.** stars: luminosity function, mass function – Galaxy: open clusters and associations: individual:  $\sigma$  Orionis – stars: low-mass, brown dwarfs

### 1. Introduction

Free-floating objects with masses of several to a few times the mass of Jupiter appear to populate young open clusters (see Lucas & Roche 2000; Zapatero Osorio et al. 2000). They could form in a similar way to stars, by gravitational fragmentation above an opacity mass limit (Hoyle 1953; Larson 1973; Low & Lynden-Bell 1976; Rees 1976; Silk 1977) or by turbulent fragmentation (Padoan & Nordlund 2002, 2004; Padoan et al. 2007) of collapsing molecular clouds, or as stellar embryos that are fragmented, photo-eroded, or ejected before they can accrete sufficient mass to become stars (see Whitworth & Goodwin 2005, and references therein). They could also form by gravitational instability in circumstellar disks (Boss 1997; Whitworth & Stamatellos 2006), then have their orbits disrupted and be

ejected (Stamatellos & Whitworth 2009; Veras et al. 2009). A better knowledge of the cluster mass function (MF; number of objects per unit mass) at these low masses will help us to determine the main formation process for these objects. Indeed, numerical simulations of opacity-limited fragmentation show a cutoff in the mass function at  $\sim 4$  Jupiter masses (Bate & Bonnell 2005; Bate 2005, 2009), whereas numerical simulations of turbulent fragmentation show an approximately log-normal, shallower drop at substellar masses (Padoan & Nordlund 2004). A detailed comparison with planets (e.g., spectral emission and chemical composition) will also provide complementary information about their origin and evolution (Fortney et al. 2008).

The  $\sigma$  Orionis open cluster in the Ori OB 1b association, together with other star-forming regions in the Orion and

Scorpius-Centaurus complexes, is well-suited to the search for free-floating planetary-mass objects. It is young ( $3 \pm 2$  Myr; Zapatero Osorio et al. 2002b), relatively nearby ( $360^{+70}_{-60}$  pc, Brown et al. 1994;  $444 \pm 20$  pc, Sherry et al. 2008), affected by very low extinction ( $A_V < 1$  mag; Sherry et al. 2008), and of solar metallicity (González Hernández et al. 2008). A revision of published, basic parameters of the cluster was provided by Caballero (2007). Caballero et al. (2007) found a smoothly continuous MF down to  $\sim 6$  Jupiter masses ( $M_{\text{Jup}}$ ) and that the brown dwarfs appear to harbour disks with a frequency similar to that of low-mass stars. This suggests that low-mass stars and substellar objects share the same formation mechanism. Also, S Ori 70, of spectral type T6, has been proposed to be a cluster member with an estimated mass of  $2\text{--}7 M_{\text{Jup}}$  (Zapatero Osorio et al. 2002a, 2008; Martín & Zapatero Osorio 2003; Burgasser et al. 2004; Scholz & Jayawardhana 2008; Luhman et al. 2008).

In this paper, we present new  $IZJHK_s$ -band photometry and a re-analysis of previous data of the  $\sigma$  Orionis cluster, allowing us to search for faint candidates in an area of  $\sim 790$  arcmin<sup>2</sup>, to the completeness magnitude  $J \approx 21.1$  mag. Our search area overlaps with those of Caballero et al. (2007) and Lodieu et al. (2009b), and its  $J$ -band completeness magnitude is about 1.5 and 2 mag fainter, respectively. We report the detection of three new cluster member candidates with theoretical masses of  $\sim 4 M_{\text{Jup}}$ .

## 2. Observations and data reduction

We discuss the new data obtained for this study and the data from Caballero et al. (2007) and Zapatero Osorio et al. (2008) that were reduced or analysed again in an attempt to increase the sensitivity to faint sources.

### 2.1. Optical data

The  $I$ -band imaging data presented in Caballero et al. (2007) were obtained with the Wide Field Camera (WFC) mounted at the Isaac Newton Telescope (INT). The WFC contains four CCD of  $2\text{ k} \times 4\text{ k}$  pixels and  $0.33$  arcsec/pixel. Figure 2 shows the area of the corresponding four images, limited to their overlap with the near-infrared data (solid and dashed lines). A new automatic search for sources was performed with the IRAF routine FINDSTAR (Almoznino), which led to a substantial increase in the number of sources at faint magnitudes with respect to those considered by Caballero et al. (2007). FINDSTAR is especially useful for detecting sources in combined dithered images (or in images with background gradients), where the standard deviation varies from centre to border. We then carried out the aperture and point-spread-function (PSF) photometry using routines within the DAOPHOT package. Objects missed by the automatic search routine but easily detected by eye in the PSF-subtracted images (e.g., sources partially hidden in the wings of bright stars) were added to the list of sources. Finally, for each of the four CCD images, the new photometry was calibrated using  $\sim 1850$  objects in common with the Caballero et al. (2007) photometry in the Cousins system. We found average completeness and limiting magnitudes of  $I_{\text{cmp}} = 23.0$  mag and  $I_{\text{lim}} = 23.9$  mag, respectively.

To determine these completeness and limiting magnitudes, we compiled the distribution of the instrumental magnitude error versus the calibrated magnitude for each image. In the bottom panel of Fig. 1, we present this with the source catalogue of one of the WFC CCD images. The completeness and limiting magnitudes were defined to be the faintest magnitude bins where the average errors are  $\leq 0.10$  and  $0.20$  mag, respectively.

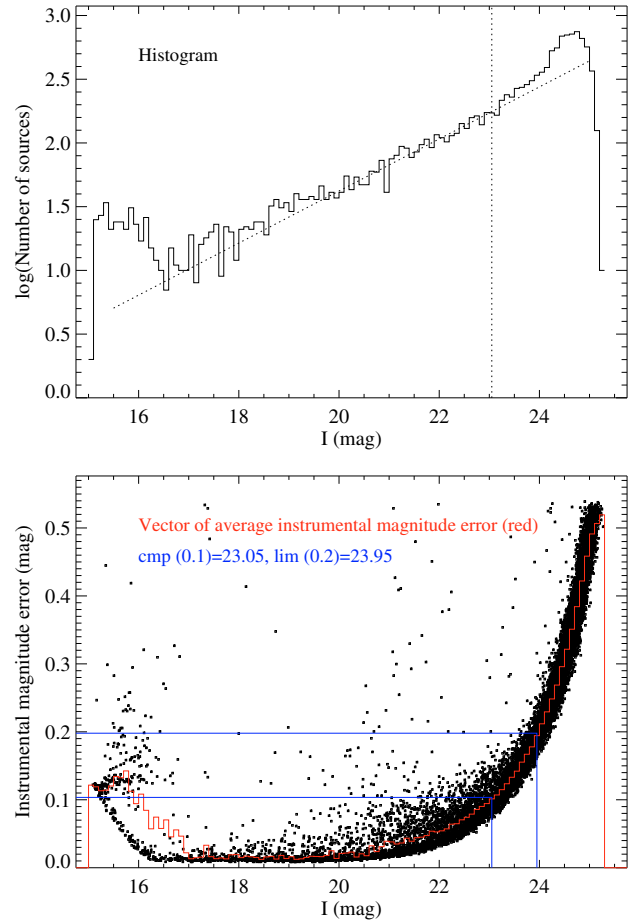


**Fig. 1.** *Upper panel.* Histogram in logarithmic scale of the  $I$ -band sources as a function of the calibrated magnitude (see text for details about the dotted lines). *Lower panel.* Instrumental magnitude error versus the calibrated magnitude of these sources (dots). The average error per magnitude bin is overlotted as a red solid line. The magnitudes of the bins just below errors of 0.1 mag (blue lower line) and 0.2 mag (blue upper line) were defined here as the completeness and limiting magnitudes, respectively.

These errors correspond to signal-to-noise ratios of  $S/N = 10$  and  $S/N = 5$ , respectively (see e.g., Newberry 1991). The average error per magnitude bin is overlotted as a red solid line. The upper panel shows the histogram of all sources on a logarithmic scale as a function of the calibrated magnitude. The inclined dotted line represents a power law fit to the histogram in the range  $[\text{mag}_{\text{cmp}} - 2.5, \text{mag}_{\text{cmp}}]$ , where  $\text{mag}_{\text{cmp}}$  is the completeness magnitude (vertical dotted line). At  $\text{mag} > \text{mag}_{\text{cmp}}$ , the histogram's deviation from the fit is most probably caused by sources affected by random upward or downward fluctuations of the background, the upward ones being preferentially detected above the detection threshold (Malmquist bias; see also Beichman et al. 2003). Comparing the counts of the histogram of sources having errors smaller than 0.10 mag with the counts of the linear extrapolation of its power law fit at the completeness magnitude, we estimated a level of completeness of  $\geq 90\%$ . This method was also applied to the other data sets.

We used broad  $IZ$ -band images from the Keck II Low Resolution Imaging Spectrograph (LRIS), associated with the discovery of S Ori 70 (see Zapatero Osorio et al. 2002a), as well as unpublished  $I$ -band images obtained with the same



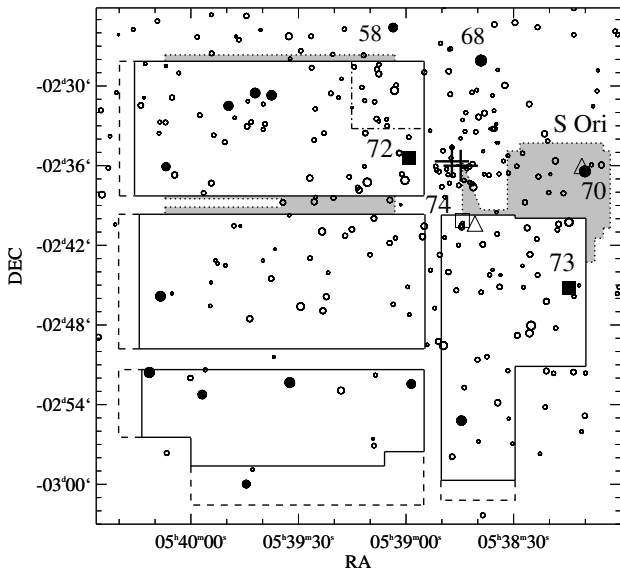


**Fig. 2.** Main search area: WFC-ISAAC  $IJ$ -band data (dashed line) together with follow-up  $H$ - or  $K$ -band data (solid line). Additional search areas: WFC  $I$ -, LRIS  $I$ -, and Omega2000  $JHK_s$ -band data (shaded regions delimited by dotted lines). Individual fields are not represented for clarity (see Fig. A.1). These areas have a completeness  $J \geq 21.1$  mag, except the upper corner in the main area (indicated by the dash-dot line) and the shaded regions on the left side. S Ori 72 and S Ori 73 are represented by filled squares, S Ori 74 by an open square, and S Ori J053840.8–024022 and S Ori J053811.0–023601 by open triangles (see finding charts of Figs. B.1–B.4). Circular symbols are cluster members and candidates (Zapatero Osorio et al. 2000; Caballero et al. 2007; Caballero 2008b); their size increases with fainter  $J$ -band magnitude, to highlight the location of the least massive objects. Filled circles are planetary-mass candidates with  $M < 0.013 M_{\odot}$ , including S Ori 70 (Zapatero Osorio et al. 2002a). Crosses are  $\sigma$  Ori AB and E, at the centre of the cluster.

instrument on 2000 January 5, in similar atmospheric conditions and for the same exposure time. Their coordinates and depths are listed in Table 1. The photometry was performed as described above. The  $I$ -band photometry was calibrated using typically 200 sources in common with the WFC survey, whereas the  $Z$ -band photometry was calibrated using on average 41 stellar sources from the Galactic Clusters Survey (GCS) component of UKIDSS<sup>1</sup> (Lawrence et al. 2007, fifth data release) and of magnitude error  $\sigma_Z(\text{UKIDSS}) < 0.1$  mag. The  $Z$ -band photometry has an average (relative) calibration error of 0.04 mag. We caution that the UKIDSS  $Z$ -band filter differs from that of the LRIS images. For the published data, we estimated that the average completeness and limiting magnitudes are  $I_{\text{cmp}} = 23.5$  mag and  $I_{\text{lim}} = 24.3$  mag, respectively, and  $Z_{\text{cmp}} = 22.3$  mag and  $Z_{\text{lim}} = 23.2$  mag, respectively. For the data from 2000, these are  $I_{\text{cmp}} = 23.5$  mag and  $I_{\text{lim}} = 24.5$  mag.

We obtained  $Z$ -band imaging data using the INT/WFC instrument on the night of 2008 November 27. We took 21 images of 900 s exposure time each and with central coordinates  $(\alpha, \delta) = (5\ 37\ 49.1, -2\ 44\ 43)$ . During the observations, thin cirrus were present and the average seeing was 1.2 arcsec. The images were reduced using routines within the IRAF

**Table 1.** Coordinates and depth of the LRIS images<sup>a</sup>.

ID	$\alpha$ (J2000)	$\delta$ (J2000)	Filter	$m_{\text{cmp}}, m_{\text{lim}}$ (mag)
1998i1	05 38 16.6	-02 37 53	$I$	23.6, 24.5
1998i2	05 38 21.0	-02 47 59	$I$	23.5, 24.4
1998i3	05 38 56.4	-02 38 57	$I$	23.5, 24.1
1998i4	05 39 21.2	-02 37 54	$I$	23.5, 24.4
1998i5	05 39 56.4	-02 34 00	$I$	23.6, 24.4
1998z1	05 38 16.6	-02 37 53	$Z$	22.1, 22.9
1998z2	05 38 21.0	-02 47 59	$Z$	22.4, 23.3
1998z3	05 38 56.4	-02 38 57	$Z$	22.4, 23.3
1998z4	05 39 21.2	-02 37 54	$Z$	22.5, 23.4
1998z5	05 39 56.4	-02 34 00	$Z$	22.4, 23.3
2000i1	05 38 17.4	-02 37 48	$I$	23.8, 24.6
2000i2	05 38 21.4	-02 48 03	$I$	23.5, 24.5
2000i3	05 38 55.2	-02 38 52	$I$	23.3, 24.3
2000i4	05 39 20.3	-02 37 58	$I$	23.7, 24.5
2000i5	05 39 57.2	-02 34 04	$I$	23.6, 24.7

<sup>a</sup> The pixel scale is  $0.210$  arcsec pixel<sup>-1</sup> and the field of view in the  $\alpha$ - $\delta$  frame is  $5.8 \times 7.2 \sim$  arcmin<sup>2</sup>. For the images 1998[i, z]3, 2000i[1, 2, 4, 5], and 2000i3, this field of view is rotated  $\sim 16, 90,$  and  $105$  deg counterclockwise, respectively.

environment, including bias and zero image subtraction and flat-field correction. Observations were done using a dithering pattern. Science images were combined to obtain flat-field images to correct for fringing. Individual images were aligned and combined to obtain final images. Aperture and PSF photometry was performed for one of the CCDs. Its photometric calibration was done using about 400 stellar sources from GCS-UKIDSS of  $\sigma_Z(\text{UKIDSS}) < 0.1$  mag, implying a relative calibration error of 0.02 mag. We caution that the UKIDSS  $Z$ -band filter is different from that of the WFC images. We estimated completeness and limiting magnitudes of 22.4 and 23.1 mag, respectively.

Astrometry was obtained for all the optical images with an accuracy of  $\sim 0.2$ – $0.05$  arcsec, using 2MASS as reference and an adaptation of the IRAF MYASTROM procedure (Puđu, see also Bihain et al. 2006). A representation of the individual fields is provided in Fig. A.1 (top left and right panels).

## 2.2. Near- and mid-infrared data

The  $J$ -band imaging data from Caballero et al. (2007) were obtained with the Infrared Spectrometer And Array Camera (ISAAC), mounted at the Very Large Telescope (VLT) and containing a Rockwell Hawaii detector of  $1\text{ k} \times 1\text{ k}$  pixels and  $0.148$  arcsec/pixel. We re-reduced these data to obtain a clean sky subtraction, remove bad pixel values, and identify more reliably charge persistencies of bright sources in the detector. The raw images were dark subtracted, superflat divided, sky subtracted (with the routine LIRISDR.LIMAGE.LRUNSKY from Acosta-Pulido, which includes object masking and vertical gradient correction), their elements flagged for bad pixel (at extreme values for thresholding) using bad pixel masks from superflats, related by pixel shifts (computed from clearly defined sources in common), and combined all at once in strips along right ascension or declination (16 strips in total). The photometry of each strip was performed similarly as for the WFC data. We ensured that all the sources remaining in the PSF-subtracted images were recovered, as we did for the Omega2000  $J$ -band images (see below). The photometry was calibrated using an average number of 12 point sources from the 2MASS catalogue (Skrutskie et al. 2006) of quality flags AAA or AAB. The average calibration

<sup>1</sup> UKIDSS uses the UKIRT Wide Field Camera (WFCAM, Casali et al. 2007) and a photometric system described in Hewett et al. (2006). The pipeline processing and science archive are described in Hambly et al. (2008).



**Table 2.** New near-infrared observations<sup>a</sup>.

ID	$\alpha$ (J2000)	$\delta$ (J2000)	Instr.	Filter	Area (arcmin <sup>2</sup> )	Date(s)	$t_{\text{exp}}$ (min)	$m_{\text{cmp}}$ (mag)	$m_{\text{lim}}$ (mag)
1-k	05 39 39.9	-02 50 26	Omega2000	$K_s$	197 (279)	2005 Jan. 31, Feb. 1, Oct. 26	326	20.5	21.2
2-j	05 39 35.1	-02 34 44	Omega2000	$J$	214 (259)	2006 Oct. 07	63	20.9	21.9
2-h	05 39 19.3	-02 33 36	Omega2000	$H$	181 (295)	2005 Oct. 19	186	21.2	21.9
2-k	05 39 21.2	-02 35 14	Omega2000	$K_s$	194 (282)	2005 Oct. 24–25	139.5	20.1	21.0
3-h	05 38 40.1	-02 48 09	SofI	$H$	21 (27)	2006 Dec. 27	147	20.3	20.9
4-h	05 38 40.0	-02 52 26	SofI	$H$	21 (27)	2006 Dec. 24	98	20.3	21.1
5-h	05 38 39.7	-02 57 09	SofI	$H$	21 (27)	2006 Dec. 27	75	20.1	20.5
6-h	05 38 20.0	-02 48 30	SofI	$H$	21 (27)	2006 Dec. 24	201	20.1	21.1
7-h	05 40 05.1	-02 30 40	SofI	$H$	21 (27)	2006 Dec. 27	132	20.3	21.1
8-h	05 40 04.9	-02 35 57	SofI	$H$	21 (27)	2006 Dec. 26	98	19.5	20.1
9-h	05 40 03.6	-02 42 10	SofI	$H$	21 (27)	2006 Dec. 25	56	19.9	20.7
10-h	05 39 09.7	-02 47 15	SofI	$H$	21 (27)	2006 Dec. 25	168	20.3	21.3
11-h	05 39 27.7	-02 47 15	SofI	$H$	21 (27)	2006 Dec. 25	95	20.1	21.1
12-h	05 39 45.7	-02 47 15	SofI	$H$	21 (27)	2006 Dec. 26	120	20.3	21.3
13-h	05 40 03.1	-02 47 04	SofI	$H$	16 (33)	2006 Dec. 26	140	20.3	21.1
14-h	05 39 09.5	-02 53 56	LIRIS	$H$	16 (20)	2006 Dec. 29	36	19.5	20.1
15-h	05 39 45.4	-02 53 57	LIRIS	$H$	16 (20)	2007 Dec. 14	45	20.3	20.9
16-h	05 40 03.6	-02 53 59	LIRIS	$H$	16 (20)	2007 Dec. 14	45	20.3	20.9

<sup>a</sup> Fields of view (and pixel scales) of the Omega2000, SofI, and LIRIS detectors are  $15.4 \times 15.4$  arcmin<sup>2</sup> ( $0.45$  arcsec pixel<sup>-1</sup>),  $4.9 \times 4.9$  arcmin<sup>2</sup> ( $0.288$  arcsec pixel<sup>-1</sup>), and  $4.2 \times 4.2$  arcmin<sup>2</sup> ( $0.25$  arcsec pixel<sup>-1</sup>), respectively.

error is 0.03 mag. The average completeness and limiting magnitudes are  $J_{\text{cmp}} = 21.6$  mag and  $J_{\text{lim}} = 22.4$  mag, respectively, in an area of  $\sim 660$  arcmin<sup>2</sup>. This area excludes  $\sim 20$  arcmin<sup>2</sup> within the region delimited by the dash dot line in Fig. 2, where  $J_{\text{cmp}} = 20.6$  mag and  $J_{\text{lim}} = 21.5$  mag, and  $\sim 100$  arcmin<sup>2</sup> corresponding to the  $\sim 0.4$  mag shallower borders of the strips.

We obtained additional near-infrared imaging data, using Omega2000 at the 3.5-m Telescope (Calar Alto, Spain), Son of Isaac (SofI) at the New Technology Telescope (La Silla, Chile), and the Long-slit Intermediate Resolution Infrared Spectrograph (LIRIS) at the William Herschel Telescope (Roque de los Muchachos Observatory, Spain). Table 2 indicates field identification, coordinates, instrument, filter, area, observing night date(s), total exposure time, and completeness- and limiting magnitudes. All the data were reduced within the IRAF environment, including (super)flat division, sky subtraction, alignment with several reference stars, and combination without trimming. SofI raw images were first row cross-talk corrected with the routine `crosstalk` (Leo Vanzi, ESO SofI tools). Omega2000 and most of the SofI images were dark subtracted before flat division. LIRIS raw images were first pixel-mapping- and row-cross-talk corrected, and then processed with the routine `LIRISDR.LIMAGE.LDEDITHER`, including sky subtraction, as applied to ISAAC  $J$ -band, and distortion correction. Bad pixel masks were used for LIRIS and SofI, whereas for Omega2000 extreme values relative to the average at each pixel were rejected during combination. Because the combined images are untrimmed, they have a deep central region surrounded by a shallower region, whose proportions depend on the observing dithers. In Table 2, we list the deep area and the total area (in parenthesis). The photometry was obtained as described above. For the Omega2000 images, the photometric calibration was obtained using  $\sim 150$  2MASS point sources of quality flags AAA or AAB (average calibration error of 0.03 mag). For each of the SofI and LIRIS images, about 10 of these calibrators were used (average calibration error of 0.04 mag). Completeness and limiting magnitudes were derived from the sources in the deeper central regions.

**Table 3.** Re-estimated depth of individual fields from Caballero et al. (2007) and Zapatero Osorio et al. (2008).

ID	$\alpha$ (J2000)	$\delta$ (J2000)	Instr.	Filter	$m_{\text{cmp}}, m_{\text{lim}}$ (mag)
1-h	05 39 37.6	-02 49 53	Omega2000	$H$	20.0, 20.9
17-h	05 38 38.7	-02 49 01	Omega2000	$H$	19.1, 19.6
17-k	05 38 37.6	-02 49 51	Omega2000	$K_s$	19.6, 20.3
18-j <sup>a</sup>	05 38 12.4	-02 35 18	Omega2000	$J$	21.1, 21.9
18-h <sup>a</sup>	05 38 11.9	-02 34 59	Omega2000	$H$	20.6, 21.4
18-k <sup>a</sup>	05 38 13.3	-02 35 37	Omega2000	$K_s$	20.0, 21.0
19-h	05 38 44.6	-02 44 35	CFHTIR	$H$	21.1, 22.1
19-k	05 38 44.6	-02 44 35	CFHTIR	$K'$	20.9, 21.9
20-h	05 38 18.3	-02 44 31	CFHTIR	$H$	20.5, 21.3
20-k	05 38 18.3	-02 44 31	CFHTIR	$K'$	20.5, 21.3
21-h	05 39 24.2	-02 29 36	CFHTIR	$H$	20.9, 21.5
21-k	05 39 25.6	-02 29 37	CFHTIR	$K'$	20.5, 21.3
22-h	05 40 06.5	-02 32 29	CFHTIR	$H$	20.7, 21.9
22-k	05 40 06.6	-02 32 29	CFHTIR	$K'$	20.5, 21.5

<sup>a</sup> Re-reduced data from Zapatero Osorio et al. (2008); deep central areas (and total areas) in  $J$ ,  $H$ , and  $K_s$  are 215 (257), 208 (265), and 197 (278) arcmin<sup>2</sup>. For the Omega2000 and CFHTIR data from Caballero et al. (2007), the deep central areas (and total areas) are 216 (236) and 6 (22) arcmin<sup>2</sup>, respectively.

Other near-infrared data, already published in Caballero et al. (2007) and Zapatero Osorio et al. (2008), were used in the search. The Omega2000 data from the latter study were re-reduced to obtain untrimmed images. Completeness and limiting magnitudes of our new photometry (obtained as described above) are listed in Table 3, except for the  $H$ -band  $\sim 1100$  arcmin<sup>2</sup> Omega2000 survey from 2003 (see Caballero et al. 2007), which is shallower. We note that the field 1-k is a combination of new data obtained on 2005 October 26 with published data obtained earlier the same year, on January 31 and February 1. The  $J$ - and  $HK$ -band data from Tables 2 and 3 correspond to overlapping areas of  $\sim 240$  arcmin<sup>2</sup> and  $\sim 690$  arcmin<sup>2</sup>

with the WFC + ISAAC survey, respectively (see Fig. 2 for the  $HK$ -band data).

Astrometry was obtained for all the near-infrared images similarly as for the optical images, with an accuracy of  $\sim 0.2$ – $0.05$  arcsec. A representation of the individual fields is provided in Fig. A.1 (top left and bottom panels).

We also used archival post-basic calibrated data (PBCD) from the *Spitzer Space Telescope* Infrared Array Camera (IRAC). For our new candidates (see Sect. 4), we have obtained the Spitzer photometry following the procedure described in Zapatero Osorio et al. (2007) and using the data published by Hernández et al. (2007) and Scholz & Jayawardhana (2008). A comparison of these two data sets is provided in Luhman et al. (2008, see e.g. Fig. 1 therein for a map of the IRAC surveys). We averaged our measurements in overlapping deep images and adopted their standard deviation as a representative error bar. We compared the [3.6]- and [4.5]-band measurements of Zapatero Osorio et al. (2007) with those of Luhman et al. (2008) for the six objects in common<sup>2</sup> and found small average differences  $[3.6]_{ZO-L} = 0.02 \pm 0.12$  mag and  $[4.5]_{ZO-L} = 0.12 \pm 0.07$  mag, implying good agreement between the two sets of measurements.

### 3. The search for $\sigma$ Orionis LT-type objects

Field dwarfs with spectral types T0–8 (effective temperature 1400–700 K) have typical colours of  $I - J > 4.5$ ,  $J - H < 1.5$ , and  $J - K_s < 2$  mag (Tinney et al. 2003; Zhang et al. 2009); the early types have redder  $J - H$  and  $J - K_s$  colours and higher effective temperatures than the later types. By extrapolating the  $\sigma$  Orionis cluster sequence using the field dwarf sequence, cluster members with a T spectral type appear to be at  $J \sim 20$  mag (see Sect. 4 and Fig. 4). About the same apparent magnitude is found using the synthetic atmosphere  $J$ -band prediction of the 3-Myr COND model isochrone from Chabrier & Baraffe (2000). However, when predicted bolometric luminosities and effective temperatures are transformed into the observable using relations for field dwarfs (see also Sect. 4 and Fig. 4), a  $J$ -band value of  $\sim 21$  mag is found.

T-type objects of this magnitude will still be detected within the completeness of the ISAAC data, whereas they will be relatively faint or undetected in the less deep  $IHK$ -band images. For example, faint T type objects with  $J = 21.5$ ,  $I - J > 4.5$ ,  $J - H < 1$ , and  $J - K_s < 1$  mag will be undetected in all the optical images and only possibly detected in the near-infrared images of ( $H$ - or  $K_s$ -band) limiting magnitudes fainter than 20.5 mag ( $\sim 470$  arcmin<sup>2</sup>). Therefore, we opted for a search relying on the ISAAC  $J$ -band photometry, i.e., the deepest near-infrared photometry over the largest area, and with an automatic selection in terms of magnitudes and colours that is not too restrictive, to allow us to recover visually any potential cluster member candidate, including L-type objects.

First, we correlated the  $\alpha - \delta$  coordinates of the  $IJK_s$ -band sources using the IDL `srcor` procedure (IDL Astronomy User’s Library, Landsman 1993); for each  $J$ -band source, we searched for the nearest counterpart within 2 arcsec in the  $H$ ,  $K_s$ , and  $I$  bands. The correlations with the WFC- and LRIS  $I$ -band catalogues were performed separately. We then selected  $19.5 < J < 21.5$  mag sources with no automatic  $I$ -band detection, or either  $I > 24$  mag  $\approx I_{\text{lim}}$  (for unreliable or spurious

<sup>2</sup> S Ori 54 was not included in the comparison because in Luhman et al. (2008) the object was probably misidentified with the brighter source [SE2004] 26, at about 5 arcsec.

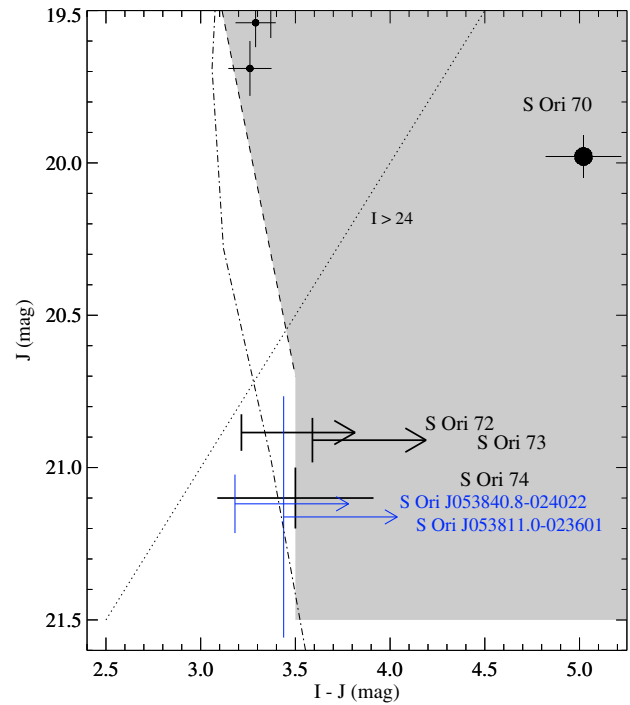


**Fig. 3.**  $J$  versus  $I - J$  colour-magnitude diagram. The shaded search region is where we expected cluster member candidates. The dashed line represents the extrapolated selection boundary from Caballero et al. (2007). The dotted line represents the  $I > 24$  mag selection sub-criterion. The dash-dot line represents the 3 Myr COND model isochrone, where  $I$  and  $J$  are in the Cousins and CIT photometric systems, respectively. The two small filled circles are the faintest objects from Caballero et al. (2007) and the large filled circle is S Ori 70. The four ( $5\sigma$ ) flux upper limits and one ( $1\sigma$ ) error cross represent our new candidates. Probable galaxies are highlighted in blue.

detections) or  $I - J > 3.5$  mag. As shown in Sect. 4, the  $I - J$  colour is essential for distinguishing LT-type objects from galaxies. The  $I - J > 3.5$  mag sub-criterion intersects at  $J = 20.7$  mag with a linear extrapolation of the selection criterion applied by Caballero et al. (2007, see therein Fig. 2) for their sources with  $I < I_{\text{cmp}} = 23$  mag. For continuity between the searches, we also selected sources redder than their  $I - J$  selection boundary and bluer than 3.5 mag. In the  $J$  versus  $I - J$  colour-magnitude diagram of Fig. 3, the shaded region represents the entire domain where we expected cluster member candidates, the dashed line represents the extrapolated selection boundary from Caballero et al. (2007), and the dotted line the  $I > 24$  mag sub-criterion. Finally, since the “2-j” Omega2000  $J$ -band image (Table 2) overlaps with the northern ISAAC scans over  $\sim 210$  arcmin<sup>2</sup>, we performed the selection process again for the sources with  $J_{\text{ISAAC}} - J_{\text{Omega2000}} > 0.2$  mag and those without ISAAC counterparts.

About 800 sources were chosen by our selection criteria from our  $IJ$ -band catalogues. We checked each source visually in all of the optical and infrared images, using the SAOImage DS9 display programme (Joye & Mandel 2003) and commands in the X Public Access (XPA) messaging system<sup>3</sup>. The simultaneous visualisation in all available bandpasses and at all observing epochs allowed us to verify whether a source is real (or of low proper motion) and unresolved. Most sources were not detected automatically in the optical, because they are faint or very

<sup>3</sup> <http://hea-www.harvard.edu/saord/xpa/>

close<sup>4</sup> to brighter ones, and their clearly bluer  $I - J$  colours imply that they should be stars or unresolved galaxies. Many are spurious detections of spikes or glares in the  $J$ -band. Others represent charge persistencies of bright sources in the ISAAC detector (following precisely and chronologically the offsets of individual pointings), resolved galaxies, sources cut at image borders, or very blended sources, which are too close to bright stars in the optical to be identified. The “2-j” Omega2000  $J$ -band sources with  $J_{\text{ISAAC}} - J_{\text{Omega2000}} > 0.2$  mag were typically galaxies, resolved in the ISAAC images, whereas those without ISAAC counterparts were sources that could not be detected in the shallower survey region (see Sect. 2.2 and Fig. 2) and the gaps between the strips.

In a similar way, we searched for candidates in the additional areas of  $\sim 15$  arcmin<sup>2</sup> and  $\sim 45$  arcmin<sup>2</sup> represented by the shaded left and right regions in Fig. 2. These areas are common to the Omega2000  $JHK_s$ -, WFC  $I$ -, and LRIS  $I$ -band data. The  $J$ -band data of the left and right regions (fields 2-j and 18-j) are complete to 20.9 and 21.1 mag, respectively. They are therefore shallower by about 0.5 mag than the ISAAC data.

These searches allowed us to find four sources that are indeed undetectable by eye in the deepest  $I$ -band images (see Sect. 4), and a half-dozen of sources at  $J > 20.7$  mag that are barely detected beyond the  $I$ -band limiting magnitudes. Most of the latter sources appear to be bluer than  $I - J \sim 3.5$  mag. They have magnitude errors  $\lesssim 0.1$  mag in the  $JHK_s$ -bands and red colours of  $J - H \approx 1$  mag or  $J - K_s \approx 2$  mag. Only one of them has a colour  $I - J \geq 3.5$  mag. It was selected as a candidate (see Sect. 4), whereas the others were rejected because they are probable galaxies or faint field M- or early L-type dwarfs. Some sources could not be verified in the  $I$ -band images because of blending with extended stellar spikes and glares. We estimated that areas of  $\sim 10$  and  $\sim 5$  arcmin<sup>2</sup> are lost in the main- and additional areas, respectively. Thus, the total search area with  $J$ -band completeness  $\geq 21.1$  mag (ISAAC and Omega2000 18-j data) amounts to  $\sim 790$  arcmin<sup>2</sup>.

#### 4. Results and discussion

Besides recovering the two faintest cluster member candidates<sup>5</sup> S Ori J053932.4–025220 and S Ori J054011.6–025135 from Caballero et al. (2007) and the T-type S Ori 70, we detect three new L- and T-type candidates and two probable galaxies (see finding charts of Figs. B.1–B.4), among many other objects rejected because they do not meet our selection criteria. As shown in Fig. 3, the new candidates are about one magnitude fainter than S Ori 70. The photometric information that we compiled from the images of different depths are listed in Tables 4 and 5, where the  $5\sigma$  flux upper limits correspond to the magnitude limits of the images.

In the  $J$  versus  $J - [3.6]$  and  $J - [4.5]$  colour–magnitude diagrams of Figs. 4 and 5, we represent the candidates together with known  $\sigma$  Orionis cluster members and candidates (Caballero et al. 2007; Zapatero Osorio et al. 2007, 2008). The solid line represents the spectrophotometric sequence of field mid-M- to late-T-type dwarfs, shifted to match the brightness of

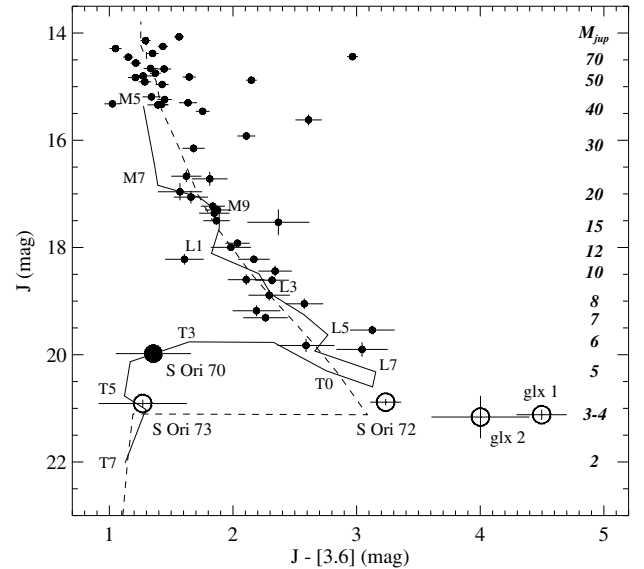


**Fig. 4.**  $J$  versus  $J - [3.6]$  colour–magnitude diagram of  $\sigma$  Orionis cluster members and candidates. The filled circles correspond to objects from Caballero et al. (2007) and Zapatero Osorio et al. (2007, 2008). The large filled circle is S Ori 70. The large open circles are the new candidates. S Ori J053840.8–024022 and S Ori J053811.0–023601 are labelled “glx 1” and “glx 2”, respectively. The solid line represents the field dwarf sequence shifted to match the brightness of the late-M-type  $\sigma$  Orionis cluster members. The dashed line represents the 3 Myr COND model isochrone (see text); masses are indicated to the right in units of Jupiter masses.

the late-M-type cluster members (Zapatero Osorio et al. 2008). For the field dwarfs, we use average absolute  $I$ -band magnitudes,  $I - J$ , and  $J - K_s$  colours compiled by Caballero et al. (2008a)<sup>6</sup>,  $J - H$  colours from Vrba et al. (2004)<sup>7</sup>, and mid-infrared magnitudes from Patten et al. (2006). In Fig. 4, the dashed line represents the 3 Myr COND model isochrone at the cluster distance, adapted by converting predicted effective temperature and luminosity into observables using relations for field dwarfs (procedure explained in Zapatero Osorio et al. 2008).

We also represent the candidates in  $I - J$  versus  $J - H$  and  $J - K_s$  colour–colour diagrams (Figs. 6 and 7) as well as in various diagrams with mid-infrared filters (Figs. 8–10), together with sources from the GOODS-MUSIC catalogue (Grazian et al. 2006) that we use as a control field to study the potential contamination by extragalactic sources in our survey. In all the figures, the open circles represent the new candidates (labelled) and the solid line represents part of the field LT-type dwarf sequence. The GOODS-MUSIC survey is centred on  $(\alpha, \delta) = (3\ 32\ 30, -27\ 48\ 30)$ , approximately, and covers an area of 143.2 arcmin<sup>2</sup> (except in the  $H$ -band, where the area is 78 arcmin<sup>2</sup>), i.e., less than a fifth of our search area. The limiting magnitudes are  $i = 26.1$ ,  $J = 23.6$ ,  $H = 22.9$ ,  $K_s = 21.9$ ,  $[3.6] = 21.2$ ,  $[4.5] = 20.1$ ,  $[5.8] = 18.3$ , and  $[8.0] = 17.6$  mag,

<sup>4</sup> De-blended in the images subtracted by the PSF fitted sources (NOAO.DIGIPHOT.DAOPHOT.ALLSTAR) or subtracted by a smoothing obtained with a moving average box much smaller than the image size (NOAO.IMRED.CCDRED.MKSKYCOR).

<sup>5</sup> For the latter, we were able to measure  $H = 18.8 \pm 0.2$  mag and  $K_s = 18.5 \pm 0.1$  mag, implying early L colours  $J - H = 0.8$  mag and  $J - K_s = 1.1$  mag.

<sup>6</sup> Note that the photometric values in Table 3 therein correspond to the spectral types M3V, M4V, M5V, ... instead of M3-4V, M4-5V, M5-6V, ... The  $I$  and  $JK_s$  magnitudes are in the Johnson-Cousins- and 2MASS photometric systems, respectively.

<sup>7</sup> The  $J - H$  colour is transformed back from the CIT- to the 2MASS photometric system using the same colour transformation of Carpenter (2001) as used in Vrba et al. (2004).

**Table 4.** Coordinates and photometry of the new L- and T-type cluster member candidates<sup>a</sup>.

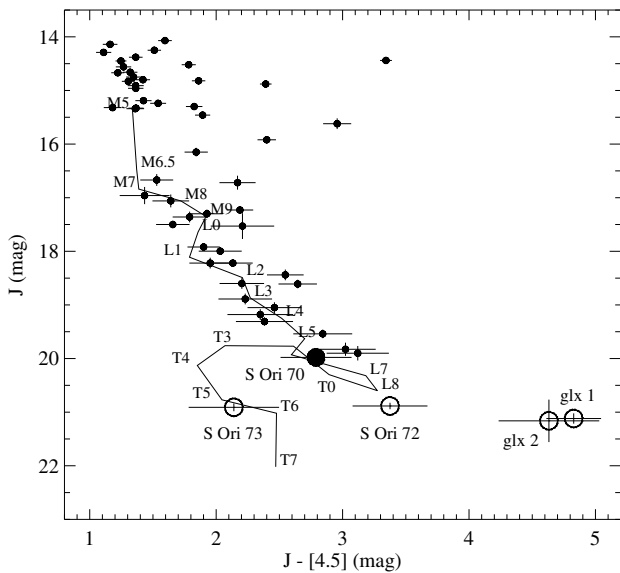
Name	$\alpha$ (J2000)	$\delta$ (J2000)	$I$ (mag)	$Z$ (mag)	$J$ (mag)	$H$ (mag)	$K_s$ (mag)	[3.6] (mag)	[4.5] (mag)	[5.8] (mag)
S Ori 72	5 38 59.17	-2 35 26.0	>24.1	>23.3	20.89 ± 0.06	19.57 ± 0.03	18.72 ± 0.05	17.65 ± 0.11	17.51 ± 0.29	17.28 ± 0.38
S Ori 73	5 38 14.49	-2 45 11.8	>24.5	23.5 ± 0.5	20.91 ± 0.07	20.83 ± 0.12	20.91 ± 0.15	19.64 ± 0.35	18.77 ± 0.35	>16.0
S Ori 74	5 38 44.27	-2 40 07.9	24.6 ± 0.4	>23.3	21.1 ± 0.1	>18.54 <sup>b</sup>	19.38 ± 0.10	... <sup>c</sup>	... <sup>c</sup>	>16.0

<sup>a</sup> All have [8.0] > 15.1 mag. <sup>b</sup> Lower magnitude limit computed for the UKIDSS GCS specific field. <sup>c</sup> Blended with a spike from the star Mayrit 260182 (located at 11.8 arcsec).

**Table 5.** Coordinates and photometry of probable galaxy candidates<sup>a</sup>.

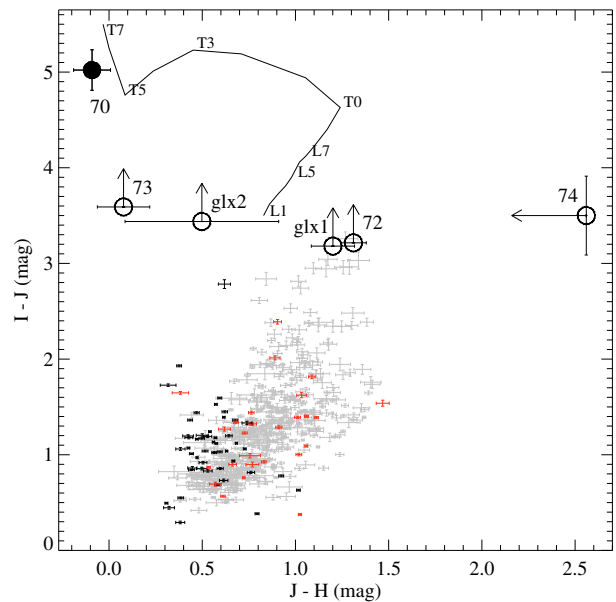
Name	$I$ (mag)	$Z$ (mag)	$J$ (mag)	$H$ (mag)	$K_s$ (mag)	[3.6] (mag)	[4.5] (mag)	[5.8] (mag)	[8.0] (mag)
S Ori J053840.8-024022	>24.3	...	21.12 ± 0.10	19.92 ± 0.07	18.94 ± 0.08	16.62 ± 0.18	16.29 ± 0.19	>16.0	>15.1
S Ori J053811.0-023601	>24.6	>22.9	21.16 ± 0.40	20.66 ± 0.11	19.61 ± 0.09	17.16 ± 0.02	16.53 ± 0.04	15.56 ± 0.06	14.69 ± 0.12

<sup>a</sup> S Ori J053811.0-023601 is at 28.0 arcsec from S Ori 70.

**Fig. 5.**  $J$  versus  $J - [4.5]$  colour-magnitude diagram. Same as in Fig. 4.

when converted from the AB system to the Vega system<sup>8</sup>. In the magnitude range  $19.5 < J < 21.5$  mag, the catalogue contains 882 galaxies, 37 active galactic nuclei (AGN), and 83 stars, and in the smaller  $H$ -band area, 505 galaxies, 27 AGN, and 49 stars. Stars and AGN are distinguished from “normal” galaxies mostly by morphological and photometric criteria, or else by spectroscopic criteria. Stars are distinguished from AGN by spectroscopic criteria. In the infrared colour-colour diagrams of Figs. 9

<sup>8</sup> The  $i$ - (or  $F775W$ ) band photometry is from *HST*/ACS and similar to that from the Sloan Digital Sky Survey (SDSS). A transformation  $I_{\text{Cousins}} = i_{\text{SDSS}} - 0.3780 * (i_{\text{SDSS}} - z_{\text{SDSS}}) - 0.3974$  ( $\sigma = 0.0063$  mag) has been obtained for stars (<http://web.archive.org/web/20071014232413/http://www.sdss.org/dr6/algorithms/sdssUBVRITransform.html>); we assumed that this transformation is also valid for galaxies. The VLT/ISAAC  $JHK_s$ -band photometry was converted to the Vega system using the transformations provided in the web page <http://web.archive.org/web/20070814141037/http://www.eso.org/science/goods/releases/20050930/>; it is found to be consistent within 0.05 mag with the 2MASS point-source photometry. For the *Spitzer*/IRAC [3.6][4.5][5.8][8.0]-band photometry, we used the transformations provided in the web page <http://web.ipac.caltech.edu/staff/gillian/cal.html>

**Fig. 6.**  $I - J$  versus  $J - H$  colour-colour diagram of stars (black crosses), AGN (red crosses), and galaxies (grey crosses) from the GOODS-MUSIC catalogue (Grazian et al. 2006), in the magnitude range  $19.5 < J < 21.5$  mag. The solid line represents the field L1-T7-type dwarf sequence, the filled circle represents S Ori 70, and the open circles represent the new candidates. S Ori J053840.8-024022 and S Ori J053811.0-023601 are labelled “glx 1” and “glx 2”, respectively.

and 10, the sequence of mid-L- to early-T type field dwarfs overlaps with the domain of galaxies and AGN; only T type dwarfs tend to have different colours. The colour-magnitude diagrams of Fig. 8 also indicate that, from  $J = 19.5$  to  $21.5$  mag, the colour ranges of galaxies and AGN become broader and the number of galaxies increases (here by a factor of 1.4 in a 0.5-mag interval). However the optical-infrared diagrams of Figs. 6 and 7 show that mid-L to mid-T type dwarfs are clearly redder in  $I - J$  than the other sources. Thus, the  $I - J$  colour is essential to distinguishing these objects from galaxies and AGN, whereas the infrared colours only help us to guess the spectral type.



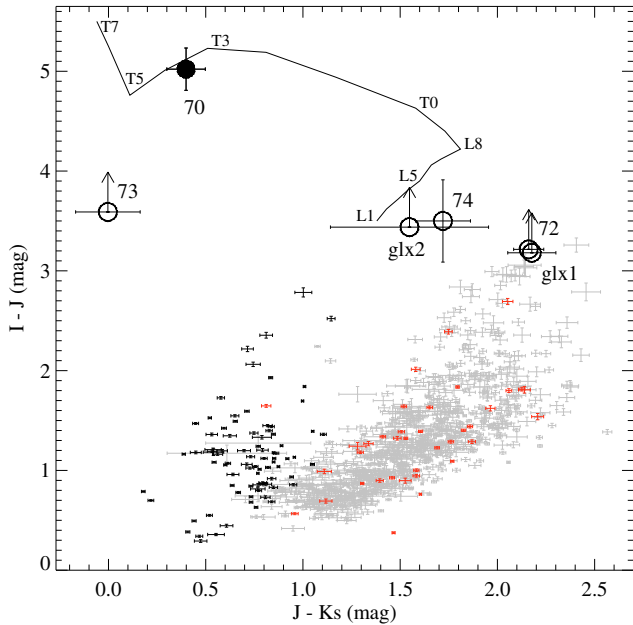


Fig. 7.  $I - J$  versus  $J - K_s$  colour-colour diagram. Same as in Fig. 6.

#### 4.1. New L- and T-type candidates

*S Ori 72*, with  $J - H \approx 1.3$  mag and  $J - K_s \approx 2.2$  mag, could be a late L-type object. It is clearly detected in the ISAAC  $J$ -band image from December 2001 and even better in Omega2000  $HK_s$ -band images (observations 2-h and 2-k, Table 2), whereas it is slightly blended but detected in the [3.6][4.5][5.8]-band images (its visual neighbour is 2MASS J05385930–0235282, a field star located 3 arcsec south-east, with  $J \approx 16.0$  mag and  $I - J \approx 0.9$  mag). *S Ori 72* is undetected in the WFC  $I$ -band image and the LRIS  $IZ$ -band images (1998iz3, Table 1). The  $FWHMs$  in the  $JHK_s$ -band images are approximately equal to those of nearby faint point-like sources, of about 0.5, 1.2, and 0.8 arcsec, respectively. Among the new candidates presented in this paper, *S Ori 72* is the only one that is detected in the GCS-UKIDSS images, with  $K_{UKIDSS} = 18.60 \pm 0.28$  mag, in agreement with our measurement. In Fig. 11, we show its spectral energy distribution, together with average ones of field dwarfs of L7- and L8 spectral types (dotted lines). *S Ori 72* is relatively brighter in the  $HK_s$ -bands. A preliminary measurement of *S Ori 72*'s proper motion using the ISAAC-Omega2000 images of 3.87 yr time baseline and the method described in Bihain et al. (2006) allows us to impose a  $2\sigma$  upper limit of 30 mas/yr. Although the estimate should be improved before comparison with the  $\mu \lesssim 5-10$  mas yr $^{-1}$  amplitude of  $\sigma$  Orionis members (Caballero 2007), it indicates that *S Ori 72* is not a high-proper motion object and unlikely to be a nearby ( $\leq 30$  pc) source. From the  $J$  versus  $J - [3.6]$  and  $J - [4.5]$  colour-magnitude diagrams of Figs. 4 and 5, *S Ori 72* could be an L/T transition cluster member candidate, but Figs. 6–10 imply that it could also be a galaxy or an AGN.

With  $J - H \sim J - K_s \sim 0$  mag, *S Ori 73* has near-infrared colours of a mid T-type object. It is clearly detected in the ISAAC  $J$ -band image, but appears very faint in the WFC  $Z$ -band image from November 2008, the CFHTIR  $HK'$ -band images from February 2004 (20-h and 20-k, Table 3), and the public *Spitzer*/IRAC [3.6]- and [4.5]-band images. It is undetected in the WFC  $I$ -band image, the LRIS  $IZ$ -band images (2000i2, 1998iz2, Table 1), and in the Omega2000  $HK_s$ -band images

(17-h and 17-k). Its  $FWHM$  in the  $J$ -band image is approximately equal to that of nearby faint point-like sources, of about 0.5 arcsec. In Fig. 11, we show its spectral energy distribution, together with average ones of field dwarfs of T4 and T6 spectral types. The position of *S Ori 73* in the  $J$  versus  $J - [3.6]$  diagram of Fig. 4 agrees with both adapted field- and model sequences, securing this source as a good T-type- and cluster member candidate. The colour-colour diagrams of Figs. 6, 7, and 9 also indicate that there are neither stars, nor AGN, nor galaxies in GOODS-MUSIC as red in  $I - J$  and blue in  $J - H$  and  $J - K_s$  as this object.

With  $I - J = 3.5 \pm 0.4$  mag and  $J - K_s \approx 1.7$  mag, *S Ori 74* could be an L-type object. It is detected in the ISAAC  $J$ -band image and in an Omega2000  $K_s$ -band image (18-k, Table 3). The object appears point-like in both images with a typical local  $FWHM$  of 0.7 and 0.9 arcsec, respectively, whereas it appears faint and blended with a stellar spike in the [3.6][4.5][5.8]-band images, preventing us from determining its IRAC photometry. The candidate is barely detected in the LRIS  $I$ -band images (2000i3 and 1998i3, Table 1) and undetected in a stellar glare in the WFC  $I$ -band- and LRIS  $Z$ -band images (1998z3). In Fig. 11, we show its spectral energy distribution, together with average ones of field dwarfs of L2- and L8 spectral types. From Fig. 7, it could also be a galaxy or an AGN. However, *S Ori 74* is located 11.8 arcsec north ( $\sim 4250$  AU; open square in Fig. 2) of the bright K7.5-type cluster star Mayrit 260182, 4.3 arcmin south of the cluster centre. The probability of chance alignment is only 5% for cluster members at this angular distance from the  $\sigma$  Orionis centre (Caballero 2009, Fig. 1). Mayrit 260182, Mayrit 270181, and Mayrit 277181 also form a possible triple system (Caballero 2006). Caballero et al. (2006) previously proposed that *S Ori 68 + SE 70* is a planet-brown dwarf system candidate, of greater mass ratio and smaller separation. There are, however, known red galaxies at comparable angular separations to  $\sigma$  Orionis cluster members. For example, the type I obscured quasi-stellar object UCM 0536–0239 is located about 14.9 arcsec south of the T Tauri star Mayrit 97212 (Caballero et al. 2008b). Observational follow-up is necessary to confirm whether *S Ori 74* is a cluster member and companion of Mayrit 260182.

#### 4.2. Probable galaxy candidates

With  $J - H \approx 1.2$  mag and  $J - K_s \approx 2.2$  mag, *S Ori J053840.8–024022* could be a late L-type object or a galaxy. It is detected with brighter magnitudes at longer wavelengths, from the Omega2000  $JHK_s$ -band images (18j–k, Table 3) to the [3.6][4.5]-band images, but is then undetected in the [5.8][8.0]-band images. It is undetected in the WFC and LRIS  $I$ -band images (2000i3, Table 1). In Fig. 11, we show its spectral energy distribution, together with average ones of field dwarfs of L7- and L8 spectral types. In the ISAAC  $J$ -band image, it is found to be slightly extended and fainter than in the lower-resolution Omega2000  $J$ -band image. The  $FWHMs$  of the object in the Omega2000  $JHK_s$ -band images are systematically larger by a factor  $\approx 1.4$  than those of nearby faint point-like sources, suggesting that it is a galaxy. *S Ori J053840.8–024022* could be an L/T transition object, but from the  $J$  versus  $J - [3.6]$  and  $J - [4.5]$  diagrams (Figs. 4 and 5), it is redder than the expected sequence of the cluster. Galaxies from the GOODS-MUSIC catalogue with these red colours appear at magnitudes  $J \geq 20.5$  mag (Fig. 8). Figure 9 illustrates its infrared excess in the  $K_s$ -, [3.6]-, and [4.5]-bands relative to the field dwarf sequence, and also suggests that this object is likely to be a galaxy.

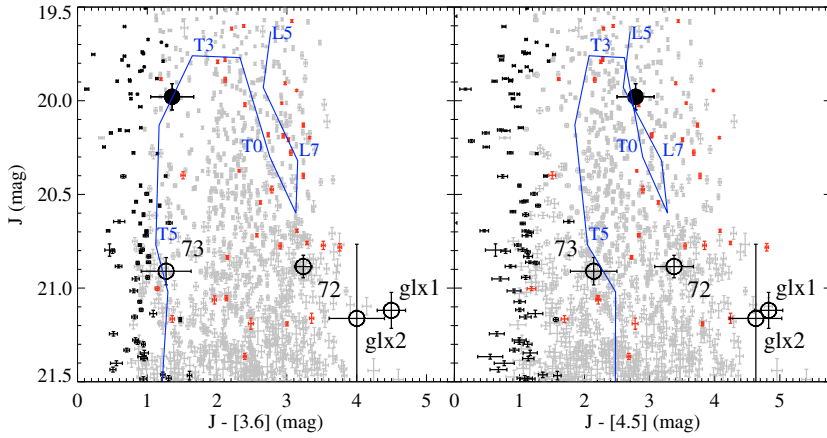


**Fig. 8.**  $J$  versus  $J - [3.6]$  and  $J - [4.5]$  colour–magnitude diagrams. Same as in Fig. 6. The blue solid line represents the field dwarf sequence shifted as in Fig. 4.

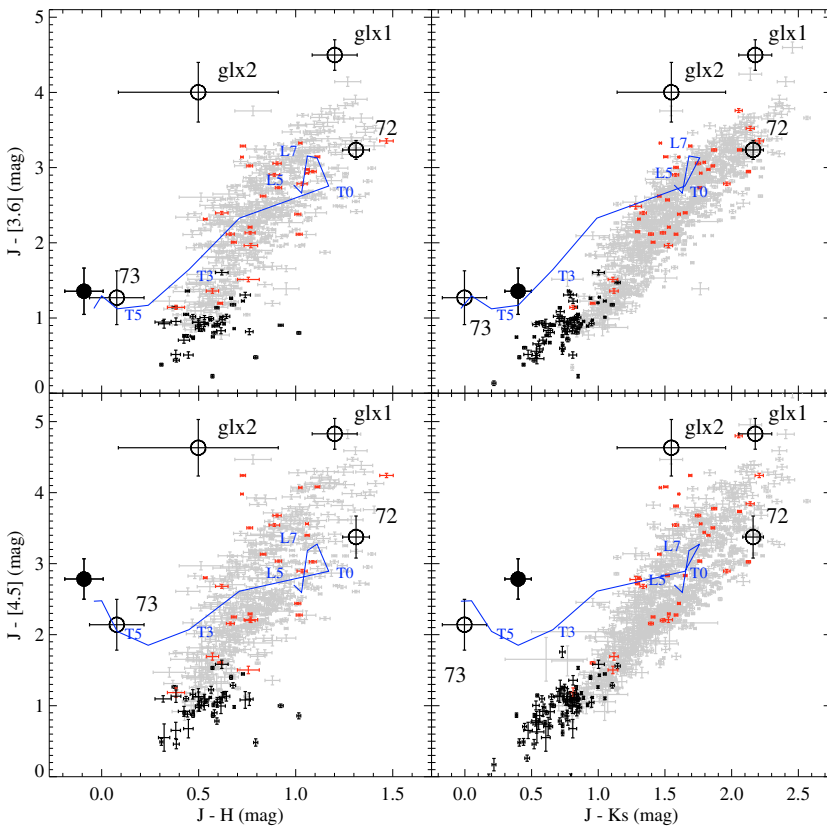


**Fig. 9.** Near- and mid-infrared colour–colour diagrams:  $J - [3.6]$  and  $J - [4.5]$  versus  $J - H$  (top- and bottom left),  $J - [3.6]$  and  $J - [4.5]$  versus  $J - K_s$  (top- and bottom right). Same as in Fig. 6.

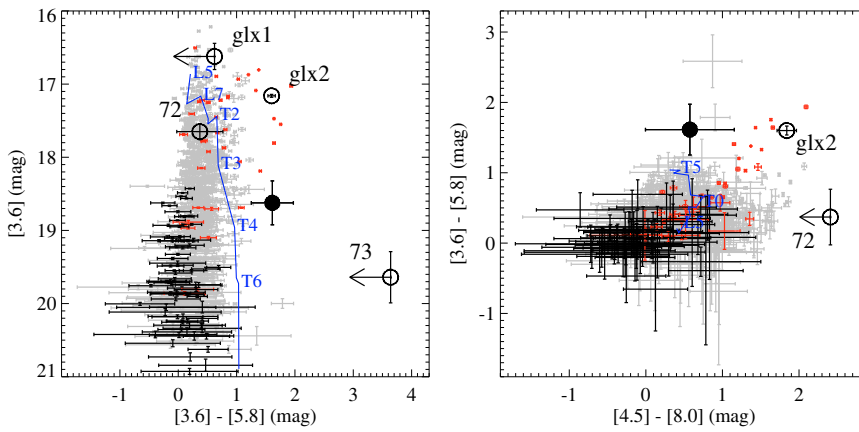


**Fig. 10.** Mid-infrared diagrams:  $[3.6]$  versus  $[3.6] - [5.8]$  (left),  $[3.6] - [5.8]$  versus  $[4.5] - [8.0]$  (right). Same as in Fig. 6.

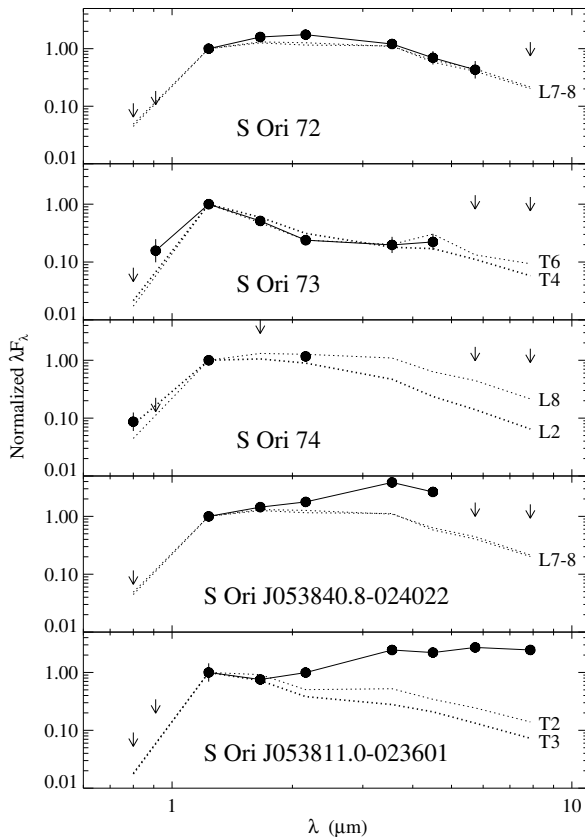


**Fig. 11.** Spectral energy distributions of the new candidates compared to average ones of field dwarfs (dotted lines).  $I\!Z\!J\!H\!K_s[3.6][4.5][5.6][8.0]$  from left to right.

*S Ori J053811.0–023601*, with  $J - H \sim 0.5$  mag and  $J - K_s \sim 1.5$  mag, could be an early T-type object or a galaxy. It is detected with brighter magnitudes at longer wavelengths, from the Omega2000  $JHK_s$ -band images (18j–k, Table 3) to the  $[3.6][4.5][5.6][8.0]$ -band images. It is undetected in the WFC  $I$ -band image and the LRIS  $I\!Z$ -band images (2000i1 and 1998iz1, Table 1). In Fig. 11, we show its spectral energy distribution, together with average ones of field dwarfs of T2 and T3 spectral types. We caution that the object appears relatively faint in the  $J$ -band and that the  $HK_s$ -band centroids are 0.8 arcsec south of the  $J$ -band centroid, although the  $JH$ -band data were obtained on the same observing night. The  $FWHMs$  in the  $HK_s$ -band images are approximately equal to those of nearby faint point-like sources, of about 1.2 and 0.9 arcsec, respectively. *S Ori J053811.0–023601* appears as an L/T transition object, but from the  $J$  versus  $J - [3.6]$  and  $J - [4.5]$  diagrams (Figs. 4 and 5) and as for *S Ori J053840.8–024022*, it is redder than the expected cluster sequence and could be a galaxy (Fig. 8). *S Ori J053811.0–023601* is particularly bright in the  $[5.8]$ - and  $[8.0]$ -bands and displays a colour  $[3.6] - [8.0] = 2.5 \pm 0.1$ , redder than most  $\sigma$  Orionis low-mass member candidates (Zapatero Osorio et al. 2007; Scholz & Jayawardhana 2008; Luhman et al. 2008). Considering that  $\geq 50\%$  of the known  $\sigma$  Orionis planetary-mass candidates exhibit excesses longward of  $5 \mu\text{m}$  (Zapatero Osorio et al. 2007), it appears to be a cluster member. In Figs. 6, 7, and 9, its optical and near-infrared colours differ from those of AGN and galaxies, but in Fig. 10, its other colours are consistent with the AGN hypothesis (see also Fig. 1 in Stern et al. 2005, representing spectroscopically identified stars, AGN,

and galaxies). Hence, although we cannot exclude completely this source being a peculiar cluster member with extreme infrared excesses, our data seem to indicate that it is more probably an AGN.

#### 4.3. Cluster membership

Because our search area is larger than that of the GOODS-MUSIC catalogue, contamination by red galaxies and AGN is even more likely to explain some of our candidates. Caballero et al. (2008b) present low-resolution optical spectroscopy and spectral energy distributions between  $0.55$  and  $24 \mu\text{m}$  of two sources fainter than the star-brown-dwarf cluster boundary, which were interpreted to be peculiar  $\sigma$  Orionis members with very red colours related to discs. They are instead two emission-line galaxies at moderate redshift, one with an AGN and the other ongoing star formation. In the present study, we assume that *S Ori J053840.8–024022* and *S Ori J053811.0–023601* are galaxy- or AGN contaminants and that the other objects are Galactic candidates awaiting confirmation by higher resolution imaging, proper motion, or spectroscopy.

In our search, we must also account for contamination by field dwarfs. Caballero et al. (2008a) provide predictions of the number of L5–T0, T0–T5, and T5–T8 field dwarf contaminants per square degree towards the  $\sigma$  Orionis region, in one-magnitude  $I$ -band intervals and from  $I = 21.0$  to  $29.0$  mag. We convert the bright and faint boundaries of the range  $J = 19.7$ – $21.1$  mag (as a prolongation of the search range of Caballero et al. 2007) into the  $I$ -band magnitudes corresponding to the earliest and latest spectral types of each of the three contaminant groups. We then sum the predicted numbers of contaminants accounting for the  $I$ -band ranges and scale the sums to the search area that is complete to  $J \geq 21.1$  mag ( $\sim 790 \text{ arcmin}^2$ ). We obtain about three L5–T8-type field dwarfs, which all contribute the most to the light close to  $J = 21.1$  mag. This predicted value remains mostly indicative, because the initial mass function and scale heights of late L- and T-type dwarfs are still uncertain. Interestingly, Caballero et al. (2008a) assume a rising mass function in the planetary mass regime and predict spatial densities of T0–8 dwarfs that are a factor of two higher than those derived from observations (Metchev et al. 2008; Lodieu et al. 2009a).

*S Ori 73* and *S Ori 70* are located<sup>9</sup> at  $11.9$  and  $8.7$  arcmin from  $\sigma$  Ori AB, respectively. *S Ori 72* and *S Ori 74* are closer, at  $3.6$  and  $4.1$  arcmin, respectively. Interestingly, the location of these faintest, presumably least massive candidates contrasts with that of the eleven  $13$ – $6 M_{\text{Jup}}$  free-floating planetary-mass candidates from Caballero et al. (2007), further out at  $26$ – $13$  arcmin in the survey area (see Fig. 2). Caballero (2008a) find an apparent deficit of low mass objects ( $M < 0.16 M_{\odot}$ ) towards the  $\sigma$  Orionis cluster centre. If the cluster membership census and the individual masses are confirmed, this configuration could be explained by several mechanisms, including e.g., a possible photo-erosion by the central OB stars (Hester et al. 1996; Whitworth & Zinnecker 2004) in the deep gravity well. Complementary studies of the dense cluster core (Bouy et al. 2009) and other cluster regions could thus help us to understand the formation of low-mass planetary-mass objects.

<sup>9</sup> *S Ori 73* is the only candidate found in one of the deeper multi-band search areas, summing up to  $\sim 470 \text{ arcmin}^2$ , see Sect. 3.

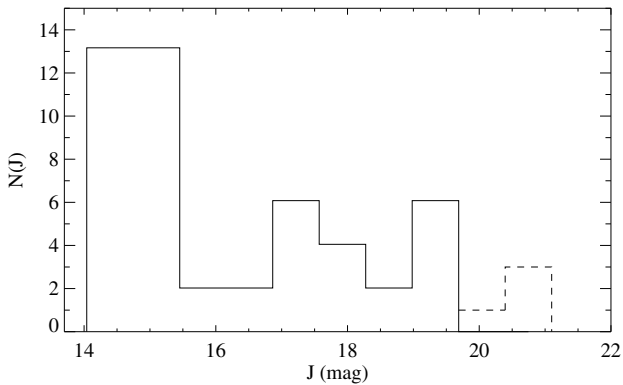


**Fig. 12.**  $J$ -band luminosity function with the LT-type candidates at  $J > 19.7$  mag (dashed line) and the brighter cluster member candidates from Caballero et al. (2007) scaled to the search area (solid line).

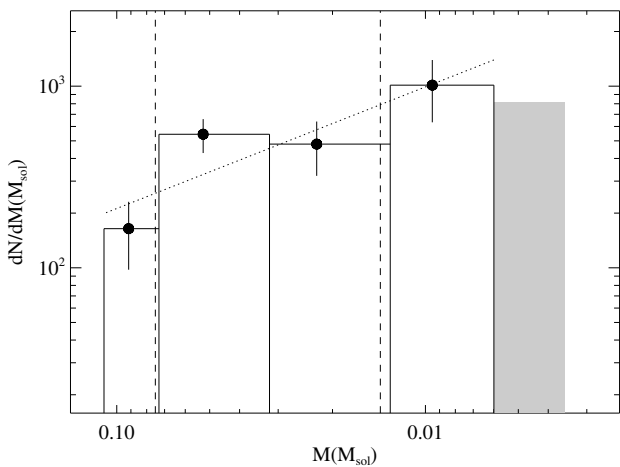


**Fig. 13.** Mass spectrum with contamination-corrected data. The dotted segment represents the linear fit to the data points from Caballero et al. (2007) in the mass range  $0.11$ – $0.006 M_{\odot}$ , which are previously scaled to the search area. The shaded region is our estimate of 0–2 cluster members in the mass range  $0.006$ – $0.004 M_{\odot}$ . From left to right, the vertical dashed lines represent the hydrogen and deuterium burning mass limits, respectively.

#### 4.4. Mass spectrum

We consider the luminosity and mass functions for the ISAAC and additional areas, where the search is complete down to  $J \geq 21.1$  mag ( $\sim 790$  arcmin<sup>2</sup>).

In Fig. 12, we show the  $J$ -band luminosity function. The magnitude bins in the range  $J = 19.7$ – $21.1$  mag correspond to the three new LT-type candidates and S Ori 70 (dashed line). The magnitude bins in the range  $J = 14.1$ – $19.7$  mag correspond to the cluster member candidates from Caballero et al. (2007), i.e., in the ISAAC area; they are scaled by the area factor  $(790)/780 = 1.0128$ . The magnitude bins have equal widths of about 0.7 mag.

We estimate the masses of our new cluster member candidates by comparing with the theoretical bolometric luminosities from the Lyon group (e.g., Baraffe et al. 2003), using exactly the same method as in Caballero et al. (2007). If cluster members, S Ori 72–74 would each have an estimated theoretical mass of  $4^{+3}_{-2} M_{\text{Jup}}$ , accounting for age, distance, and photometric uncertainties. This rounded up result does not change significantly by using a cluster distance of 400 pc (Mayne & Naylor 2008)

or 440 pc (Sherry et al. 2008) instead of 360 pc (Brown et al. 1994). The effective temperature corresponding to that mass would be of  $\sim 1400$  K. In Fig. 13, we display the mass spectrum ( $\Delta N/\Delta M$ ). The filled circles represent the contamination-corrected data points from Caballero et al. (2007) scaled to the search area of  $\sim 790$  arcmin<sup>2</sup>. The last bin (shaded region) corresponds to the result from the present study for the magnitude range  $J = 19.7$ – $21.1$  mag. Subtracting the three possible contaminants (see Sect. 4.3) from the four LT-type candidates and accounting for the Poissonian error, we estimate 0–2 cluster members with a mass of  $0.006$ – $0.004 M_{\odot}$ .

Previous studies of the substellar population in the  $\sigma$  Orionis cluster find that the mass spectrum increases toward lower masses. Béjar et al. (2001) show that it can be represented by a potential law ( $\Delta N/\Delta M \propto M^{-\alpha}$ ) with an  $\alpha$  index of 0.8 in the mass range  $0.11$ – $0.013 M_{\odot}$ . González-García et al. (2006) and Caballero et al. (2007) extend this mass spectrum to  $0.006 M_{\odot}$  and find a slightly lower index  $\alpha = 0.6$ . For the substellar mass range of  $0.073$ – $0.006 M_{\odot}$ , Caballero et al. (2007) obtain an even lower  $\alpha$  index of 0.4. An extrapolation of the mass spectrum with an index  $\alpha = 0.4$ – $0.8$  predicts 3–7 objects in the mass range  $0.006$ – $0.004 M_{\odot}$ . From our survey, the most likely number of cluster members in this mass interval is in the range 0–2. This could be an indication of a turnover in the substellar mass spectrum. However, given the low statistics and the possibility that the number of contaminants could be overestimated, such a change in the slope of the mass spectrum should be considered with caution. If real, the turnover could be related to an opacity mass limit, turbulence effects, or a different mass-luminosity relation (if less massive objects were fainter than predicted). Wider and deeper searches would be very valuable in constraining the mass spectrum more reliably at these and lower masses.

## 5. Conclusions

The mass function in young open clusters can provide clues about the formation mechanism of free-floating planetary-mass objects. We therefore decided to explore the substellar mass function for  $M < 6 M_{\text{Jup}}$  in the  $\sim 3$  Myr old  $\sigma$  Orionis open cluster. We extended to  $J = 19.5$ – $21.5$  mag the  $\sim 780$  arcmin<sup>2</sup> INT/WFC-VLT/ISAAC  $IJ$ -band search of Caballero et al. (2007).  $J$ -band sources (ISAAC and CAHA 3.5 m/Omega2000) were cross-matched with  $I$ - (WFC and Keck/LRIS) and  $HK$ -band sources (Omega2000, NTT/SofI, WHT/LIRIS, and CFHT/CFHTIR). We selected sources redder than a boundary at  $I - J > 3.1$ – $3.5$  or without an  $I$ -band detection or fainter than  $I = 24$  mag. These sources were then checked visually in all available images, including  $Z$ -band images from LRIS and WFC, and archival mid-infrared images from *Spitzer*/IRAC.

We recover S Ori 70 and the two faintest cluster member candidates from Caballero et al. (2007), and we find five red  $I - J$  sources, with  $J \sim 21$  mag, located within 12 arcmin of the cluster centre. The near- and mid-infrared colours indicate that one of the sources, S Ori 73, is probably of T spectral type. If confirmed as a cluster member, it would be the least massive free-floating T type object detected in  $\sigma$  Orionis, with  $4^{+3}_{-2} M_{\text{Jup}}$ . The four other sources appear to be L/T transition objects, but two are likely to be galaxies because of their strong mid-infrared excesses, similar to those of galaxies at  $J \geq 20.5$  mag. S Ori 72 and S Ori 73 are relatively close to the expected cluster sequence in the  $J$  versus  $J - [3.6]$  and  $J - [4.5]$  colour–magnitude diagrams. S Ori 74 is located 11.8 arcsec ( $\sim 4250$  AU) away from the solar-type cluster star Mayrit 260182. From the effective search area



## Appendix A: Representation of individual fields in the IZJHK-bands

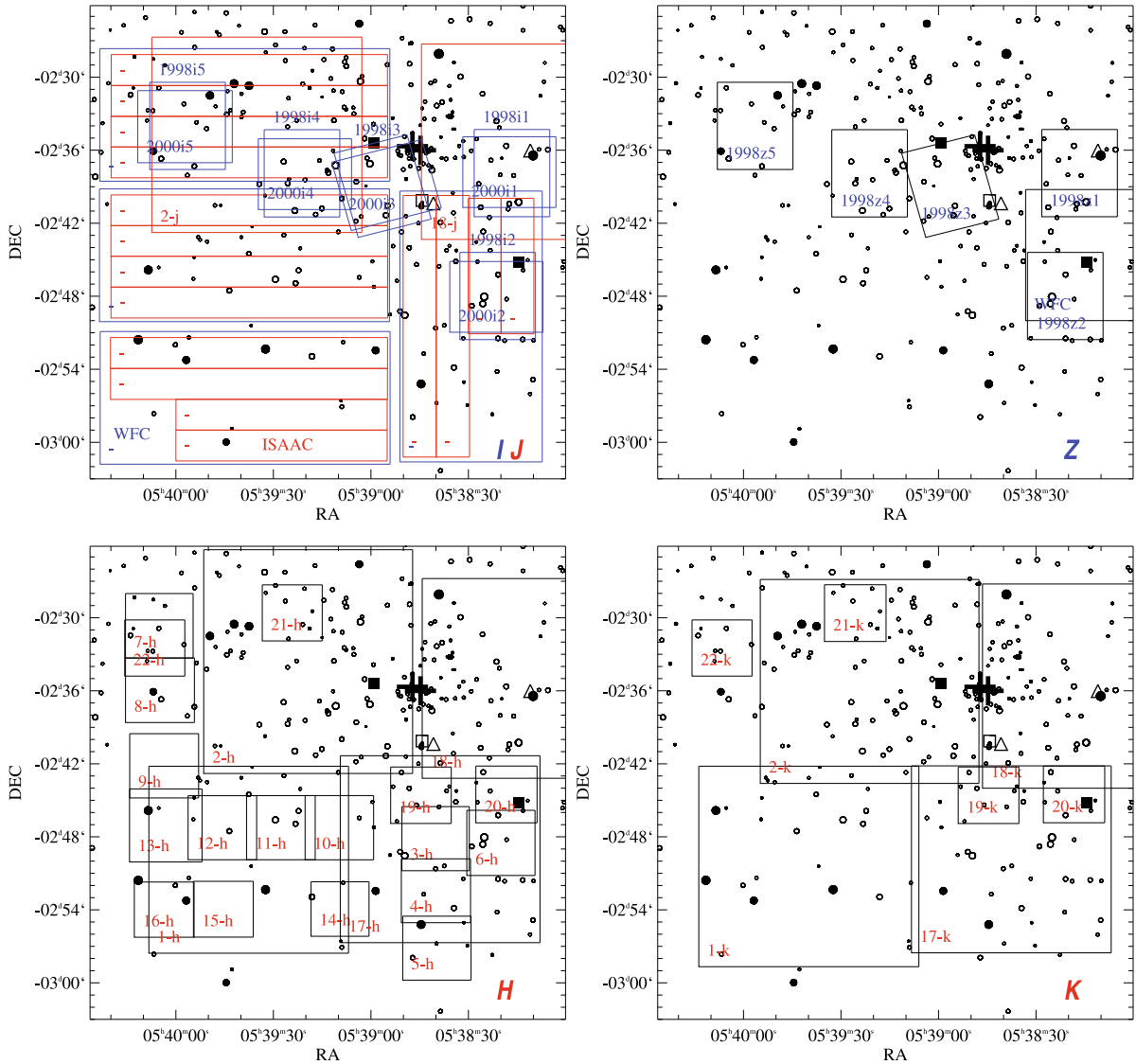


**Fig. A.1.** Individual fields used in the search: *IJ*-bands (top left), *Z*-band (top right), *H*-band (bottom left), and *K*-band (bottom right). Symbols are defined as in Fig. 2.

of  $\sim 790$  arcmin<sup>2</sup> complete to  $J = 21.1$  mag, we estimate there to be, after contaminant correction, between zero and two cluster members in the mass interval  $6\text{--}4 M_{\text{Jup}}$ . The low number of candidates in this mass bin may be indicative of a turnover in the substellar mass function. Wider and deeper optical-to-infrared surveys are required to confirm whether this is the case, by constraining the mass function more tightly at lower masses.

*Acknowledgements.* We thank the referee Kevin Luhman. We thank Claire Halliday (A&A language editor) and Terry Mahoney (IAC, Spain) for revising the English of the manuscript. We acknowledge Project No. 03065/PI/05 from the Fundación Séneca. Partially funded by the Spanish MEC under the Consolider-Ingenio 2010 Programme grant CSD2006-00070 (First Science with the GTC, <http://www.iac.es/consolider-ingenio-gtc/>). Based on observations made with ESO Telescopes at the La Silla or Paranal Observatories under programmes ID 068.C-0553(A) and 078.C-0402(A). Based on observations obtained at the Canada-France-Hawaii Telescope (CFHT), which is operated by the National Research Council of Canada, the Institut National des Sciences de l'Univers of the Centre National de la Recherche Scientifique

of France, and the University of Hawaii. Based on observations collected at the German-Spanish Astronomical centre, Calar Alto, jointly operated by the Max-Planck-Institut für Astronomie Heidelberg and the Instituto de Astrofísica de Andalucía (CSIC). We thank Calar Alto Observatory for allocation of director's discretionary time to this programme. Based on observations made with the Isaac Newton Telescope (INT) and the William Herschel Telescope (WHT) operated on the island of La Palma by the Isaac Newton Group in the Spanish Observatorio del Roque de los Muchachos of the Instituto de Astrofísica de Canarias. This research has been supported by the Spanish Ministry of Science and Innovation (MICINN) under the grant AYA2007-67458. Some of the data presented herein were obtained at the W.M. Keck Observatory, which is operated as a scientific partnership among the California Institute of Technology, the University of California, and the National Aeronautics and Space Administration. The Observatory was made possible by the generous financial support of the W.M. Keck Foundation. The authors wish to recognise and acknowledge the very significant cultural role and reverence that the summit of Mauna Kea has always had within the indigenous Hawaiian community. We are most fortunate to have the opportunity to conduct observations from this mountain. This work is based in part on observations made with the Spitzer Space Telescope, which is operated by the Jet Propulsion Laboratory,

## Appendix B: Finding charts

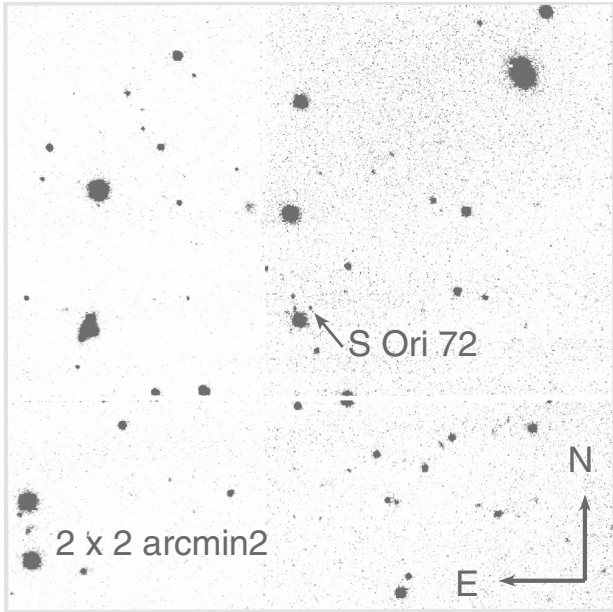


**Fig. B.1.** ISAAC *J*-band image of S Ori 72.

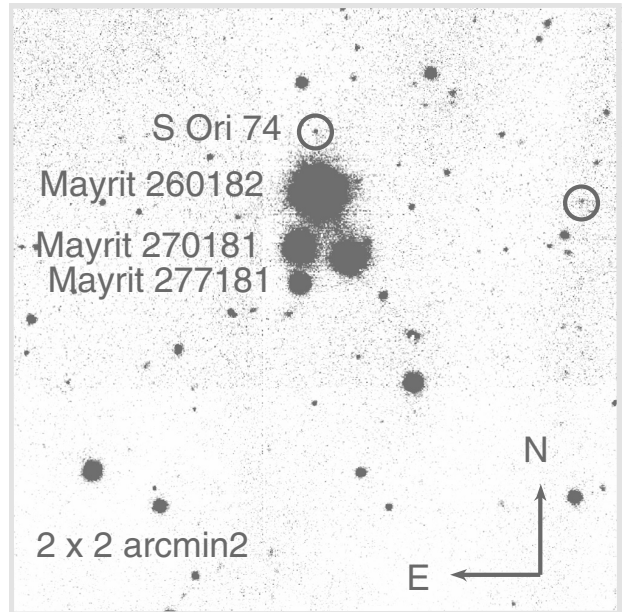


**Fig. B.3.** ISAAC *J*-band image of S Ori 74 and S Ori J053840.8-024022 (unlabelled circle).

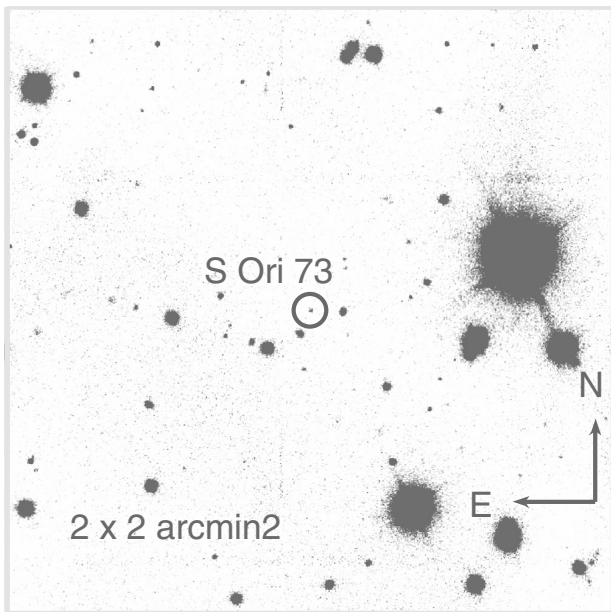


**Fig. B.2.** ISAAC *J*-band image of S Ori 73.

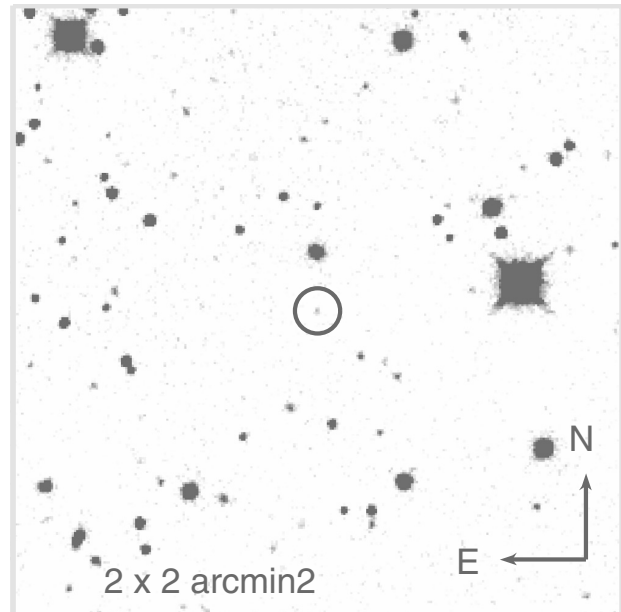


**Fig. B.4.** Omega2000 *H*-band image of S Ori J053811.0-023601.

California Institute of Technology under a contract with NASA. IRAF is distributed by the National Optical Astronomy Observatories, which are operated by the Association of Universities for Research in Astronomy, Inc., under cooperative agreement with the National Science Foundation. This publication makes use of data products from the Two Micron All Sky Survey, which is a joint project of the University of Massachusetts and the Infrared Processing and Analysis centre/California Institute of Technology, funded by the National Aeronautics and Space Administration and the National Science Foundation. This research has made use of SAOImage DS9, developed by Smithsonian Astrophysical Observatory. This research has made use of the SIMBAD database, operated at CDS, Strasbourg, France.

## References

- Baraffe, I., Chabrier, G., Barman, T. S., Allard, F., & Hauschildt, P. H. 2003, *A&A*, 402, 701  
 Bate, M. R. 2005, *MNRAS*, 363, 363  
 Bate, M. R. 2009, *MNRAS*, 392, 590  
 Bate, M. R., & Bonnell, I. A. 2005, *MNRAS*, 356, 1201  
 Beichman, C. A., Cutri, R., Jarrett, T., Stiening, R., & Skrutskie, M. 2003, *AJ*, 125, 2521  
 Béjar, V. J. S., Martín, E. L., Zapatero Osorio, M. R., et al. 2001, *ApJ*, 556, 830  
 Bihain, G., Rebolo, R., Béjar, V. J. S., et al. 2006, *A&A*, 458, 805  
 Boss, A. P. 1997, *Science*, 276, 1836  
 Bouy, H., Huélamo, N., Martín, E. L., et al. 2009, *A&A*, 493, 931

- Brown, A. G. A., de Geus, E. J., & de Zeeuw, P. T. 1994, *A&A*, 289, 101
- Burgasser, A. J., Kirkpatrick, J. D., McGovern, M. R., et al. 2004, *ApJ*, 604, 827
- Caballero, J. A. 2006, Ph.D. Thesis, Universidad de La Laguna, Spain
- Caballero, J. A. 2007, *A&A*, 466, 917
- Caballero, J. A. 2008a, *MNRAS*, 383, 375
- Caballero, J. A. 2008b, *A&A*, 478, 667
- Caballero, J. A. 2009, in *The 15th Cambridge Workshop on Cool Stars, Stellar Systems, and the Sun*, ed. E. Stempels, AIP Conf. Proc., 1094, 912
- Caballero, J. A., Martín, E. L., Dobbie, P. D., & Barrado y Navascués, D. 2006, *A&A*, 460, 635
- Caballero, J. A., Béjar, V. J. S., Rebolo, R., et al. 2007, *A&A*, 470, 903
- Caballero, J. A., Burgasser, A. J., & Klement, R. 2008a, *A&A*, 488, 181
- Caballero, J. A., Valdivielso, L., Martín, E. L., et al. 2008b, *A&A*, 491, 515
- Carpenter, J. M. 2001, *AJ*, 121, 2851
- Casali, M., Adamson, A., Alves de Oliveira, C., et al. 2007, *A&A*, 467, 777
- Chabrier, G., & Baraffe, I. 2000, *ARA&A*, 38, 337
- Fortney, J. J., Marley, M. S., Saumon, D., & Lodders, K. 2008, *ApJ*, 683, 1104
- González-García, B. M., Zapatero Osorio, M. R., Béjar, V. J. S., et al. 2006, *A&A*, 460, 799
- González Hernández, J. I., Caballero, J. A., Rebolo, R., et al. 2008, *A&A*, 490, 1135
- Grazian, A., Fontana, A., de Santis, C., et al. 2006, *A&A*, 449, 951
- Hambly, N. C., Collins, R. S., Cross, N. J. G., et al. 2008, *MNRAS*, 384, 637
- Hernández, J., Hartmann, L., Megeath, T., et al. 2007, *ApJ*, 662, 1067
- Hester, J. J., Scowen, P. A., Sankrit, R., et al. 1996, *AJ*, 111, 2349
- Hewett, P. C., Warren, S. J., Leggett, S. K., & Hodgkin, S. T. 2006, *MNRAS*, 367, 454
- Hoyle, F. 1953, *ApJ*, 118, 513
- Joye, W. A., & Mandel, E. 2003, in *Astronomical Data Analysis Software and Systems XII*, ed. H. E. Payne, R. I. Jedrzejewski, & R. N. Hook, PASPC, 295, 489
- Landsman, W. B. 1993, in *PASPC, Astronomical Data Analysis Software and Systems II*, ed. R. J. Hanisch, R. J. V. Brissenden, & J. Barnes, 52, 246
- Larson, R. B. 1973, *MNRAS*, 161, 133
- Lawrence, A., Warren, S. J., Almaini, O., et al. 2007, *MNRAS*, 379, 1599
- Lodieu, N., Dobbie, P. D., Deacon, N. R., Venemans, B. P., & Durant, M. 2009a, *MNRAS*, 395, 1631
- Lodieu, N., Zapatero Osorio, M. R., Rebolo, R., Martín, E. L., & Hambly, N. C. 2009b, *A&A*, 505, 1115
- Low, C., & Lynden-Bell, D. 1976, *MNRAS*, 176, 367
- Lucas, P. W., & Roche, P. F. 2000, *MNRAS*, 314, 858
- Luhman, K. L., Hernández, J., Downes, J. J., Hartmann, L., & Briceño, C. 2008, *ApJ*, 688, 362
- Martín, E. L., & Zapatero Osorio, M. R. 2003, *ApJ*, 593, L113
- Mayne, N. J., & Naylor, T. 2008, *MNRAS*, 386, 261
- Metchev, S. A., Kirkpatrick, J. D., Berriman, G. B., &Looper, D. 2008, *ApJ*, 676, 1281
- Newberry, M. V. 1991, *PASP*, 103, 122
- Padoan, P., & Nordlund, Å. 2002, *ApJ*, 576, 870
- Padoan, P., & Nordlund, Å. 2004, *ApJ*, 617, 559
- Padoan, P., Nordlund, Å., Kritsuk, A. G., Norman, M. L., & Li, P. S. 2007, *ApJ*, 661, 972
- Patten, B. M., Stauffer, J. R., Burrows, A., et al. 2006, *ApJ*, 651, 502
- Rees, M. J. 1976, *MNRAS*, 176, 483
- Scholz, A., & Jayawardhana, R. 2008, *ApJ*, 672, L49
- Sherry, W. H., Walter, F. M., Wolk, S. J., & Adams, N. R. 2008, *AJ*, 135, 1616
- Silk, J. 1977, *ApJ*, 214, 152
- Skrutskie, M. F., Cutri, R. M., Stiening, R., et al. 2006, *AJ*, 131, 1163
- Stamatellos, D., & Whitworth, A. P. 2009, *MNRAS*, 392, 413
- Stern, D., Eisenhardt, P., Gorjian, V., et al. 2005, *ApJ*, 631, 163
- Tinney, C. G., Burgasser, A. J., & Kirkpatrick, J. D. 2003, *AJ*, 126, 975
- Veras, D., Crepp, J. R., & Ford, E. B. 2009, *ApJ*, 696, 1600
- Vrba, F. J., Henden, A. A., Luginbuhl, C. B., et al. 2004, *AJ*, 127, 2948
- Whitworth, A. P., & Goodwin, S. P. 2005, *Astron. Nachr.*, 326, 899
- Whitworth, A. P., & Stamatellos, D. 2006, *A&A*, 458, 817
- Whitworth, A. P., & Zinnecker, H. 2004, *A&A*, 427, 299
- Zapatero Osorio, M. R., Béjar, V. J. S., Martín, E. L., et al. 2000, *Science*, 290, 103
- Zapatero Osorio, M. R., Béjar, V. J. S., Martín, E. L., et al. 2002a, *ApJ*, 578, 536
- Zapatero Osorio, M. R., Béjar, V. J. S., Pavlenko, Y., et al. 2002b, *A&A*, 384, 937
- Zapatero Osorio, M. R., Caballero, J. A., Béjar, V. J. S., et al. 2007, *A&A*, 472, L9
- Zapatero Osorio, M. R., Béjar, V. J. S., Bihain, G., et al. 2008, *A&A*, 477, 895
- Zhang, Z. H., Pokorny, R. S., Jones, H. R. A., et al. 2009, *A&A*, 497, 619

**Date:** Tue, 18 May 2010 15:05:59 +0200 [02:05:59 PM WEST]

---


**From:** aanda.paris@obspm.fr

**To:** gbihain@iac.es

---

**Subject:** AA/2009/13676: paper sent to language-editor

---

 1 unnamed [text/plain] 0.66 KB

18/05/2010

Mr Gabriel Bihain  
Instituto de Astrofísica de Canarias  
c/ Vía Láctea, s/n  
38205 La Laguna  
SPAIN

gbihain@iac.es

Our Ref. : AA/2009/13676

Dear Mr Bihain,

I am pleased to inform you that your paper entitled "Near-infrared low-resolution spectroscopy of Pleiades L-type brown dwarfs" is now accepted for publication in section 7. Stellar structure and evolution of Astronomy and Astrophysics. The official date of acceptance is 18/05/2010.

Your paper is being sent to our language editor and the annotated copy will be forwarded to you. We will contact you again as soon as possible.

Sincerely yours,

C. Bertout  
Editorial Office Paris

---

# Near-infrared low-resolution spectroscopy of Pleiades L-type brown dwarfs

G. Bihain<sup>1,2</sup>, R. Rebolo<sup>1,2,3</sup>, M. R. Zapatero Osorio<sup>4</sup>, V. J. S. Béjar<sup>1,3</sup>, and J. A. Caballero<sup>4,5</sup>

<sup>1</sup> Instituto de Astrofísica de Canarias, c/ vía Láctea, s/n, 38205 La Laguna, Tenerife, Islas Canarias, Spain  
e-mail: gbihain@iac.es

<sup>2</sup> Consejo Superior de Investigaciones Científicas (CSIC), Spain

<sup>3</sup> Departamento de Astrofísica, Universidad de La Laguna, 38205 La Laguna, Tenerife, Islas Canarias, Spain

<sup>4</sup> Centro de Astrobiología (CSIC-INTA), Carretera de Ajalvir, km 4. 28850 Torrejón de Ardoz, Madrid, Spain

<sup>5</sup> Dpto. de Astrofísica y Ciencias de la Atmósfera, Facultad de Física, Universidad Complutense de Madrid, 28040 Madrid, Spain

Received 16 November 2009 / Accepted 18 May 2010

## ABSTRACT

**Context.** The fundamental properties of brown dwarfs evolve with age. Models describing the evolution of luminosities and effective temperatures, among other physical parameters, can be empirically constrained using brown dwarfs of various masses in star clusters of well-determined age and metallicity.

**Aims.** We aim to carry out a spectroscopic and photometric characterization of low-mass brown dwarfs in the  $\sim 120$  Myr old Pleiades open cluster.

**Methods.** We obtained low-resolution, near-infrared spectra of the  $J = 17.4\text{--}18.8$  mag candidate L-type brown dwarfs PLIZ 28 and 35, BRB 17, 21, 23, and 29, which are Pleiades members by photometry and proper motion. We also obtained spectra of the well-known  $J = 15.4\text{--}16.1$  mag late M-type cluster members PPI 1, Teide 1, and Calar 3.

**Results.** We find that the first six objects have early- to mid-L spectral types and confirm previously reported M-types for the three other objects. The spectra of the L0-type BRB 17 and PLIZ 28 present a triangular  $H$ -band continuum shape, indicating that this peculiar spectral feature persists until at least the age of the Pleiades. We add to our sample 36 reported M5–L0-type cluster members and collect their  $I_C$ - and UKIDSS  $ZYJHK$ -band photometry. We confirm a possible interleaving of the Pleiades and field L-type sequences in the  $JHK$  absolute magnitude versus spectral type diagrams, and quantify marginally redder Pleiades  $J - K$  colours, by  $0.11 \pm 0.20$  mag, possibly related to both reddening and youth. Using field dwarf bolometric correction – and effective temperature – spectral type relations, we obtain the Hertzsprung-Russell diagram of the Pleiades sample. Theoretical models reproduce the spectral sequence at M5.5–9, but appear to overestimate the luminosity or underestimate the effective temperature at L0–5.

**Conclusions.** We classify six faint Pleiades brown dwarfs as early to mid L-type objects using low-resolution near-infrared spectra. We compare their properties to field dwarfs and theoretical models and estimate their masses to be in the range  $0.025\text{--}0.035 M_{\odot}$ .

**Key words.** open clusters and associations: individual: Pleiades – brown dwarfs – stars: fundamental parameters

## 1. Introduction

About 600 field L-type dwarfs have been spectroscopically identified to date<sup>1</sup>. Most of them have been discovered by large sky-area surveys such as 2MASS (Skrutskie et al. 2006) and SDSS (Abazajian et al. 2009). Spectroscopy has allowed the determination of physical properties and the derivation of effective temperatures (in the range  $\sim 2300\text{--}1400$  K, e.g. Leggett et al. 2001), and parallax studies have provided distances and luminosities for about 10% of these objects, indicating that they are most probably very low-mass stars or massive brown dwarfs. For individual field L-dwarfs, an estimation of mass from the luminosity and effective temperature requires additional information on age, which is in general difficult to obtain. This limits our ability to determine the field substellar mass function and formation history (Reid et al. 1999; Chabrier 2002, 2003; Kroupa & Bouvier 2003; Burgasser 2004; Allen et al. 2005; Pinfield et al. 2006).

An empirical determination of the evolution of effective temperature and luminosity with age for L-type dwarfs could be obtained by identifying such objects in stellar associations of various ages. Brown dwarf- and planetary-mass candidates of (mostly early) L-type have been studied photometrically and spectroscopically in the Serpens- (Lodieu et al. 2002), Ophiuchus- (Jayawardhana & Ivanov 2006a), Chamaeleon I- (Luhman et al. 2006, 2008; Luhman & Muench 2008; Schmidt et al. 2008), Chamaeleon II- (Jayawardhana & Ivanov 2006b; Allers et al. 2007), Taurus- (Itoh et al. 2005; Luhman et al. 2009), Trapezium- (Lucas et al. 2001, 2006; Weights et al. 2009), and Lupus 1 clouds (Neuhäuser et al. 2005; McElwain et al. 2007), the  $\sigma$  Orionis open cluster (Zapatero Osorio et al. 1999a, 2000; Béjar et al. 2001; Martín et al. 2001; Barrado y Navascués et al. 2001, 2002; McGovern et al. 2004), and the TW Hydrae- (Gizis 2002; Chauvin et al. 2004;Looper et al. 2007), Upper Scorpius- (Lodieu et al. 2008; Lafrenière et al. 2008; Béjar et al. 2008), and Tucana-Horologium associations (Chauvin et al. 2005). All these star-forming regions are very young, with ages of a few Myr to a few tens of Myr. Finally,

<sup>1</sup> <http://spider.ipac.caltech.edu/staff/davy/ARCHIVE/index.shtml>, 2010 May 17.



**Table 1.** Spectroscopic observations.

Object	$J^b$ (mag)	Opt. SpT <sup>c</sup>	Instrument	Date	$T_{\text{exp}}^d$ (min)	Airmass	$\Delta\text{airmass}_{\text{T-S}}$	$S/N$	Near-IR SpT
PPI 1	$15.36 \pm 0.01$	M6.5	NICS( <i>JHK</i> )	2002 Oct. 31	$8 \times 2$	1.08	0.14	50	$M7.0 \pm 0.5$
Calar 3	$16.08 \pm 0.01$	M8	NICS( <i>JHK</i> )	2002 Oct. 31	$8 \times 2$	1.15	0.07	49	$M8.0 \pm 0.5$
Teide 1	$16.21 \pm 0.01$	M8	NICS( <i>JHK</i> )	2002 Nov. 27	$8 \times 2$	1.03	0.73	32	$M8.0 \pm 0.5$
BRB 17	$17.41 \pm 0.03$	...	LIRIS( <i>zJ, HK</i> )	2006 Dec. 28	$(12, 18) \times 2$	1.74, 1.41	0.44, 0.89	4, 6	$L0.0 \pm 1.0$
PLIZ 28	$17.60 \pm 0.04$	...	NICS( <i>JHK</i> )	2005 Nov. 20	$15 \times 2$	1.11	0.57	18	$L0.0 \pm 1.0$
PLIZ 35	$18.07 \pm 0.05$	...	NICS( <i>JHK</i> )	2005 Sep. 18	$65 \times 0.6$	1.03	-0.03	15	$L2.0 \pm 1.0$
BRB 21	$18.14 \pm 0.06$	...	NICS( <i>JHK</i> )	2005 Sep. 18	$80 \times 0.5$	1.21	0.15	7	$L3.0 \pm 1.0$
BRB 23	$18.23 \pm 0.04$	...	NICS( <i>JHK</i> )	2007 Feb. 7	$10 \times 5$	1.33	-0.27	14	$L3.5 \pm 1.0$
BRB 29	$18.69 \pm 0.10$	...	LIRIS( <i>HK</i> )	2006 Dec. 29	$12 \times 2$	1.09	-0.02	3	$L4.5 \pm 1.5$
J0829 <sup>a</sup>	$12.80 \pm 0.03$	L2V	LIRIS( <i>zJ, HK</i> )	2006 Dec. 28	$(4, 6) \times 1.5$	1.38, 1.36	0.80, 0.94	29, 37	$L2.0 \pm 1.0$

**Notes.** <sup>(a)</sup> SSSPM J0829–1309. <sup>(b)</sup> From the Galactic Clusters Survey (GCS) component of UKIDSS (Lawrence et al. 2007, sixth data release) for the Pleiades members and from 2MASS (Skrutskie et al. 2006) for the field object. <sup>(c)</sup> From Martín et al. (1996) for the three Pleiades objects and from Scholz & Meusinger (2002) and Lodieu et al. (2005) for the field object. <sup>(d)</sup> Dithers  $\times$  detector integration time.

several L-type dwarfs characterized photometrically and spectroscopically have been associated with moving groups, such as the all-sky,  $400 \pm 100$  Myr old Ursa Major moving group (Bannister & Jameson 2007; Jameson et al. 2008; Casewell et al. 2008).

In this context, the Pleiades open cluster is well-suited to providing a reference sequence for L- and T-dwarfs at an age of  $\sim 120$  Myr. Proper-motion studies (Moraux et al. 2003; Bihain et al. 2006; Lodieu et al. 2007) have shown that there is a significant population of low-luminosity members of the cluster that, based on their optical and near-infrared colours, are likely to be of spectral type L. Casewell et al. (2007) have extended the brown dwarf search beyond these objects with some candidate members of spectral type T. Here, we report near-infrared spectroscopy for six of the nine L-type candidates confirmed as Pleiades proper motion members by Bihain et al. (2006), which allows us to study the relationship between spectral type and luminosity for L dwarfs at a homogeneous age and solar metallicity.

## 2. Observations and data reduction

Low-resolution spectra of four candidate L-type Pleiades brown dwarfs and three well-known late M-type Pleiads were obtained with the Near Infrared Camera Spectrometer (NICS) and its Amici prism, mounted on the 3.6 m Telescopio Nazionale Galileo (TNG; Observatorio del Roque de Los Muchachos –ORM–, Spain). Additional spectra of two other candidate L-type Pleiades brown dwarfs and an L2-type field dwarf were obtained with the Long-slit Intermediate Resolution Infrared Spectrograph (LIRIS), mounted on the 4.2 m William Hershel Telescope (WHT, ORM). Table 1 lists the object names,  $J$ -band magnitudes, optical spectral types (when available), instruments (and bandpass coverage), observing-night dates, exposure times, mean airmasses, differences in mean airmasses between telluric standard stars (T) and the science objects (S), and pseudo-continuum signal-to-noise ratios. The weather conditions were clear, except on the nights of 2002 November 27 and 2006 December 28, when some clouds were present. The seeing ( $0.6$ – $1.5$  arcsec) implied in most cases the use of a slit width of  $1.0$  arcsec and in the case of Calar 3 and PPI 1 a slit width of  $1.5$  arcsec. The NICS/Amici spectra have a constant resolving power  $R = \lambda/\Delta\lambda \approx 50$  in the range  $0.8$ – $2.5 \mu\text{m}$  (dispersion  $3$ – $10$  nm  $\text{pix}^{-1}$ ); for Calar 3 and PPI 1,  $R \approx 33$ . The LIRIS  $zJ$ -

band ( $0.887$ – $1.531 \mu\text{m}$ ) spectra have  $R \approx 960$  at  $\lambda \approx 1.17 \mu\text{m}$  and a constant dispersion of  $0.61$  nm  $\text{pix}^{-1}$ , whereas the  $HK$ -band ( $1.388$ – $2.419 \mu\text{m}$ ) spectra have  $R \approx 945$  at  $\lambda \approx 1.83 \mu\text{m}$  and a constant dispersion of  $0.97$  nm  $\text{pix}^{-1}$ . Small dithers over two or three different positions along the slits were performed to allow for sky subtraction. Spectra of hot, B9–A1V stars were obtained during each observing night, except in 2002, when the spectra of a DAO white dwarf and a K1 dwarf were obtained, relatively close in coordinates to the scientific targets, for the correction of the instrumental response and the telluric absorption.

The raw spectroscopic data were reduced using standard routines within the IRAF<sup>2</sup> environment. Amici spectra were sky-subtracted, flat-fielded, aligned, combined, optimally extracted, and wavelength-calibrated using the look-up table provided on the instrument’s webpage<sup>3</sup> and the deep telluric absorption features. LIRIS raw images were corrected for pixel mapping and row cross-talk, and the spectra were sky-subtracted, flat-fielded, wavelength-calibrated (using vacuum wavelengths of Ar arc lamps), shifted, and combined using routines in the LIRISDR package developed by J. A. Acosta-Pulido before they were optimally extracted. The instrumental response and telluric bands were removed by dividing by the “telluric” spectra and multiplying by black-body spectra with the same effective temperature. The intrinsic lines in the LIRIS hot-star spectra were removed before dividing the science spectra. A vacuum-to-air correction was applied to the LIRIS spectra, using the default standard temperature and pressure. As indicated in the column  $\Delta\text{airmass}_{\text{T-S}}$  of Table 1, some of our science spectra were acquired at airmasses quite different to the telluric spectra, thus yielding a poor correction of telluric bands. The reduced Amici spectrum of BRB 23 was cut longwards of  $2.245 \mu\text{m}$  because the level of the sky counts entered the non-linear regime of the detector. The LIRIS  $zJ$  and  $HK$  spectra were flux-calibrated using published  $JH$ -band photometry, allowing us to combine both parts. The pseudo-continuum signal-to-noise ratios (Table 1) were measured in the interval  $2.14$ – $2.24 \mu\text{m}$ , or for the LIRIS  $zJ$ -band data, in the interval  $1.28$ – $1.32 \mu\text{m}$ .

<sup>2</sup> IRAF is distributed by the National Optical Astronomy Observatories, which are operated by the Association of Universities for Research in Astronomy, Inc., under cooperative agreement with the National Science Foundation.

<sup>3</sup> <http://web.archive.org/web/20071126094610/http://www.tng.iac.es/instruments/nics/spectroscopy.html>

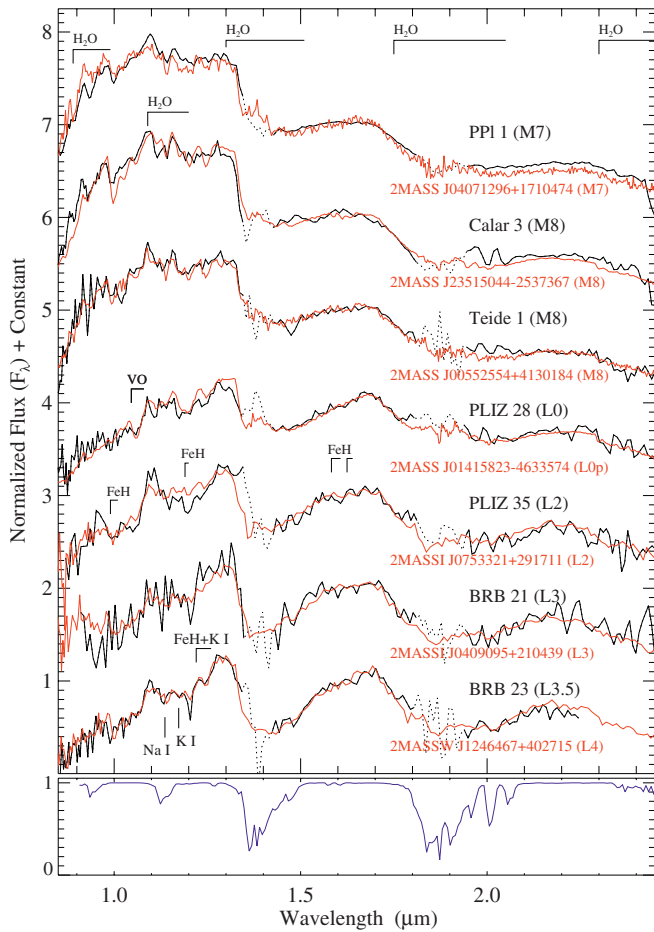


**Fig. 1.** NICS/Amici low-resolution 0.85–2.40  $\mu\text{m}$  spectra of Pleiades low-mass members (black lines). The spectra are in air wavelengths, normalized to the average flux between 1.56 and 1.74  $\mu\text{m}$ , and offset by constants. The main regions affected by tellurics are represented by dotted lines. Field dwarf spectra are overplotted in red and their references are: 2MASS J04071296+1710474 and 2MASS J00552554+4130184 (Burgasser et al. 2004), 2MASS J23515044–2537367 (Burgasser et al. 2008), 2MASS J01415823–4633574 (Kirkpatrick et al. 2006), 2MASS J0753321+2917111, 2MASS J0409095+210439, and 2MASSW J1246467+402715 (Testi 2009). A model atmospheric transmission rebinned to a dispersion of 7  $\text{nm pix}^{-1}$  is represented in blue in the lower panel.

### 3. Spectral types

In Figs. 1 and 2, we show the reduced Amici and LIRIS spectra, respectively, and also a model atmospheric transmission (Hammersley 1998). The main absorption features of our target spectra are indicated (see Cushing et al. 2005 for details). As expected for late M- and L-type objects, the spectra display intense water absorption bands at 1.3–1.51 and 1.75–2.05  $\mu\text{m}$ . Also, as expected for lower effective temperatures and dustier atmospheres (see Fig. 2 in Tsuji et al. 1996), the fainter objects have a flux at 0.85–1.3  $\mu\text{m}$  that is decreased compared to that at *H* or *K* band.

The Amici spectra were classified spectroscopically by comparison with spectra of the Amici (Testi et al. 2001; Testi 2009) and SpeX Prism libraries<sup>4</sup> (Adam Burgasser), with resolving power  $R \sim 100$  and *JHK*-bandpass coverage. The LIRIS spec-

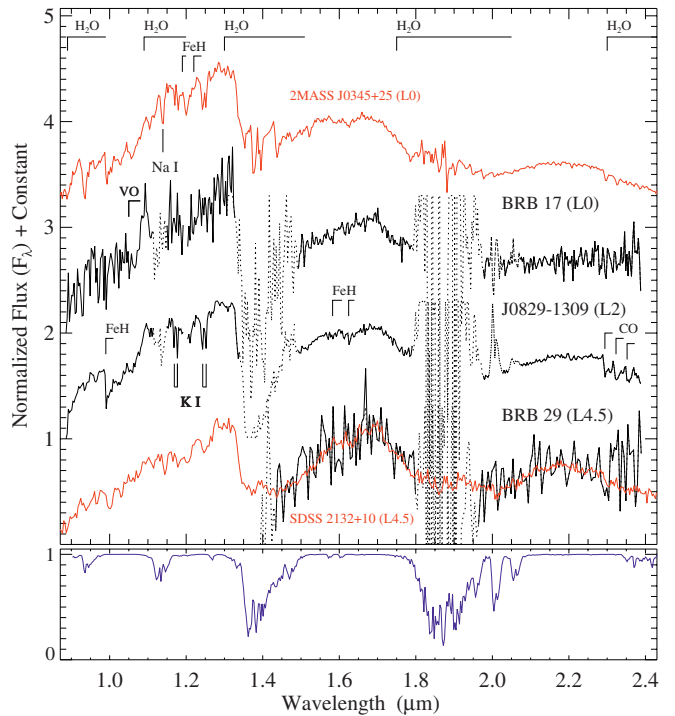


**Fig. 2.** LIRIS intermediate-resolution spectra of the Pleiades low-mass members BRB 17 and BRB 29 and the field dwarf SSSPM J0829–130 (black lines). The spectra are in air wavelengths, normalized by the average flux between 1.56 and 1.74  $\mu\text{m}$ , rebinned to dispersions of 3 (BRB 17 and SSSPM J0829–1309) and 5  $\text{nm pix}^{-1}$  (BRB 29), and offset by constants. The main regions affected by tellurics are represented by dotted lines. The spectra of the field dwarfs 2MASS J03454316+2540233 (composite spectrum of Leggett et al. 2001, rebinned to 3  $\text{nm pix}^{-1}$ ) and SDSS J213240.36+102949.4 ( $R \sim 150$ ; Chiu et al. 2006) are shown in red. A model atmospheric transmission rebinned to 3  $\text{nm pix}^{-1}$  is represented in blue in the lower panel.

tra were classified similarly using in addition the  $R \sim 150$ –600 spectra from the L- and T-type dwarf data archive of Sandy Leggett<sup>5</sup>. The first, second, and third libraries adopt L spectral types from (i) the far-red optical (classification scheme of Kirkpatrick et al. 1999); (ii) the far-red optical or near-infrared; and (iii) the near-infrared (classification scheme of Geballe et al. 2002, which agrees in the L0–L5 range with the optical schemes of Martín et al. 1999; and Kirkpatrick et al. 1999), respectively. For the objects of the second and third libraries, we preferred to adopt their optical spectral types, when available<sup>6</sup>.

We classified the spectra first visually by considering the change in the continuum shape from the earlier to the later spectral types (e.g. the 0.85–1.3  $\mu\text{m}$  region and the  $\text{H}_2\text{O}$  absorption bands), and then by chi-squared minimization for optimization. The errors were obtained by accounting for the plausible earliest- and latest-type field dwarf spectra matching those of our targets. For BRB 17 and PLIZ 28, however, the spectra differ notably from those of normal field dwarfs. Figure 3 illustrates this with a sequence of field dwarfs whose optical-typing references are LP 944-20 (Kirkpatrick et al. 1999), 2MASS J12212770+0257198 (Reid et al. 2008), 2MASS J01415823–4633574 (Kirkpatrick et al. 2006, 2008; Cruz et al. 2009), GJ 1048B (Gizis et al.

<sup>5</sup> <http://staff.gemini.edu/~sleggett/LTdata.html>

<sup>6</sup> <http://www.dwarfarchives.org>

<sup>4</sup> <http://www.browndwarfs.org/spexprism>

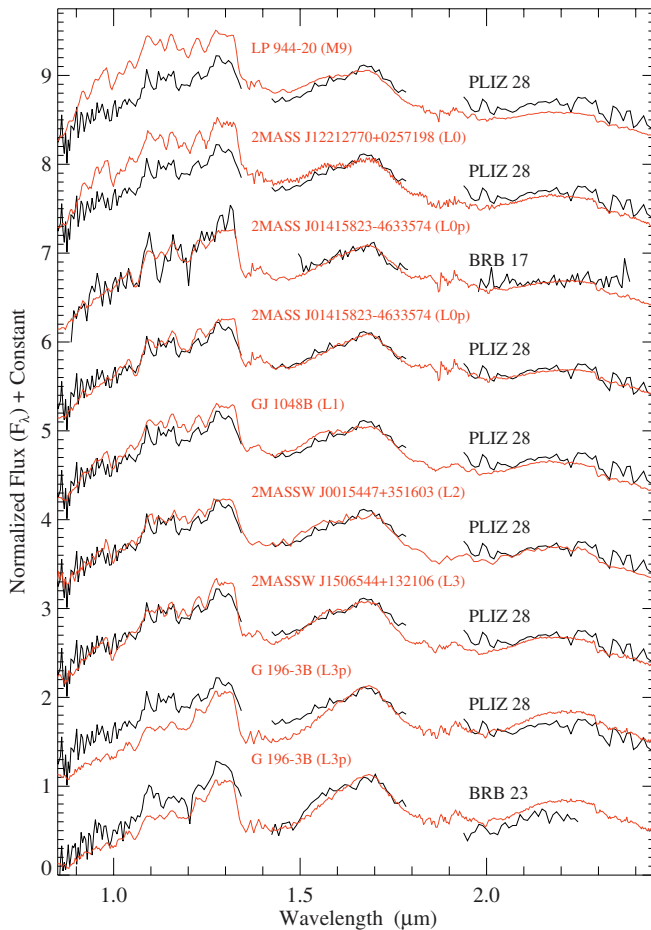


**Fig. 3.** Spectra of Pleiades L-type brown dwarfs compared to field dwarf spectra (overplotted in red). The spectra are normalized to the average flux between 1.56 and 1.74  $\mu\text{m}$  and offset by constants. The LIRIS spectrum of BRB 17 is rebinned to a dispersion of 7 nm  $\text{pix}^{-1}$ . The references of the field spectra are: LP 944-20, 2MASS J12212770+0257198, and GJ 1048B (Burgasser et al. 2008), 2MASS J01415823-4633574 (Kirkpatrick et al. 2006), 2MASSW J0015447+351603 (Testi et al. 2001), 2MASSW J1506544+132106 (Burgasser 2007), and G 196-3B (Allers et al. 2010).

2001), 2MASSW J0015447+351603 (Kirkpatrick et al. 2000), 2MASSW J1506544+132106 (Gizis et al. 2000), and G 196-3B (Cruz et al. 2009). The best match is with the spectrum of the low surface-gravity field dwarf 2MASS J01415823-4633574 (Kirkpatrick et al. 2006). Therefore we adopted its  $L0 \pm 1$  (peculiar) spectral type. The match is less good with the spectrum of G 196-3B, another low surface-gravity field dwarf (Rebolo et al. 1998; Martín et al. 1999; Kirkpatrick et al. 2001; Allers et al. 2007; Kirkpatrick et al. 2008). For the other Pleiades spectra, the best match is with the spectra of the normal field dwarfs overplotted in Figs. 1 and 2. We verified whether the  $J - H$  and  $H - K$  colours of our nine Pleiades targets agree with those of the specific field dwarfs providing the best spectral match. For the Pleiades dwarfs we used UKIDSS<sup>7</sup> photometry and for the field dwarfs we used 2MASS photome-

<sup>7</sup> UKIDSS uses the UKIRT Wide Field Camera (WFCAM, Casali et al. 2007) and a photometric system described in Hewett et al. (2006). The pipeline processing and science archive are described in Hambly et al. (2008).

try converted to the WFCAM photometric system using the transformations of Hodgkin et al. (2009), or else when available UKIDSS- (2MASS J0409095+210439) or MKO photometry (SDSS J213240.36+102949.4; Chiu et al. 2006). On average, the colours agree within the error bars, and, in all cases but two, better than about 1.5 times the sum of the error bars. 2MASS J00552554+4130184, with  $H - K \approx 0.0$  mag, is 0.5 mag bluer than Teide 1, which disagrees with the very similar fluxes in the spectra of the two objects (Fig. 1). 2MASS J01415823-4633574 is 0.20 mag redder in  $H - K$  than BRB 17.

Our derived spectral types (Table 1) indicate that the low-mass brown dwarfs confirmed by proper motion in Bihain et al. (2006) are indeed ultra-cool dwarfs of spectral type L. They also indicate that our near-infrared classification of the late M-type Amici spectra is consistent with their optical spectral classification. Steele et al. (1995), Williams et al. (1996), and Greissl et al. (2007) have already presented near-infrared, low-resolution spectra of Pleiades early M- to L0-type dwarfs, including PPI 1, Teide 1, Roque 33, and Roque 25, which at least qualitatively support the optical classification.

For the Pleiades L-type spectra, we measured five field-dwarf spectral indices, in regions less affected by telluric absorption bands:  $sHJ$ ,  $sKJ$ ,  $sH_2O^J$ , and  $sH_2O^{H1}$  from Testi et al. (2001) and  $sH_2O^B$  from Reid et al. (2001). For BRB 17, only the  $sHJ$  and  $sKJ$  indices could be measured. We note that the indices depend on narrow regions that are significantly affected by noise in our data, implying that they are less reliable than comparisons using all the available spectral regions. The average spectral types derived from the field dwarf indices are shown in the left part of Table 2 and agree with our adopted spectral types (Table 1) except for BRB 17 and PLIZ 28. We also measured the  $H_2O$  1.5  $\mu\text{m}$  (Geballe et al. 2002),  $H_2O$  (Allers et al. 2007), and  $H_2O-2$  (Slesnick et al. 2004) spectral indices, expected to be gravity-independent in early to mid L-types. The two last indices are more appropriate for spectra of higher spectral resolution than the Amici data. Nevertheless, we find good agreement between the average spectral types derived from the field-dwarf and “gravity-independent” indices. In the case of PLIZ 28 and BRB 17, the spectral indices independent of the  $J$  band – especially the gravity-independent indices – give earlier spectral types that are more consistent with the spectral type L0. This results from the apparently shallower water bands at  $\sim 1.4$  and  $\sim 1.9 \mu\text{m}$  for the relatively depressed continuum at  $0.85-1.3 \mu\text{m}$ , as compared to normal field dwarfs. Spectra of improved signal-to-noise ratio and flux correction will permit us to confirm or refute this unusual combination of spectral features.

## 4. Discussion

### 4.1. Spectroscopic properties

In Fig. 2, we compare the spectrum of the L0-type BRB 17 with those of two field dwarfs, the optical L0 standard 2MASS J03454316+2540233 of Kirkpatrick et al. (1999) and the L2-type SSSPM J0829-1309. In the blue part, the Pleiades spectrum displays the VO band at  $\sim 1.05 \mu\text{m}$ , which appears more clearly than other local features. The FeH band at  $1.2 \mu\text{m}$  is not covered because of bad pixel columns in the LIRIS frames. In the central part ( $H$  band), the shape of the continuum is triangular, instead of approximately flat-topped as in the comparison spectra. These peculiarities can also be seen in the lower resolution spectrum of PLIZ 28 (Figs. 1 and 3). Deep VO bands and triangular  $H$ -band continuum shapes, as well as weak FeH and



**Table 2.** Field-dwarf- and gravity-independent spectral indices<sup>a</sup> (left and right parts of the table, respectively).

Object	sHJ (1.265–1.305, 1.60–1.70)	sKJ (1.265–1.305, 2.12–2.16)	sH <sub>2</sub> O <sup>J</sup> (1.09–1.13, 1.265–1.305)	sH <sub>2</sub> O <sup>H1</sup> (1.45–1.48, 1.60–1.70)	sH <sub>2</sub> O <sup>B</sup> (1.47–1.49, 1.59–1.61)	⟨SpT⟩ <sup>b</sup>	H <sub>2</sub> O 1.5 μm (1.46–1.48, 1.57–1.59)	H <sub>2</sub> O (1.492–1.502, 1.55–1.56)	H <sub>2</sub> O-2 (2.035–2.045, 2.145–2.155)	⟨SpT⟩ <sup>b</sup>
BRB 17	0.23; L2.4	0.63; L2.6	...	...	...	(L2.5)	...	1.22; L0.6	0.95; M8.4	(M9.5)
PLIZ 28	0.12; L4.5	0.51; L4.0	0.21; L3.0	0.35; L2.0	0.78; L0.8	(L3)	1.30; L1	1.17; M9.5	0.88; L0.3	(L0.5)
PLIZ 35	0.21; L2.7	0.66; L2.2	0.09; L1.2	0.37; L2.3	0.79; L0.6	(L2)	1.31; L1	1.36; L4.0	0.80; L2.6	(L2.5)
BRB 21	0.19; L3.1	0.55; L3.5	0.35; L5.2	0.38; L2.4	0.67; L3.6	(L3.5)	1.39; L2	1.42; L5.2	0.89; L0.0	(L2.5)
BRB 23	0.18; L3.4	0.55; L3.5	0.29; L4.3	0.58; L5.0	0.58; L6.2	(L4.5)	1.67; L7	1.51; L7.2	0.79; L2.8	(L5.5)
BRB 29	...	...	...	0.65; L5.8	0.68; L3.4	(L4.5)	1.56; L5	1.25; L1.3	0.68; L5.6	(L4)

**Notes.** <sup>(a)</sup> Their spectral ranges in μm are also indicated. <sup>(b)</sup> Average spectral types derived from the spectral indices are approximated to the nearest half subclasses.

CO bands and weak Na I and K I lines, have been observed in spectra of L-type objects in star-forming regions and have been associated with lower surface gravity (Martín et al. 1998b; Lucas et al. 2001; McGovern et al. 2004; Allers et al. 2007). The triangular *H*-band continuum shape could be explained by a reduction in the H<sub>2</sub> collision-induced and H<sub>2</sub>O absorptions in lower surface-gravity and dustier atmospheres (Borysow et al. 1997; Kirkpatrick et al. 2006; Mohanty et al. 2007). Possibly, the entire apparently peculiar continuum of PLIZ 28 and BRB 17 (see Sect. 3) could be explained by dustier atmospheres (see Fig. 2 in Tsuji et al. 1996).

#### 4.2. Spectrophotometric properties

We compare now the spectrophotometric properties of Pleiades L-type brown dwarfs mainly with those of field dwarfs of known parallax. We use *I*<sub>C</sub>- and UKIDSS *ZYJHK*-band photometry. To our nine Pleiades targets, we add 36 other low-mass Pleiades stars and brown dwarfs with spectral type measurements (Table A.1). They are cluster members confirmed by proper motion or the lithium test (Rebolo et al. 1992), and many present spectral features of low surface gravity (see spectroscopic references in the table). We include the M9-type Roque 4 and the L0-type Roque 25, which have spectral features consistent with cluster membership (Zapatero Osorio et al. 1997; Martín et al. 1998b, 2000; Kirkpatrick et al. 2008); furthermore, Roque 25 has a proper motion consistent with cluster membership (see Appendix B). To obtain *JHK*-band absolute magnitudes, we use the Pleiades revised trigonometric parallax distance of  $120.2 \pm 1.9$  pc (van Leeuwen 2009a,b). We do not account for the distance uncertainty due to cluster depth ( $\approx \pm 0.2$  mag towards the cluster centre, Pinfield et al. 1998). We compute average *JHK*-band absolute magnitudes and average *I*<sub>C</sub> – *J*, *Z* – *J*, and *Y* – *J* colours in the spectral type intervals  $[4.75+i/2, 5.25+i/2]$  with  $i = 0, \dots, 19$  (where 5.0 corresponds to M5.0, 14.5 to L4.5) and excluding known binaries. We also obtain chi-squared linear fits to the *J* – *H*, *H* – *K*, and *J* – *K* colours as a function of spectral type, including these binaries.

For field dwarfs compiled with trigonometric parallaxes and spectral types (van Altena et al. 1995; Dahn et al. 2000, 2002; Henry et al. 2004; Faherty et al. 2009), we use *I*<sub>C</sub>- (Leggett et al. 2000; Dahn et al. 2000, 2002; Henry et al. 2004; Phan-Bao et al. 2008) and 2MASS or MKO *JHK*-band photometry. We convert the 2MASS photometry to the (MKO-)WFCAM system using the transformations of Hodgkin et al. (2009). For some field dwarfs, we use available WFCAM *ZYJHK*-band photometry (UKIDSS DDR6) or WFCAM *Z* – *J* and *Y* – *J* synthetic colours

(Hewett et al. 2006; Rayner et al. 2009). We cautiously assume errors of 0.10 mag and 0.05 mag in the colours of the former and latter studies, respectively. For all the field dwarfs, we preferentially adopt their optical spectral types. Late M- and L-type close binaries resolved by imaging (see references in Faherty et al. 2009) are accounted for in the comparison. We compute average absolute magnitudes, average colours and linear fits in a similar way to the Pleiades sample, but using values with total errors smaller than 0.4 mag. For illustrative purpose, we highlight four relatively bright L4-type field dwarfs (HD 130948B and C, Potter et al. 2002; Dupuy et al. 2009; HD 49197B, Metchev & Hillenbrand 2004; 2MASSW J1841086+311727, Kirkpatrick et al. 2000) and we add five subdwarfs associated with the thick-disc or halo population (Bowler et al. 2009), three low-mass substellar members of relatively young associations (2M1207AB, Chauvin et al. 2004; Mohanty et al. 2007; Ducourant et al. 2008; AB Pic B, Chauvin et al. 2005; Bonnefoy et al. 2010), and three field dwarfs without parallax measurements (2MASS J01415823–4633574, G 196–3B and the candidate young L4.5-type 2MASS J18212815+1414010, Looper et al. 2008).

As claimed in Bihain et al. (2006), the Pleiades and field L-type dwarfs may have similar spectral energy distributions and luminosities, and thus possibly similar (but not necessarily equal) radii, based on the apparent overlapping of these objects in the *J* versus *I* – *J*, *J* – *H*, and *J* – *K* colour-magnitude diagrams. Indeed, our near-infrared absolute magnitude versus spectral type diagrams (Fig. 4) indicate that, unlike the Pleiades M-type dwarfs, the L-type dwarfs appear no brighter than a few tenths of magnitude than their field counterparts, especially in the *J* band. Nevertheless, if we adopt the larger Pleiades distance of  $133.8 \pm 3.0$  pc (Percival et al. 2005) as in Bihain et al. (2006) – obtained by main sequence fitting in the optical and near-infrared using field stars – the Pleiades L-type dwarfs would be brighter by 0.23 mag, implying less similar luminosities to those of field L-type dwarfs. Besides, the diagrams in Figs. 5 and 6 show no significant differences between the colours of Pleiades and field L-type dwarfs.

At the M/L transition (see Fig. 4), we note that four Pleiades brown dwarfs (NPL 40, BRB 17, PLIZ 28, and Roque 25) appear to have a relatively lower flux towards the *J* band, which could be due to too early spectral typing or some atmospheric or interstellar extinction. The effect is stronger for the  $\sim 30$  Myr old low-mass brown dwarf or massive planet AB Pic B, and even stronger for the later-type  $\sim 8$  Myr few-Jupiter-mass

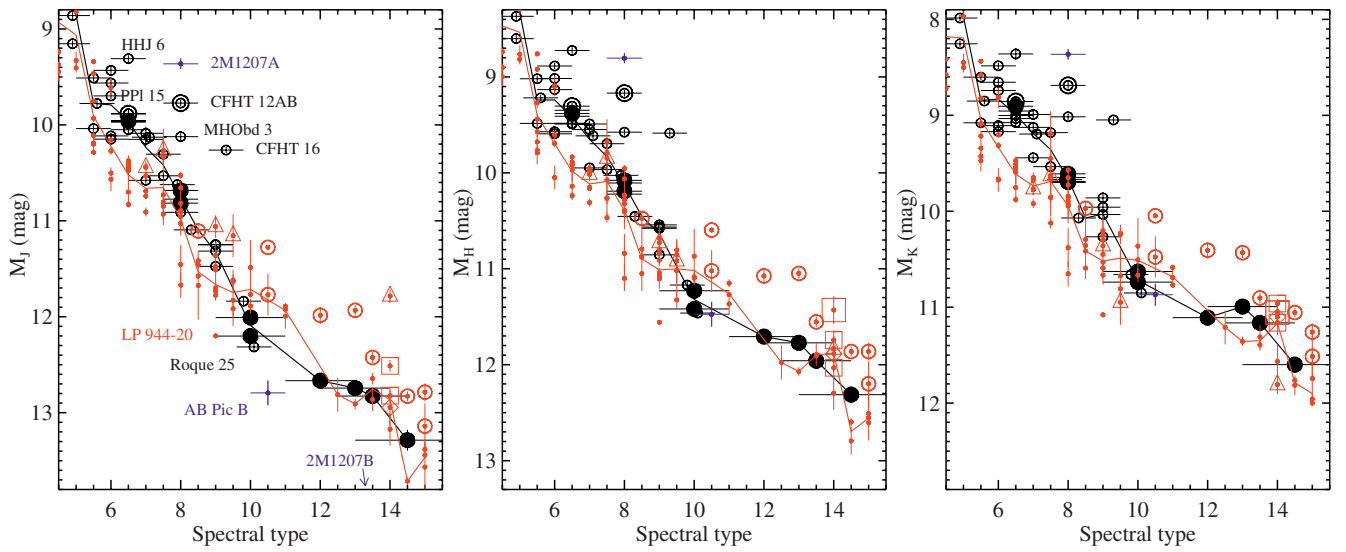


**Fig. 4.** Absolute magnitude  $M_J$ ,  $M_H$ , and  $M_K$  versus spectral type (M6 = 6, L0 = 10) diagrams (*left-, middle-, and right panels*, respectively), with Pleiades members (*black filled circles* for new data and *black small open circles* for previous data) and field dwarfs (*red dots*). Resolved close binaries are *encircled*. Average Pleiades and field values are represented by the *black- and red solid lines*, respectively. For illustrative purpose, we highlight four relatively bright field L4-type dwarfs (HD 130948B and C by *small squares*, HD 49197B by *large square*, and 2MASSW J1841086+311727 by *diamond*) and we add five subdwarfs (*triangles*) and three low-mass substellar members of very young associations (*blue dots*; we assume an L5 type for 2M1207B). All three diagrams span 5.0 mag. The photometry is in the MKO-WFCAM system.

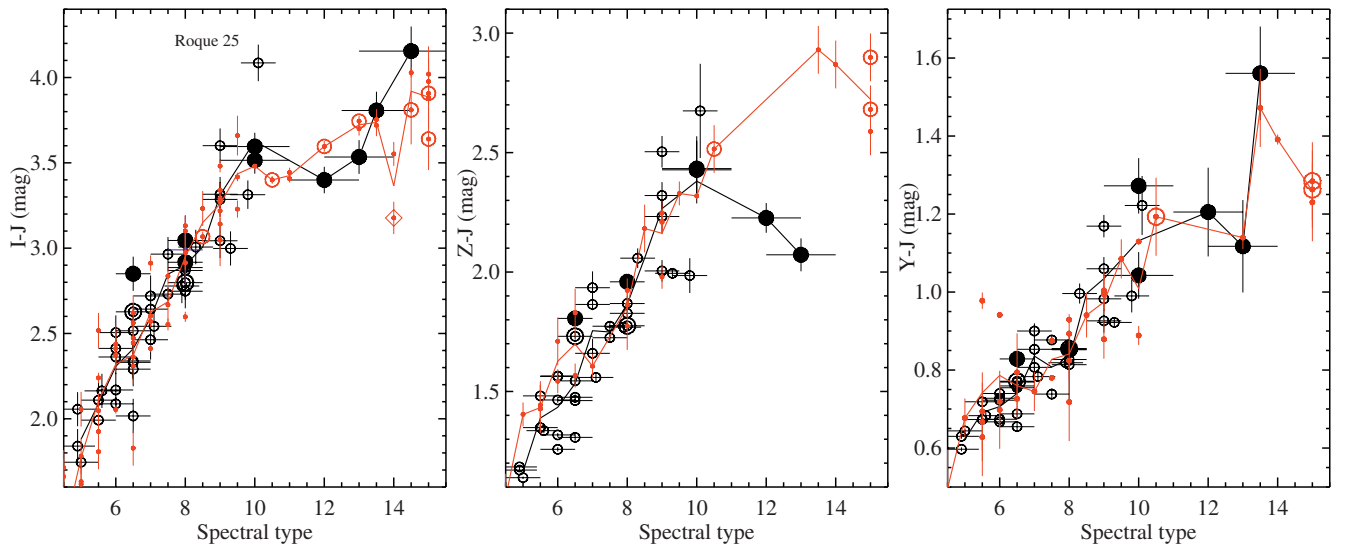


**Fig. 5.**  $I_C - J$ ,  $Z - J$ , and  $Y - J$  versus spectral type diagrams (*left-, middle-, and right panels*, respectively). Same symbol definitions as in Fig. 4.

2M1207B<sup>8</sup>, for which ongoing accretion/formation processes have been proposed (Mohanty et al. 2007; Mamajek & Meyer 2007; Ducourant et al. 2008; Patience et al. 2010). Finally, the very nearby (5 pc) M9-type field brown dwarf LP 944-20, with lithium absorption and an age estimated to be of several hundred Myr (Tinney 1998; Ribas 2003) appears also to be fainter, but equally in the  $HK$  bands as in the  $J$  band, an effect that could be real or related to uncertainties in the parallax measurement.

The near-infrared colour diagrams of Fig. 6 indicate that late M- and L-type Pleiades dwarfs are marginally redder in  $J-H$  and  $H-K$  than their field counterparts. The difference reaches  $0.11 \pm$

<sup>8</sup> 2M1207B is less luminous than the Pleiades and field dwarf sequences, by about 3, 2, and 1 mag in the  $J$ ,  $H$ , and  $K$  bands, respectively, assuming a spectral type L5.

0.20 mag in  $J-K$  and at spectral type L3, using the chi-squared linear fits. If we consider only the field dwarfs with UKIDSS photometry (10 M6–L4-type dwarfs), the  $J-K$  difference at L3 increases by 0.08 mag. This suggests that the slightly redder colour is not due to some bias in the photometric transformations of Hodgkin et al. (2009). It could be associated with both:

1. the reddening in the line of sight of the faint Pleiades brown dwarfs. The  $E(B-V)$  values could be in the range 0.02–0.14 mag (Taylor 2008), which using the  $E(J-K_s)/E(B-V)$  relation of An et al. (2007), would lead to small infrared excesses  $E(J-K_s) = 0.01-0.09$  mag for an intrinsic colour  $(J-K_s)_0 = 1.5$  mag;
2. the youth of the Pleiades brown dwarfs. Indeed, the  $J-K$  colour is found to be redder, on average, for L-type field

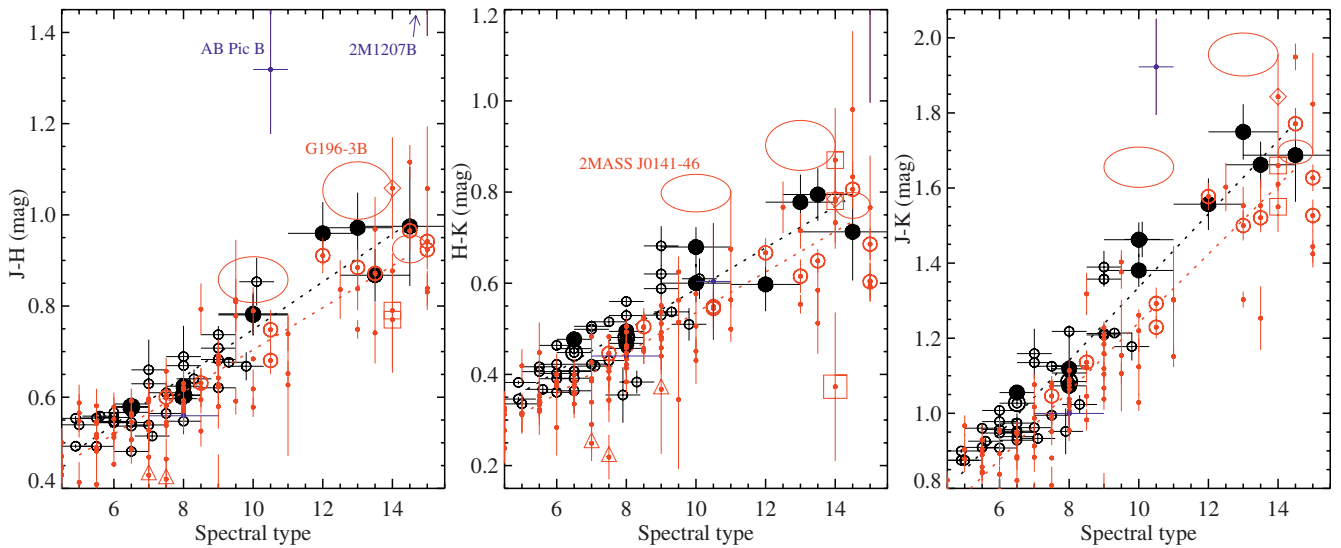


**Fig. 6.**  $J - H$ ,  $H - K$ , and  $J - K$  versus spectral type diagrams (*left-, middle-, and right panels*, respectively). Same symbol definitions as in Fig. 4. Pleiades and field chi-squared linear fits to the colours as a function of spectral type are represented by the *black- and red dashed lines*, respectively. For illustrative purpose, we add the low surface gravity field dwarfs 2MASS J01415823–4633574 and G 196–3B and the candidate young field dwarf 2MASS J18212815+1414010, represented by error *ellipses* for clarity.

dwarfs with smaller velocity dispersion, and thus of younger age (Faherty et al. 2009; Schmidt et al. 2010). The 0.1 Gyr old Pleiads would likely have lower surface gravities than those of the older field dwarfs, which furthermore could have lower metallicities than the Pleiades ( $[\text{Fe}/\text{H}]_{\text{Pleiades}} = 0.03 \pm 0.05$  dex, Funayama et al. 2009; Soderblom et al. 2009). Both lower surface gravities and higher metallicities may cause lower  $\text{H}_2$  collision-induced absorption or dustier atmospheres, and therefore redder  $J - K$  colours (Linsky 1969; Saumon et al. 1994; Borysow et al. 1997; Mohanty et al. 2007). Also, several field L-type dwarfs with spectral features of low surface gravity have very red near-infrared colours (see Fig. 6 and Kirkpatrick et al. 2008; Cruz et al. 2009).

### 4.3. Hertzsprung-Russell diagram

Altogether, the L-type Pleiades and field dwarf sequences appear to be rather close in the photometric – spectral-type diagrams. We now build the Hertzsprung-Russell (HR) diagram of our sample of 45 Pleiades members. We convert observed  $J$ -band magnitudes into luminosities using the open cluster revised parallax distance and an average of field dwarf  $J$ -band bolometric corrections  $BC_J$  (Dahn et al. 2002; Vrba et al. 2004) as a function of spectral type. The  $J$  band is chosen because the spectral energy distributions of the Pleiades objects peak in this band, and the  $J - K$  colour excesses with respect to their field dwarf spectral type counterparts are only 0.1–0.2 mag. For the effective temperatures ( $T_{\text{eff}}$ ), we use an average of field dwarf  $T_{\text{eff}}$  determinations (Basri et al. 2000; Dahn et al. 2002; Vrba et al. 2004) also as a function of spectral type. We provide the luminosity and  $T_{\text{eff}}$  values for our nine Pleiades targets in Table 3, where the error bars account for the uncertainties in the photometry, cluster distance, spectral types, and the spread in the field dwarf  $BC_J$  and  $T_{\text{eff}}$ . Figure 7 shows the Hertzsprung-Russell diagram. The Pleiades substellar sequence clearly extends to mid-L spectral types or  $T_{\text{eff}} \sim 1700$  K. The “single-object” sequence has a

luminosity dispersion of about 0.1 dex (except at  $\sim\text{M9-L0}$ ) and no apparent temperature gap between 2900 and 1700 K. The sequence of suspected equal-mass binaries is clearly seen at the warmest temperatures, whereas below 2400 K there is no obvious hint of such objects, despite the photometric surveys tending to be biased towards their detection.

We overplot the theoretical 120-Myr isochrones of Chabrier et al. (2000, DUSTY model) and Burrows et al. (1997) in Fig. 7. Both models make similar predictions for luminosity,  $T_{\text{eff}}$ , and mass, and both appear to reproduce the slope of the mid- to late-M single-object sequence of the Pleiades within about  $1-\sigma$  uncertainty. There is, however, a discrepancy between theory and observations in the L-type regime ( $\leq 2400$  K): our objects appear 100–400 K warmer (1–3 spectral subclasses earlier) or 0.1–0.4 dex less luminous than the isochrones. Using the absolute  $K$ -band magnitude and the field dwarf bolometric correction  $BC_K$  from Golimowski et al. (2004) increase the luminosities by  $\lesssim 0.10$  dex for the Pleiades L-type objects with the largest  $J - K$  colour excess, thus only slightly reducing the discrepancy. It is uncertain whether the field dwarf bolometric correction- and  $T_{\text{eff}}$ -spectral type relations may be valid for the Pleiades L-type brown dwarfs because of gravity dependence. However, these objects appear to have spectral energy distributions and luminosities that are in general very close to those of their field spectral type counterparts. Thus, the discrepancy in the Hertzsprung-Russell diagram may also come from incorrect model predictions, such as an underestimation of the contraction rate of the Pleiades L-type dwarfs.

The luminosity range of the spectroscopic sample as compared to the theoretical luminosities of the 120 Myr DUSTY isochrone (Fig. 7) would imply a mass range of  $\sim 0.025\text{--}0.1 M_{\odot}$  (without accounting for the brightest, probable binaries). In Table 3, we list individual masses for our targets, obtained by interpolating linearly between the model points using our estimated luminosities. The faintest and coolest brown dwarf is BRB 29, with an estimated mass of  $25 \pm 8 M_{\text{Jup}}$ .

**Table 3.** Luminosities, effective temperatures, and masses for our Pleiades targets.

Object	SpT	$\log L/L_{\odot}$ (dex)	$T_{\text{eff}}$ (K)	$M$ ( $M_{\odot}$ )
PPI 1	$M6.5 \pm 0.5$	$-2.90 \pm 0.04$	$2676 \pm 120$	$\sim 0.074$
Calar 3	$M8.0 \pm 0.5$	$-3.18 \pm 0.04$	$2584 \pm 100$	$\sim 0.054$
Teide 1	$M8.0 \pm 0.5$	$-3.24 \pm 0.04$	$2584 \pm 100$	$\sim 0.052$
BRB 17	$L0.0 \pm 1.0$	$-3.68 \pm 0.06$	$2350 \pm 100$	$\sim 0.035$
PLIZ 28	$L0.0 \pm 1.0$	$-3.76 \pm 0.06$	$2350 \pm 100$	$\sim 0.033$
PLIZ 35	$L2.0 \pm 1.0$	$-3.94 \pm 0.06$	$2110 \pm 180$	$\sim 0.028$
BRB 21	$L3.0 \pm 1.0$	$-3.95 \pm 0.06$	$1950 \pm 150$	$\sim 0.028$
BRB 23	$L3.5 \pm 1.0$	$-3.98 \pm 0.06$	$1875 \pm 150$	$\sim 0.027$
BRB 29	$L4.5 \pm 1.5$	$-4.14 \pm 0.12$	$1735 \pm 190$	$\sim 0.024$

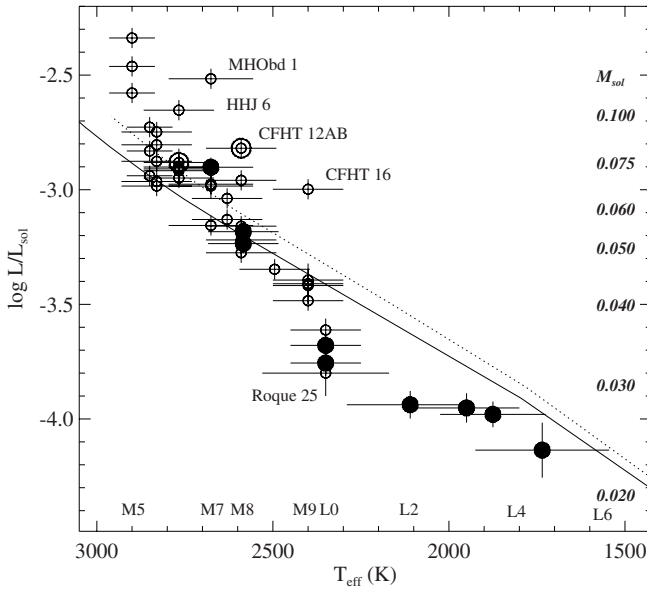


**Fig. 7.** Hertzsprung-Russell diagram of Pleiades low-mass stars and brown dwarfs. Same symbol definitions as in Fig. 4. Theoretical 120 Myr isochrones of Chabrier et al. (2000, DUSTY) and Burrows et al. (1997) are represented by dotted and solid lines, respectively. Spectral types and DUSTY theoretical masses are indicated.

## 5. Conclusions

We obtained near-infrared NICS/Amici and LIRIS spectra of six  $J = 17.4\text{--}18.8$  mag candidate L-type brown dwarfs of the  $\sim 120$  Myr old Pleiades cluster, as well as Amici spectra of three other members that are well-known late M-type brown dwarfs. We confirm that the former objects have early- to mid-L spectral types and also confirm the optical spectral types reported for the last objects. PLIZ 28 and BRB 17, the two earliest L-type brown dwarfs, present a triangular  $H$ -band continuum shape and a noticeable VO band, associated to low surface gravity, dust and youth. The Pleiades L-type brown dwarfs appear to have similar absolute magnitudes and colours as their field counterparts, but have slightly redder near-infrared colours, possibly related to both reddening and youth.

We build the Hertzsprung-Russell diagram of our Pleiades sample using field dwarf relations and find good agreement with theoretical models for the M5.5–9 type objects. However, for the L0–5 type brown dwarfs, models appear to overpredict the luminosity ( $\Delta \log L/L_{\odot} = 0.1 - 0.4$  dex) or underestimate the effective temperature ( $\Delta T_{\text{eff}} = 100\text{--}400$  K). It is also possi-

ble that the adopted field-dwarf relations are not truly valid for  $\sim 120$  Myr-old objects. Additional optical-to-infrared spectroscopy and higher resolution imaging of the Pleiades L-type brown dwarfs may allow us to account more for dust opacities and binarity (e.g. Knapp et al. 2004; Burgasser et al. 2008), and refine our estimates of spectral types, effective temperatures, luminosities, and masses. Current models predict masses in the range  $0.025\text{--}0.035 M_{\odot}$  for the Pleiades L0–5 type brown dwarfs.

**Acknowledgements.** We thank the anonymous referee for her/his valuable comments and suggestions, and Terry Mahoney for correcting the English text. We thank Katelyn N. Allers for providing the spectrum of G 196-3B. The study presented here is based on observations made with the Italian Telescopio Nazionale Galileo (TNG) and the William Herschel Telescope (WHT) operated on the island of La Palma by the Fundación Galileo Galilei of the INAF (Istituto Nazionale di Astrofisica) and the Isaac Newton Group, respectively, in the Spanish Observatorio del Roque de los Muchachos of the Instituto de Astrofísica de Canarias. We thank the TNG for allocation of director's discretionary time to this programme. Based on observations collected at the German-Spanish Astronomical Center, Calar Alto, jointly operated by the Max-Planck-Institut für Astronomie Heidelberg and the Instituto de Astrofísica de Andalucía (CSIC). We thank Calar Alto Observatory for allocation of director's discretionary time to this programme. This research has been supported by the Spanish Ministry of Science and Innovation (MICINN). This research has benefitted from the SpeX Prism Spectral Libraries maintained by Adam Burgasser, the L and T dwarf data archive maintained by Sandy K. Leggett, and the M, L, and T dwarf compendium housed at DwarfArchives.org and maintained by Chris Gelino, Davy Kirkpatrick, and Adam Burgasser. This research has made use of SAOImage DS9, developed by Smithsonian Astrophysical Observatory. This research has made use of the SIMBAD database, operated at CDS, Strasbourg, France. This publication makes use of data products from the Two Micron All Sky Survey, which is a joint project of the University of Massachusetts and the Infrared Processing and Analysis Centre/California Institute of Technology, funded by the National Aeronautics and Space Administration and the National Science Foundation. This research has made use of NASA's Astrophysics Data System Bibliographic Services.

## Appendix A: Pleiades spectroscopic sample of low-mass stars and brown dwarfs

## Appendix B: Cluster membership confirmation of Roque 25 by proper motion

As part of the project to characterize the Pleiades L-type population by both proper motion and spectroscopy, we obtained  $H$ -band imaging data of Roque 25, the first L-type object identified in the Pleiades (Martín et al. 1998b, 2000), to assess its cluster membership by proper motion. The observations were done on the night of 2006 February 15 with the Omega-2000 instrument ( $15.4 \times 15.4$  arcmin<sup>2</sup>,  $0.45$  arcsec pix<sup>-1</sup>) mounted on the 3.5 m Telescope (Centro Astronómico Hispano-Alemán de Calar Alto, Spain). They consisted of  $1.6 \text{ s} \times 23$  coadds  $\times 36$  dithers on the science target, as well as dome flats. These data were reduced as in Bihain et al. (2006). We performed aperture and point-spread-function (PSF) photometry using routines within the DAOPHOT package. The  $H$ -band photometry was calibrated using 341 stellar sources from UKIDSS GCS DDR6, with aperture corrected magnitudes of errors  $\sigma_H(\text{UKIDSS}) < 0.1$  mag ( $2.0$  arcsec aperture diameter). The photometry has an average relative calibration error of  $0.04$  mag. For Roque 25, we measure  $H = 16.85 \pm 0.05$  mag, in agreement with  $H(\text{UKIDSS}) = 16.86 \pm 0.04$  mag. Using the Omega-2000 image of Roque 25 and the discovery  $I$ -band image (Zapatero Osorio et al. 1999b), corresponding to a time baseline of  $10.01$  yr, and the method described in Bihain et al. (2006), we obtain a proper motion  $(\mu_{\alpha} \cos \delta, \mu_{\delta}) = (27.4 \pm 7.3, -32.6 \pm 3.9)$  mas yr<sup>-1</sup>. Considering the average cluster proper motion  $(\mu_{\alpha} \cos \delta, \mu_{\delta}) = (19.15 \pm 0.23, -45.72 \pm 0.18)$  mas yr<sup>-1</sup> (Robichon et al. 1999) and the fact that the low mass cluster members have a larger intrinsic



**Table A.1.** Pleiades spectroscopic sample of 45 low-mass stars and brown dwarfs.

Object	SpT	$\alpha^a$	$\delta^a$	$I_C$ (mag)	$Z^b$ (mag)	$Y^b$ (mag)	$J^b$ (mag)	$H^b$ (mag)	$K^b$ (mag)	Ref. <sup>c</sup>
HHJ 2	M6.5	03 38 27.52	25 30 18.1	17.30	16.591 ± 0.011	15.938 ± 0.007	15.284 ± 0.007	14.747 ± 0.005	14.355 ± 0.006	1,-,1,7
HHJ 3	M6.0	03 48 50.45	22 44 29.9	17.51	16.562 ± 0.010	15.825 ± 0.006	15.098 ± 0.006	14.531 ± 0.005	14.141 ± 0.004	1,-,1,7
HHJ 6	M6.5	03 41 42.41	23 54 57.1	17.00	16.171 ± 0.007	15.464 ± 0.006	14.709 ± 0.004	14.124 ± 0.004	13.760 ± 0.050	1,-,1,7
HHJ 7	M6.0	03 57 49.37	22 08 31.0	17.00	16.149 ± 0.007	15.498 ± 0.005	14.831 ± 0.005	14.286 ± 0.005	13.884 ± 0.003	1,-,1,7
PPI 1	M6.5	03 45 41.27	23 54 09.8	18.21	17.166 ± 0.014	16.189 ± 0.008	15.360 ± 0.006	14.782 ± 0.005	14.305 ± 0.006	4,8,7,5
PPI 14	M5.5	03 44 34.30	23 51 24.6	17.43	16.920 ± 0.011	16.157 ± 0.007	15.438 ± 0.007	14.884 ± 0.005	14.478 ± 0.006	4,2,7,1
PPI 15	M6.5	03 48 04.66	23 39 30.2	17.91	17.014 ± 0.012	16.054 ± 0.007	15.283 ± 0.006	14.704 ± 0.005	14.256 ± 0.006	4,2,7,2
Calar 3	M8.0	03 51 25.57	23 45 21.3	19.00	...	...	16.083 ± 0.010	15.478 ± 0.009	15.009 ± 0.011	4,3,5,3
Teide 1	M8.0	03 47 17.92	24 22 31.7	19.26	18.174 ± 0.029	17.067 ± 0.013	16.215 ± 0.010	15.591 ± 0.009	15.096 ± 0.011	4,3,5,2
PIZ 1	M9.0	03 48 31.52	24 34 37.3	20.00	19.218 ± 0.065	17.883 ± 0.025	16.715 ± 0.015	15.977 ± 0.012	15.357 ± 0.014	5,-,7,6
Roque 4 <sup>d</sup>	M9.0	03 43 53.55	24 31 11.6	20.25	18.970 ± 0.054	17.709 ± 0.025	16.649 ± 0.016	15.942 ± 0.016	15.260 ± 0.040	6,-,-,5
Roque 11	M8.0	03 47 12.08	24 28 31.7	19.06	...	16.988 ± 0.013	16.174 ± 0.087	15.505 ± 0.009	15.048 ± 0.012	6,-,8,2
Roque 13	M7.5	03 45 50.66	24 09 03.5	18.67	17.478 ± 0.017	16.582 ± 0.010	15.705 ± 0.008	15.095 ± 0.006	14.580 ± 0.008	6,8,7,5
Roque 14	M7.0	03 46 42.98	24 24 50.7	18.27	17.484 ± 0.018	16.403 ± 0.009	15.550 ± 0.066	14.890 ± 0.006	14.391 ± 0.007	6,-,8,7
Roque 16	M6.0	03 47 39.02	24 36 22.2	17.91	17.112 ± 0.013	16.271 ± 0.008	15.548 ± 0.007	14.992 ± 0.006	14.570 ± 0.008	6,8,7,3
Roque 17	M6.5	03 47 23.97	22 42 37.4	17.87	...	16.123 ± 0.008	15.354 ± 0.007	14.809 ± 0.006	14.402 ± 0.007	6,-,2,7
Teide 2	M6.0	03 52 06.72	24 16 00.5	18.02	17.079 ± 0.013	16.255 ± 0.009	15.515 ± 0.008	14.971 ± 0.008	14.507 ± 0.008	7,7,7,3
CFHT 9	M6.5	03 49 15.12	24 36 22.5	17.71	16.847 ± 0.011	16.059 ± 0.007	15.371 ± 0.006	14.890 ± 0.005	14.433 ± 0.007	8,8,7,3
CFHT 10	M6.5	03 44 32.32	25 25 18.0	17.78	16.994 ± 0.012	16.209 ± 0.009	15.450 ± 0.008	14.883 ± 0.007	14.476 ± 0.007	8,8,7,3
CFHT 12	M8.0	03 53 55.12	23 23 36.2	17.97	16.947 ± 0.012	16.027 ± 0.007	15.172 ± 0.006	14.569 ± 0.005	14.088 ± 0.005	8,8,3,3
CFHT 15	M7.0	03 55 12.60	23 17 37.3	18.62	17.842 ± 0.022	16.877 ± 0.012	15.977 ± 0.010	15.348 ± 0.009	14.842 ± 0.010	8,8,3,3
MHObd 3	M8.0	03 41 54.16	23 05 04.7	18.27	17.349 ± 0.016	16.376 ± 0.010	15.522 ± 0.008	14.975 ± 0.007	14.415 ± 0.007	8,8,7,4
NPL 26	M5.0	03 47 07.89	24 23 37.9	15.70	15.094 ± 0.004	14.598 ± 0.003	13.954 ± 0.003	13.415 ± 0.002	13.080 ± 0.002	9,-,4,2
NPL 34	M6.0	03 48 55.65	24 21 40.1	17.05	16.220 ± 0.007	15.636 ± 0.005	14.963 ± 0.005	14.416 ± 0.004	14.055 ± 0.005	9,-,1,2
NPL 36	M7.5	03 48 19.02	24 25 12.7	18.66	17.655 ± 0.020	16.668 ± 0.011	15.930 ± 0.009	15.365 ± 0.008	14.935 ± 0.011	9,-,7,2
NPL 38	M8.0	03 47 50.41	23 54 47.9	19.18	18.179 ± 0.028	17.138 ± 0.014	16.311 ± 0.011	15.622 ± 0.009	15.093 ± 0.012	9,-,8,2
MHObd 1	M7.0	03 44 52.42	24 36 49.5	17.95	17.147 ± 0.014	16.294 ± 0.008	15.487 ± 0.059	14.948 ± 0.006	14.525 ± 0.007	10,10,-,4
Roque 5	M9.0	03 44 22.44	23 39 01.3	20.19	19.107 ± 0.064	17.857 ± 0.025	16.874 ± 0.017	16.254 ± 0.016	15.666 ± 0.018	11,-,7,5
CFHT 1	M4.9	03 51 51.56	23 34 49.1	16.10	15.431 ± 0.005	14.857 ± 0.004	14.260 ± 0.003	13.768 ± 0.003	13.385 ± 0.003	12,-,3,3
CFHT 2	M4.9	03 52 44.29	23 54 15.0	16.61	15.738 ± 0.005	15.184 ± 0.004	14.554 ± 0.004	14.000 ± 0.004	13.654 ± 0.004	12,-,3,3
CFHT 5	M5.5	03 48 44.69	24 37 23.5	17.02	16.260 ± 0.008	15.584 ± 0.005	14.911 ± 0.005	14.419 ± 0.004	14.002 ± 0.005	12,-,7,3
CFHT 7	M5.6	03 52 05.83	24 17 31.0	17.34	16.512 ± 0.009	15.860 ± 0.007	15.176 ± 0.006	14.618 ± 0.006	14.251 ± 0.007	12,-,7,3
CFHT 16	M9.3	03 44 35.16	25 13 42.8	18.66	17.656 ± 0.020	16.584 ± 0.010	15.662 ± 0.007	14.985 ± 0.006	14.448 ± 0.008	12,12,7,3
CFHT 17	M7.9	03 43 00.17	24 43 52.3	18.80	17.791 ± 0.021	16.841 ± 0.013	16.022 ± 0.010	15.425 ± 0.010	15.070 ± 0.060	12,-,3,3
CFHT 25	M9.0	03 54 05.35	23 33 59.3	19.69	18.651 ± 0.041	17.573 ± 0.024	16.647 ± 0.018	15.964 ± 0.016	15.434 ± 0.017	12,-,3,3
NPL 40	M9.8	03 48 49.03	24 20 25.4	20.55	19.222 ± 0.069	18.227 ± 0.035	17.237 ± 0.023	16.569 ± 0.020	16.059 ± 0.029	12,-,8,2
Roque 7	M8.3	03 43 40.31	24 30 11.2	19.50	18.552 ± 0.038	17.490 ± 0.021	16.494 ± 0.014	15.853 ± 0.015	15.470 ± 0.020	12,-,3,3
Roque 25	L0.1	03 48 30.75	22 44 50.4	21.80	20.389 ± 0.193	18.936 ± 0.065	17.714 ± 0.039	16.861 ± 0.035	16.251 ± 0.027	12,-,9,5
BPL 327	M7.1	03 55 23.08	24 49 04.9	18.07	17.087 ± 0.014	16.311 ± 0.009	15.528 ± 0.008	15.013 ± 0.007	14.595 ± 0.008	13,-,6,5
BRB 17	L0.0	03 54 07.98	23 54 27.9	20.92	19.841 ± 0.111	18.451 ± 0.050	17.408 ± 0.033	16.628 ± 0.030	16.028 ± 0.029	14,-,5,6
PLIZ 28	L0.0	03 54 14.06	23 17 52.0	21.20	20.028 ± 0.136	18.873 ± 0.062	17.601 ± 0.035	16.818 ± 0.031	16.138 ± 0.030	14,-,5,6
PLIZ 35	L2.0	03 52 39.16	24 46 29.5	21.46	20.292 ± 0.030	19.271 ± 0.100	18.066 ± 0.055	17.106 ± 0.042	16.509 ± 0.042	14,-,5,6
BRB 21	L3.0	03 54 10.27	23 41 40.2	21.68	20.215 ± 0.030	19.260 ± 0.101	18.143 ± 0.062	17.171 ± 0.046	16.393 ± 0.040	14,-,5,6
BRB 23	L3.5	03 50 39.54	25 02 54.7	22.03	...	19.786 ± 0.112	18.225 ± 0.044	17.358 ± 0.038	16.563 ± 0.043	14,-,5,6
BRB 29	L4.5	03 54 01.43	23 49 57.7	22.84	...	...	18.686 ± 0.103	17.711 ± 0.081	16.999 ± 0.070	14,-,5,6

**Notes.** <sup>(a)</sup> Coordinates from UKIDSS Galaxy Cluster Survey DDR6. <sup>(b)</sup> *ZYJHK*-band photometry from UKIDSS Galaxy Cluster Survey DDR6, except for the measurements at *Z* band of PLIZ 35 and BRB 21 (Casewell et al. 2007), MKO *K* band of HHJ 6, Roque 4, CFHT 17, and Roque 7 (Pinfield et al. 2003), and *J* band of MHObd 1 (2MASS, converted to UKIDSS photometric system). <sup>(c)</sup> References for the quadruplet (SpT, Li,  $\mu$ ,  $I_C$ ): *Spectral type or lithium test*: 1) Steele & Jameson (1995); 2) Basri et al. (1996); 3) Rebolo et al. (1996); 4) Martín et al. (1996); 5) Cossburn et al. (1997); 6) Zapatero Osorio et al. (1997); 7) Martín et al. (1998a); 8) Stauffer et al. (1998b); 9) Festin (1998b); 10) Stauffer et al. (1998a); 11) Martín et al. (1998b); 12) Martín et al. (2000); 13) Pinfield et al. (2003); 14) this study. Spectral type uncertainties for our L-type targets are listed in Table 1; for the other objects the uncertainties are typically of half a subclass. *Proper motion*: 1) Hambly et al. (1993); 2) Pinfield et al. (2000); 3) Moraux et al. (2001); 4) Deacon & Hambly (2004); 5) Bihain et al. (2006); 6) Casewell et al. (2007); 7) Lodieu et al. (2007); 8) Stauffer et al. (2007); 9) this study. *I<sub>C</sub>-band photometry*: 1) Stauffer et al. (1994); 2) Festin (1998a); 3) Bouvier et al. (1998); 4) Stauffer et al. (1998a); 5) Jameson et al. (2002); 6) Bihain et al. (2006); 7) Stauffer et al. (2007). Magnitude errors are of 0.05–0.1 mag. <sup>(d)</sup> Roque 4 has radial velocity and spectral features consistent with cluster membership (Zapatero Osorio et al. 1997; Kirkpatrick et al. 2008).

velocity dispersion than that of the high-mass members (Pinfield et al. 1998; Bihain et al. 2006), our result confirms that Roque 25 is also a Pleiades member by proper motion.

## References

Abazajian, K. N., Adelman-McCarthy, J. K., Agüeros, M. A., et al. 2009, *ApJS*, 182, 543  
 Allen, P. R., Koerner, D. W., Reid, I. N., & Trilling, D. E. 2005, *ApJ*, 625, 385  
 Allers, K. N., Jaffe, D. T., Luhman, K. L., et al. 2007, *ApJ*, 657, 511  
 Allers, K. N., Liu, M. C., Dupuy, T. J., & Cushing, M. C. 2010, *ApJ*, 715, 561

An, D., Terndrup, D. M., & Pinsonneault, M. H. 2007, *ApJ*, 671, 1640  
 Bannister, N. P., & Jameson, R. F. 2007, *MNRAS*, 378, L24  
 Barrado y Navascués, D., Zapatero Osorio, M. R., Béjar, V. J. S., et al. 2001, *A&A*, 377, L9  
 Barrado y Navascués, D., Zapatero Osorio, M. R., Martín, E. L., et al. 2002, *A&A*, 393, L85  
 Basri, G., Marcy, G. W., & Graham, J. R. 1996, *ApJ*, 458, 600  
 Basri, G., Mohanty, S., Allard, F., et al. 2000, *ApJ*, 538, 363  
 Béjar, V. J. S., Martín, E. L., Zapatero Osorio, M. R., et al. 2001, *ApJ*, 556, 830  
 Béjar, V. J. S., Zapatero Osorio, M. R., Pérez-Garrido, A., et al. 2008, *ApJ*, 673, L185  
 Bihain, G., Rebolo, R., Béjar, V. J. S., et al. 2006, *A&A*, 458, 805

- Bonnefoy, M., Chauvin, G., Rojo, P., et al. 2010, *A&A*, 512, A52
- Borysow, A., Jorgensen, U. G., & Zheng, C. 1997, *A&A*, 324, 185
- Bouvier, J., Stauffer, J. R., Martín, E. L., et al. 1998, *A&A*, 336, 490
- Bowler, B. P., Liu, M. C., & Cushing, M. C. 2009, *ApJ*, 706, 1114
- Burgasser, A. J. 2004, *ApJS*, 155, 191
- Burgasser, A. J. 2007, *ApJ*, 659, 655
- Burgasser, A. J., Liu, M. C., Ireland, M. J., Cruz, K. L., & Dupuy, T. J. 2008, *ApJ*, 681, 579
- Burgasser, A. J., McElwain, M. W., Kirkpatrick, J. D., et al. 2004, *AJ*, 127, 2856
- Burrows, A., Marley, M., Hubbard, W. B., et al. 1997, *ApJ*, 491, 856
- Casali, M., Adamson, A., Alves de Oliveira, C., et al. 2007, *A&A*, 467, 777
- Casewell, S. L., Dobbie, P. D., Hodgkin, S. T., et al. 2007, *MNRAS*, 378, 1131
- Casewell, S. L., Jameson, R. F., & Burleigh, M. R. 2008, *MNRAS*, 390, 1517
- Chabrier, G. 2002, *ApJ*, 567, 304
- Chabrier, G. 2003, *PASP*, 115, 763
- Chabrier, G., Baraffe, I., Allard, F., & Hauschildt, P. 2000, *ApJ*, 542, 464
- Chauvin, G., Lagrange, A.-M., Dumas, C., et al. 2004, *A&A*, 425, L29
- Chauvin, G., Lagrange, A.-M., Zuckerman, B., et al. 2005, *A&A*, 438, L29
- Chiu, K., Fan, X., Leggett, S. K., et al. 2006, *AJ*, 131, 2722
- Cosburn, M. R., Hodgkin, S. T., Jameson, R. F., & Pinfield, D. J. 1997, *MNRAS*, 288, L23
- Cruz, K. L., Kirkpatrick, J. D., & Burgasser, A. J. 2009, *AJ*, 137, 3345
- Cushing, M. C., Rayner, J. T., & Vacca, W. D. 2005, *ApJ*, 623, 1115
- Dahn, C. C., Guetter, H. H., Harris, H. C., et al. 2000, in *From Giant Planets to Cool Stars*, ASP Conf. Ser. 212, 74
- Dahn, C. C., Harris, H. C., Vrba, F. J., et al. 2002, *AJ*, 124, 1170
- Deacon, N. R., & Hambly, N. C. 2004, *A&A*, 416, 125
- Ducourant, C., Teixeira, R., Chauvin, G., et al. 2008, *A&A*, 477, L1
- Dupuy, T. J., Liu, M. C., & Ireland, M. J. 2009, *ApJ*, 692, 729
- Faherty, J. K., Burgasser, A. J., Cruz, K. L., et al. 2009, *AJ*, 137, 1
- Festini, L. 1998a, *A&A*, 333, 497
- Festini, L. 1998b, *MNRAS*, 298, L34
- Funayama, H., Itoh, Y., Oasa, Y., et al. 2009, *PASJ*, 61, 930
- Geballe, T. R., Knapp, G. R., Leggett, S. K., et al. 2002, *ApJ*, 564, 466
- Gizis, J. E. 2002, *ApJ*, 575, 484
- Gizis, J. E., Kirkpatrick, J. D., & Wilson, J. C. 2001, *AJ*, 121, 2185
- Gizis, J. E., Monet, D. G., Reid, I. N., et al. 2000, *AJ*, 120, 1085
- Golimowski, D. A., Leggett, S. K., Marley, M. S., et al. 2004, *AJ*, 127, 3516
- Greissl, J., Meyer, M. R., Wilking, B. A., et al. 2007, *AJ*, 133, 1321
- Hambly, N. C., Collins, R. S., Cross, N. J. G., et al. 2008, *MNRAS*, 384, 637
- Hambly, N. C., Hawkins, M. R. S., & Jameson, R. F. 1993, *A&AS*, 100, 607
- Hammersley, P. L. 1998, *New Astron. Rev.*, 42, 533
- Henry, T. J., Subasavage, J. P., Brown, M. A., et al. 2004, *AJ*, 128, 2460
- Hewett, P. C., Warren, S. J., Leggett, S. K., & Hodgkin, S. T. 2006, *MNRAS*, 367, 454
- Hodgkin, S. T., Irwin, M. J., Hewett, P. C., & Warren, S. J. 2009, *MNRAS*, 394, 675
- Itoh, Y., Hayashi, M., Tamura, M., et al. 2005, *ApJ*, 620, 984
- Jameson, R. F., Casewell, S. L., Bannister, N. P., et al. 2008, *MNRAS*, 384, 1399
- Jameson, R. F., Dobbie, P. D., Hodgkin, S. T., & Pinfield, D. J. 2002, *MNRAS*, 335, 853
- Jayawardhana, R., & Ivanov, V. D. 2006a, *Science*, 313, 1279
- Jayawardhana, R., & Ivanov, V. D. 2006b, *ApJ*, 647, L167
- Kirkpatrick, J. D., Barman, T. S., Burgasser, A. J., et al. 2006, *ApJ*, 639, 1120
- Kirkpatrick, J. D., Cruz, K. L., Barman, T. S., et al. 2008, *ApJ*, 689, 1295
- Kirkpatrick, J. D., Dahn, C. C., Monet, D. G., et al. 2001, *AJ*, 121, 3235
- Kirkpatrick, J. D., Reid, I. N., Liebert, J., et al. 1999, *ApJ*, 519, 802
- Kirkpatrick, J. D., Reid, I. N., Liebert, J., et al. 2000, *AJ*, 120, 447
- Knapp, G. R., Leggett, S. K., Fan, X., et al. 2004, *AJ*, 127, 3553
- Kroupa, P., & Bouvier, J. 2003, *MNRAS*, 346, 369
- Lafrenière, D., Jayawardhana, R., & van Kerkwijk, M. H. 2008, *ApJ*, 689, L153
- Lawrence, A., Warren, S. J., Almaini, O., et al. 2007, *MNRAS*, 379, 1599
- Leggett, S. K., Allard, F., Dahn, C., et al. 2000, *ApJ*, 535, 965
- Leggett, S. K., Allard, F., Geballe, T. R., Hauschildt, P. H., & Schweitzer, A. 2001, *ApJ*, 548, 908
- Linsky, J. L. 1969, *ApJ*, 156, 989
- Lodieu, N., Caux, E., Monin, J.-L., & Klotz, A. 2002, *A&A*, 383, L15
- Lodieu, N., Dobbie, P. D., Deacon, N. R., et al. 2007, *MNRAS*, 380, 712
- Lodieu, N., Hambly, N. C., Jameson, R. F., & Hodgkin, S. T. 2008, *MNRAS*, 383, 1385
- Lodieu, N., Scholz, R., McCaughrean, M. J., et al. 2005, *A&A*, 440, 1061
- Looper, D. L., Burgasser, A. J., Kirkpatrick, J. D., & Swift, B. J. 2007, *ApJ*, 669, L97
- Looper, D. L., Kirkpatrick, J. D., Cutri, R. M., et al. 2008, *ApJ*, 686, 528
- Lucas, P. W., Roche, P. F., Allard, F., & Hauschildt, P. H. 2001, *MNRAS*, 326, 695
- Lucas, P. W., Weights, D. J., Roche, P. F., & Riddick, F. C. 2006, *MNRAS*, 373, L60
- Luhman, K. L., Allen, L. E., Allen, P. R., et al. 2008, *ApJ*, 675, 1375
- Luhman, K. L., Mamajek, E. E., Allen, P. R., & Cruz, K. L. 2009, *ApJ*, 703, 399
- Luhman, K. L., & Muench, A. A. 2008, *ApJ*, 684, 654
- Luhman, K. L., Wilson, J. C., Brandner, W., et al. 2006, *ApJ*, 649, 894
- Mamajek, E. E., & Meyer, M. R. 2007, *ApJ*, 668, L175
- Martín, E. L., Basri, G., Gallegos, J. E., et al. 1998a, *ApJ*, 499, L61
- Martín, E. L., Basri, G., Zapatero Osorio, M. R., Rebolo, R., & López, R. J. G. 1998b, *ApJ*, 507, L41
- Martín, E. L., Brandner, W., Bouvier, J., et al. 2000, *ApJ*, 543, 299
- Martín, E. L., Delfosse, X., Basri, G., et al. 1999, *AJ*, 118, 2466
- Martín, E. L., Rebolo, R., & Zapatero Osorio, M. R. 1996, *ApJ*, 469, 706
- Martín, E. L., Zapatero Osorio, M. R., Barrado y Navascués, D., Béjar, V. J. S., & Rebolo, R. 2001, *ApJ*, 558, L117
- McElwain, M. W., Metchev, S. A., Larkin, J. E., et al. 2007, *ApJ*, 656, 505
- McGovern, M. R., Kirkpatrick, J. D., McLean, I. S., et al. 2004, *ApJ*, 600, 1020
- Metchev, S. A. & Hillenbrand, L. A. 2004, *ApJ*, 617, 1330
- Mohanty, S., Jayawardhana, R., Huéramo, N., & Mamajek, E. 2007, *ApJ*, 657, 1064
- Moraux, E., Bouvier, J., & Stauffer, J. R. 2001, *A&A*, 367, 211
- Moraux, E., Bouvier, J., Stauffer, J. R., & Cuillandre, J.-C. 2003, *A&A*, 400, 891
- Neuhäuser, R., Guenther, E. W., Wuchterl, G., et al. 2005, *A&A*, 435, L13
- Patience, J., King, R. R., De Rosa, R. J., & Marois, C. 2010, *A&A* in press, DOI: 10.1051/0004-6361/201014173
- Percival, S. M., Salaris, M., & Groenewegen, M. A. T. 2005, *A&A*, 429, 887
- Phan-Bao, N., Bessell, M. S., Martín, E. L., et al. 2008, *MNRAS*, 383, 831
- Pinfield, D. J., Dobbie, P. D., Jameson, R. F., et al. 2003, *MNRAS*, 342, 1241
- Pinfield, D. J., Hodgkin, S. T., Jameson, R. F., et al. 2000, *MNRAS*, 313, 347
- Pinfield, D. J., Jameson, R. F., & Hodgkin, S. T. 1998, *MNRAS*, 299, 955
- Pinfield, D. J., Jones, H. R. A., Lucas, P. W., et al. 2006, *MNRAS*, 368, 1281
- Potter, D., Martín, E. L., Cushing, M. C., et al. 2002, *ApJ*, 567, L133
- Rayner, J. T., Cushing, M. C., & Vacca, W. D. 2009, *ApJS*, 185, 289
- Rebolo, R., Martín, E. L., Basri, G., Marcy, G. W., & Zapatero Osorio, M. R. 1996, *ApJ*, 469, L53
- Rebolo, R., Martín, E. L., & Magazzù, A. 1992, *ApJ*, 389, L83
- Rebolo, R., Zapatero Osorio, M. R., Madruga, S., et al. 1998, *Science*, 282, 1309
- Reid, I. N., Burgasser, A. J., Cruz, K. L., Kirkpatrick, J. D., & Gizis, J. E. 2001, *AJ*, 121, 1710
- Reid, I. N., Cruz, K. L., Kirkpatrick, J. D., et al. 2008, *AJ*, 136, 1290
- Reid, I. N., Kirkpatrick, J. D., Liebert, J., et al. 1999, *ApJ*, 521, 613
- Ribas, I. 2003, *A&A*, 400, 297
- Robichon, N., Arenou, F., Mermilliod, J.-C., & Turon, C. 1999, *A&A*, 345, 471
- Saumon, D., Bergeron, P., Lunine, J. I., Hubbard, W. B., & Burrows, A. 1994, *ApJ*, 424, 333
- Schmidt, S. J., West, A. A., Hawley, S. L., & Pineda, J. S. 2010, *AJ*, 139, 1808
- Schmidt, T. O. B., Neuhäuser, R., Seifahrt, A., et al. 2008, *A&A*, 491, 311
- Scholz, R.-D. & Meusinger, H. 2002, *MNRAS*, 336, L49
- Skrutskie, M. F., Cutri, R. M., Stiening, R., et al. 2006, *AJ*, 131, 1163
- Slesnick, C. L., Hillenbrand, L. A., & Carpenter, J. M. 2004, *ApJ*, 610, 1045
- Soderblom, D. R., Laskar, T., Valenti, J. A., Stauffer, J. R., & Rebull, L. M. 2009, *AJ*, 138, 1292
- Stauffer, J. R., Hamilton, D., & Probst, R. G. 1994, *AJ*, 108, 155
- Stauffer, J. R., Hartmann, L. W., Fazio, G. G., et al. 2007, *ApJS*, 172, 663
- Stauffer, J. R., Schild, R., Barrado y Navascués, D., et al. 1998a, *ApJ*, 504, 805
- Stauffer, J. R., Schultz, G., & Kirkpatrick, J. D. 1998b, *ApJ*, 499, L199
- Steele, I. A. & Jameson, R. F. 1995, *MNRAS*, 272, 630
- Steele, I. A., Jameson, R. F., Hodgkin, S. T., & Hambly, N. C. 1995, *MNRAS*, 275, 841
- Taylor, B. J. 2008, *AJ*, 136, 1388
- Testi, L. 2009, *A&A*, 503, 639
- Testi, L., D'Antona, F., Ghinassi, F., et al. 2001, *ApJ*, 552, L147
- Tinney, C. G. 1998, *MNRAS*, 296, L42
- Tsuji, T., Ohnaka, K., & Aoki, W. 1996, *A&A*, 305, L1
- van Altena, W. F., Lee, J. T., & Hoffleit, E. D. 1995, *The general catalogue of trigonometric stellar parallaxes*, ed. W. F. van Altena, J. T. Lee, & E. D. Hoffleit
- van Leeuwen, F. 2009a, *A&A*, 497, 209
- van Leeuwen, F. 2009b, *A&A*, 500, 505
- Vrba, F. J., Henden, A. A., Luginbuhl, C. B., et al. 2004, *AJ*, 127, 2948
- Weights, D. J., Lucas, P. W., Roche, P. F., Pinfield, D. J., & Riddick, F. 2009, *MNRAS*, 392, 817
- Williams, D. M., Boyle, R. P., Morgan, W. T., et al. 1996, *ApJ*, 464, 238
- Zapatero Osorio, M. R., Béjar, V. J. S., Martín, E. L., et al. 2000, *Science*, 290, 103
- Zapatero Osorio, M. R., Béjar, V. J. S., Rebolo, R., Martín, E. L., & Basri, G. 1999a, *ApJ*, 524, L115
- Zapatero Osorio, M. R., Rebolo, R., Martín, E. L., et al. 1997, *ApJ*, 491, L81
- Zapatero Osorio, M. R., Rebolo, R., Martín, E. L., et al. 1999b, *A&AS*, 134, 537